

NOAA Data Report ERL PMEL-34



---

A TOGA ARRAY OF DRIFTING THERMISTOR CHAINS IN THE  
WESTERN EQUATORIAL PACIFIC OCEAN: OCTOBER 1989-JANUARY 1990

M.J. McPhaden  
A.J. Shepherd  
W.G. Large  
P.P. Niiler

Pacific Marine Environmental Laboratory  
Seattle, Washington  
June 1991

---

**noaa**

NATIONAL OCEANIC AND  
ATMOSPHERIC ADMINISTRATION

Environmental Research  
Laboratories

NOAA Data Report ERL PMEL-34

A TOGA ARRAY OF DRIFTING THERMISTOR CHAINS IN THE  
WESTERN EQUATORIAL PACIFIC OCEAN: OCTOBER 1989-JANUARY 1990

M.J. McPhaden  
A.J. Shepherd  
Pacific Marine Environmental Laboratory

W.G. Large  
National Center for Atmospheric Research  
Boulder, Colorado

P.P. Niiler  
Scripps Institution of Oceanography  
La Jolla, California

Pacific Marine Environmental Laboratory  
Seattle, Washington  
June 1991



**UNITED STATES  
DEPARTMENT OF COMMERCE**

**Robert A. Mosbacher  
Secretary**

**NATIONAL OCEANIC AND  
ATMOSPHERIC ADMINISTRATION**

**John A. Knauss  
Under Secretary for Oceans  
and Atmosphere/Administrator**

**Environmental Research  
Laboratories**

**Joseph O. Fletcher  
Director**

## NOTICE

Mention of a commercial company or product does not constitute an endorsement by NOAA/ERL. Use of information from this publication concerning proprietary products or the tests of such products for publicity or advertising purposes is not authorized.

Contribution No. 1280 from NOAA/Pacific Marine Environmental Laboratory

---

For sale by the National Technical Information Service, 5285 Port Royal Road  
Springfield, VA 22161

## CONTENTS

	PAGE
1. INTRODUCTION . . . . .	1
2. BUOY DESIGN . . . . .	4
3. ON-BOARD DATA PROCESSING AND SATELLITE TRANSMISSION . . . . .	6
4. SYSTEM PERFORMANCE . . . . .	7
5. DATA EDITING AND PROCESSING . . . . .	8
a. Position . . . . .	8
b. Pressure . . . . .	10
c. Temperature . . . . .	10
d. Wind . . . . .	11
6. ACKNOWLEDGMENTS . . . . .	11
7. REFERENCES . . . . .	11
8. LIST OF FIGURES . . . . .	13

## TABLES

1. Drifting buoy launch dates and positions . . . . .	2
2. Temperature and pressure sensor specifications . . . . .	3
3. Argos data transmission format . . . . .	5
4. Data return . . . . .	9

# A TOGA Array of Drifting Thermistor Chains in the Western Equatorial Pacific Ocean: October 1989–January 1990

M.J. McPhaden<sup>1</sup>, A.J. Shepherd<sup>1</sup>, W.G. Large<sup>2</sup>, and P.P. Niiler<sup>3</sup>

**ABSTRACT.** This report presents data collected from 19 drifting thermistor chains in the western equatorial Pacific Ocean between October 1989 and January 1990. The drifters were deployed as part of the TOGA program to study variability in the western equatorial Pacific warm pool. All drifters were equipped with 300 m long thermistor chains and 3 drifters were equipped with wind sensors. Data were telemetered in real-time to satellite via Service Argos. Drifter design, Argos data stream, data processing procedures, and overall system performance are described in detail.

## 1. INTRODUCTION

This report describes data collected from a satellite-tracked array of drifting thermistor chains deployed in the western equatorial Pacific as part of the Tropical Ocean-Global Atmosphere (TOGA) program. Deployments took place during October–November 1989 from the Xiangyanghong #14 on cruise #7 of the US/PRC Bilateral Air-Sea Interaction Program (Fig. 1, Table 1). A total of 19 buoys were launched, 3 of which were equipped with wind sensors. All buoys were manufactured by Polar Research Laboratory (PRL) of Carpinteria, California. An earlier pilot array of 4 PRL buoys deployed in February 1988 between 0°–6°N, 165°E is described in Taft and McPhaden (1990).

The primary goals of the 1989 drifter deployments were:

- 1) to determine space and time scales of upper ocean temperature variability in the western Pacific warm pool near the equator over the course of a season or longer; and
- 2) to determine the relationship between surface winds, sea surface temperature and upper ocean heat content on daily to seasonal time scales in the warm pool.

The timing of the deployments during the monsoon transition was meant to maximize the probability of observing the response to westerly wind bursts which occur most frequently during this season. Several such wind bursts were in fact observed during and after the drifter deployments as described in a preliminary presentation of the data in McPhaden *et al.* (1990).

The remainder of this report is outlined as follows. Section 2 briefly describes the drifting thermistor chain design, followed by a description in Section 3 of on-board data processing and

---

<sup>1</sup> Pacific Marine Environmental Laboratory, 7600 Sand Point Way N.E., Seattle, WA 98115-0070.

<sup>2</sup> National Center for Atmospheric Research, Boulder, CO 80307.

<sup>3</sup> Scripps Institution of Oceanography, La Jolla, CA 92093.

TABLE 1. Drifting buoy launch dates and positions, end dates and positions, and number of days transmitting.

Buoy ID	Launch Date (Yr,Mo,Dy)	Launch Time (z)	Launch Position (Lat. Long.)		Last Date (Yr,Mo,Dy)	Last Time (z)	Last Position (Lat. Long.)		Days Operating
8120	89 10 31	09:57	1.50S	152.51E	90 11 14	03:22	2.35S	154.02E	379
8121	89 10 28	01:49	3.00N	145.00E	90 7 26	08:28	0.56N	155.64E	271
8122	89 10 28	13:33	1.48N	147.51E	90 5 20	21:37	3.92N	144.42E	204
8126	89 11 18	10:50	1.53S	164.97E	90 10 26	01:49	1.11S	174.71E	342
*8127	89 10 25	14:06	1.49N	141.52E	91 2 18	10:52	1.15N	130.68E	481
*8129	89 10 29	23:49	1.50S	147.50E	91 2 18	15:01	4.69N	180.70E	477
8131	89 11 1	08:30	0.00N	155.00E	89 12 20	21:59	1.79N	159.60E	49
8132	89 11 22	09:30	2.97S	159.42E	89 12 5	16:22	3.79S	159.63E	13
8133	89 10 31	21:12	3.00S	155.00E	90 7 2	09:17	1.41S	156.41E	244
*8134	89 10 30	11:31	2.99N	150.00E	91 2 18	15:00	12.18N	184.68E	476
8135	89 11 23	05:13	1.49N	156.86E	90 2 6	20:34	4.11N	160.45E	75
8136	89 10 30	22:34	1.49N	152.49E	90 9 26	22:25	7.50N	155.20E	331
8137	89 10 29	10:48	3.01S	150.00E	90 5 21	22:54	0.14S	149.94E	204
8138	89 10 26	04:27	1.50S	141.51E	90 1 3	21:45	0.55S	143.23E	69
8139	89 10 27	20:03	3.00S	145.00E	90 1 28	09:42	1.51S	144.80E	93
8140	89 11 23	18:36	3.00N	156.00E	90 7 8	16:13	9.22N	165.52E	227
†10066	89 11 2	04:43	0.01N	160.00E	89 11 23	04:02	0.54S	160.55E	21
†10067	89 10 27	07:21	0.01N	145.00E	90 1 9	21:12	0.36S	151.97E	74
†10068	89 10 29	22:51	0.02N	150.01E	90 4 19	03:00	2.28N	152.66E	172

\* Buoys still transmitting as of February 18, 1991.

† Equipped with wind sensor

TABLE 2. Temperature and pressure sensor specifications for the PRL buoys. Reporting ranges (rounded to nearest integer values) and Argos bit resolution (rounded to nearest 0.001°C and 0.01 db) are as provided by the manufacturer. These numbers are approximate; more precise determination of reporting range and bit resolution were made for each individual sensor based on calibrations performed at PMEL.

Sensor ID	Depth (m)	Bus No.	Buoys 8120–8126		Buoys 8127, 8129		Buoys 8130–8140 10066–10068	
			Reporting Range	Bit Resolution	Reporting Range	Bit Resolution	Reporting Range	Bit Resolution
T1	1	1	15–31°C	0.063°C	22–31°C	0.035°C	15–33°C	0.070°C
T2	5	1	15–31°C	0.063°C	22–31°C	0.035°C	15–33°C	0.070°C
T3	10	2	15–31°C	0.063°C	22–31°C	0.035°C	15–33°C	0.070°C
T4	25	3	15–31°C	0.063°C	22–31°C	0.035°C	15–33°C	0.070°C
T5	50	1	15–31°C	0.063°C	22–31°C	0.035°C	15–33°C	0.070°C
T6	80	3	15–31°C	0.063°C	15–31°C	0.063°C	15–33°C	0.070°C
T7	110	1	12–30°C	0.070°C	12–30°C	0.070°C	12–30°C	0.070°C
T8	140	2	10–28°C	0.070°C	10–28°C	0.070°C	10–28°C	0.070°C
T9	170	3	9–27°C	0.070°C	9–27°C	0.070°C	9–27°C	0.070°C
T10	200	1	9–27°C	0.070°C	9–27°C	0.070°C	9–27°C	0.070°C
T11	230	2	8–24°C	0.063°C	8–24°C	0.063°C	8–26°C	0.070°C
T12	260	3	8–24°C	0.063°C	8–24°C	0.063°C	8–26°C	0.070°C
T13	300	2	8–24°C	0.063°C	8–24°C	0.063°C	8–26°C	0.070°C
P4	25	3	0–28 db	0.11 db	0–28 db	0.11 db	0–28 db	0.11 db
P7	110	1	0–122 db	0.48 db	0–122 db	0.48 db	0–122 db	0.48 db
P13	300	2	90–320 db	0.90 db	90–320 db	0.90 db	90–320 db	0.90 db

the Argos data stream. Overall buoy performance is evaluated in Section 4. Data editing and processing procedures are discussed in Section 5, followed by a presentation of the data in various formats.

## 2. BUOY DESIGN

A schematic of the satellite-tracked PRL drifter used in this study is shown in Fig. 2. The hull design incorporating electronic, batteries, satellite antenna and sea surface temperature (SST) sensor was similar to that developed for the FGGE experiment in the late 1970's. Attached to this hull was a 300 m long electromechanical cable supporting a vertical array of 12 thermoliner YSI temperature sensors and 3 Sensometrics Series SP97 pressure transducers. A 40 kg anchor was attached to the bottom of the chain.

The thermistor chain was 1.55 cm in diameter and consisted of a 0.23 cm black polyurethane outer jacket surrounding electrical conducting cable for multiplexing temperature and pressure sensor data to the surface buoy. Sensors were independently bussed on 3 electrical circuits (each with 4 temperature sensors and 1 pressure sensor) to minimize the loss of data in the event of fishbite or other damage to the electrical cabling. Sensors were mounted in housings along the axis of the cable in modular pressure resistant aluminum cannisters. The housings were approximately 50 cm long and oval in crosssection with 6.5 cm by 9.0 cm semiminor and semimajor axes. A similar buoy design was used in STREX (Large *et al.*, 1986), except that in the STREX buoys sensors were directly wired to circuits in the hull and thermistors were permanently potted along a 125 m long line.

Table 2 lists the temperature and pressure sensor depths, reporting ranges, Argos bit resolution, and bus configuration for the PRL buoys. The SST sensor is located on the buoy at a nominal depth of 1 m below the surface. The depths and reporting ranges of the subsurface temperature sensors were chosen to resolve variations in the surface layer and upper thermocline of the western equatorial Pacific. Pressure sensors were positioned to determine the 2-dimensional shape of the chain in the event of uplift by the horizontal shear flow. Bit resolution was determined by the range specification and the Argos word length discussed below. In most cases the resolution for temperature was 0.06°C–0.07°C, except for 2 “high resolution” buoys (#8127, #8129) which had a bit resolution of 0.035°C near the surface to accurately resolve the diurnal cycle in the mixed layer. Pressure and temperature sensors were calibrated at PMEL. Calibration residuals were typically 0.03°C–0.04°C for temperature; pressure was accurate to within the manufacturer's specification of  $\pm 1$ –1.5% full range. All pressure sensors were calibrated to read gauge pressure, i.e., pressure relative to atmospheric pressure.

Three of the buoys (#10066, #10067, #10068) were instrumented with RM Young 5103 wind monitors mounted atop a 3 m mast. Buoys were orientated into the wind by a 30 cm  $\times$  75 cm fixed vane assembly on the mast. Direction relative to magnetic north was measured with a



TABLE 3. Argos data transmission format for the PRL buoys. Tn and VTn are 3-hourly temperatures and variances for sensor n at the depths shown in parentheses; Pn and VPn are corresponding 3-hourly pressure means and variances. Buffer number (byte 31) indicates which of 3 buffers are being transmitted (1 = most recent data, 2 = next most recent data, 3 = oldest data). Sequence number (byte 32) indicates the sample number being collected at the time of transmission (effectively a clock word for temperature and pressure). WS1 and WD1 are wind speed and direction with conditional compass and vane sampling; WS2 and WD2 are wind speed and direction with conditional compass sampling only; WS is wind speed unconditionally sampled; Q contains 2 4-bit words with the percentage of data used in the 2 computations of conditionally sampled wind speed and direction; HR1 and HR2 indicate the sequencing in time of the hourly wind data ensembles written to memory at time WT.

Byte#	Buoys 8120-8140	Buoys 10066-10068
1	T1 (1 m)	T1 (1 m)
2	T2 (5 m)	T2 (5 m)
3	T3 (10 m)	T3 (10 m)
4	T4 (25 m)	T4 (25 m)
5	T5 (50 m)	T5 (50 m)
6	T6 (80 m)	T6 (80 m)
7	T7 (110 m)	T7 (110 m)
8	T8 (140 m)	T8 (140 m)
9	T9 (170 m)	T9 (170 m)
10	T10 (200 m)	T10 (200 m)
11	T11 (230 m)	T11 (230 m)
12	T12 (260 m)	T12 (260 m)
13	T13 (300 m)	T13 (300 m)
14	P4 (25 m)	P4 (25 m)
15	P7 (110 m)	P7 (110 m)
16	P13 (300 m)	P13 (300 m)
17	VT2 (5 m)	WS1 (HR1)
18	VT3 (10 m)	WD1 (HR1)
19	VT4 (25 m)	WS2 (HR1)
20	VT5 (50 m)	WD2 (HR1)
21	VT6 (80 m)	WS (HR1)
22	VT7 (110 m)	Q (HR1)
23	VT8 (140 m)	WS1 (HR2)
24	VT9 (170 m)	WD1 (HR2)
25	VT10 (200 m)	WS2 (HR2)
26	VT11 (230 m)	WD2 (HR2)
27	VT12 (260 m)	WS (HR2)
28	VT13 (300 m)	Q (HR2)
29	VP7 (110 m)	WT
30	VP13 (300 m)	Air Temperature (inoperative)
31	Buffer number	Buffer number
32	Sequence number	Sequence number

Digicourse fluxgate compass having a bit resolution of  $1.4^{\circ}\text{C}$ . RM Young speeds were calibrated in PMEL's wind tunnel; calibration residuals were typically  $0.1\text{ m s}^{-1}$ .

### 3. ON-BOARD DATA PROCESSING AND SATELLITE TRANSMISSION

Each buoy transmitted data to Service Argos receivers on board two of NOAA's polar orbiting Tiros series weather satellites. Individual transmissions were limited to 256 bits of information in 32 8-bit bytes. Transmissions were every 60 seconds, although data were received only when the buoy was in view of one of the satellites. Argos satellites passed within sight of the buoys typically 6–8 times per day, and for each overpass 6–10 transmissions were usually received. Considerable on board data processing and transmission scheduling were required in order to obtain a continuous data record because of the limited data rate and irregular reception of Service Argos.

Argos data transmission formats for the PRL thermistor chains with wind sensors (#10066–10068) and for those without wind sensors (#8120–8140) are shown in Table 3. Both types of buoys transmitted data in a "normal" and a "deployment" mode of operation. During "normal mode" operation, 3-hour means were computed for each temperature and pressure sensor based on 180 1-minute samples. For buoys #8120–8140, 3-hour variances were also computed, except for SST and P4 (25 m) pressure. Temperature and pressure statistics plus a corresponding clock word constituted a 3-hour data ensemble, and at any time the 3 most recent ensembles were stored in 3 separate memory buffers. Buffers were transmitted sequentially, so that every ensemble was transmitted at 3 minute intervals throughout the 9 hours following its formation. In this way a very nearly continuous record of 3 hourly means and variances of the temperatures and pressures was obtained.

The nature of wind variability required more frequent averages and more rapid sampling. A separate wind processor sampled and stored the wind speed and direction relative to the buoy hull every second, and the hull orientation (compass) every 5 seconds. After 375 seconds, the vane and compass data were used to compute a time series of wind direction, and from this time series the most common direction was determined over the interval. Speed and direction data were then subsampled to include only those directions within  $\pm 30$  degrees of this most common direction. In previous pilot experiments, directions outside this range were found to correspond to instances of violent buoy motion that could contaminate the wind measurement. The average speed computed from this subsample was reduced by  $\frac{1}{2}\%$  to eliminate the effects of turbulent fluctuations (Pond et al., 1979). Average speed and direction were then used to compute zonal and meridional wind components from the 375-second interval.

To guard against complete data loss in the case of vane signal failure, a second computation similar to that described above was performed, assuming that the fixed vane aligned the buoy into wind. In this instance, only compass variations can cause the wind direction to be outside the sampling range. Wind speed, direction and velocity components were otherwise calculated as

above. Finally, a third calculation of wind speed was performed by averaging over all samples in the interval, so that a wind speed would still be available in the case of compass failure.

Following these computations, the processor was shut down for 512 seconds to conserve power, after which sampling resumed for the next 375 second interval. Wind components (computed using the 2 different subsampling schemes) and scalar speed were then averaged over 4 such sampling intervals. A wind record thus consisted of an approximate hourly average for the two wind vectors (transformed into a wind speed and direction in order to reduce the required number of data bits); the scalar average speed; and the percentage of samples used in each of the two subsampling schemes. Every 2 hours the two most recent 1-hour wind data were loaded into one of the three memory buffers for transmission. Thus at any time the memory buffers contained the 6 most recent 1-hour wind speeds and directions, each of which was transmitted every 3 minutes for 6 hours.

During the first 3 hours after switch on, the buoys operated in a "deployment mode" to allow an immediate evaluation of temperature and pressure sensor performance using a portable uplink receiver. In this mode, the buoys transmitted instantaneous 1 minute temperature and pressure samples for 8 minutes followed by an 8 minute average and variance in the ninth transmission. This sequence was repeated until the system switched to "normal mode" after 3 hours.

#### **4. SYSTEM PERFORMANCE**

The time history of sensor performance is shown in Figure 3 for the PRL drifter array. The number of temperature and pressure sensors deployed was 304 (247 temperature sensors, 57 pressure sensors). By 30 March 1990 (i.e., about 120–150 days after the drifters were deployed) only 66 temperature sensors and 14 pressure sensors were functioning. Overall failure rate was 74% (73% for temperature and 78% for pressure). In November 1990 after approximately 1 year, only 4 buoys were transmitting (Table 1) with 10 functional temperature sensors and 3 functional pressure sensors (overall failure rate of 96%). The buoys had a design lifetime of 1 year according to the manufacturer.

Three modes of failure affected the transmission of temperature and pressure data from the drifters. The first (and least significant) was an occasional, apparently random, sensor failure. The second failure mode was more severe and involved bus or chain failures on 13 buoys. In some cases, all sensors on a particular bus failed at the same time. In other cases affecting at least 10 buoys, the deepest sensors on a bus failed first, followed by failure of the shallower sensors after several days to weeks. Similar gradual bus failures had been noticed in the 1988 pilot deployment of 4 PRL drifting thermistor chains in the western equatorial Pacific (Taft and McPhaden, 1990), and in an earlier TOGA test deployment of 2 PRL drifting thermistor chains in the California Current in July–August 1987. The PRL buoys deployed in October–November 1989 were of a newer design and construction which, according to the manufacturer, should have remedied this gradual bus failure problem.

The third failure mode affecting the drifters was one of catastrophic data loss through the premature termination of satellite transmissions. These catastrophic losses, which affected 7 buoys in the first 120 days of the experiment, could have been due to either a power failure or a failure of the satellite transmitter.

Temperature data return was also affected by uplift of the chain, which in extreme cases was 150 m or more in response to strong westerly wind forcing. This uplift caused some of deep thermistors to be located in water temperatures outside the sensor measurement range. Sensor output during these periods was pinned at top of range until the chain relaxed.

The longest wind record collected was 21 days in duration on buoy #10066 which stopped transmitting on 23 November 1989. Five days of wind data were collected from buoy #10067 and no wind data from buoy #10068. It has not been possible to recover any of the buoys to investigate the causes behind the transmission failures, wind system failures, or thermistor chain failures.

## **5. DATA EDITING AND PROCESSING**

Data editing and processing has been restricted to the period October 1989–January 1990 in view of the unexpectedly rapid decrease of the drifter data return resulting from failures and problems discussed in the previous section. This period is of the greatest interest scientifically because it encompassed 4 westerly wind episodes near the equator. Data for the period after January 1990 will be processed at a later time.

The data were first edited to remove transmission errors, then screened bit-by-bit to eliminate duplicate transmissions. Deployment mode data (i.e., data transmitted <3 hours after deployment) were eliminated. Subsequent transmissions were accepted only if the Argos time word was properly sequenced. After this preliminary processing, position, temperature, pressure and wind data were edited to produce a final data set. Overall temperature and pressure data return for the 19 PRL drifters during October 1989–January 1990 was 63.6% after editing (Table 4). Details of the editing procedures are discussed below.

### **a. Position**

On average, there were about 6 position fixes per day per buoy (Fig. 4), with a maximum of 7 per day for buoy 8132 and a minimum of 3 per day for buoy 8122. Class 2 position fixes, which according to Service Argos (1988) have a 1 standard deviation location accuracy of 350 m, comprised 72% of the total. Class 1 positions fixes (accuracy of 1 km) comprised 17% of the total, and class 3 position fixes (accuracy of 150 m) comprised the remaining 11%. Position fixes were not evenly distributed throughout the day, but tended to cluster around times of most frequent satellite overpasses (Fig. 4). We interpolated all position data using cubic splines to an evenly spaced time series of 4-hourly values based on the array average of 6 position fixes per day. Plots of buoy positions smoothed to approximately daily means with a 9-point, 36-hour

TABLE 4. Good 3-hour averages and percentage data return for PRL drifting buoy temperature and pressure data. Statistics are from time of deployment to 31 January 1990. Percent data return for sensors is based on a potential of 13,274 good 3-hourly values from the 19 buoys. Percent data return for all buoys and sensors (63.6%) is highlighted at lower right.

Buoy		08120	08121	08122	08126	08127	08129	08131	08132	08133	08134	08135	08136	08137	08138	08139	08140	10066	10067	10068	Sensor Total	% Return
Sensor																						
T01	731	761	591	591	774	732	394	109	150	736	556	163	751	204	736	550	167	146	563	9405	70.9	
T02	733	761	589	443	664	735	394	109	143	735	556	143	751	5	213	550	167	0	276	7967	60.0	
T03	733	330	589	591	780	735	394	109	144	508	556	722	751	545	681	550	167	0	732	9617	72.5	
T04	733	761	357	591	780	735	394	109	375	508	556	724	751	545	736	550	167	0	732	10104	76.1	
T05	139	761	586	591	778	735	394	29	148	508	556	164	751	204	728	550	167	146	563	8498	64.0	
T06	139	761	1	591	780	735	394	109	112	508	556	723	751	545	736	550	167	192	732	9082	68.4	
T07	139	761	130	591	778	735	389	109	146	508	556	163	751	204	717	550	167	144	563	8101	61.0	
T08	92	738	458	141	763	447	153	9	44	499	494	414	642	417	267	514	119	3	409	6623	49.9	
T09	137	303	333	309	778	526	277	33	299	500	510	625	719	463	440	543	130	215	564	7704	58.0	
T10	137	761	561	387	338	157	319	107	153	506	526	360	743	506	443	550	161	0	613	7328	55.2	
T11	137	761	565	94	34	496	325	109	145	508	534	166	749	204	597	550	167	146	453	6740	50.8	
T12	137	761	282	432	780	688	330	109	374	508	540	720	751	540	626	550	167	159	642	9096	68.5	
T13	137	761	580	298	780	729	346	109	145	508	553	724	751	545	304	550	167	0	714	8701	65.6	
P04	733	761	391	591	780	734	394	109	375	509	556	724	751	545	736	550	167	0	732	10138	76.4	
P07	137	758	0	591	620	735	394	109	145	509	556	164	751	204	692	550	167	146	563	7791	58.7	
P13	139	758	589	430	780	735	389	109	132	507	556	724	0	545	298	550	167	0	732	8140	61.3	
Buoy Totals		5133	11258	6602	7262	10987	10389	5680	1486	3030	8565	8717	7423	11114	6221	8950	8757	2581	1297	9583	135035	
Buoy Potential		11728	12176	9456	9456	12480	11760	11696	9024	11744	11792	8896	11584	12016	12416	12240	8800	11616	11792	11712	212384	
% Return		43.8	92.5	69.8	76.8	88.0	88.3	48.6	16.5	25.8	72.6	98.0	64.1	92.5	50.1	73.1	99.5	22.2	11.0	81.8	63.6	

Hanning filter (zero amplitude at periods of 18 hrs.) are shown in Fig. 5 for the entire array, and in Figs. 6–15 for individual buoys.

Velocity time series were computed using centered differences on the interpolated position data. The differenced time series were noisy, and in many cases were characterized by large velocity spikes. We eliminated these spikes by filtering with a 9-point, 36-hour running median filter (Brock, 1986). The data were then smoothed with a 36-hour Hanning filter to remove high frequency noise. The resulting velocity time series are shown in Figs. 16–34. Scalar speeds are also shown in Figs. 16–34. These are based on 4-hourly data filtered in the same manner as zonal and meridional velocity components.

#### **b. Pressure**

Pressure data were manually edited for outliers. Questionable 3-hour means with erratic variances were likewise eliminated. About 3% of the original data were culled by these procedures.

Edited 3-hourly pressure time series are shown in Figs. 35–53. Features of note include an apparent drift in the 300 m pressure sensor on buoy #8121 (Fig. 36). Though uncorrectable, this drift has not been edited out since it was relatively modest and viewed as acceptable relative to the alternative of no pressure data at 300 m. The shallowest pressure sensor on buoy #8139 (Fig. 49) consistently registered values 3–5 db less than expected from its location at a nominal depth 25 m. This may have been due to positioning of the sensor at an incorrect depth on the thermistor chain.

Time series of thermistor chain shape are shown in Figs. 54–72. These have been computed by block averaging the pressure data to daily means for each sensor based on 4 or more 3-hourly values. Chain shapes have then been estimated by linear interpolation between pressure sensors, assuming a pressure of zero at the surface.

#### **c. Temperature**

Temperature data were edited in a manner similar to that described for pressure data. In addition, suspicious temperature data were checked for consistency with data from neighboring depths. Temperature values pinned at top-of-range were eliminated. About 5% of the original data were removed by these editing procedures.

Edited 3-hourly temperature time series are shown in Figs. 73–91. Temperature inversions of  $O(0.1^{\circ}\text{C})$ , in some cases lasting several days or longer, are evident in the upper sensors from a few of the buoys (e.g., #8121, #8129, #8131, #10066). These inversions could be due to an offset or drift in sensor calibrations. However, rainfall rates in the western Pacific are the highest in the world ocean, and buoyancy in the surface layer is significantly affected by this fresh water flux (Lukas and Lindstrom, 1990). Hence, we have not edited or adjusted the time series for

these inversions, the nature of which may become clearer in further scientific analyses of the data.

Data gaps of 6 hours or less in these edited time series were filled by linear interpolation. The resultant data set contains less than 0.5% interpolations, with the maximum number of interpolated data for any single buoy being 1.4% of the total (buoy #8122). Temperature data were then adjusted for the shape of the thermistor chain by linearly interpolating 3-hourly pressure data to determine the depth of a particular temperature sensor. Temperature data from these positions were next linearly interpolated to the nominal depths of the temperature sensors. The 3-hourly temperature time series adjusted for the shape of the thermistor chain are shown in Figs. 92–110. Daily averaged versions of these time series, based on block averaging a minimum of four 3-hourly values, are shown in Figs. 111–129; corresponding daily averaged isotherm depth plots are shown in Figs. 130–147.

#### d. Wind

Wind data from buoys #10066 and #10067 were edited in a manner similar to that described for temperature and pressure. However, there were no bad data or data gaps for the time period that the wind sensors were working on these buoys. Wind speed and wind direction computed from each of the methods described in Section 3 are shown in Fig. 148. There is almost no distinction between the two methods of subsampling wind speed and direction. Hourly time series of wind velocity components are shown in Fig. 149.

## 6. ACKNOWLEDGMENTS

We would like to thank Ansley Manke and Marguerite McCarty of PMEL for their programming assistance in producing this report. We would also like to acknowledge Susan Hirst (formerly of PMEL) who wrote much of the original code for downloading and processing the Argos data stream, and who was instrumental in developing programs to process calibration data from the PRL drifters. Carol Coho (also formerly of PMEL) helped in testing, calibrating, and deploying the drifters; and monitoring their performance at sea. Funds for this program were provided by the National Science Foundation (grant OCE-89-23053) and the US TOGA Project Office.

## 7. REFERENCES

- Brock, F.V. (1986): A nonlinear filter to remove noise from meteorological data. *J. Atmos. Ocean. Tech.*, 3, 51–58.
- Large, W.G., J.C. McWilliams, and P.P. Niiler (1986): Upper ocean thermal response to strong autumnal forcing in the northeast Pacific. *J. Phys. Oceanogr.*, 16, 1524–1550.

- McPhaden, M.J., P.P. Niiler, and P.L. Richardson (1990): The response of the western equatorial Pacific to westerly wind burst forcing in November 1989–January 1990. *Eos, Trans. Am. Geophys. Union*, 71, 1231.
- Pond, S., W.G. Large, M. Miyake and R.W. Burling (1979): A Gill twin propellor-vane anemometer for flux measurements during moderate and strong winds. *Bound.-Layer Meteor.*, 16, 351-364.
- Service Argos (1988): User's Manual, Version 1. Service Argos, Inc. Landover, MD.
- Taft, B.A., and M.J. McPhaden (1990): Diurnal cycle of sea surface temperature in the western tropical Pacific. Proceedings of the Symposium on US/PRC Bilateral Air-Sea Interaction Program, Beijing, PRC, 15–17 November 1988, China Ocean Press, Beijing, 343–352.



## 8. LIST OF FIGURES

- Fig. 1. Cruise track of the Xiangyanghong #14 in October–November 1989 indicating the locations of drifting thermistor chain deployments (x). Also indicated are the positions of current meter moorings (■), ATLAS moorings (◆) and island wind/sea level stations (●).
- Fig. 2. Schematic diagram of a PRL drifting thermistor chain.
- Fig. 3. Time history of PRL sensor performance from 22 October 1989 to 30 March 1990.
- Fig. 4. Histogram of location fixes as a function of time of day for PRL buoys during the period October 1989–January 1990, inclusive. Total number of fixes and average number of fixes per day are indicated.
- Fig. 5. Buoy positions smoothed with a 9-point, 36-hour Hanning filter. Deployment location is indicated by a large circle. Squares indicate sequential positions separated by 5 days. Buoy ID numbers and deployment dates are indicated near each deployment site. Trajectories are shown through 31 January 1990.
- Figs. 6–15. Individual buoy positions smoothed with a 9-point, 36-hour Hanning filter. Diamonds indicate positions at the middle of each day; squares indicate sequential positions separated by 5 days. Trajectories from deployment through 31 January 1990 are shown, with start and end dates indicated.
- Figs. 16–34. Zonal velocity, meridional velocity and scalar speed for individual drifters.
- Figs. 35–53. Time series of 3-hourly pressure data at nominal sensor depths for the PRL drifters.
- Figs. 54–72. Time series of daily averaged thermistor chain shapes for the PRL drifters. Dots below the surface indicate depths of pressure sensors.
- Figs. 73–91. Time series of 3-hourly temperature sensor data for PRL drifters.
- Figs. 92–110. Time series of 3-hourly temperatures at fixed depths for PRL drifters.
- Figs. 111–129. Daily averaged temperature time series at fixed depths for PRL drifters.
- Figs. 130–147. Contour plots of daily averaged temperatures for PRL drifters. No plot is shown for buoy #10067 due to lack of sufficient data.
- Fig. 148. Hourly time series of wind speed and direction (measured counterclockwise relative to east) for PRL buoys #10066 and #10067. Time series from the 2 buoys are non-overlapping and separated by the record gap on November 1. Direction computed from subsampled compass data (solid line) and subsampled compass and vane data (dashed line) are overplotted, as are speeds based on data with and without subsampling. There is almost no distinction between the two methods of subsampling wind speed and direction.
- Fig. 149. Hourly time series of wind velocity components for PRL buoys #10066 and #10067. Time series from the 2 buoys are non-overlapping and separated by the record gap on November 1. Components computed from subsampled compass only (solid line) and subsampled compass and vane (dashed line) are overplotted. There is almost no distinction between the two methods of computing wind components.

US/PRC Bilateral Cruise #7  
 Xiangyanghong #14  
 Guangzhou, PRC – Guam  
 12 October – 26 November 1989

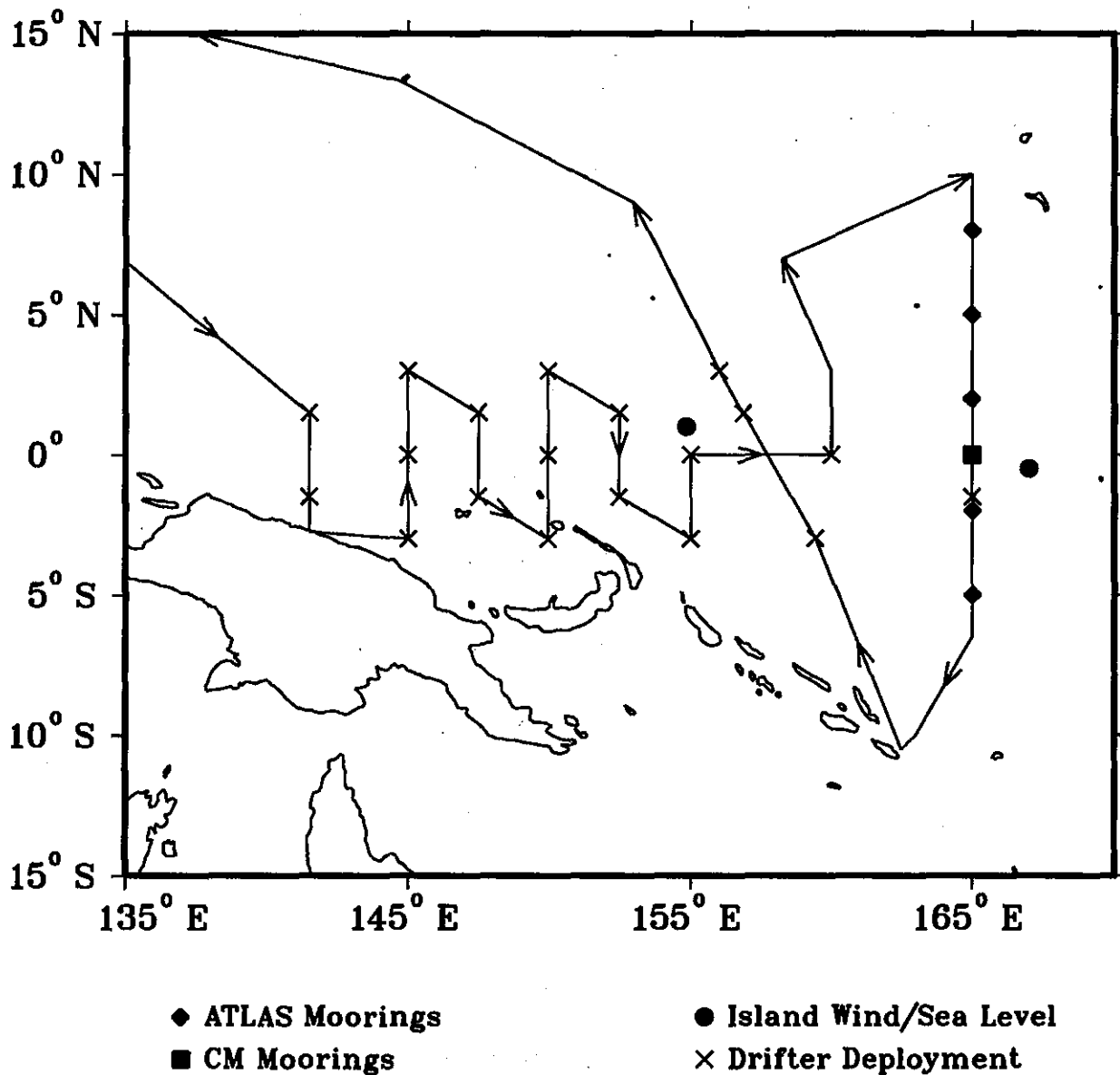


Figure 1. Cruise track of the Xiangyanghong #14 in October–November 1989 indicating the locations of drifting thermistor chain deployments (x). Also indicated are the positions of current meter moorings (■), ATLAS moorings (◆) and island wind/sea level stations (●).

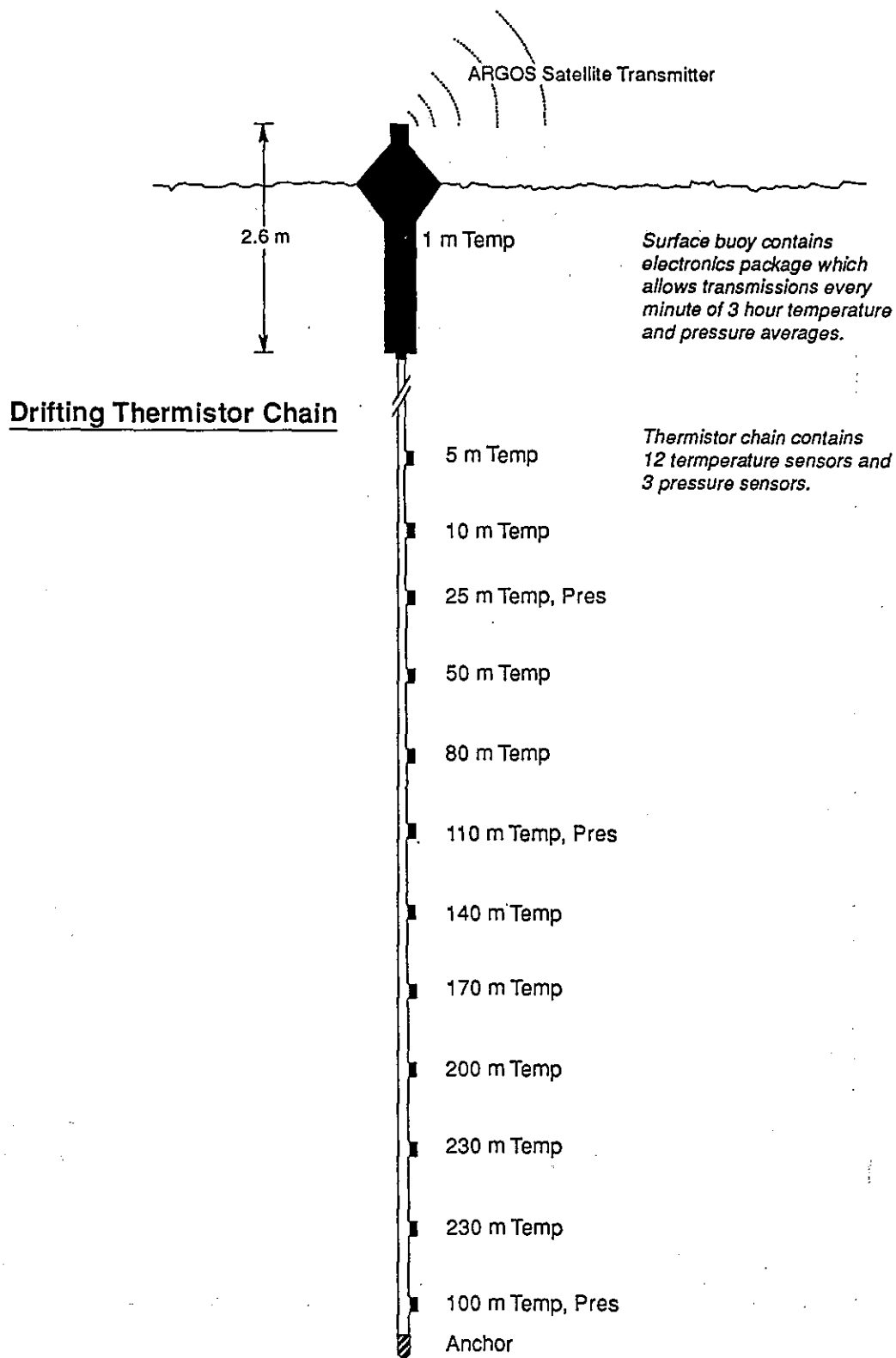


Figure 2. Schematic diagram of a PRL drifting thermistor chain.

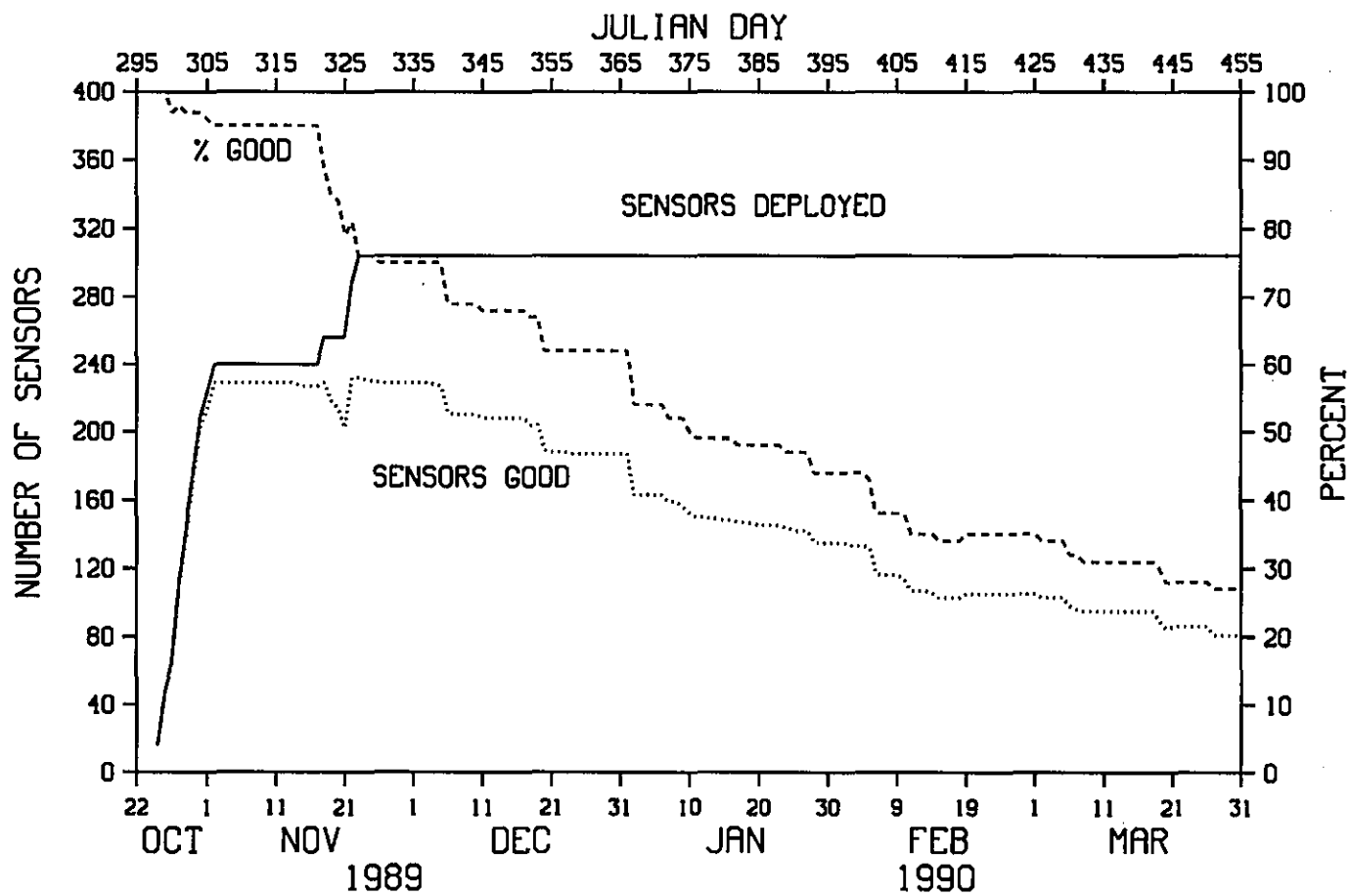


Figure 3. Time history of PRL sensor performance from 22 October 1989 to 30 March 1990.

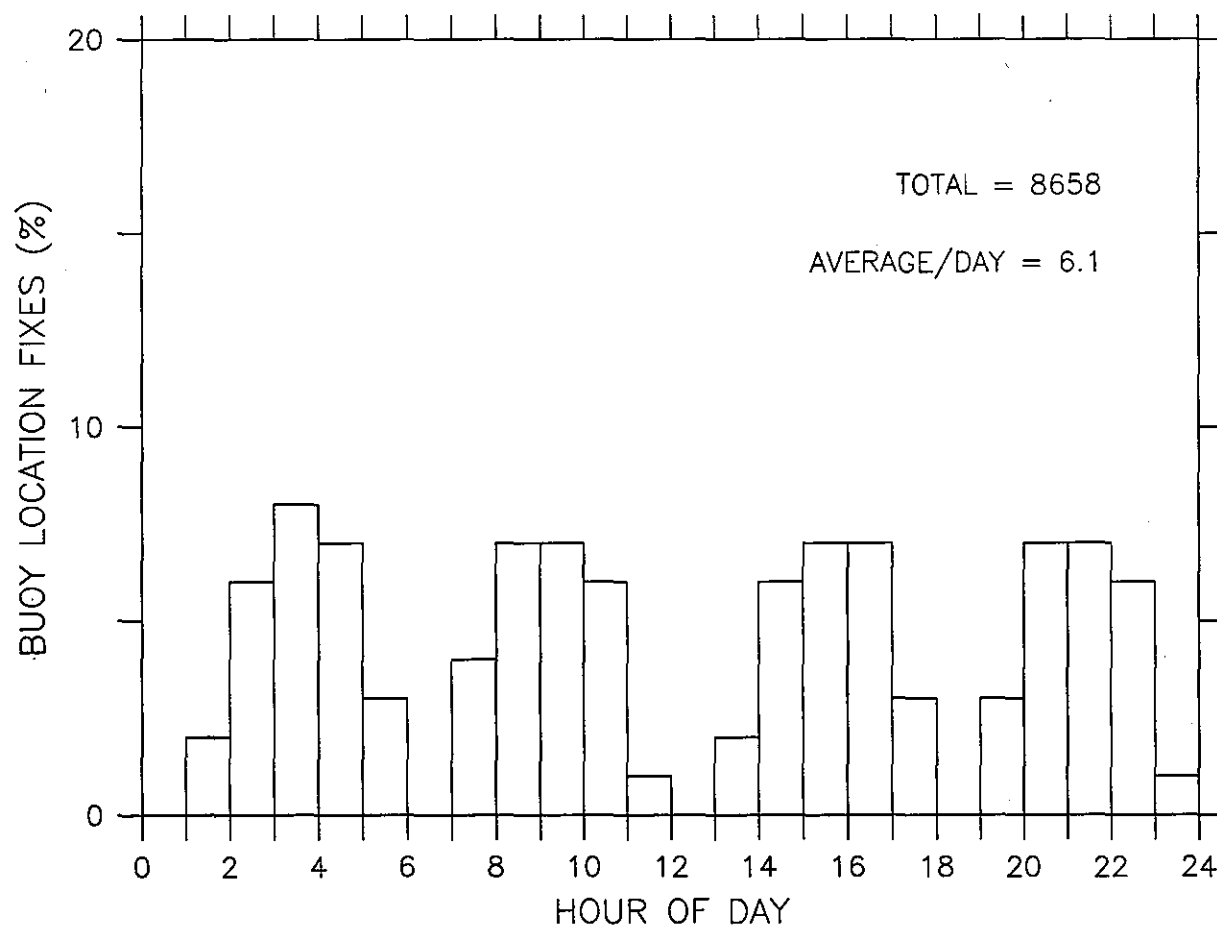


Figure 4. Histogram of location fixes as a function of time of day for PRL buoys during the period October 1989–January 1990, inclusive. Total number of fixes and average number of fixes per day are indicated.

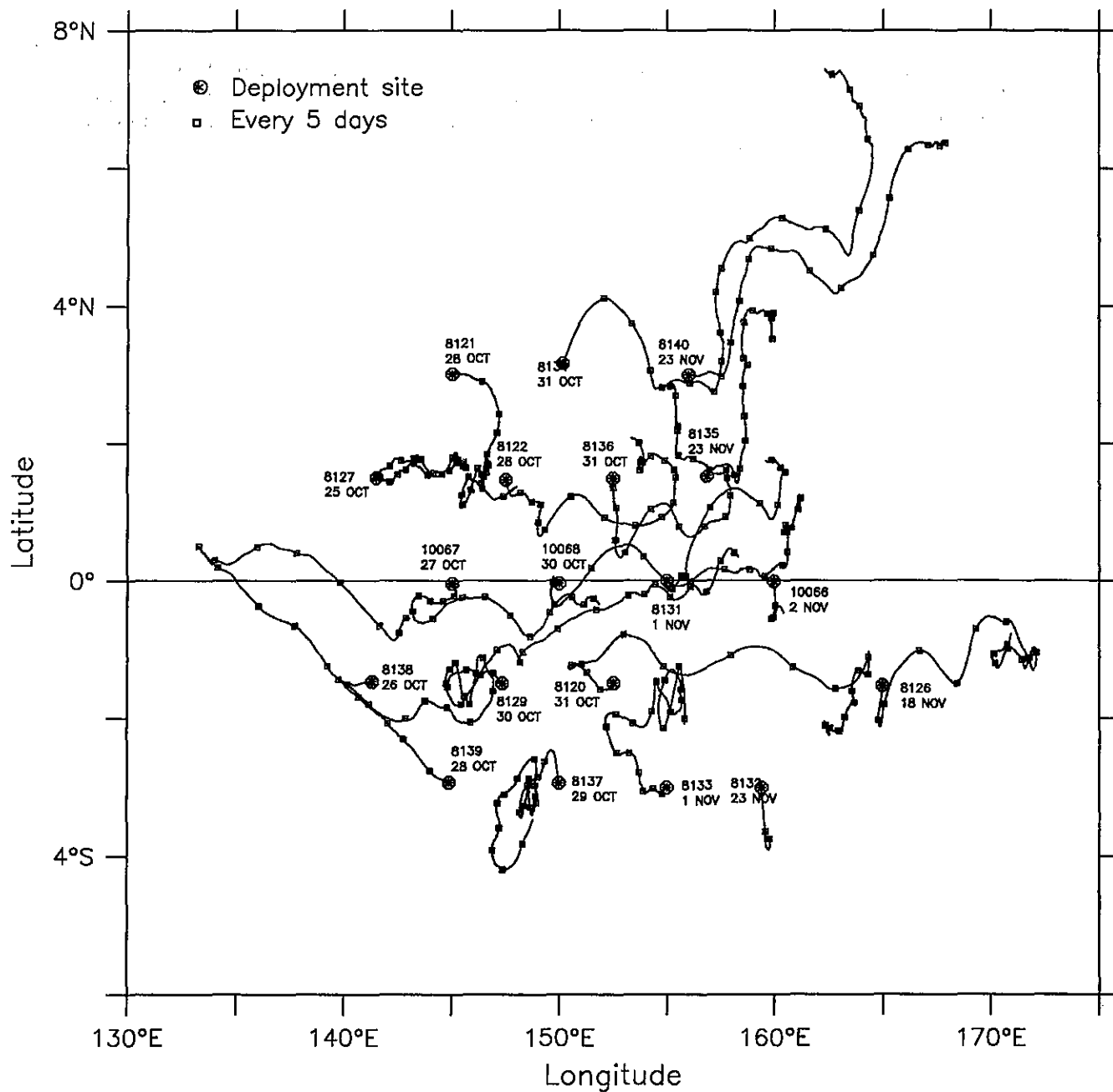


Figure 5. Buoy positions smoothed with a 9-point, 36-hour Hanning filter. Deployment location is indicated by a large circle. Squares indicate sequential positions separated by 5 days. Buoy ID numbers and deployment dates are indicated near each deployment site. Trajectories are shown through 31 January 1990.

Figures 6–15. Individual buoy positions smoothed with a 9-point, 36-hour Hanning filter. Diamonds indicate positions at the middle of each day; squares indicate sequential positions separated by 5 days. Trajectories from deployment through 31 January 1990 are shown, with start and end dates indicated.

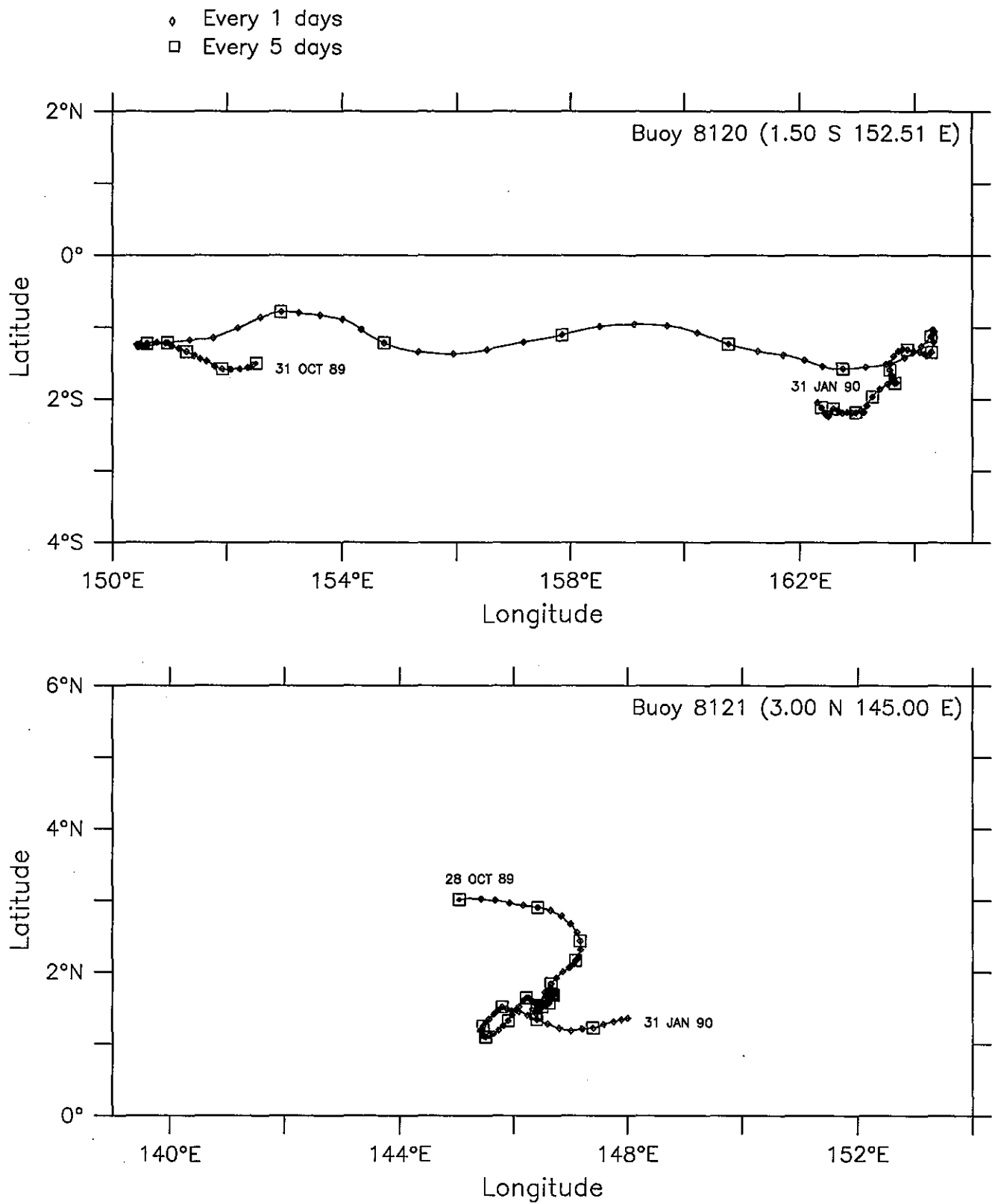


Figure 6.



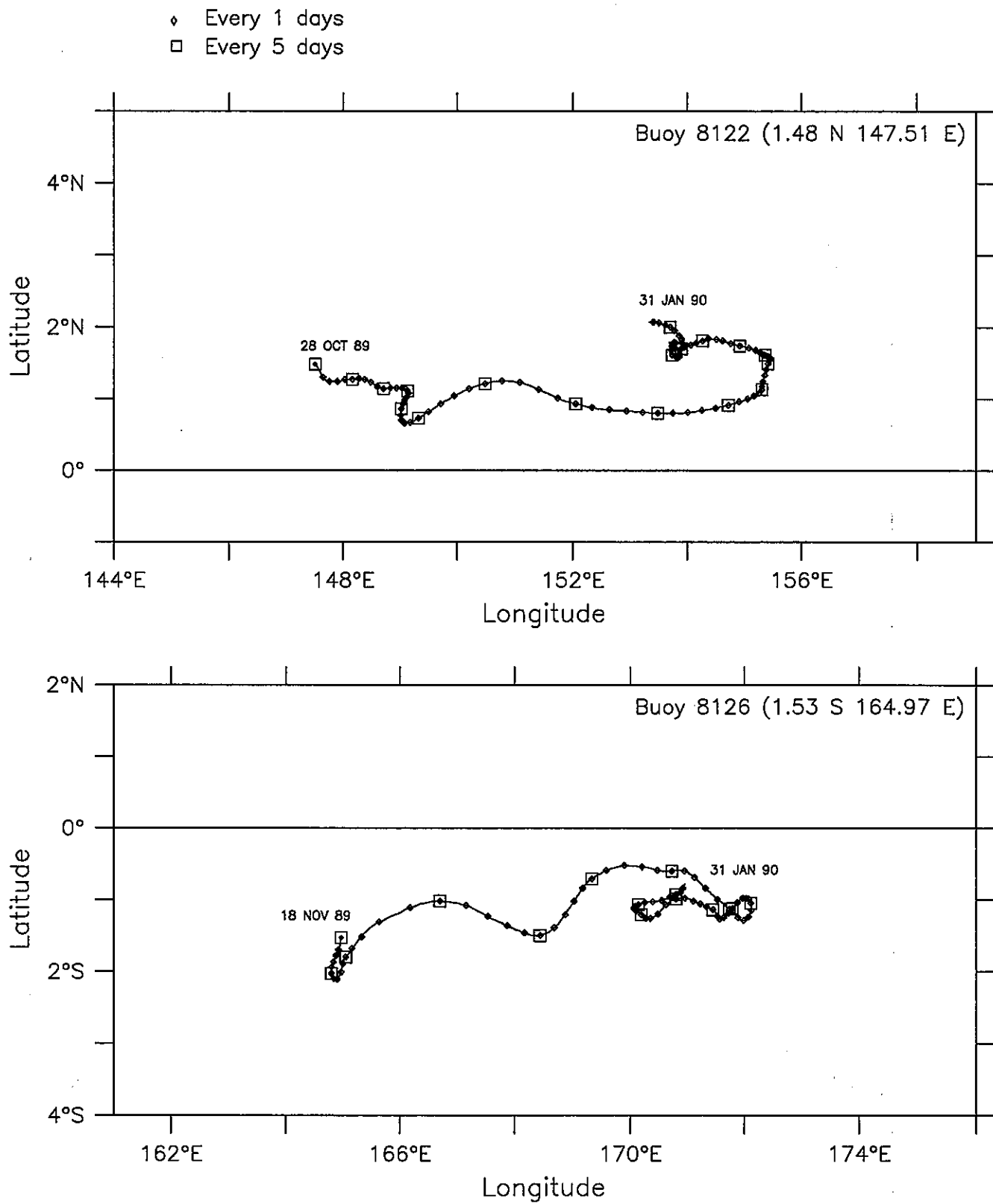


Figure 7.

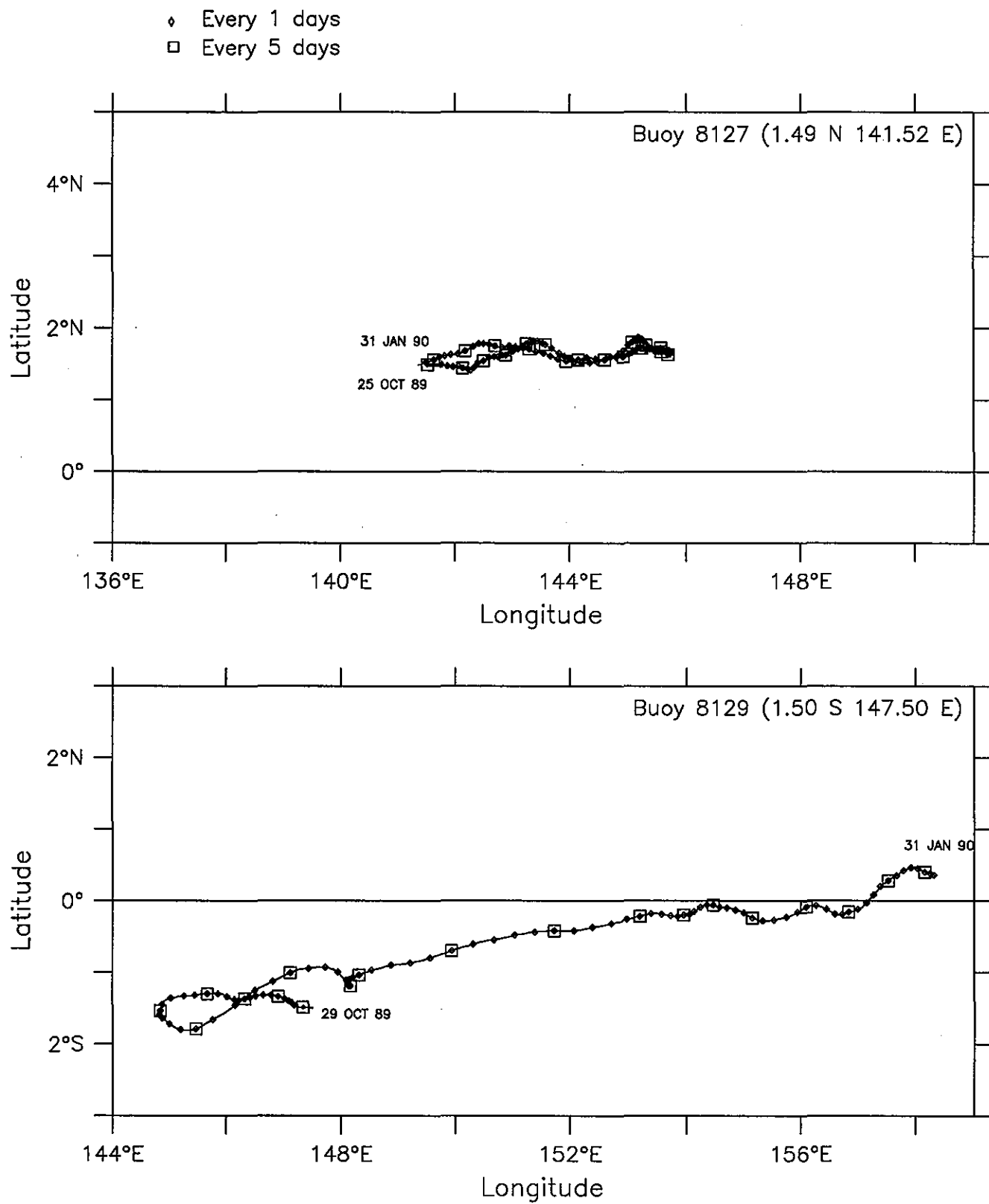


Figure 8.

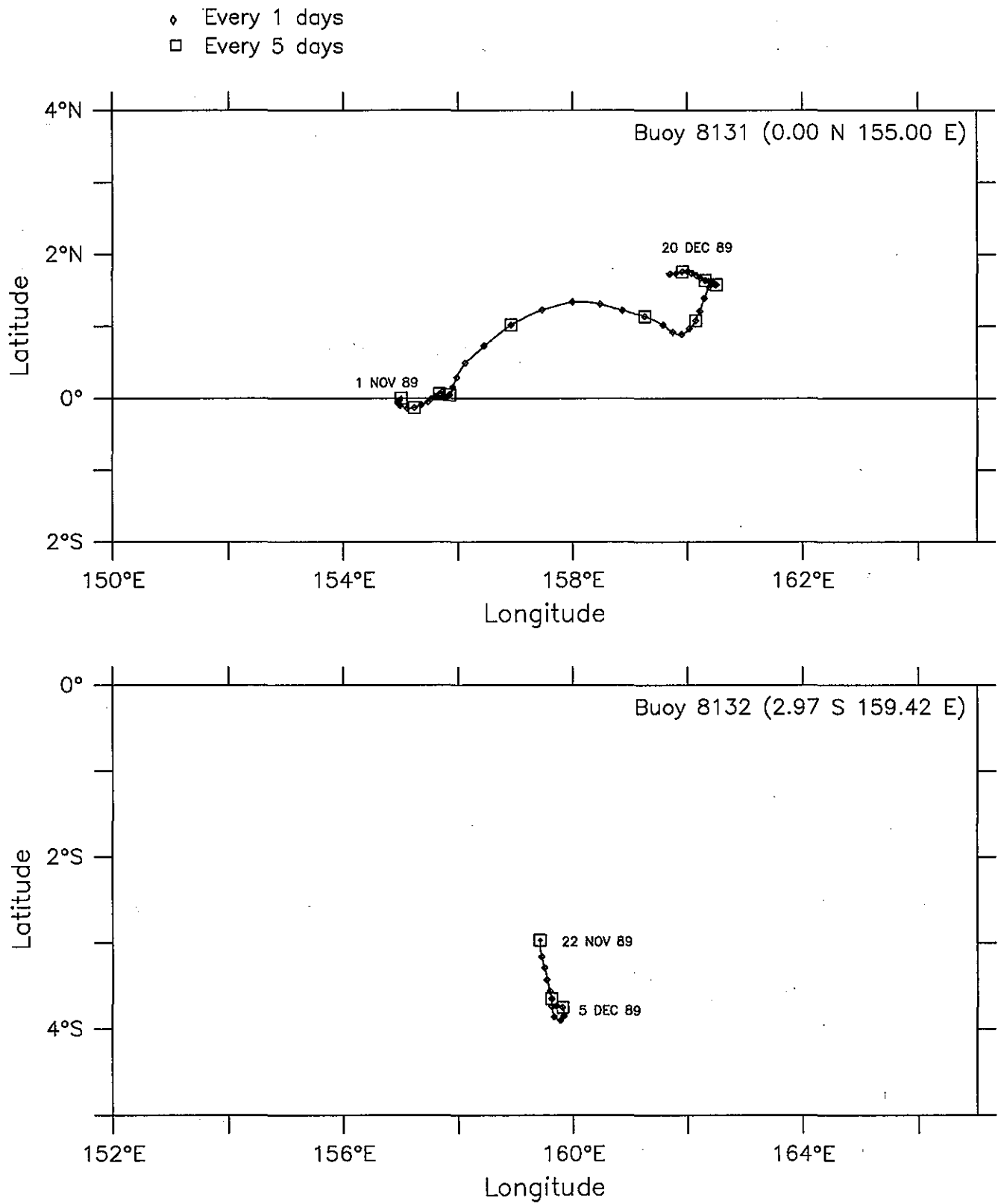


Figure 9.

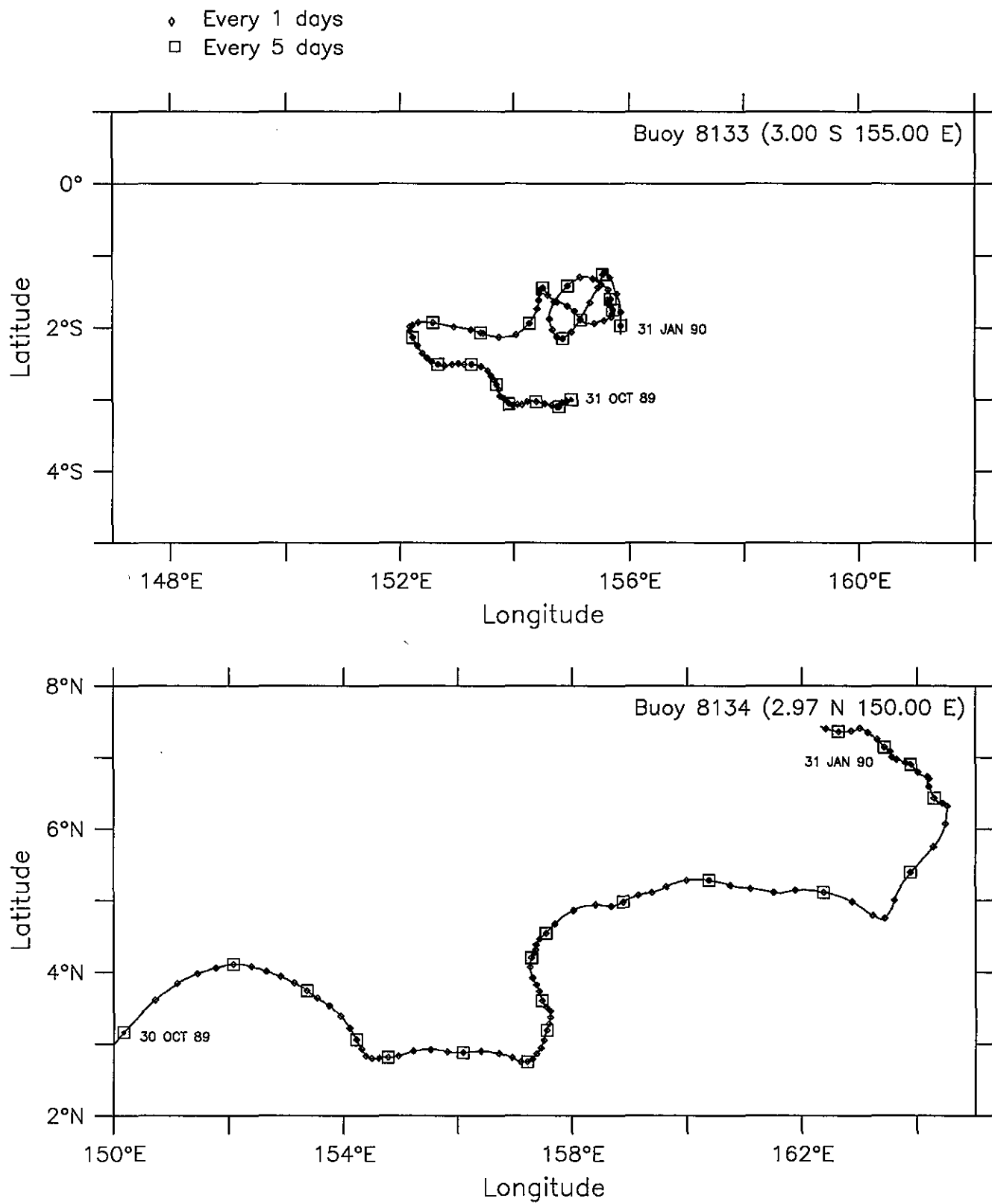


Figure 10.

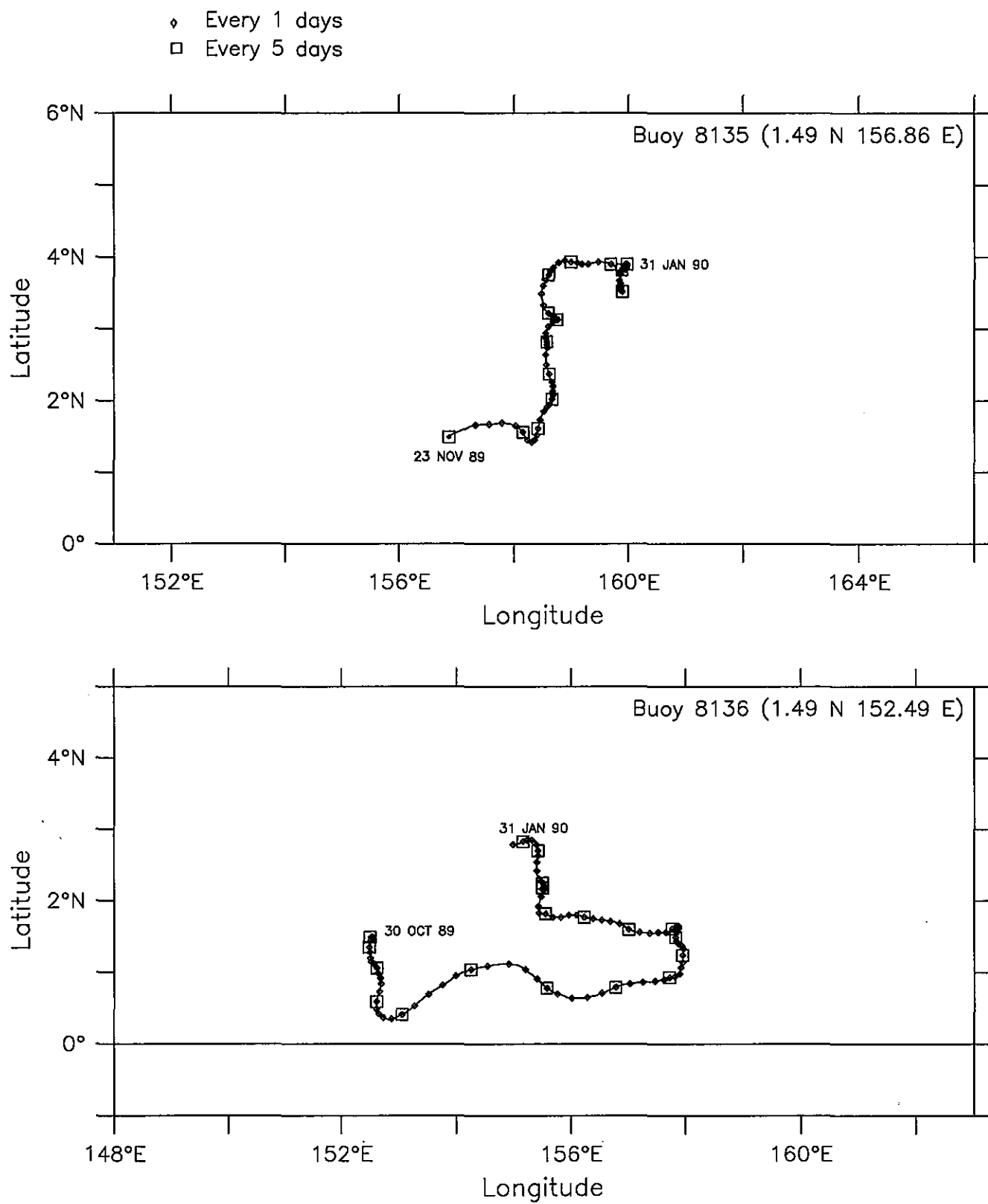


Figure 11.

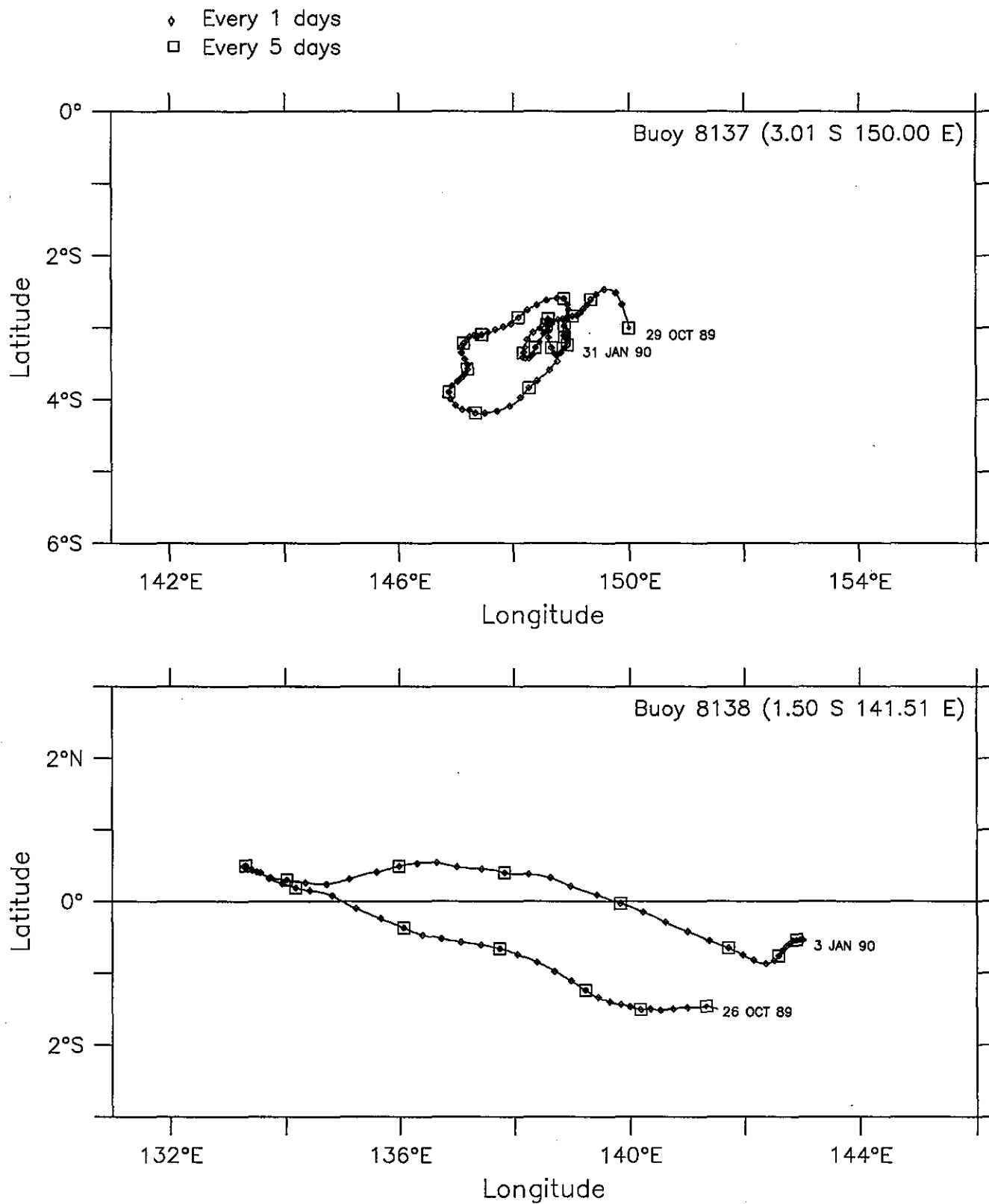


Figure 12.

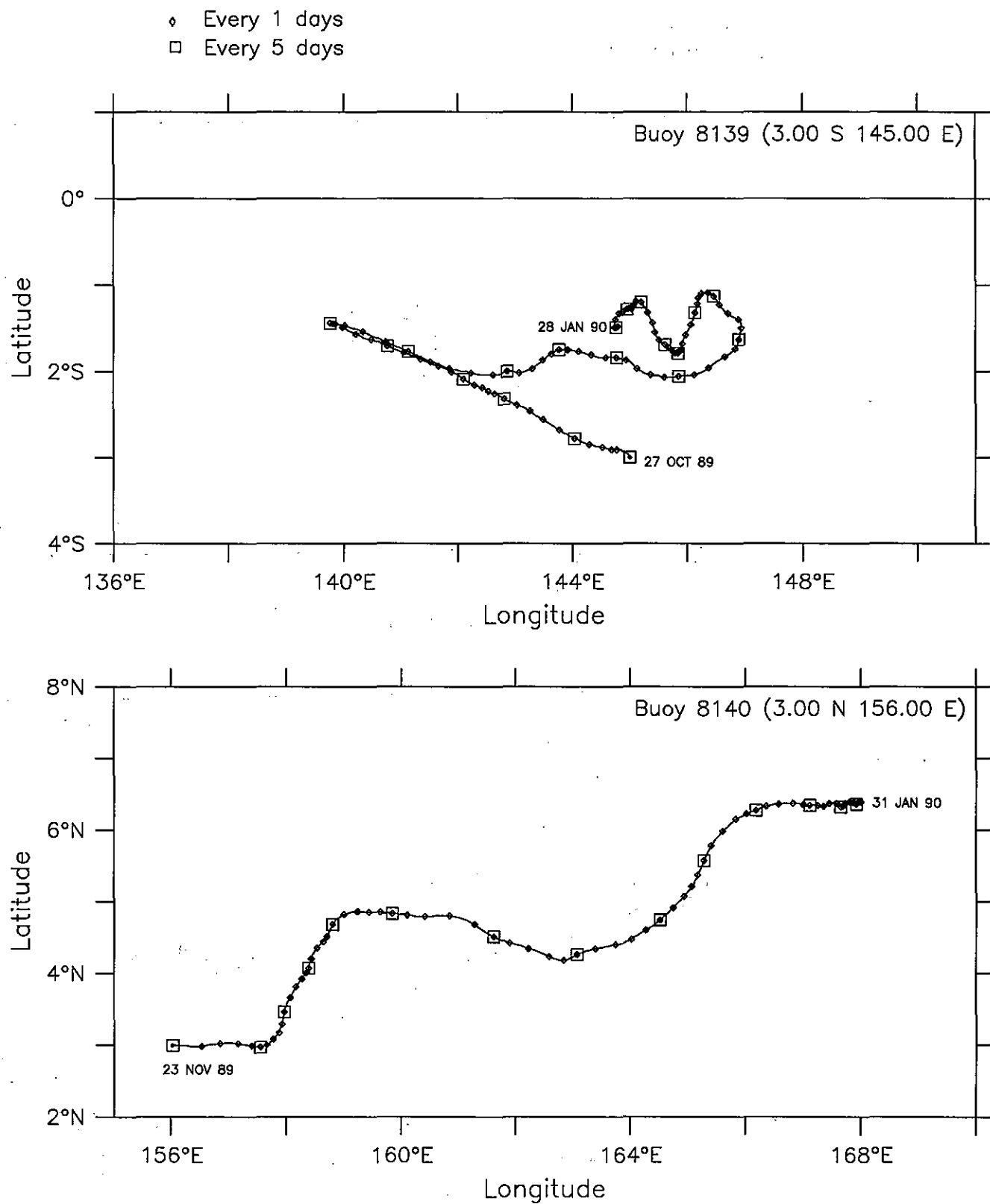


Figure 13.

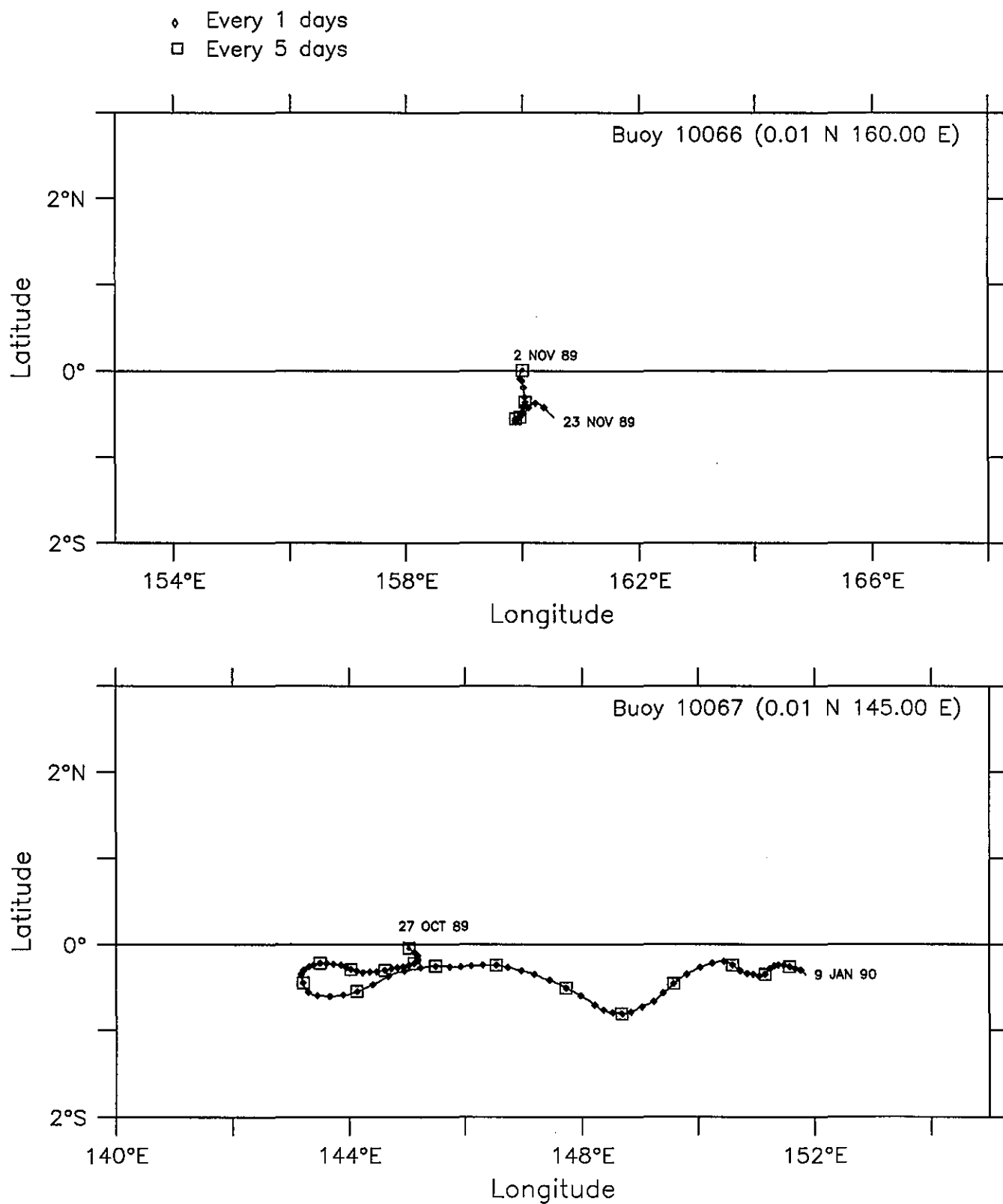


Figure 14.



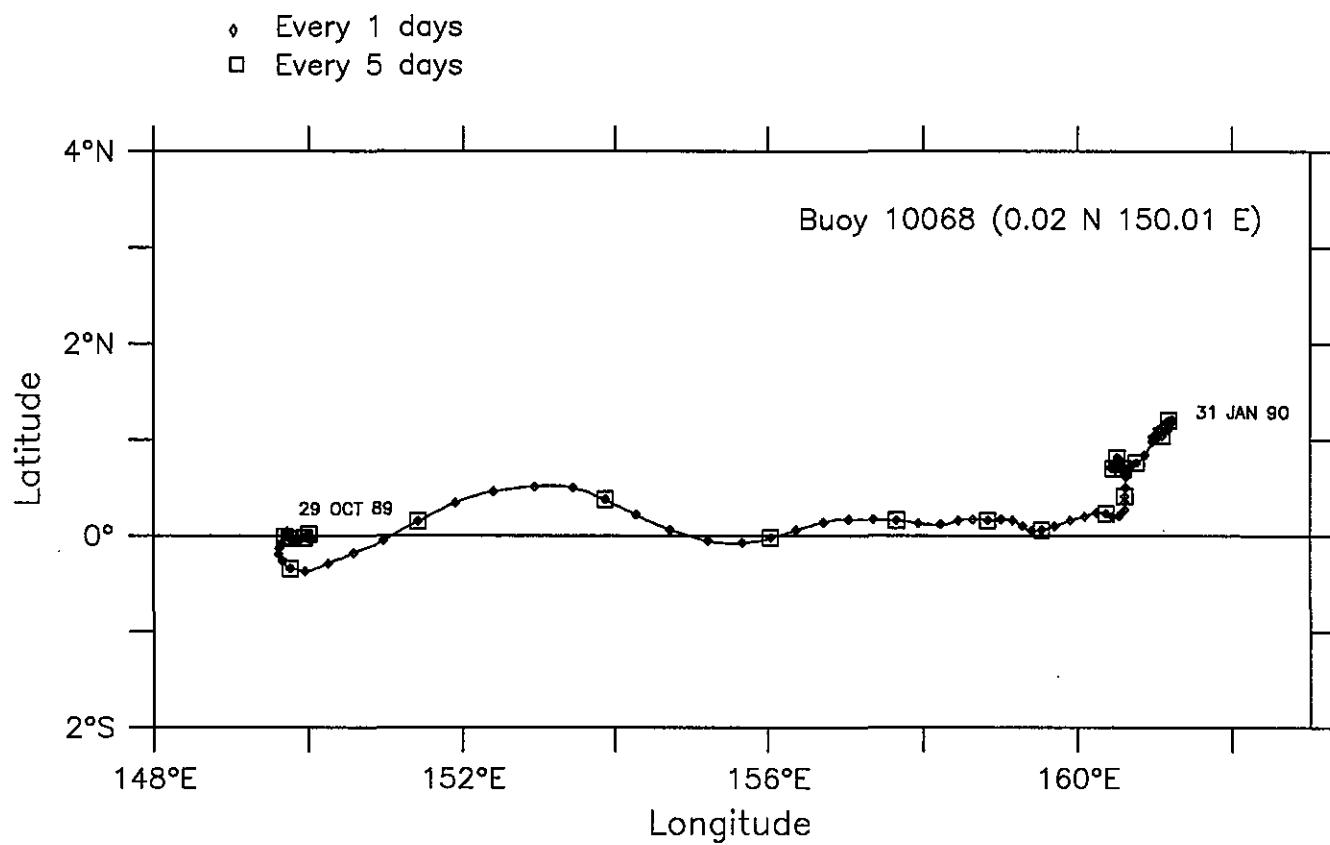


Figure 15.



Figures 16–34. Zonal velocity, meridional velocity and scalar speed for individual drifters.

BUOY 08120 (1.50 S 152.51 E)

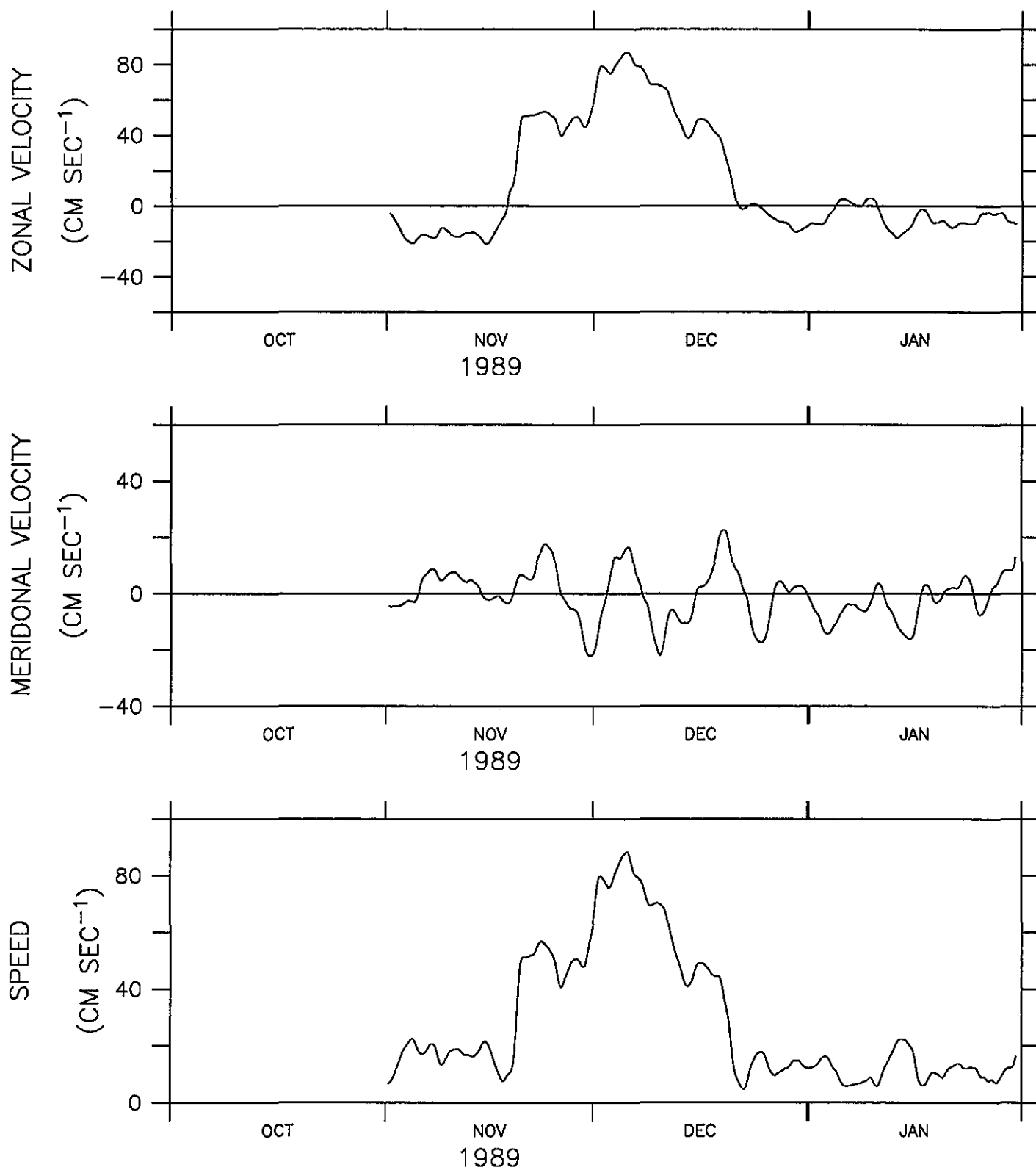


Figure 16.

BUOY 08121 (3.00 N 145.00 E)

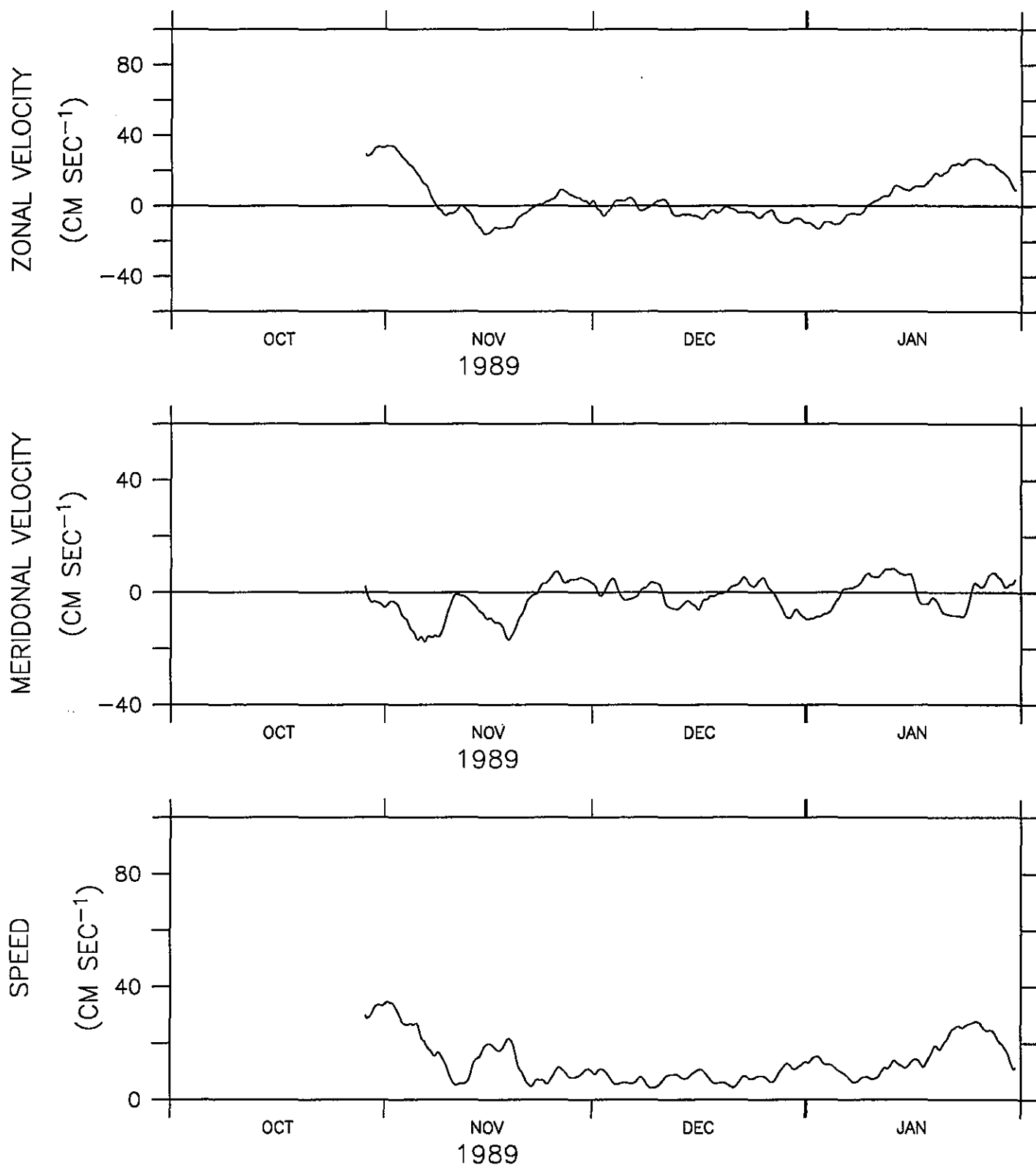


Figure 17.

BUOY 08122 (1.48 N 147.51 E)

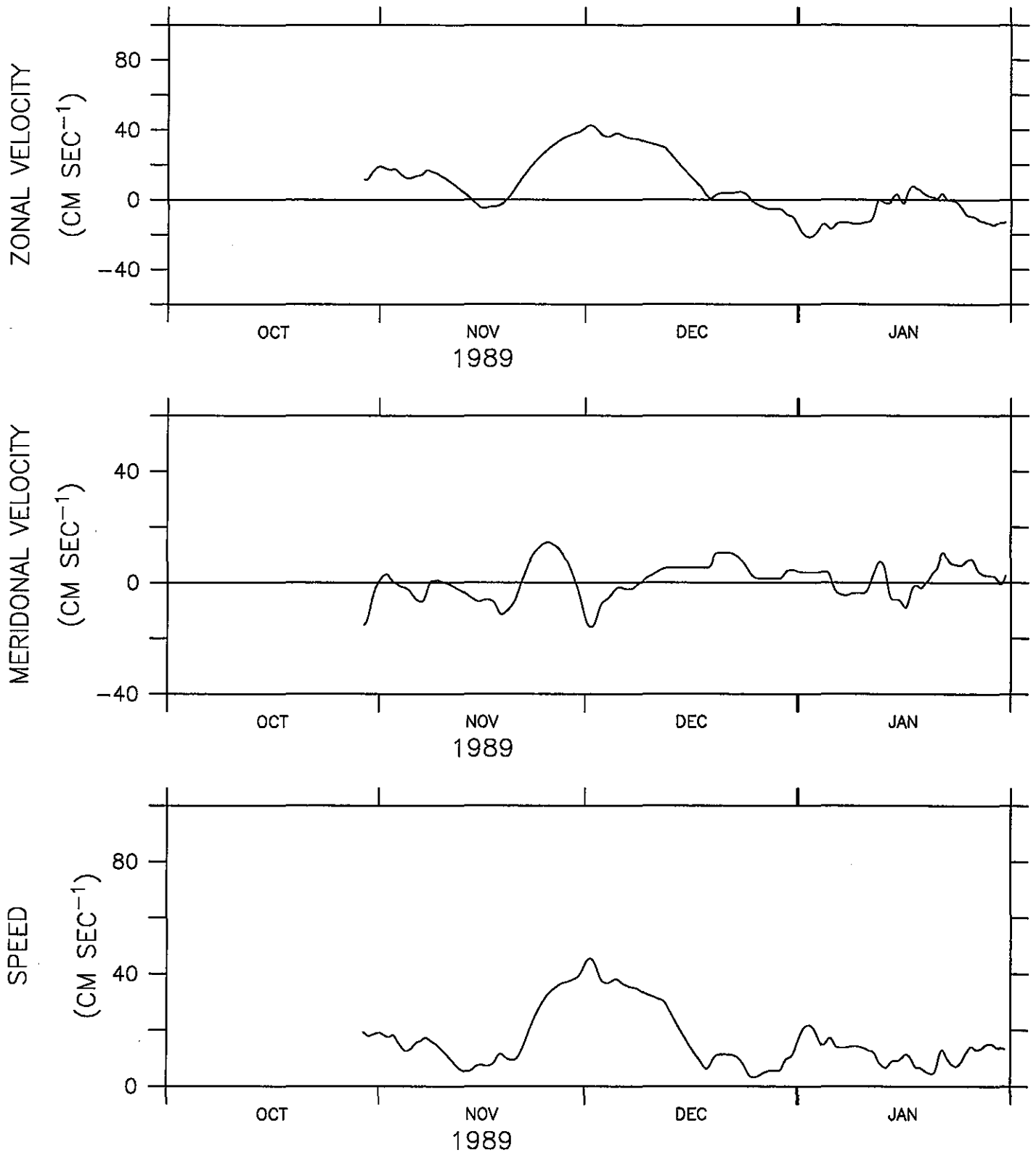


Figure 18.

BUOY 08126 (1.53 S 164.97 E)

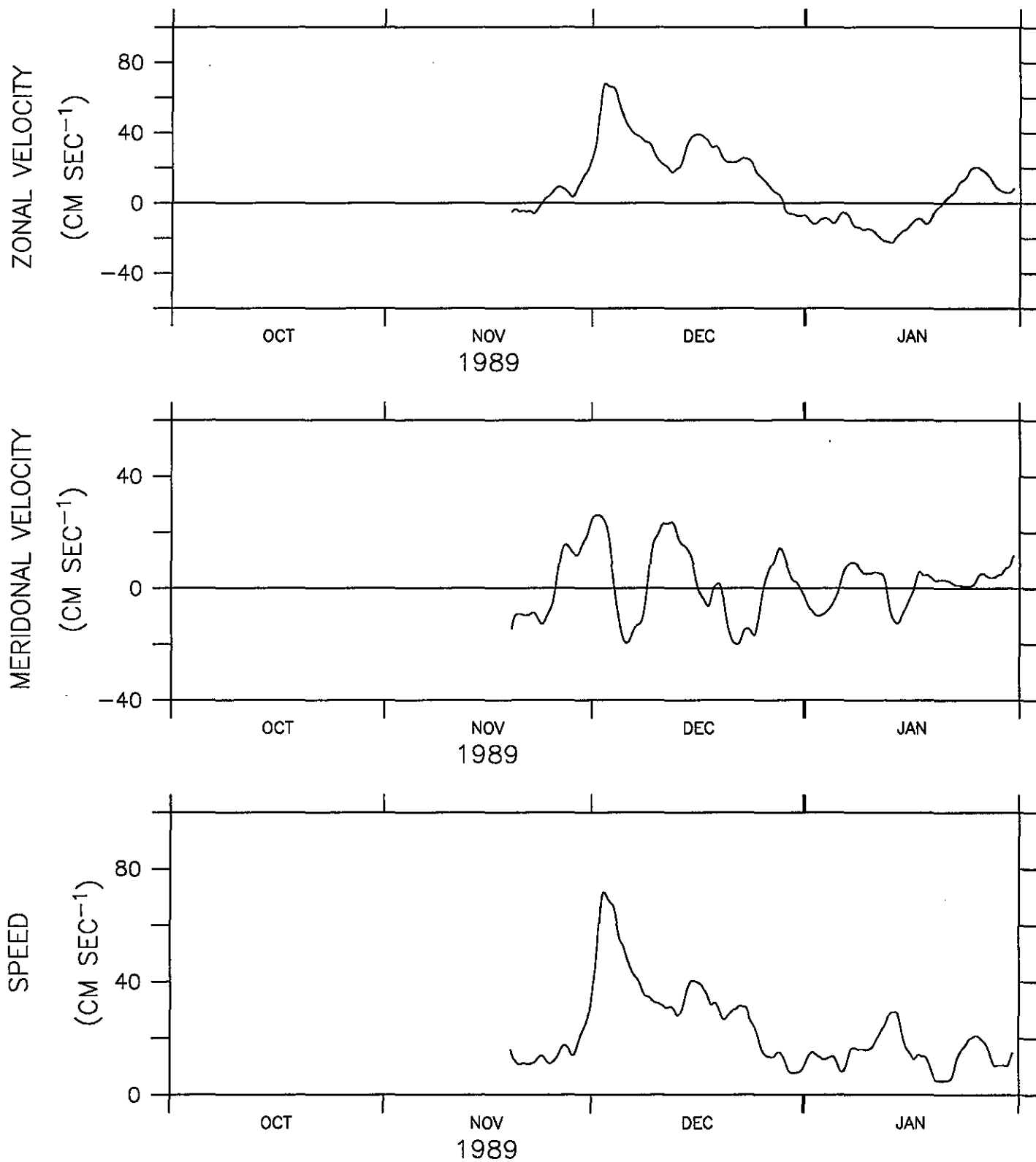


Figure 19.

BUOY 08127 (1.49 N 141.52 E)

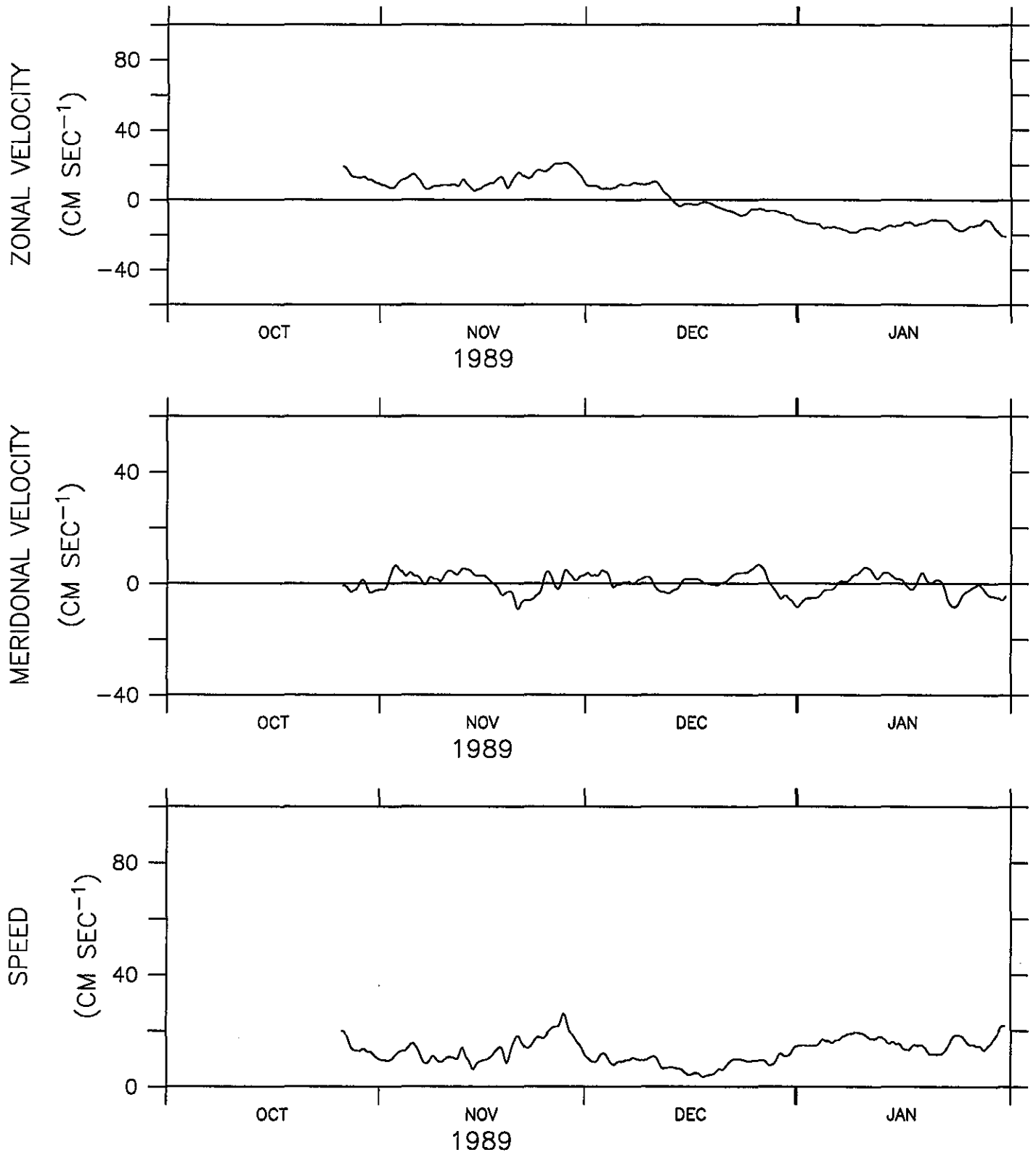


Figure 20.



BUOY 08129 (1.50 S 147.50 E)

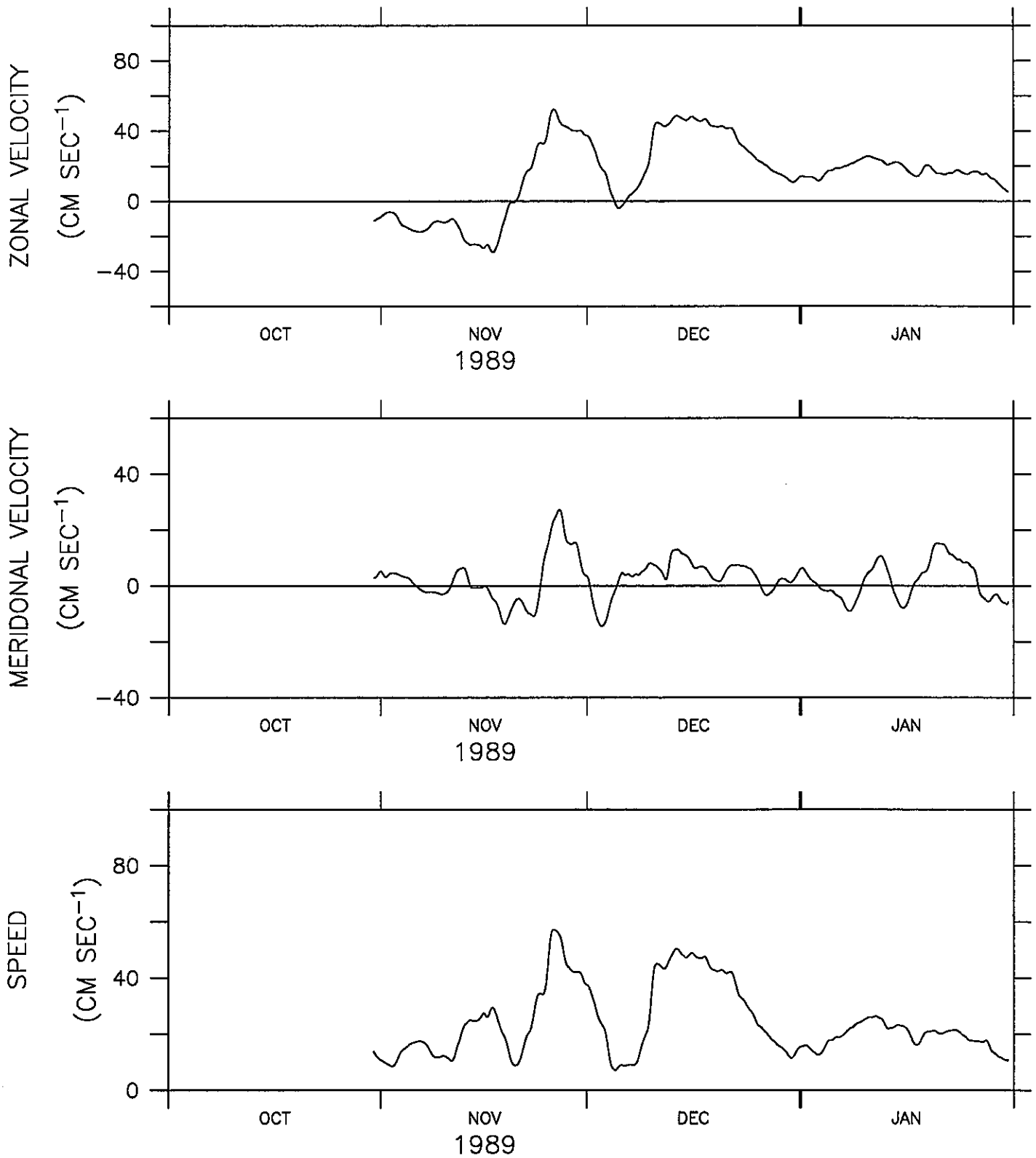


Figure 21.

BUOY 08131 (0.00 N 155.00 E)

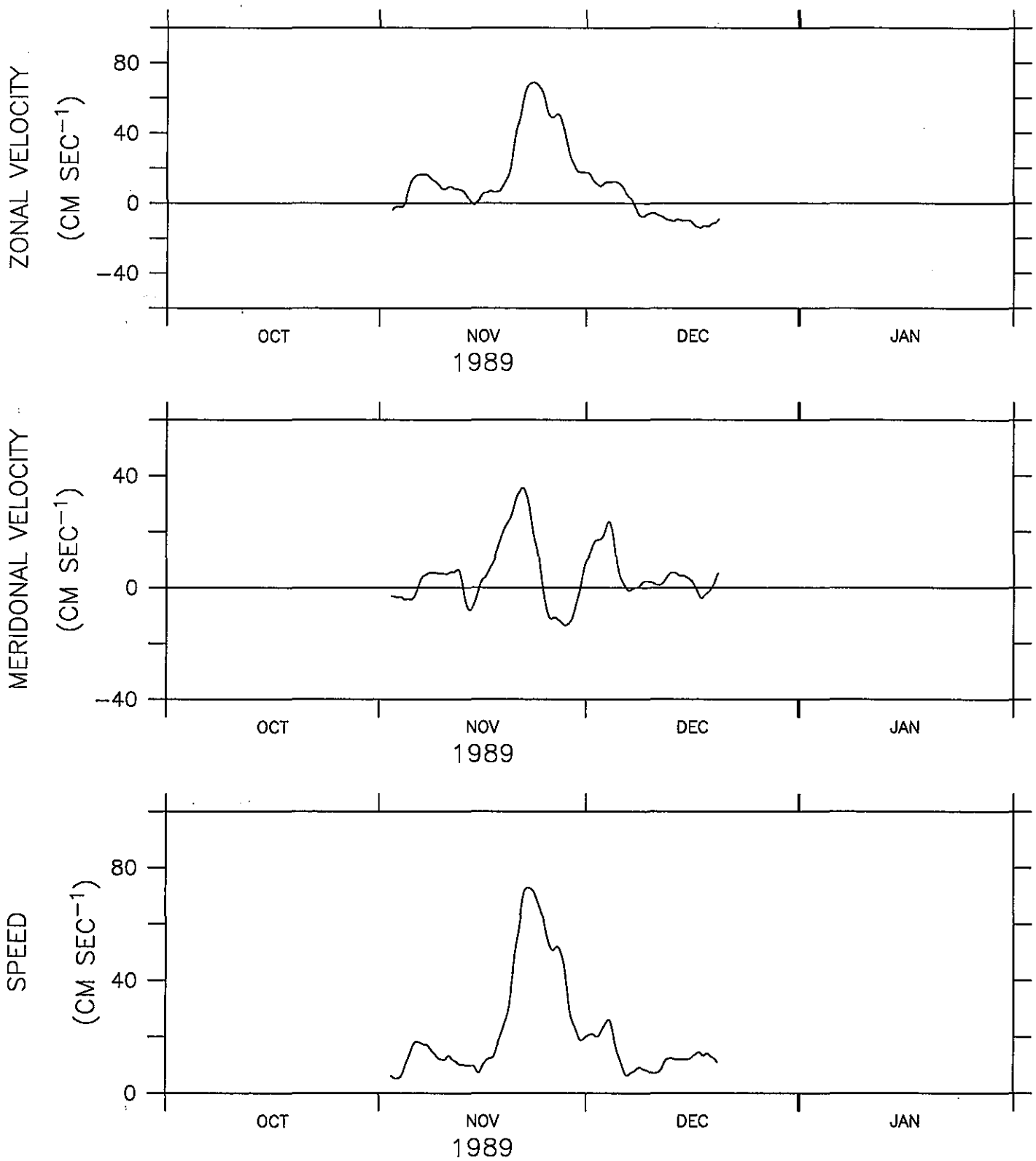


Figure 22.

BUOY 08132 (2.97 S 159.42 E)

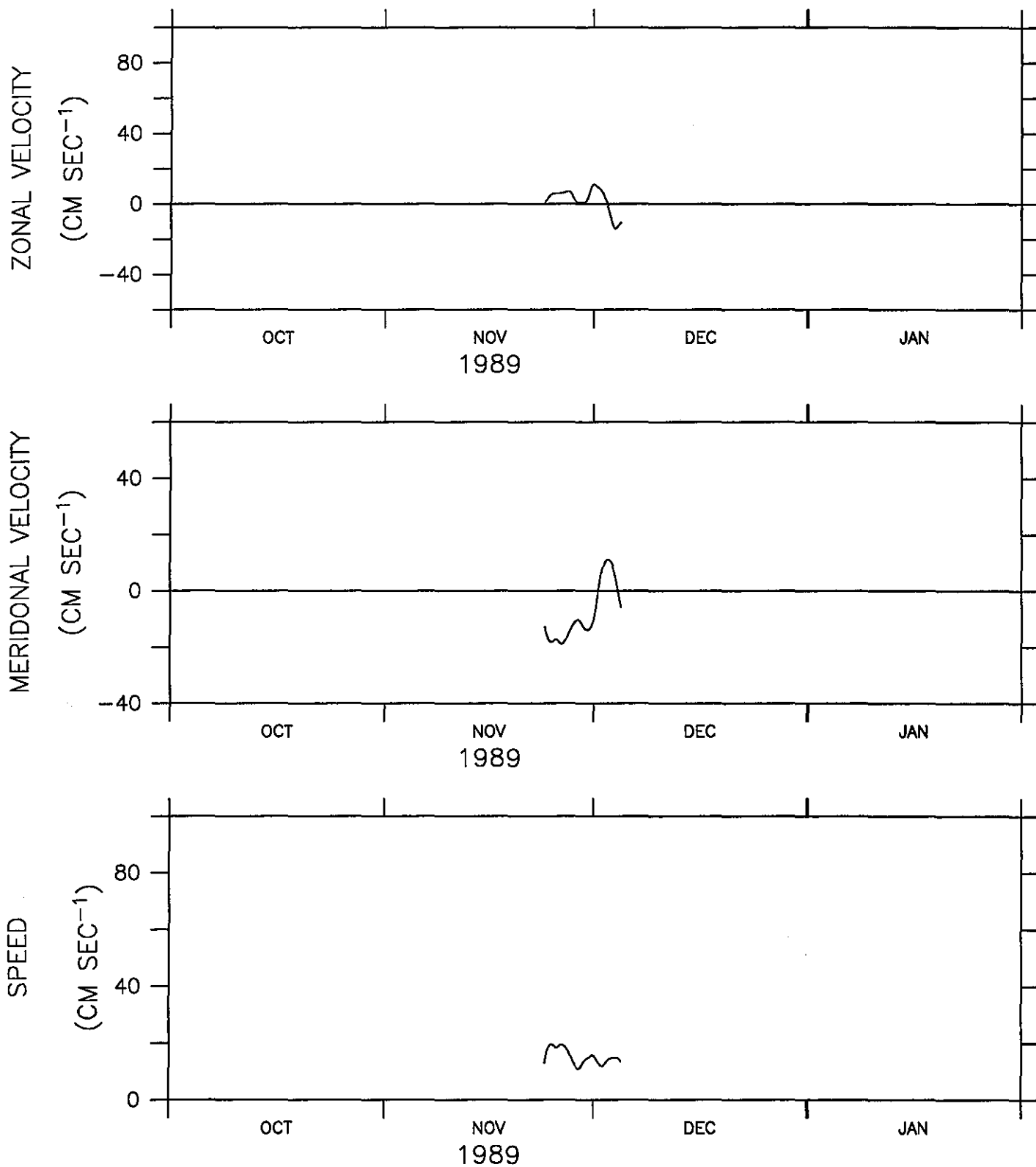


Figure 23.

BUOY 08133 (3.00 S 155.00 E)

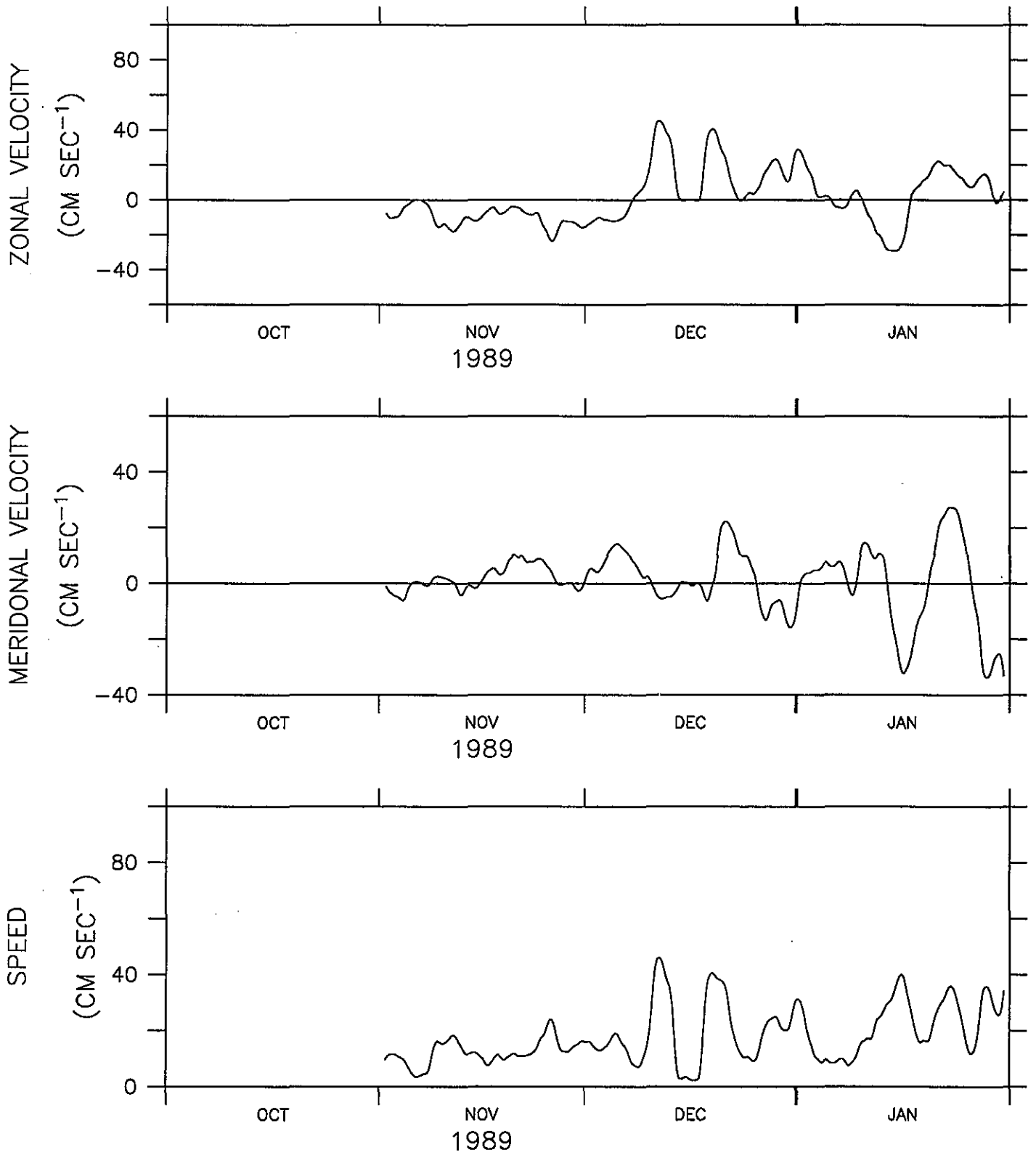


Figure 24.

BUOY 08134 (2.97 N 150.00 E)

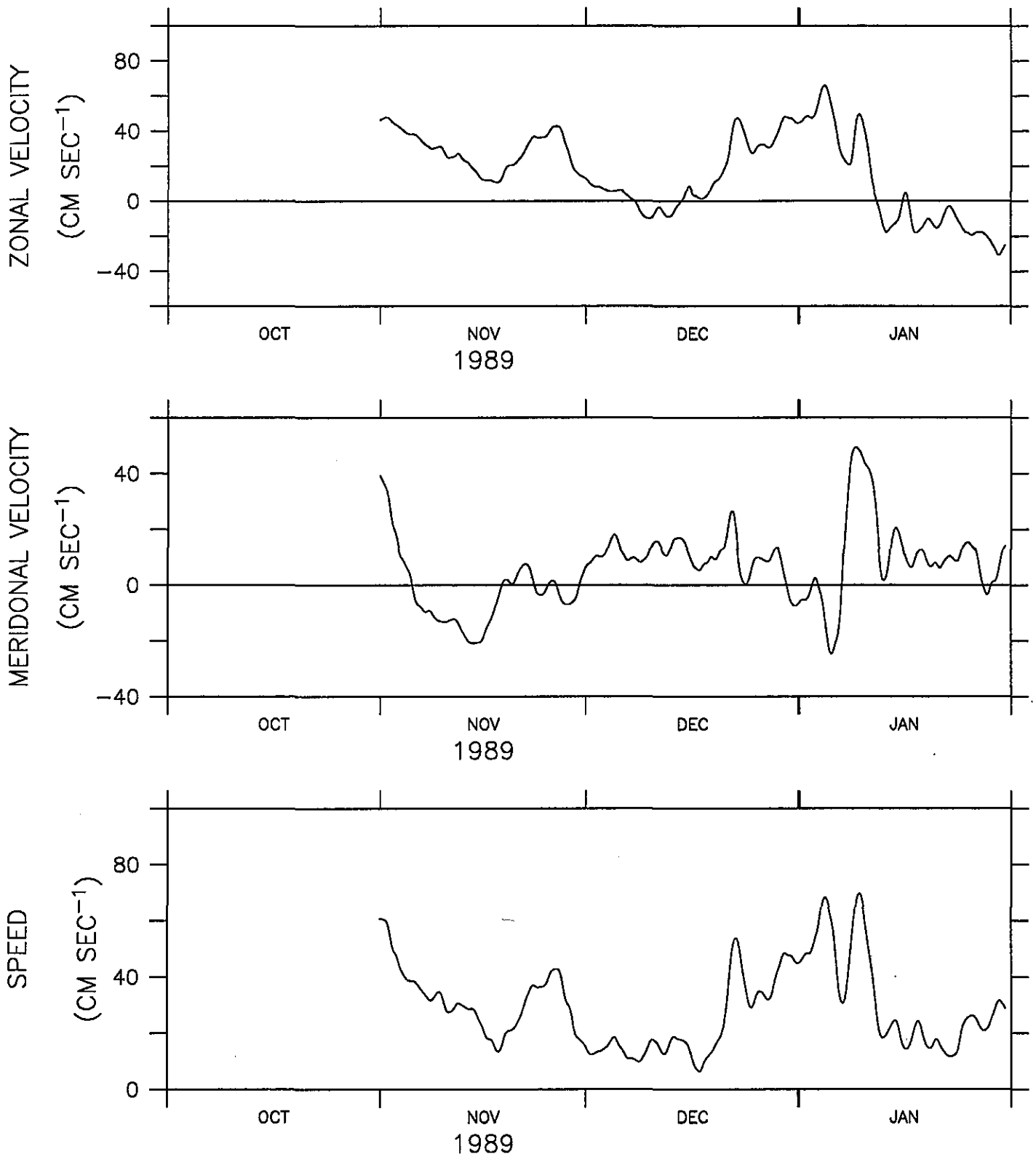


Figure 25.

BUOY 08135 (1.49 N 156.86 E)

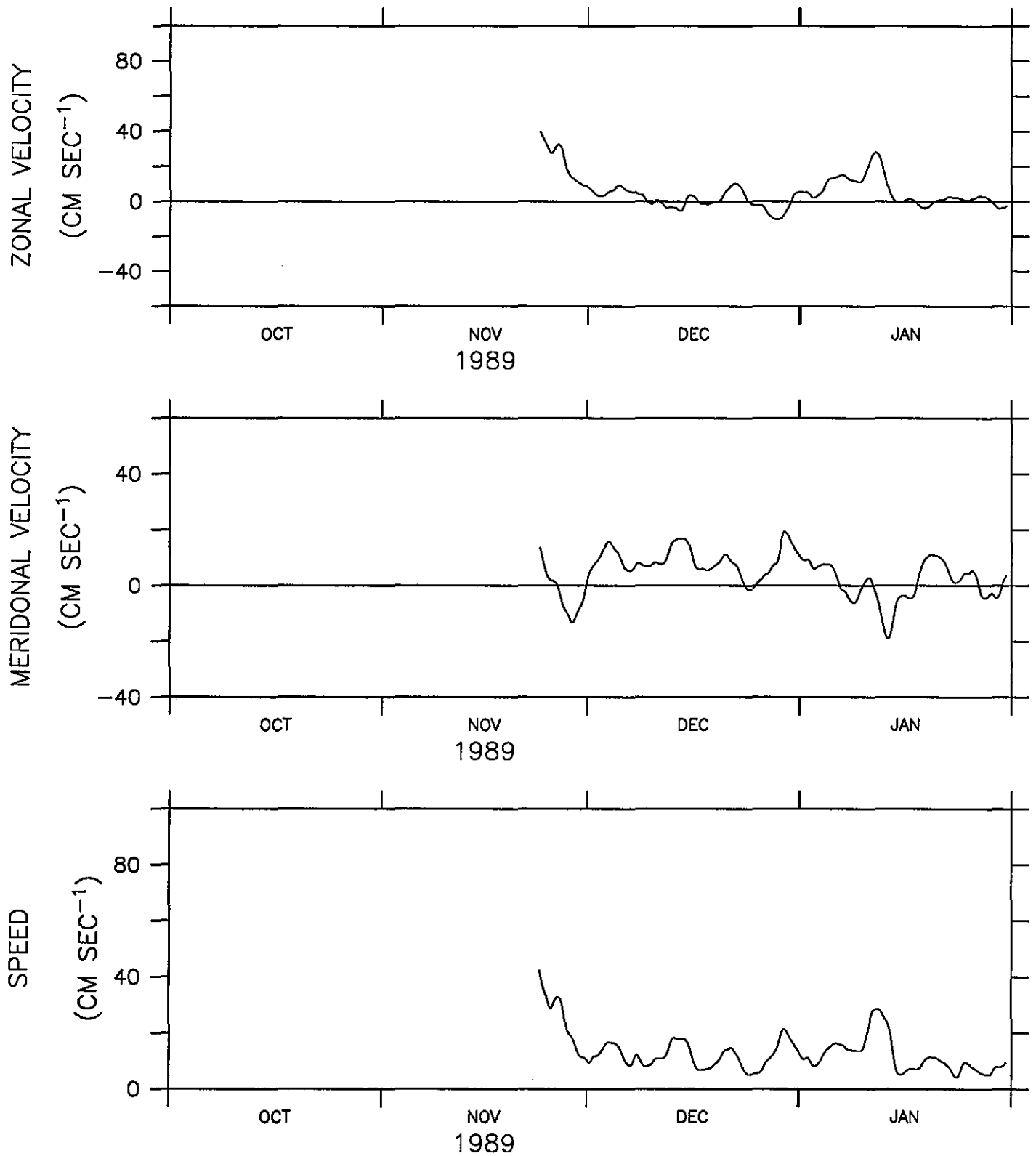


Figure 26.

BUOY 08136 (1.49 N 152.49 E)

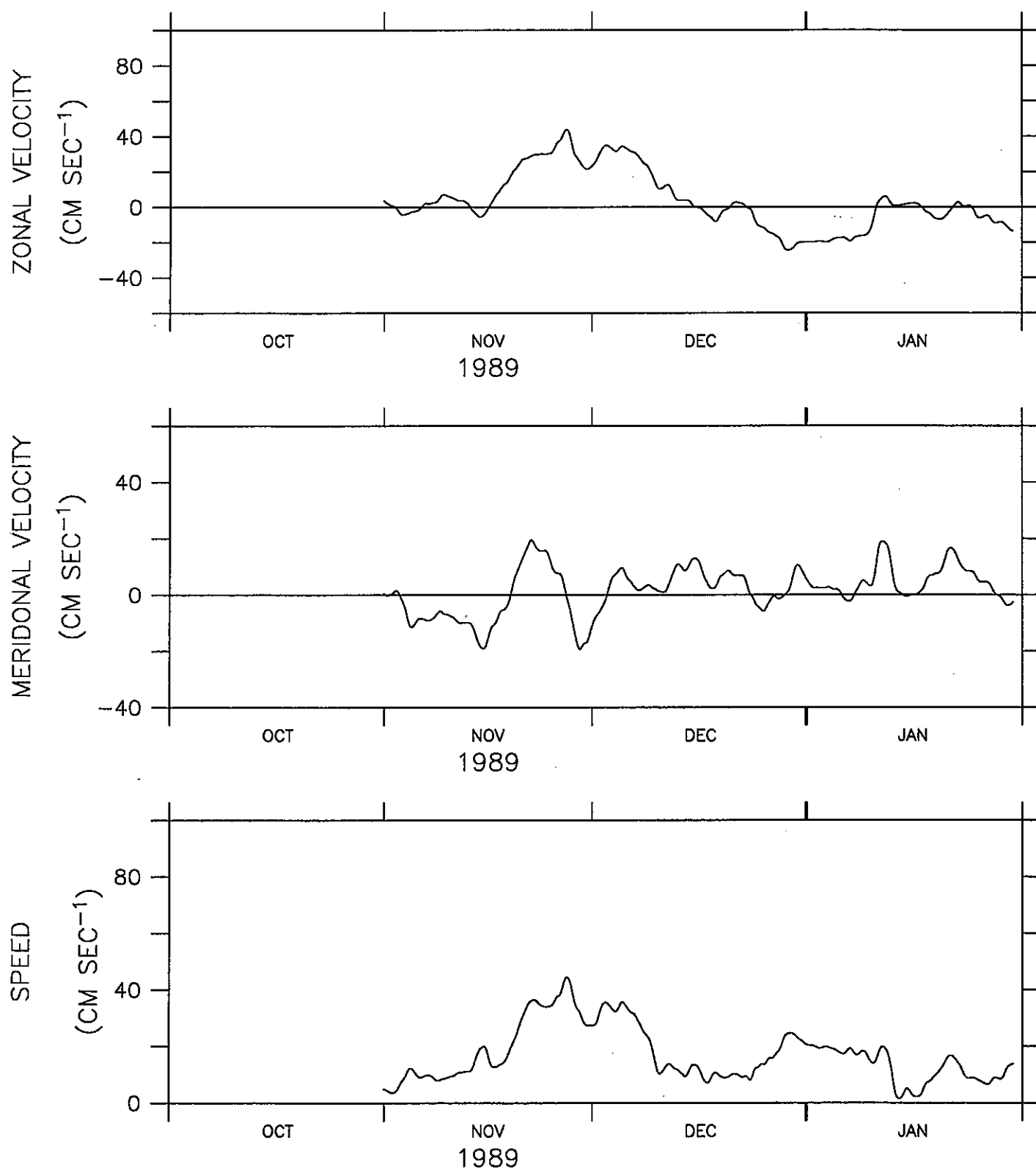


Figure 27.

BUOY 08139 (3.00 S 145.00 E)

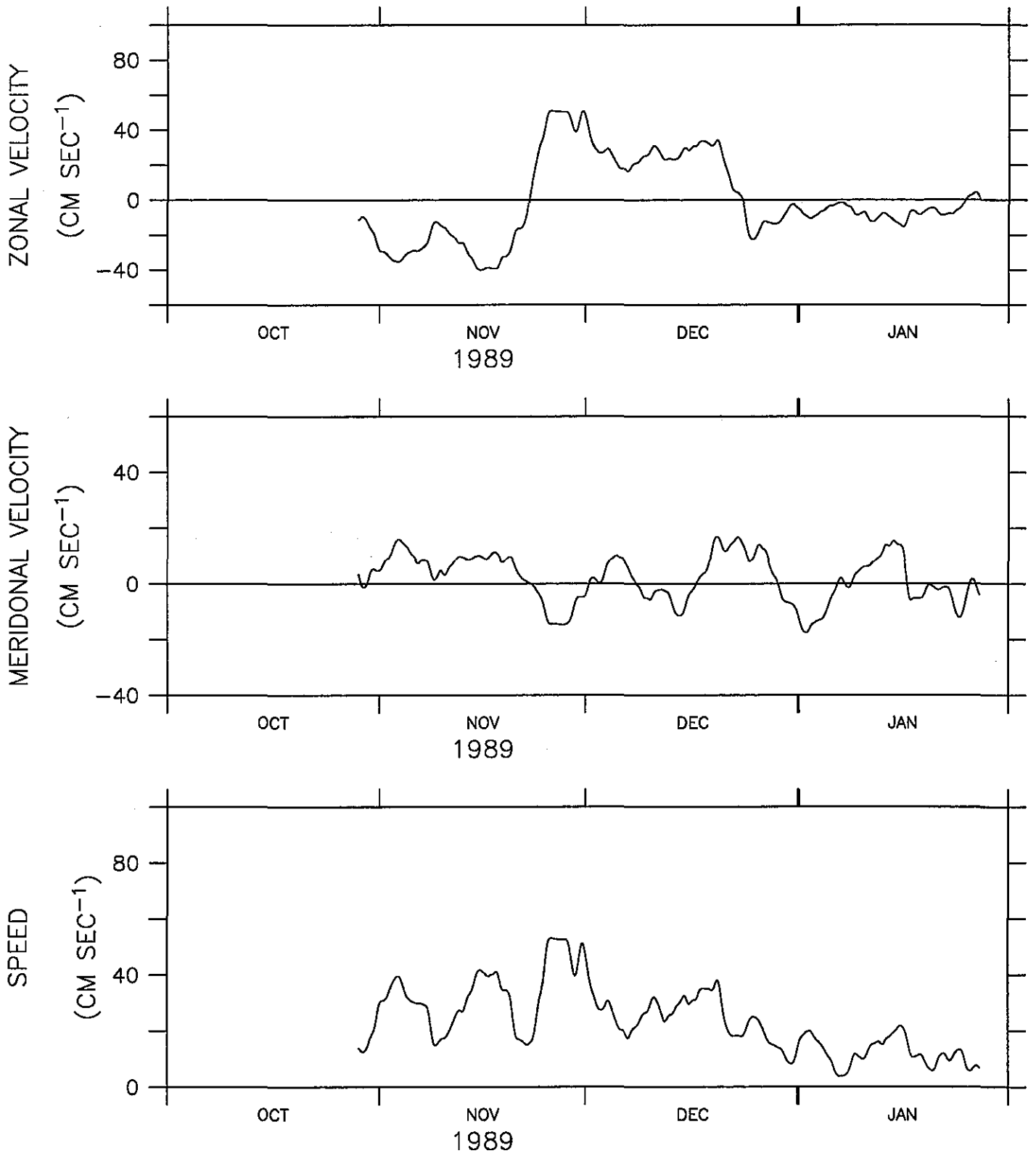


Figure 30.



BUOY 08140 (3.00 N 156.00 E)

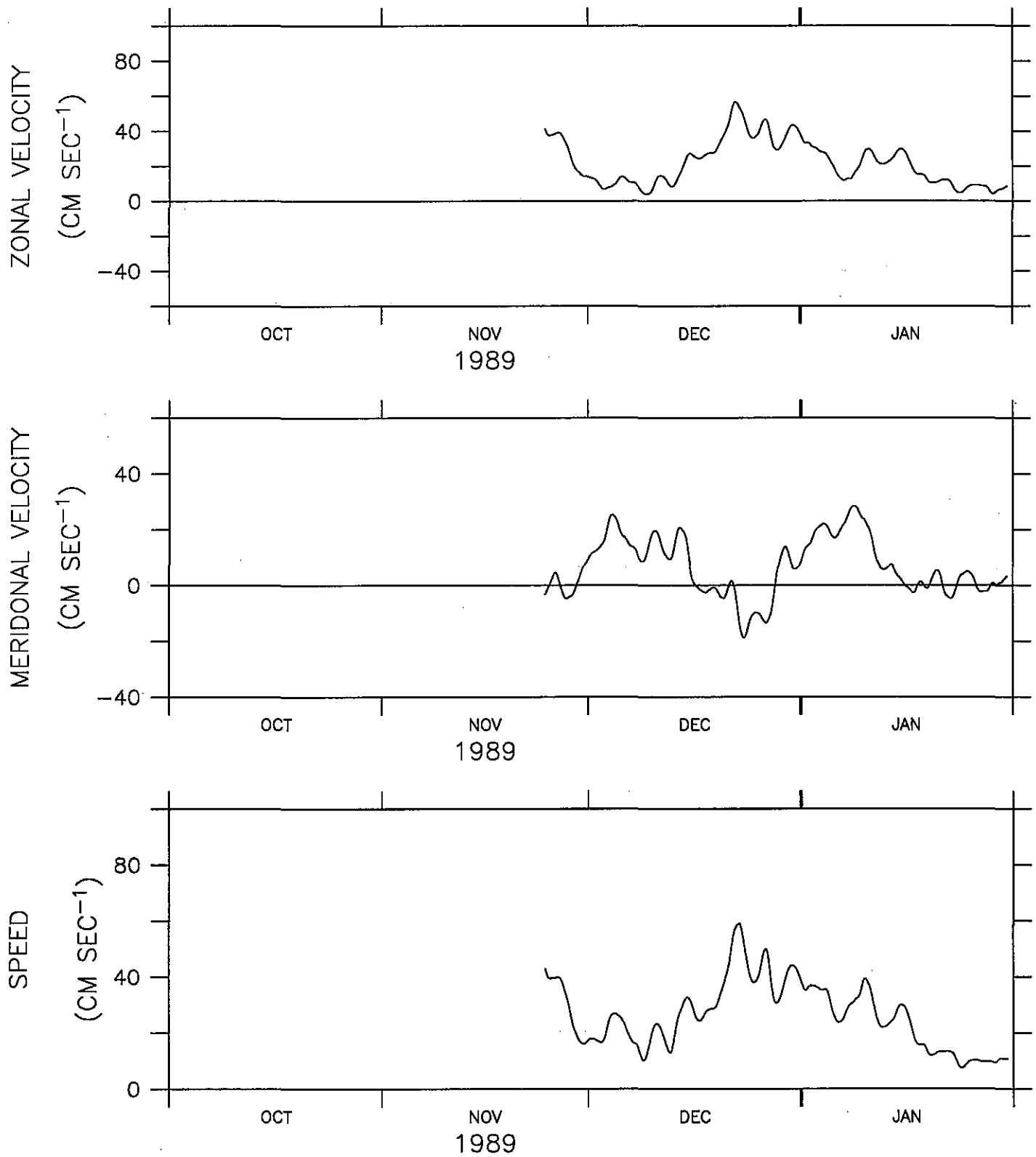


Figure 31.

BUOY 10066 (0.01 N 160.00 E)

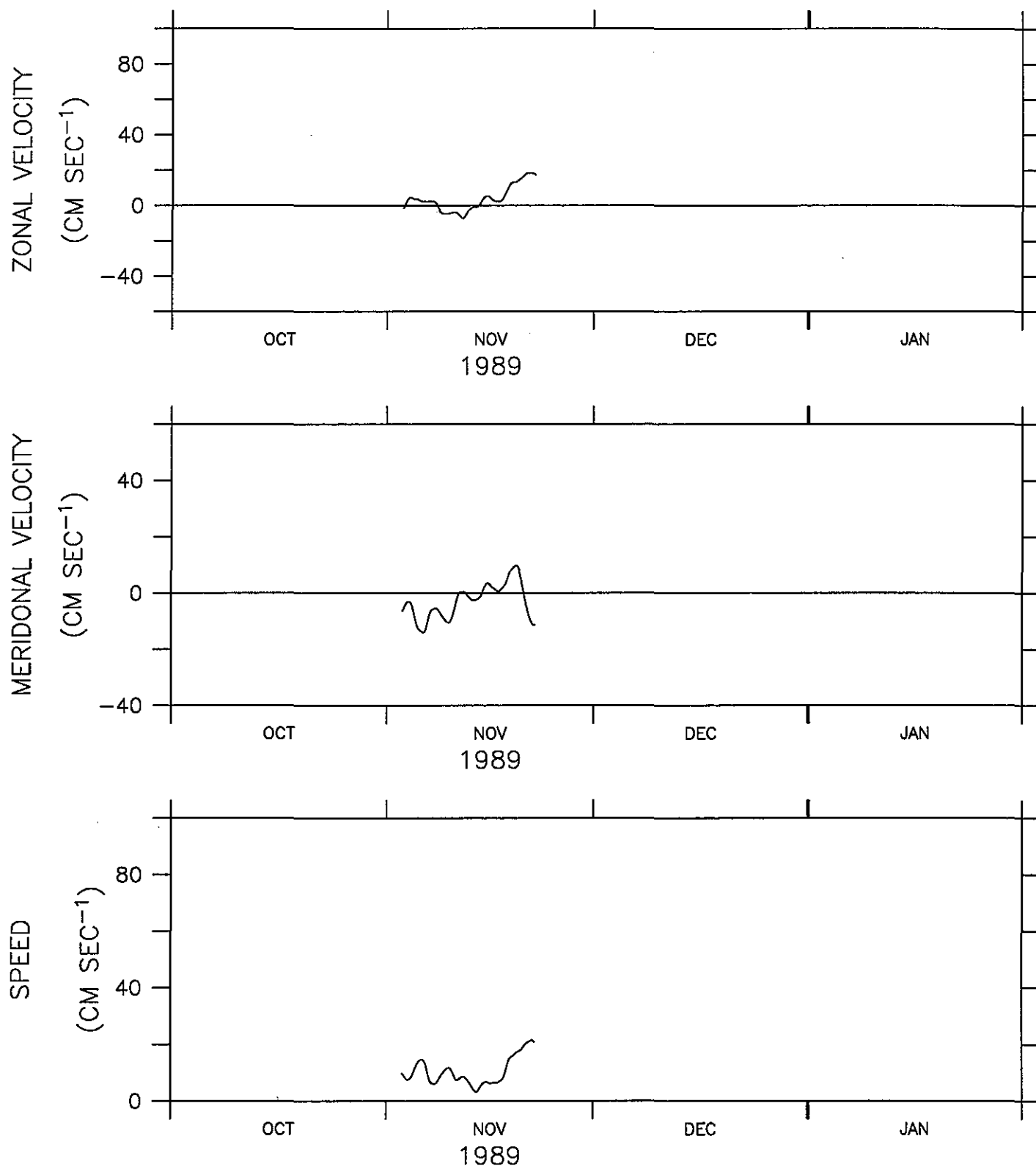


Figure 32.

BUOY 10067 (0.01 N 145.00 E)

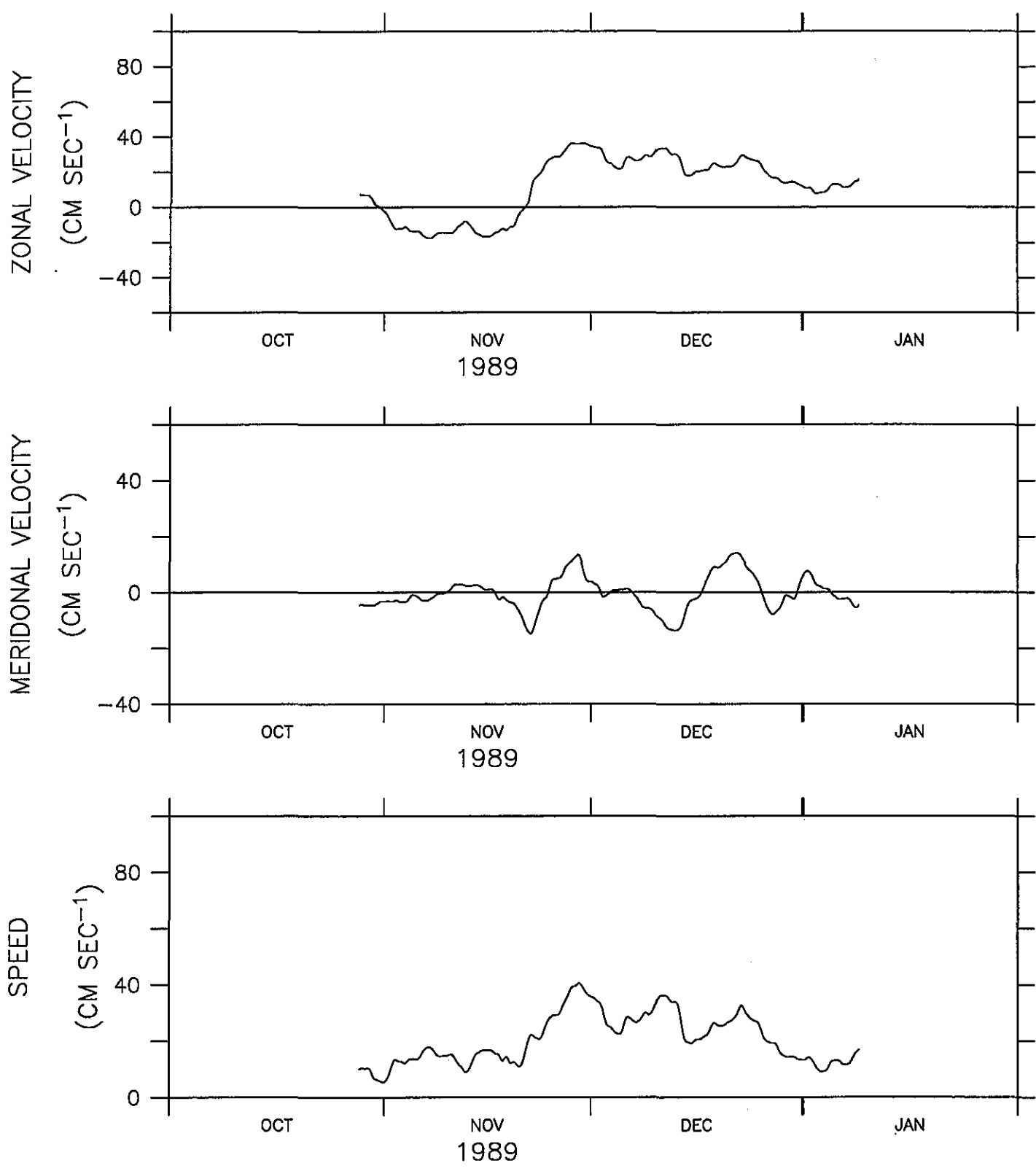


Figure 33.

BUOY 10068 (0.02 N 150.01 E)

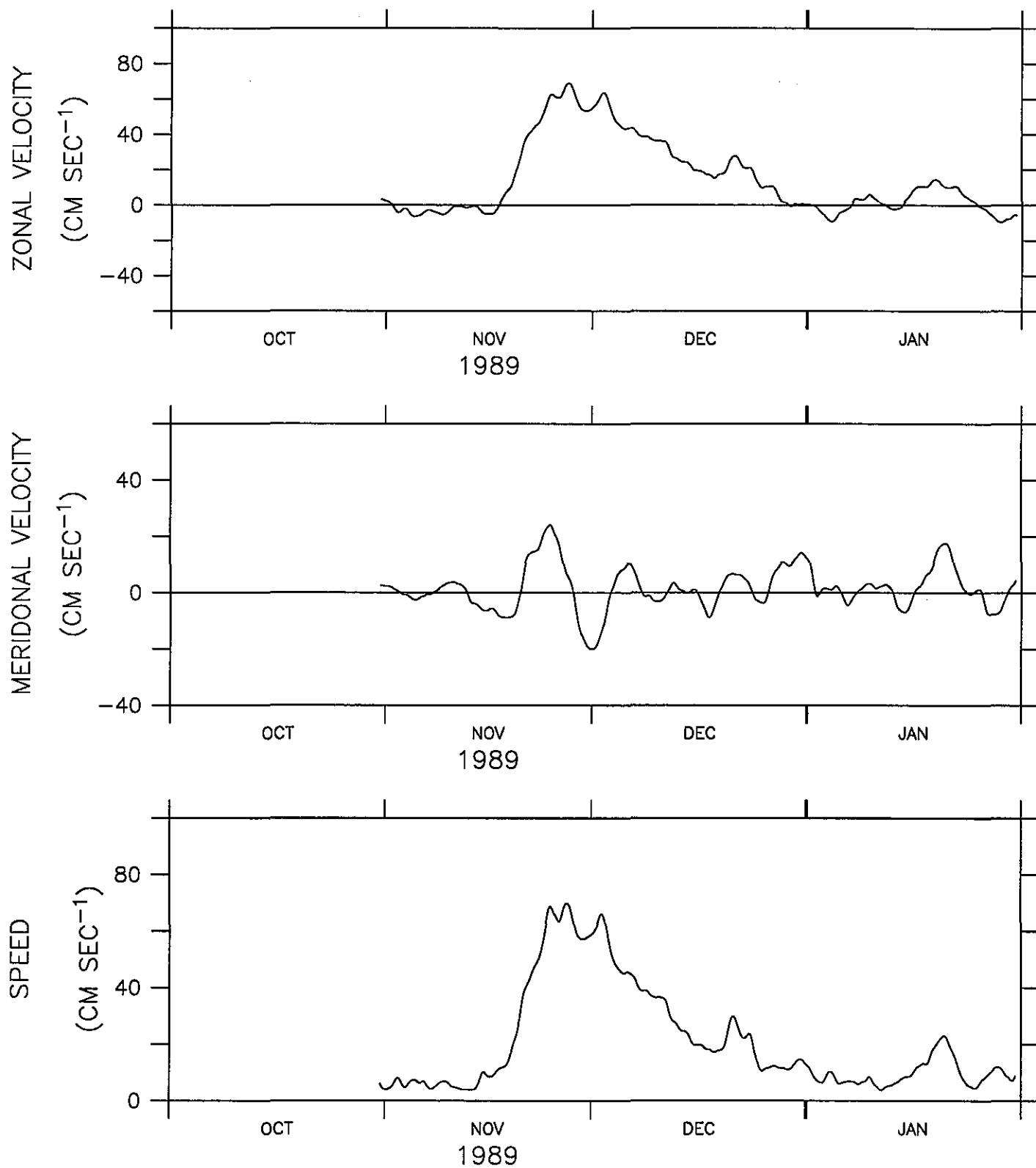


Figure 34.

Figures 35–53. Time series of 3-hourly pressure data at nominal sensor depths for the PRL drifters.

BUOY 08120 (1.50 S, 152.51 E)

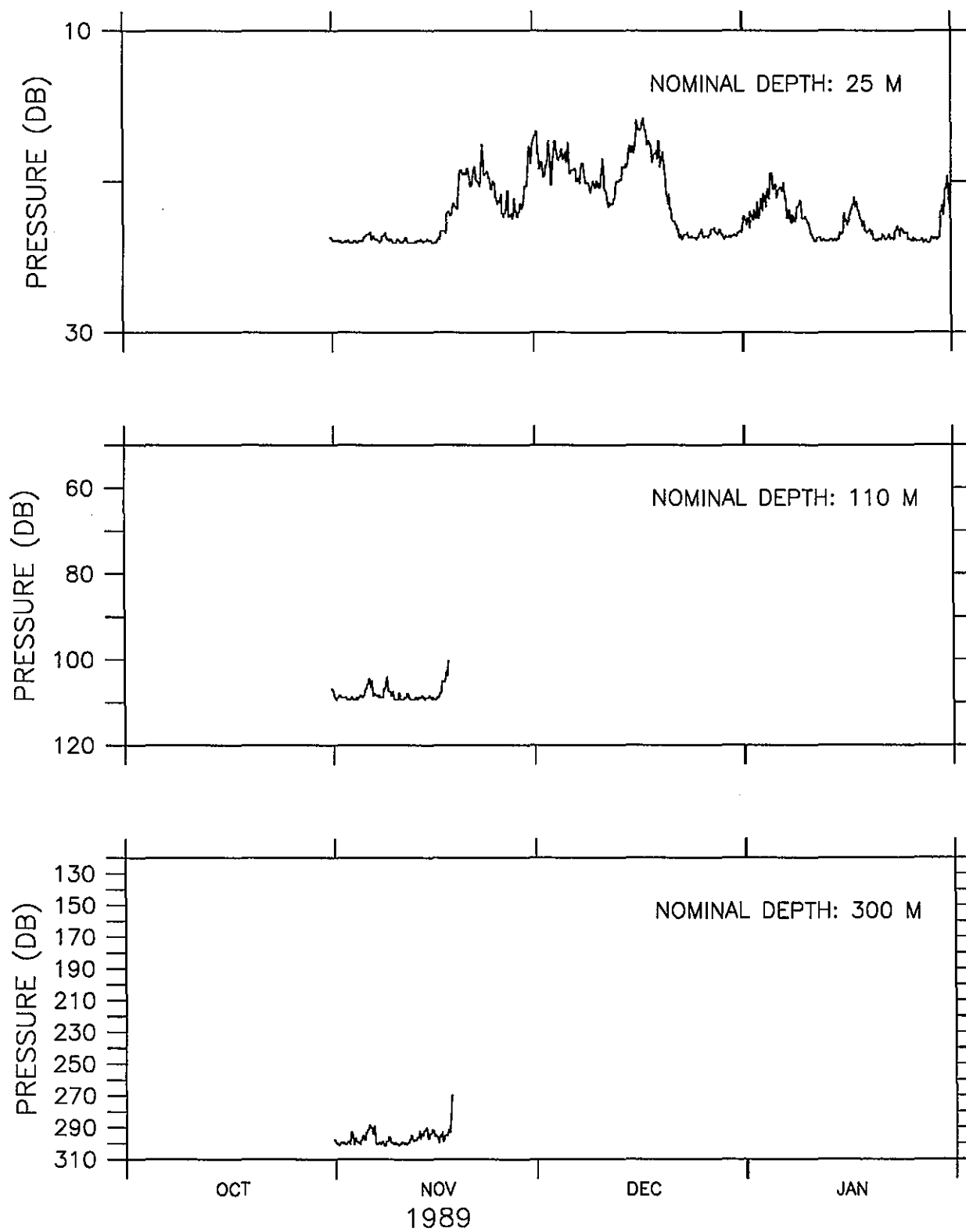


Figure 35.

BUOY 08121 (3.00 N, 145.00 E)

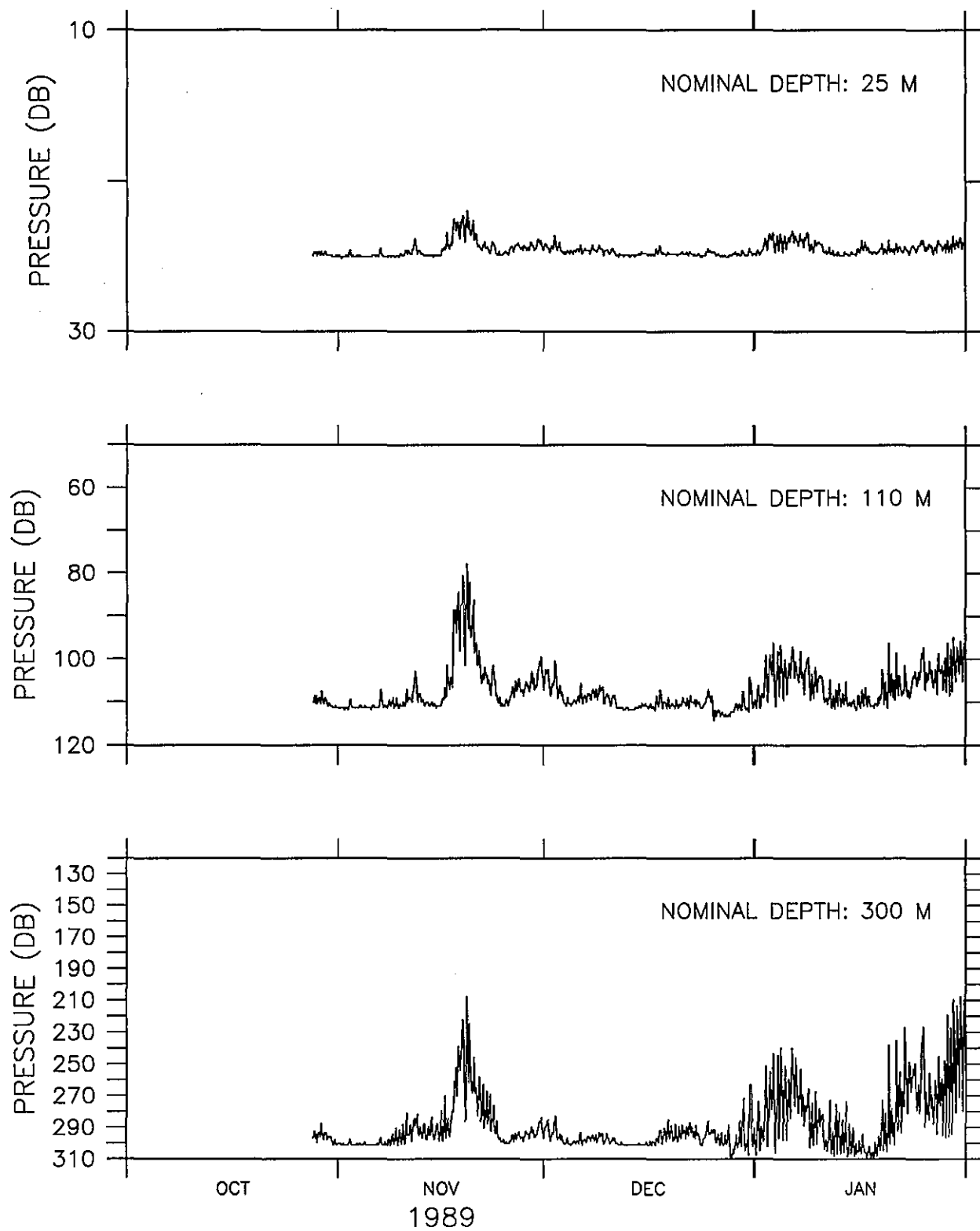


Figure 36.

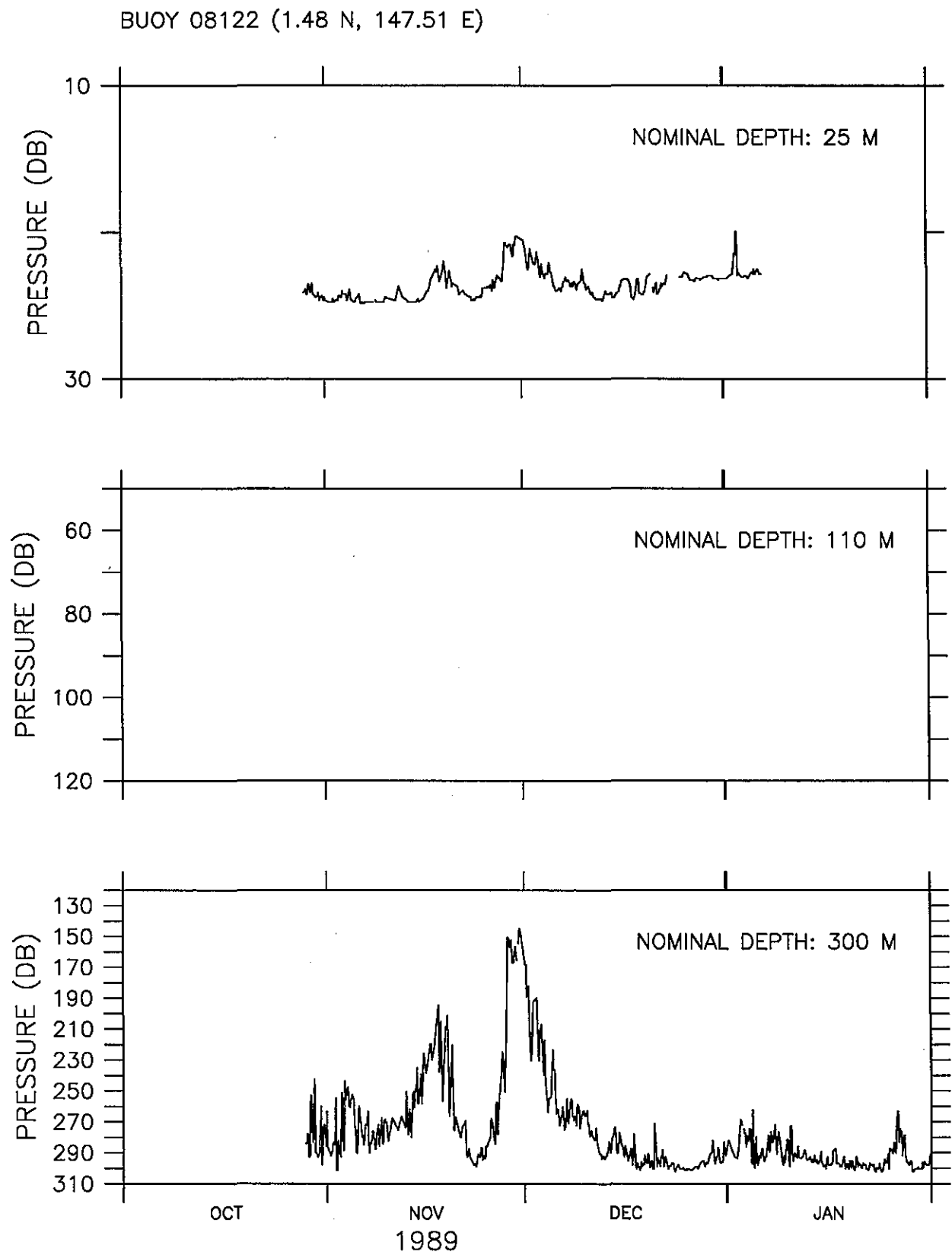


Figure 37.



BUOY 08126 (1.53 S, 164.97 E)

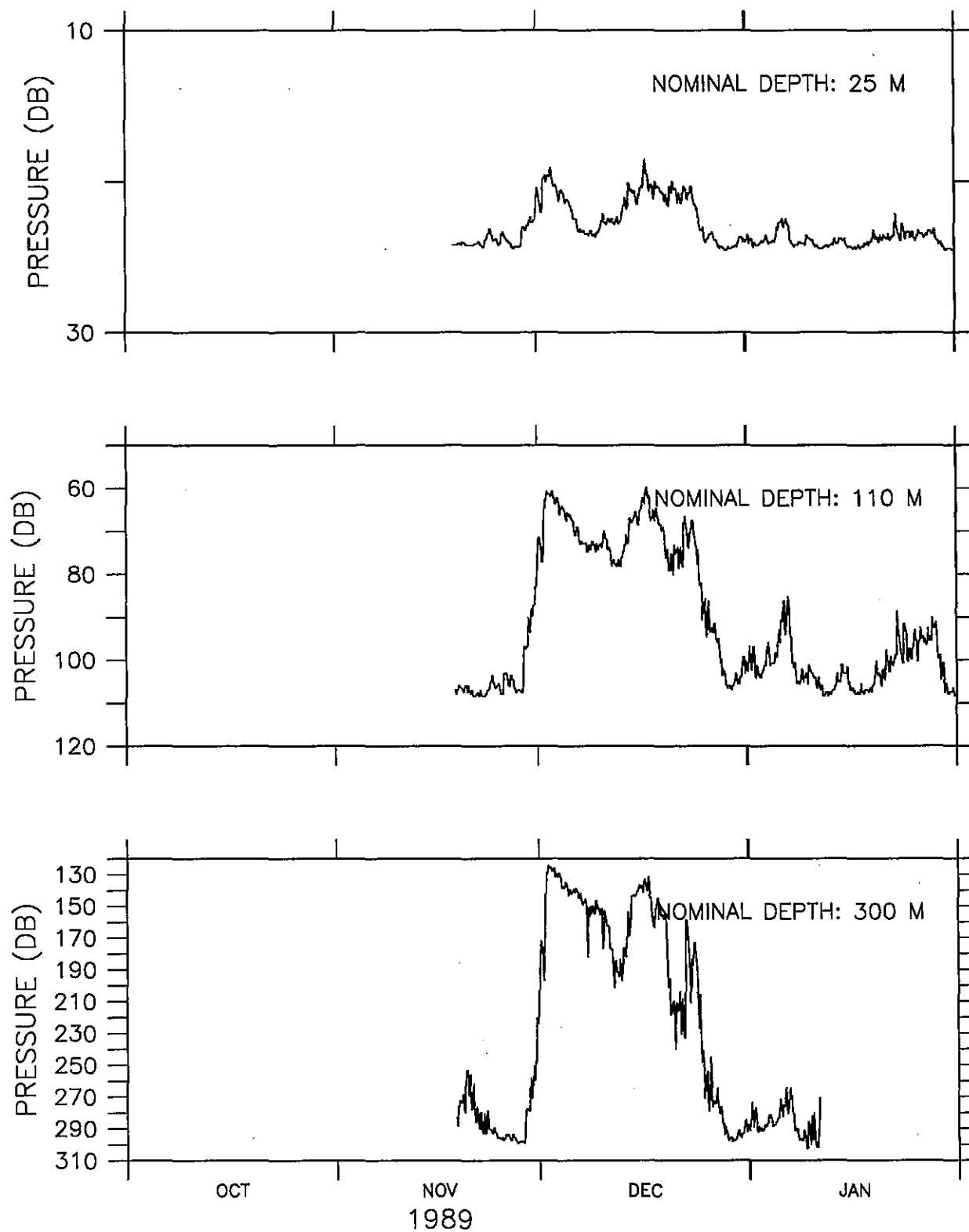


Figure 38.

BUOY 08127 (1.49 N, 141.52 E)

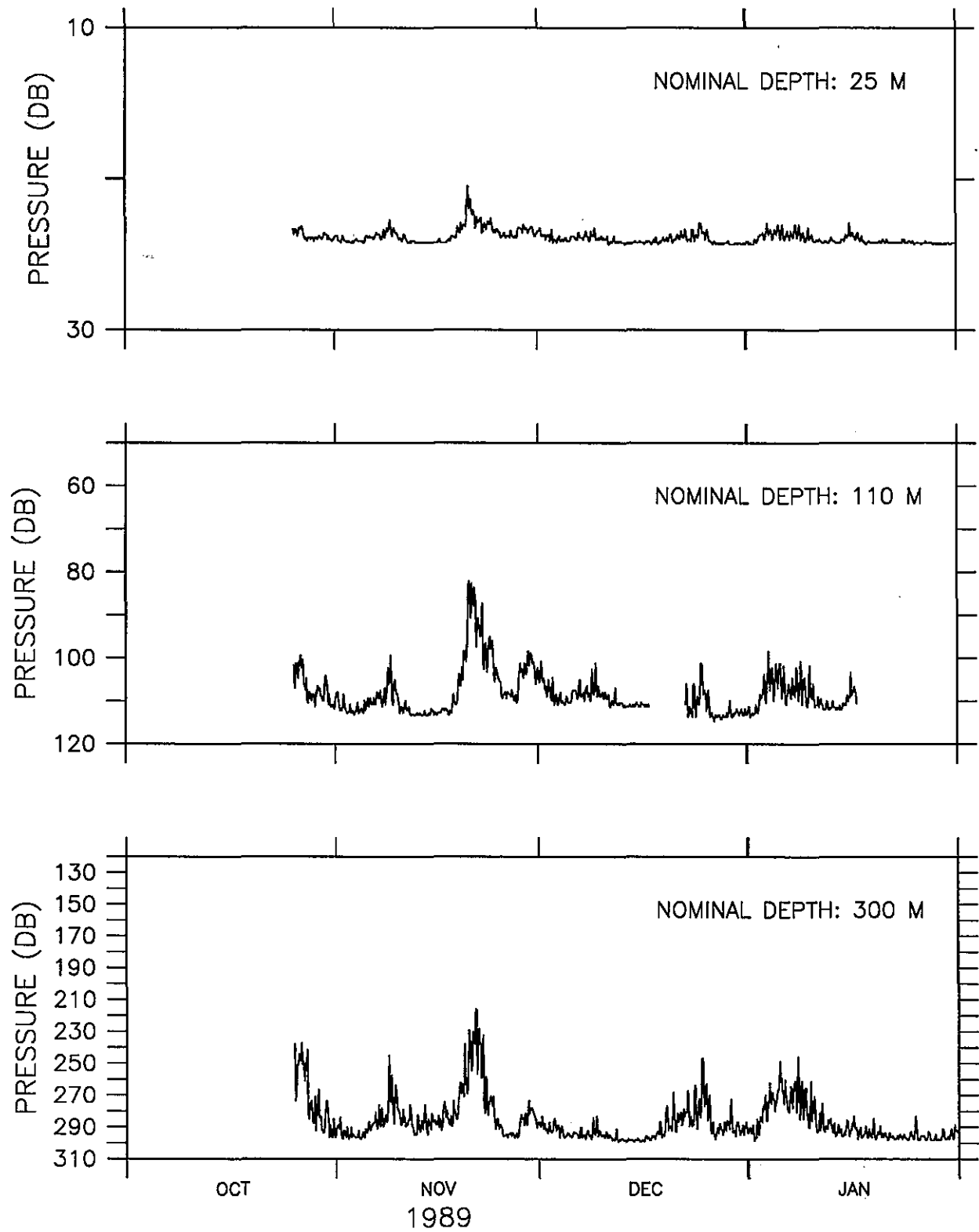


Figure 39.

BUOY 08129 (1.50 S, 147.50 E)

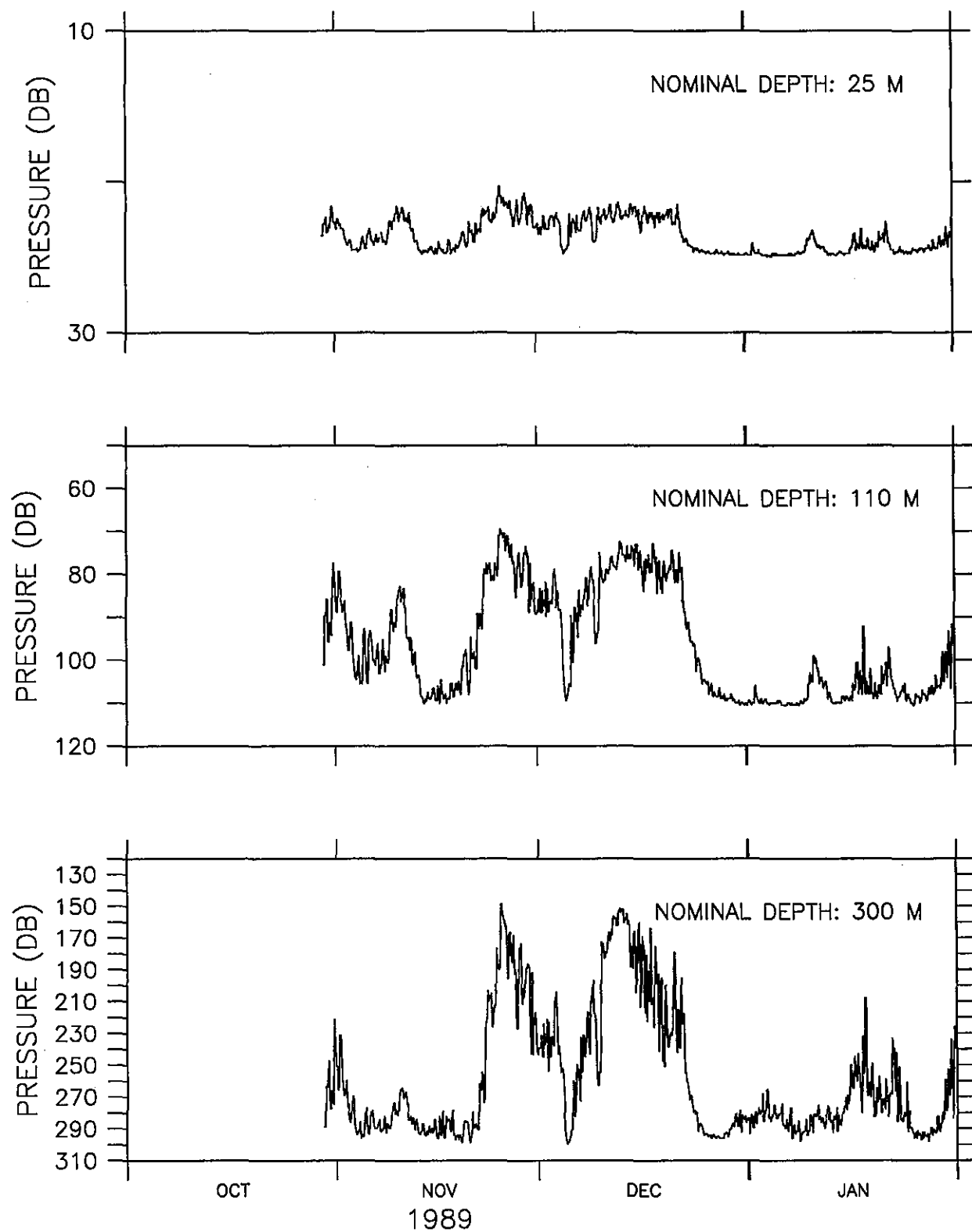


Figure 40.

BUOY 08131 (0.00 N, 155.00 E)

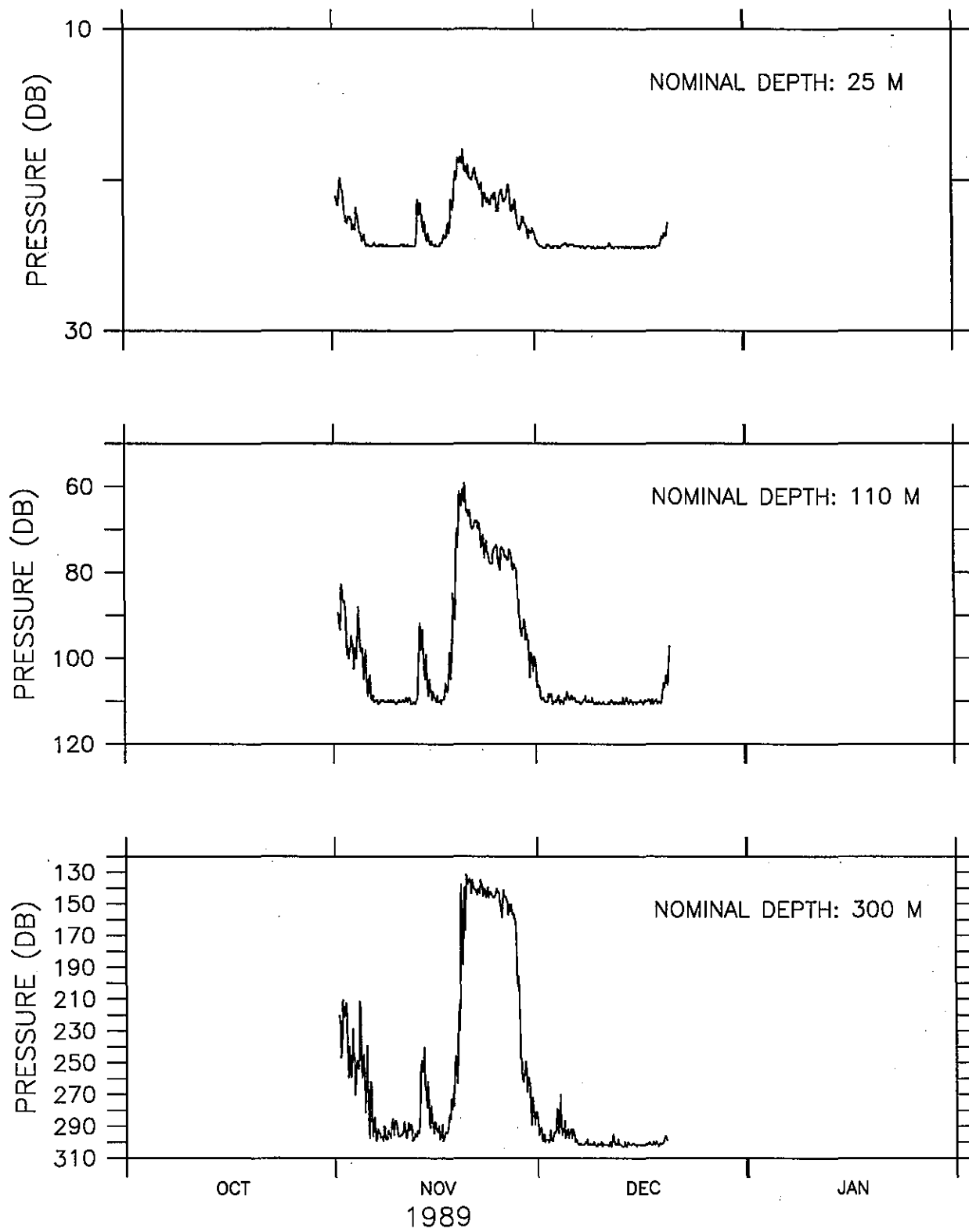


Figure 41.

BUOY 08132 (2.97 S, 159.42 E)

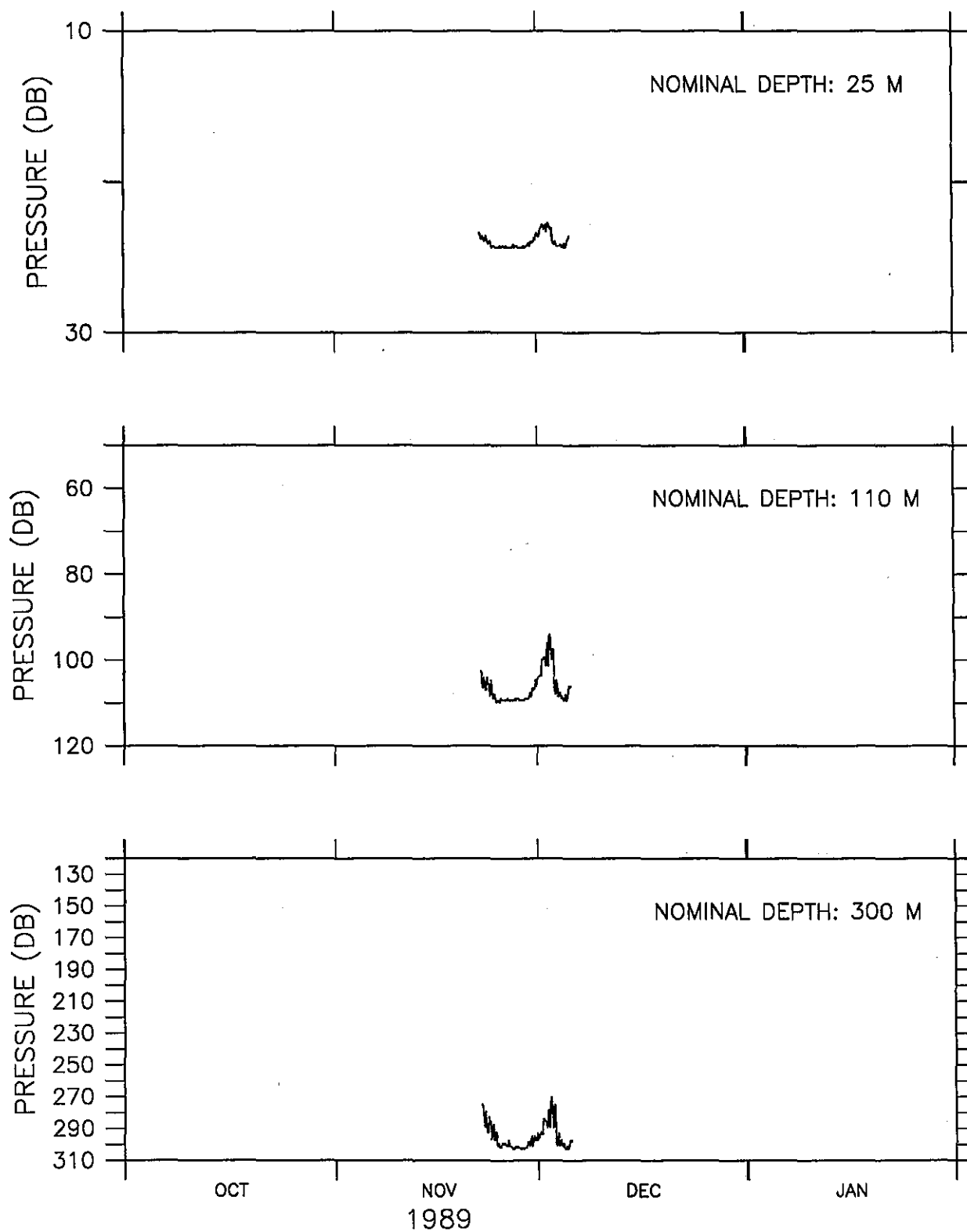


Figure 42.

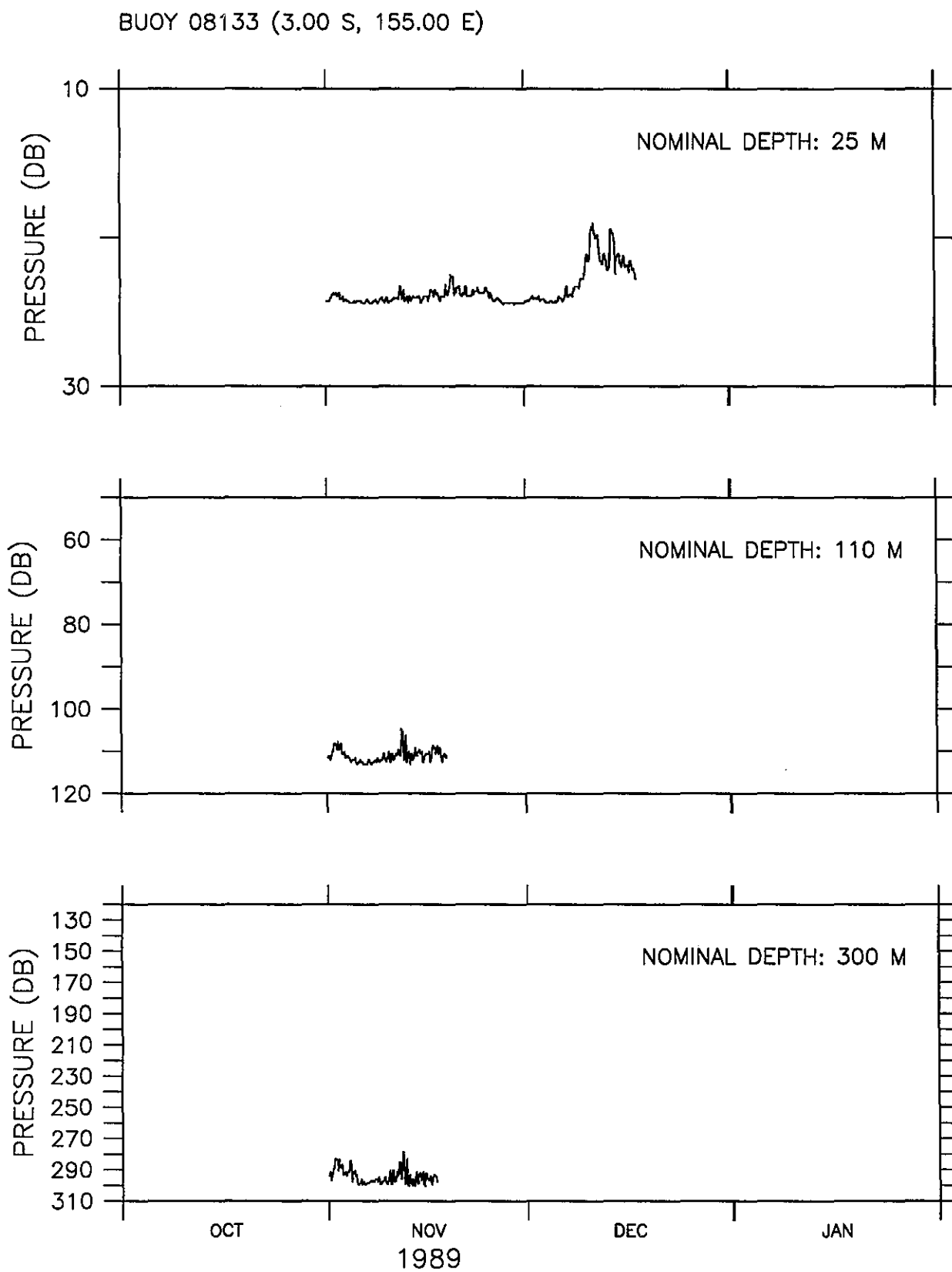


Figure 43.

BUOY 08134 (2.97 N, 150.00 E)

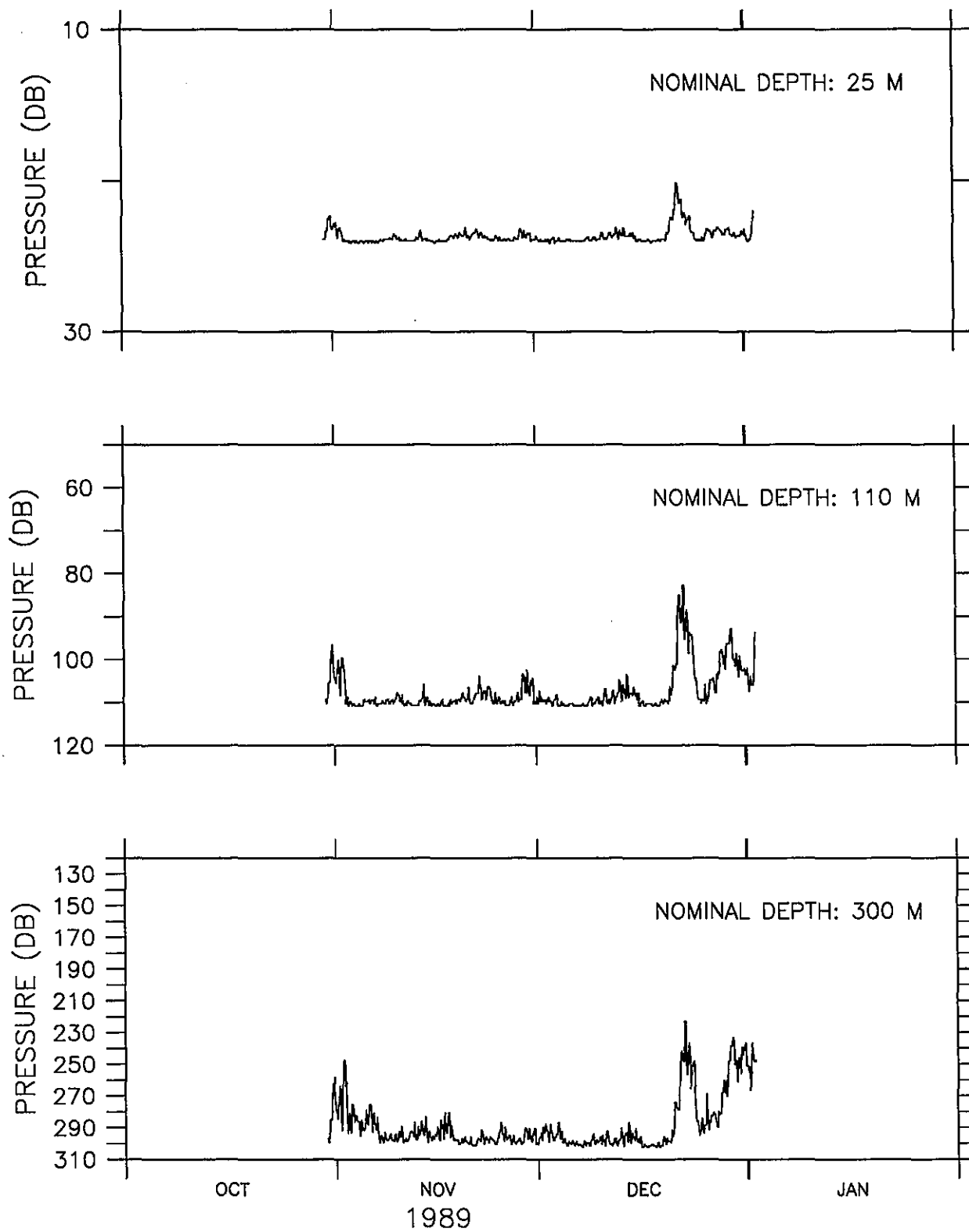


Figure 44.

BUOY 08135 (1.49 N, 156.86 E)

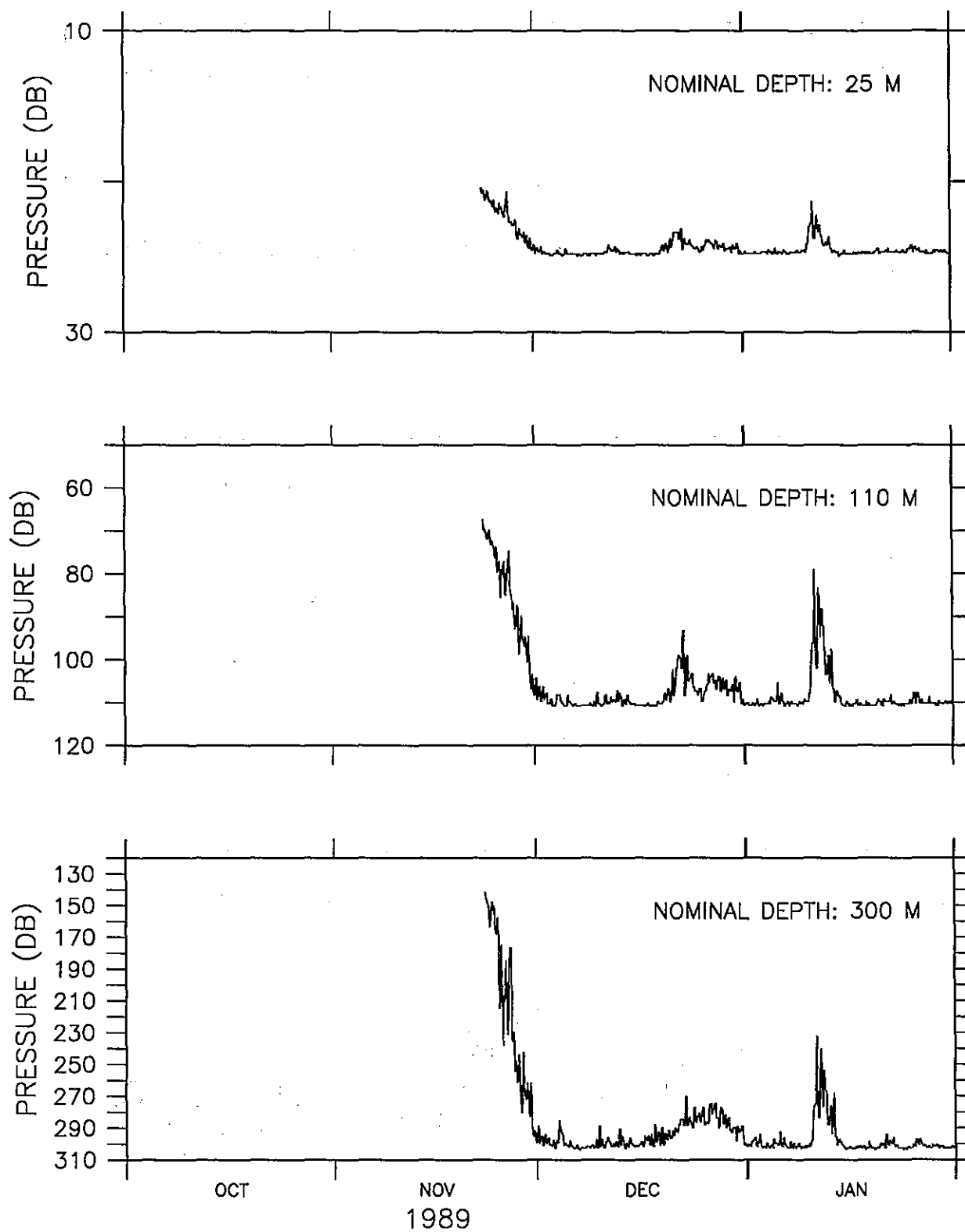


Figure 45.



BUOY 08136 (1.49 N, 152.49 E)

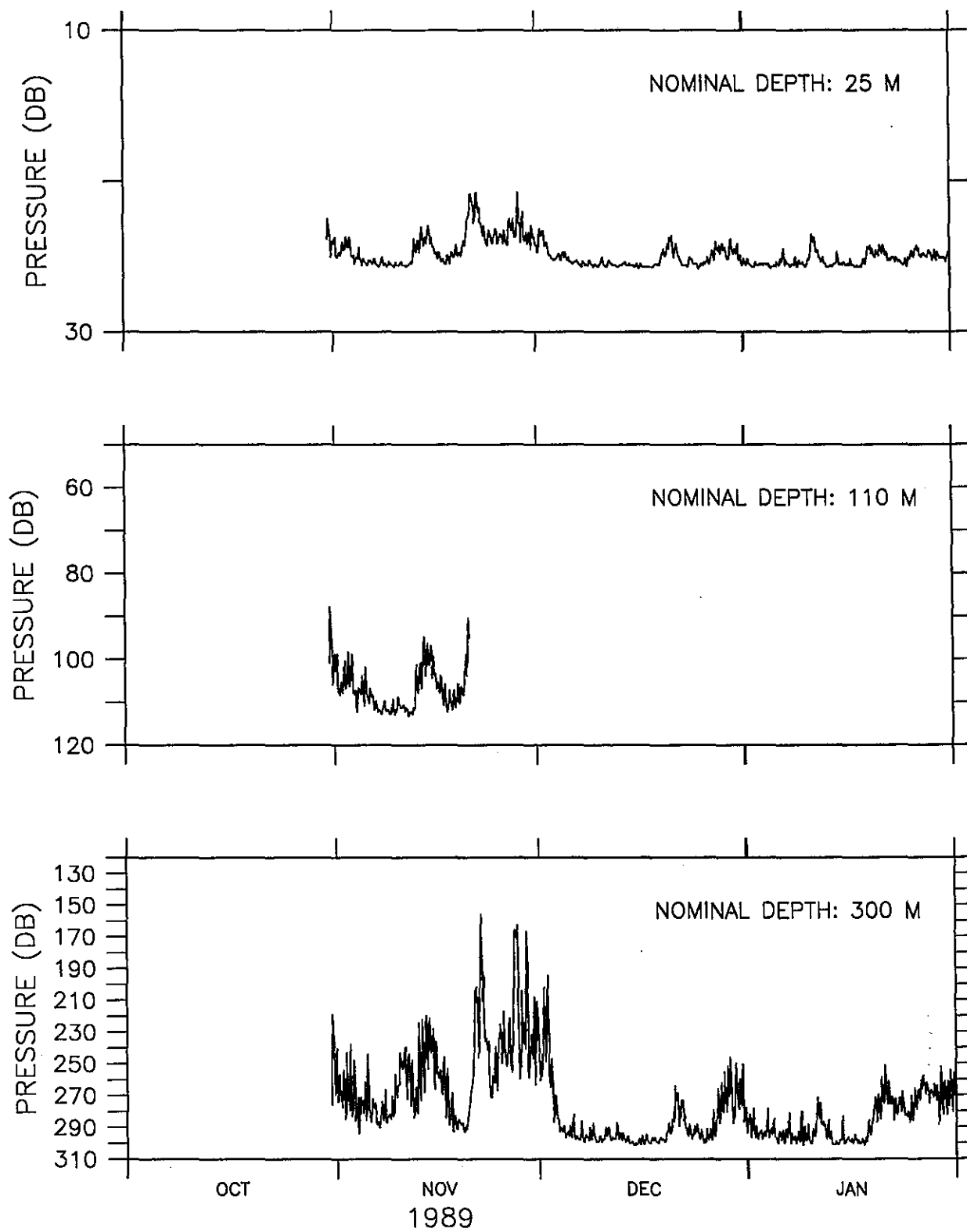


Figure 46.

BUOY 08137 (3.01 S, 150.00 E)

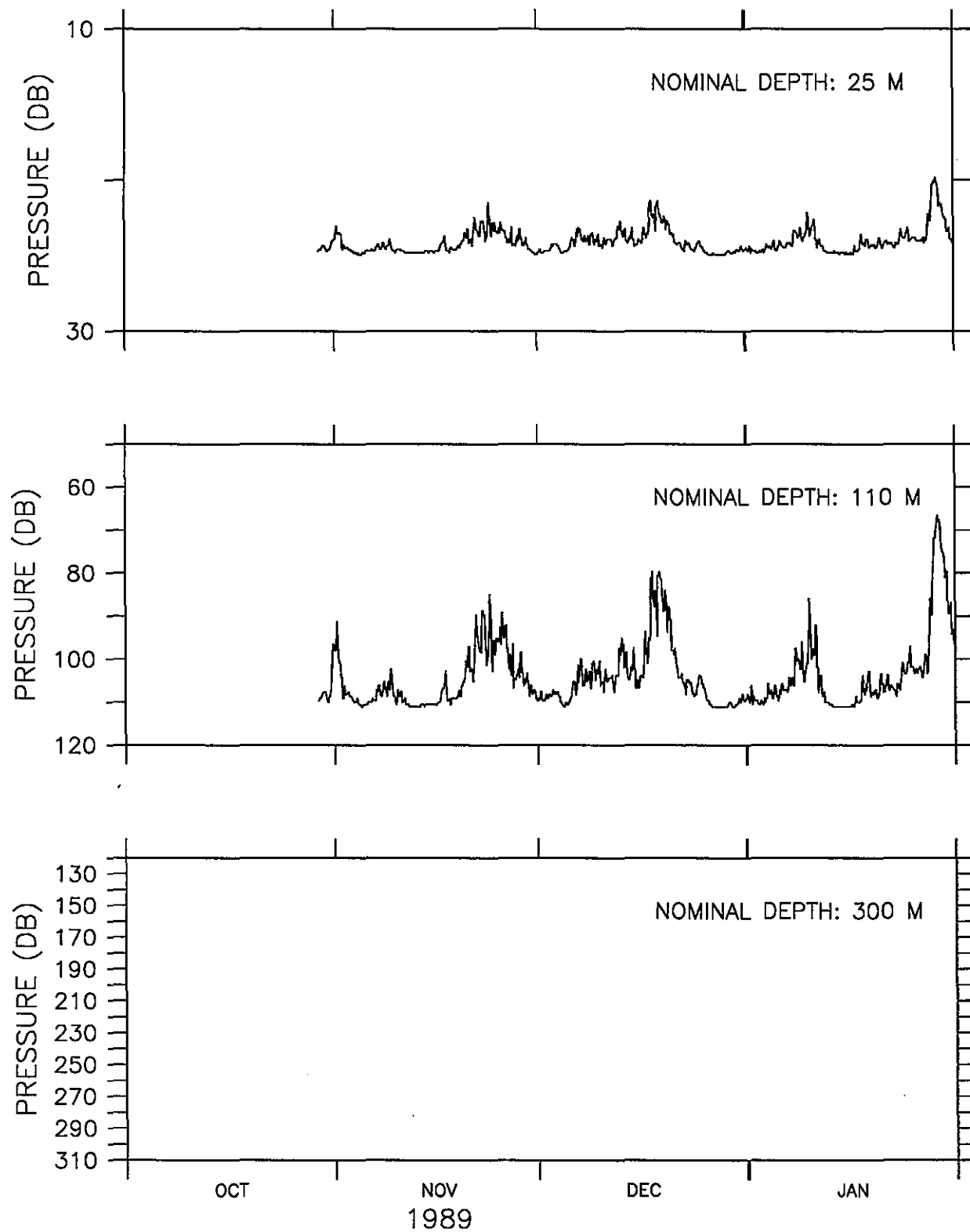


Figure 47.

BUOY 08138 (1.50 S, 141.51 E)

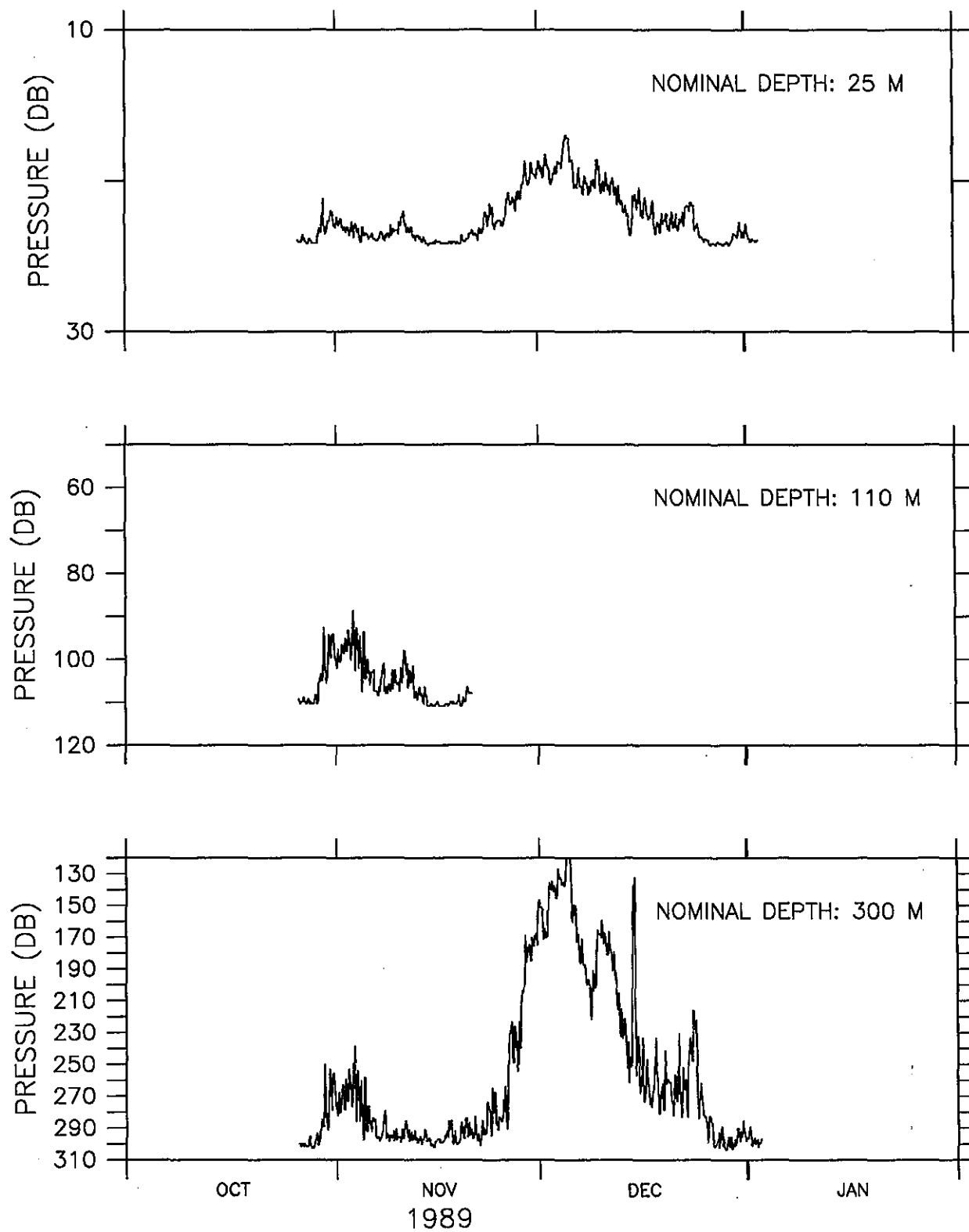


Figure 48.

BUOY 08139 (3.00 S, 145.00 E)

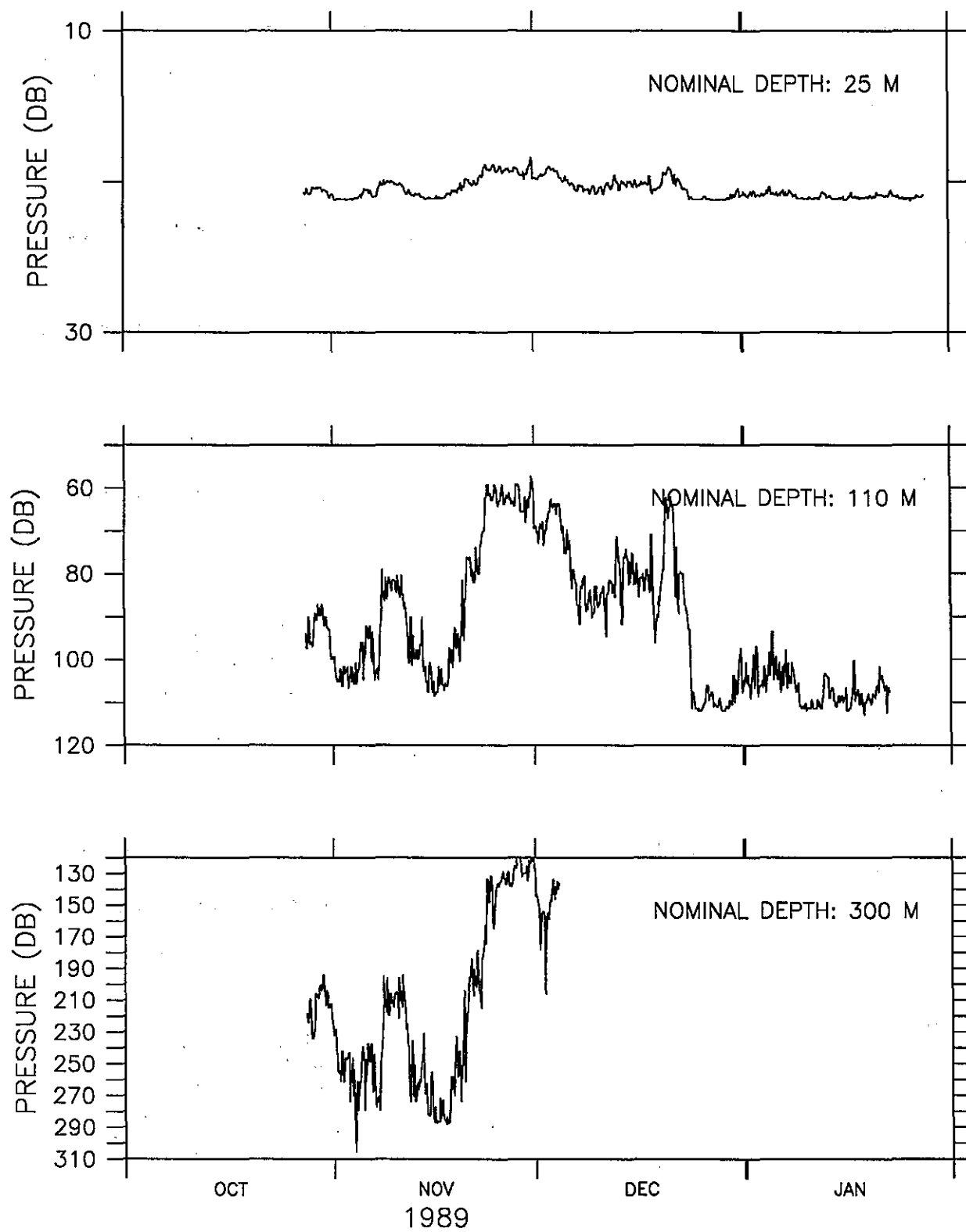


Figure 49.

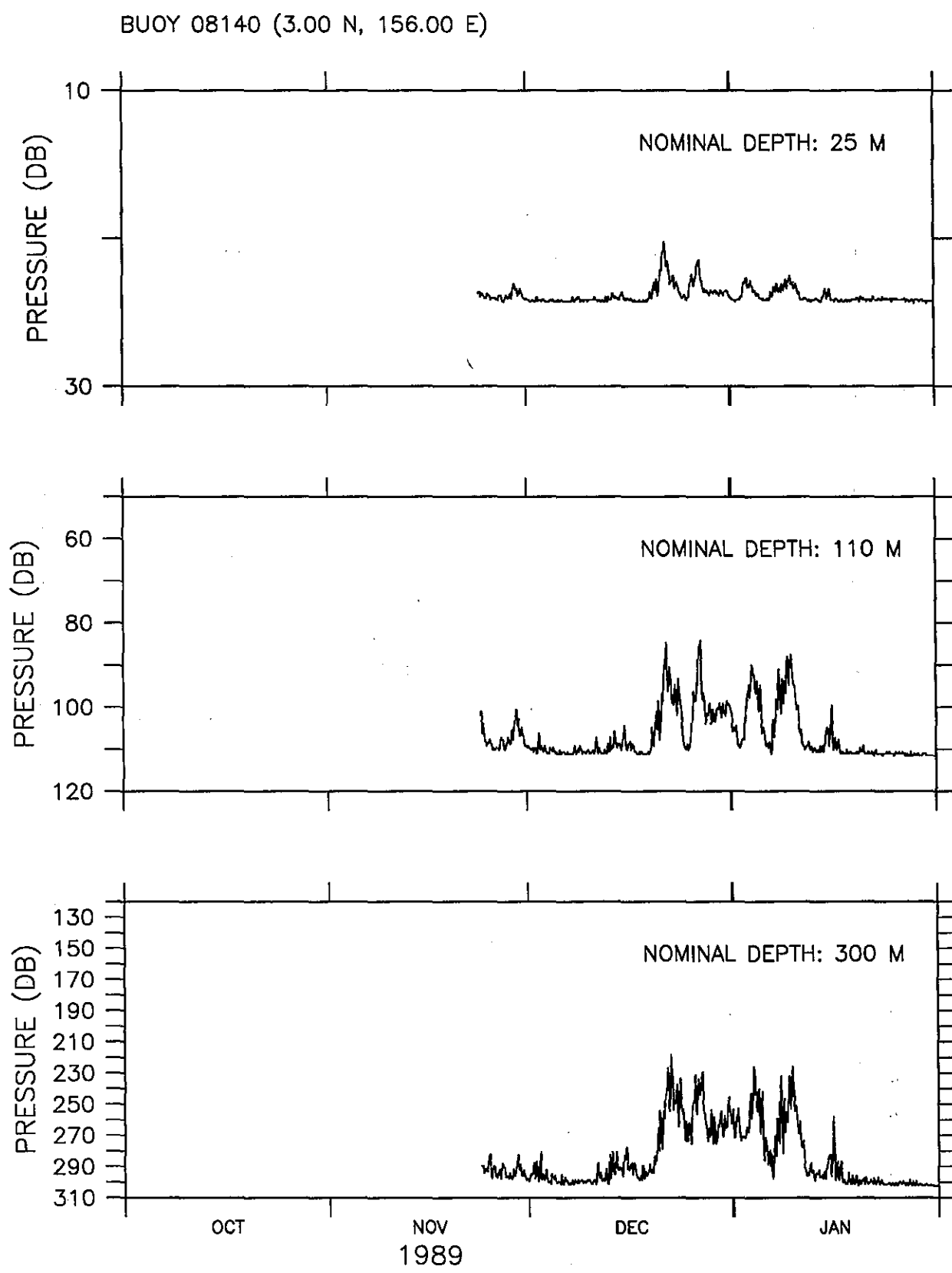


Figure 50.

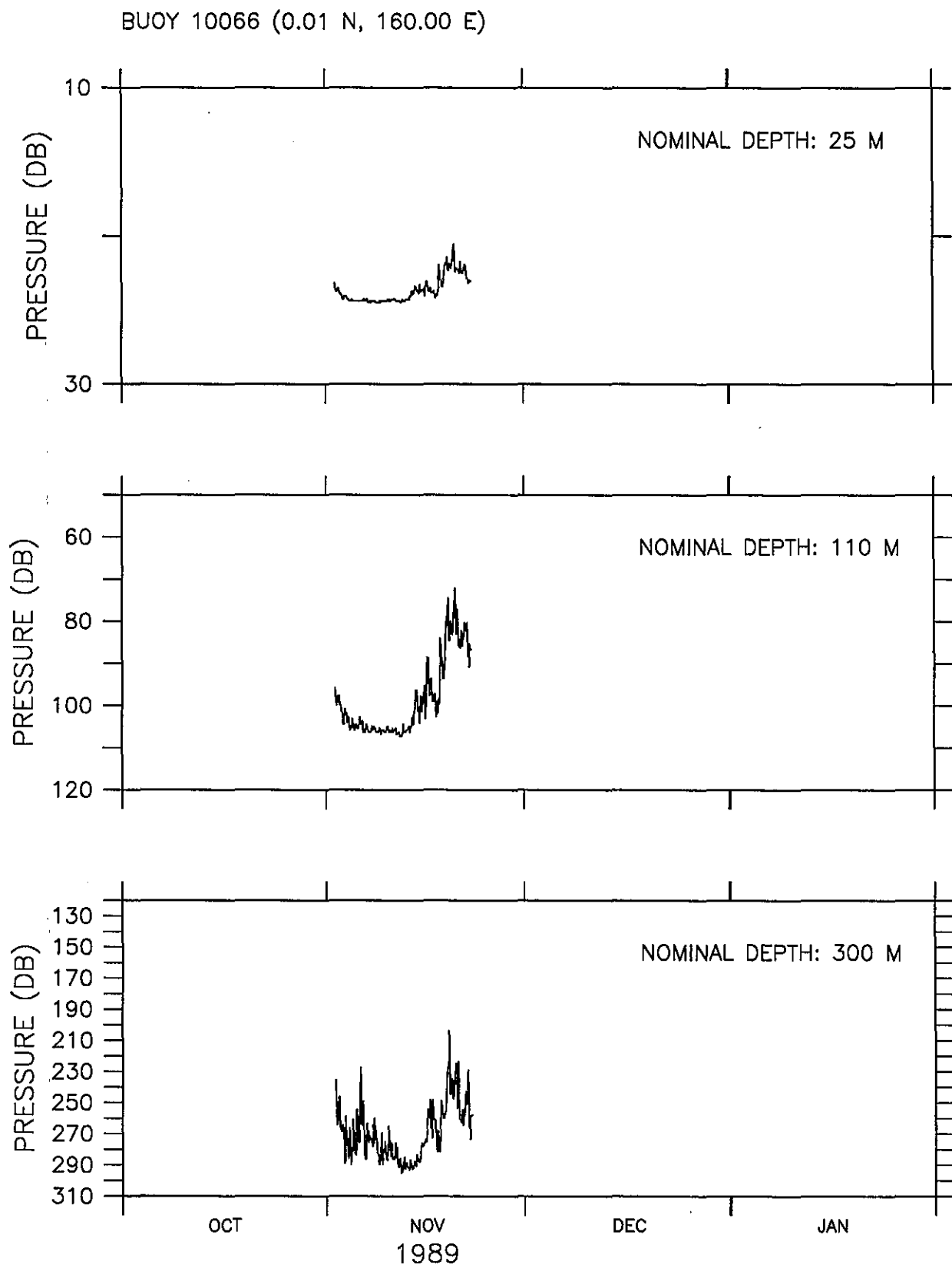


Figure 51.

BUOY 10067 (0.01 N, 145.00 E)

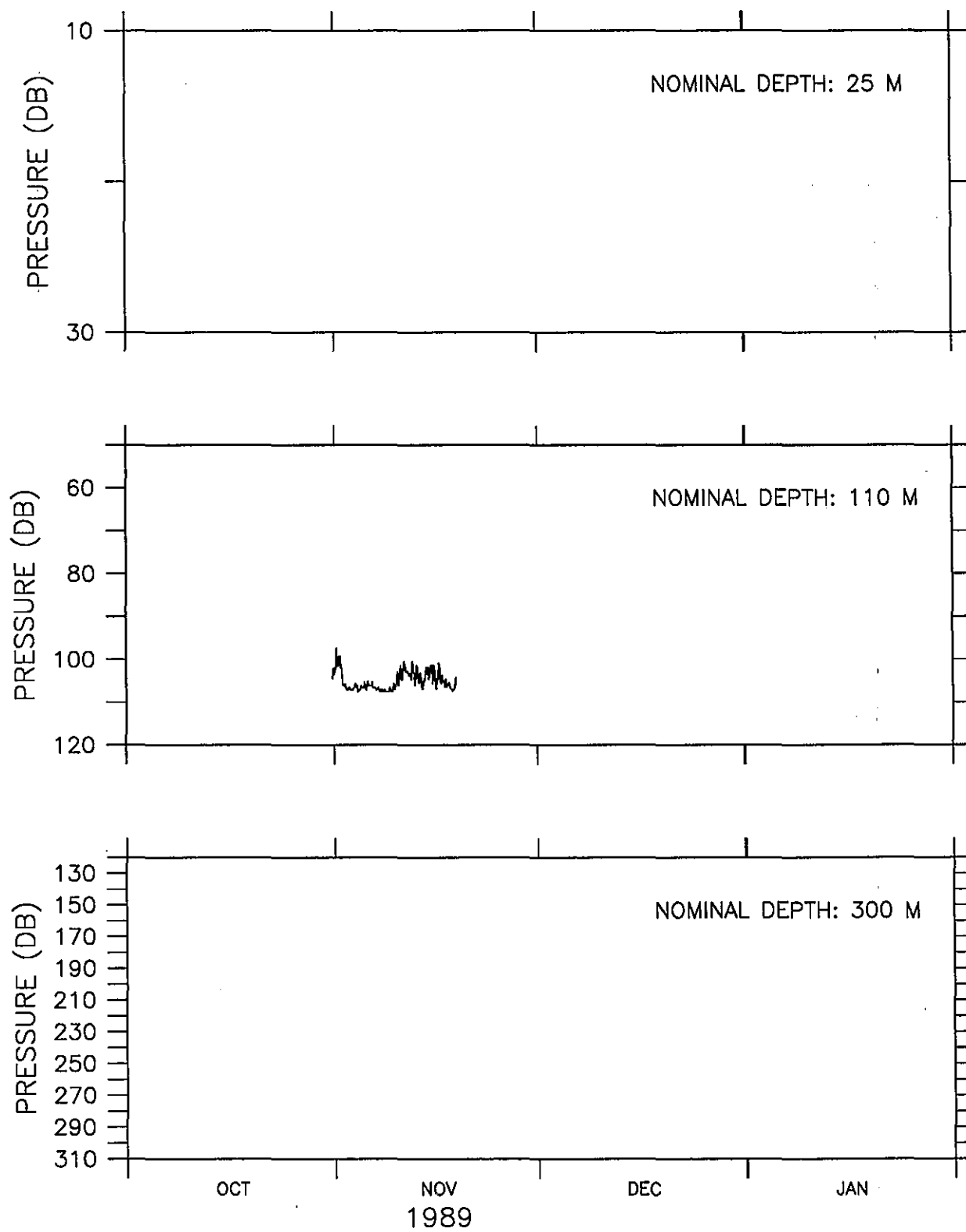


Figure 52.

BUOY 10068 (0.02 N, 150.01 E)

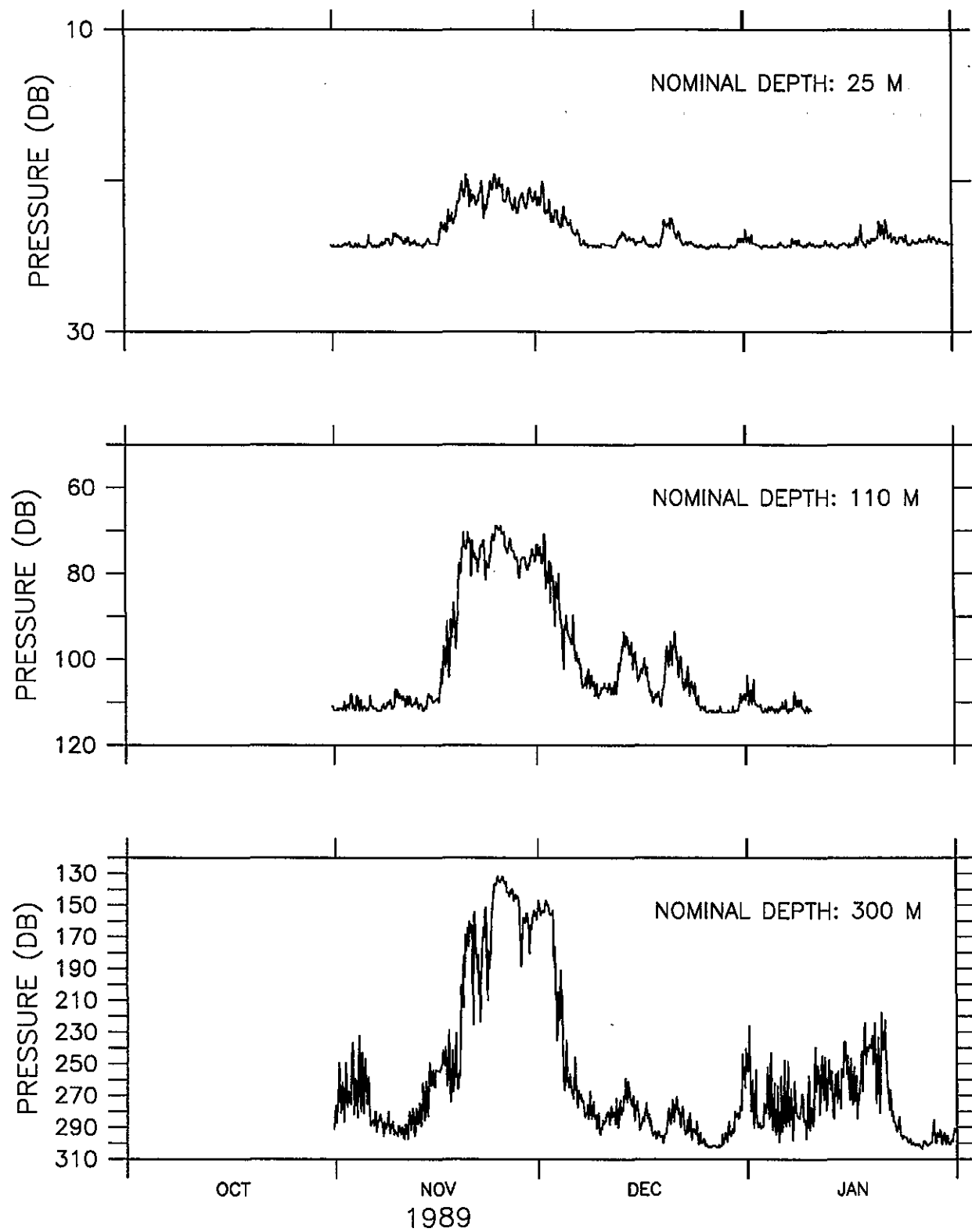


Figure 53.



Figures 54–72. Time series of daily averaged thermistor chain shapes for the PRL drifters. Dots below the surface indicate depths of pressure sensors.

# CHAIN SHAPE

BUOY 08120 (1.50 S 152.51 E)

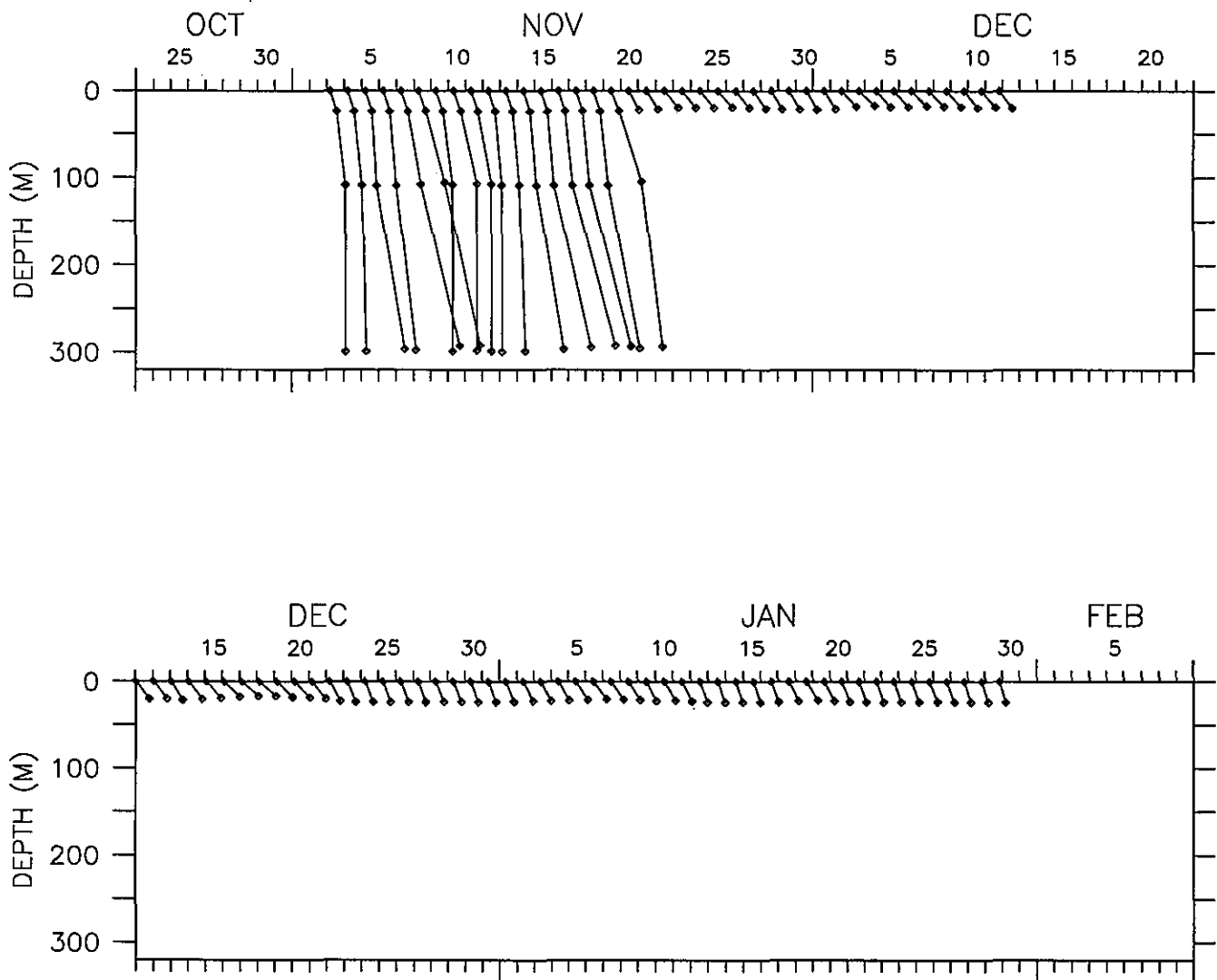


Figure 54.

# CHAIN SHAPE

BUOY 08121 (3.00 N 145.00 E)

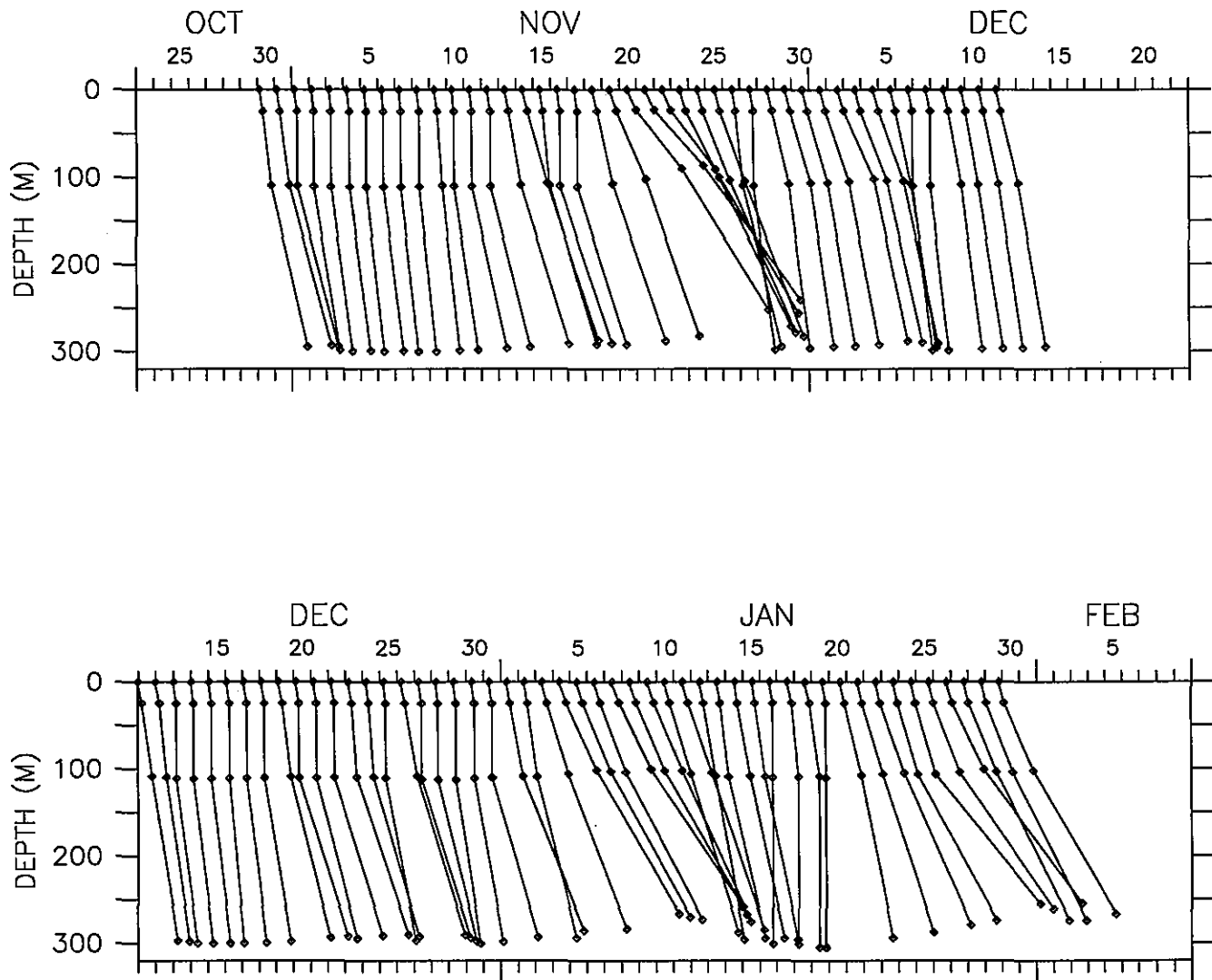


Figure 55.

# CHAIN SHAPE

BUOY 08122 (1.48 N 147.51 E)

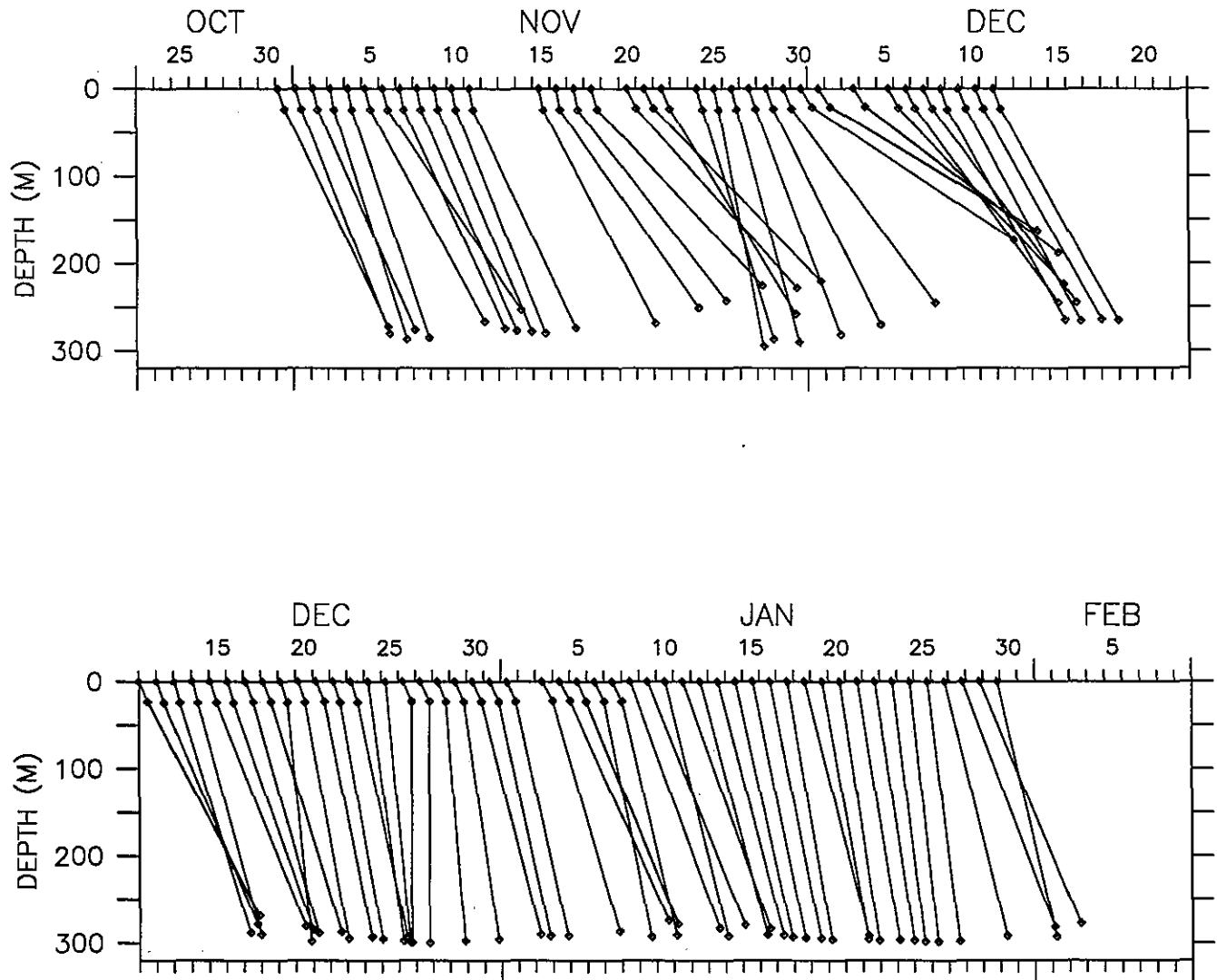


Figure 56.

# CHAIN SHAPE

BUOY 08126 (1.53 S 164.97 E)

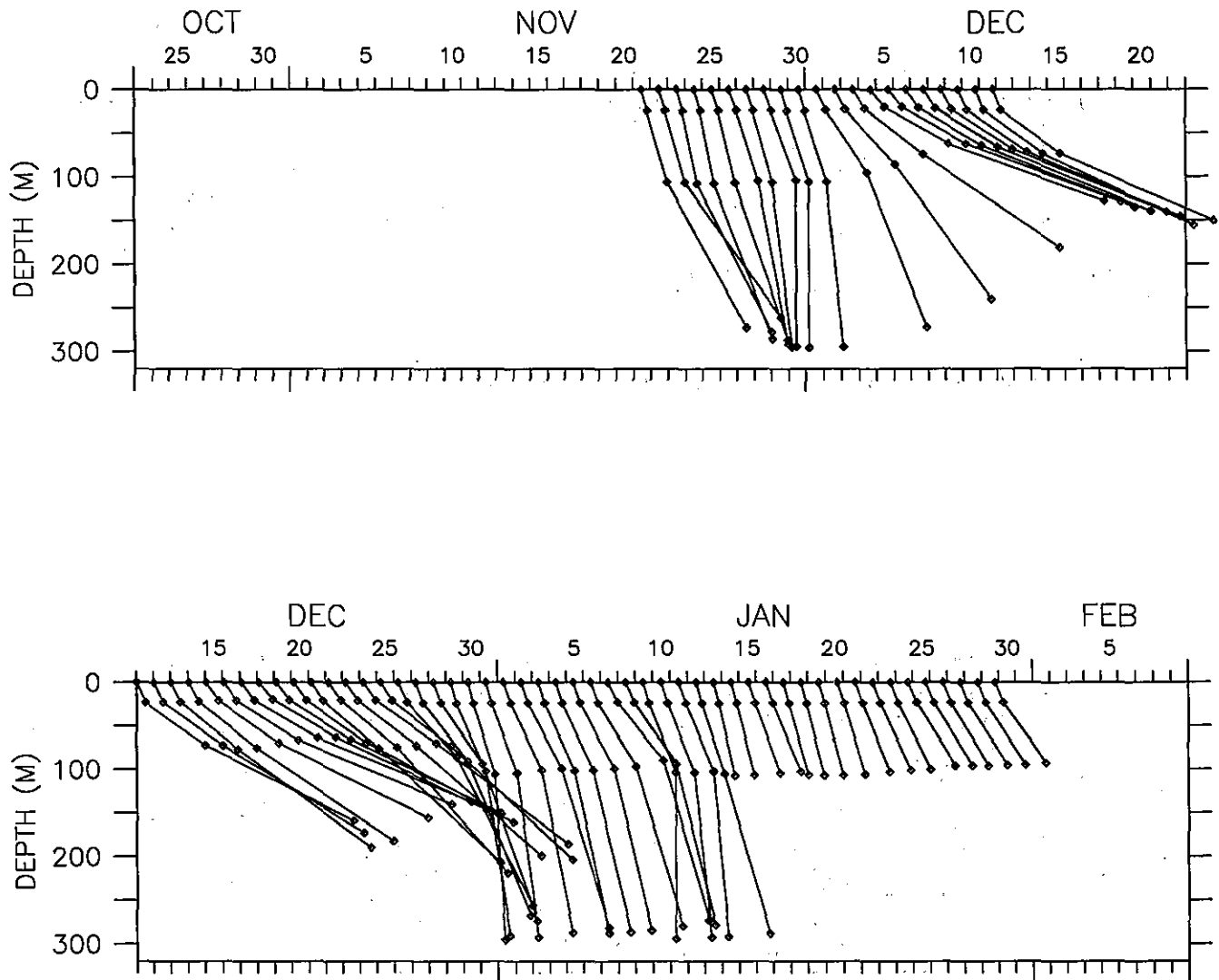


Figure 57.

# CHAIN SHAPE

BUOY 08131 (0.00 N 155.00 E)

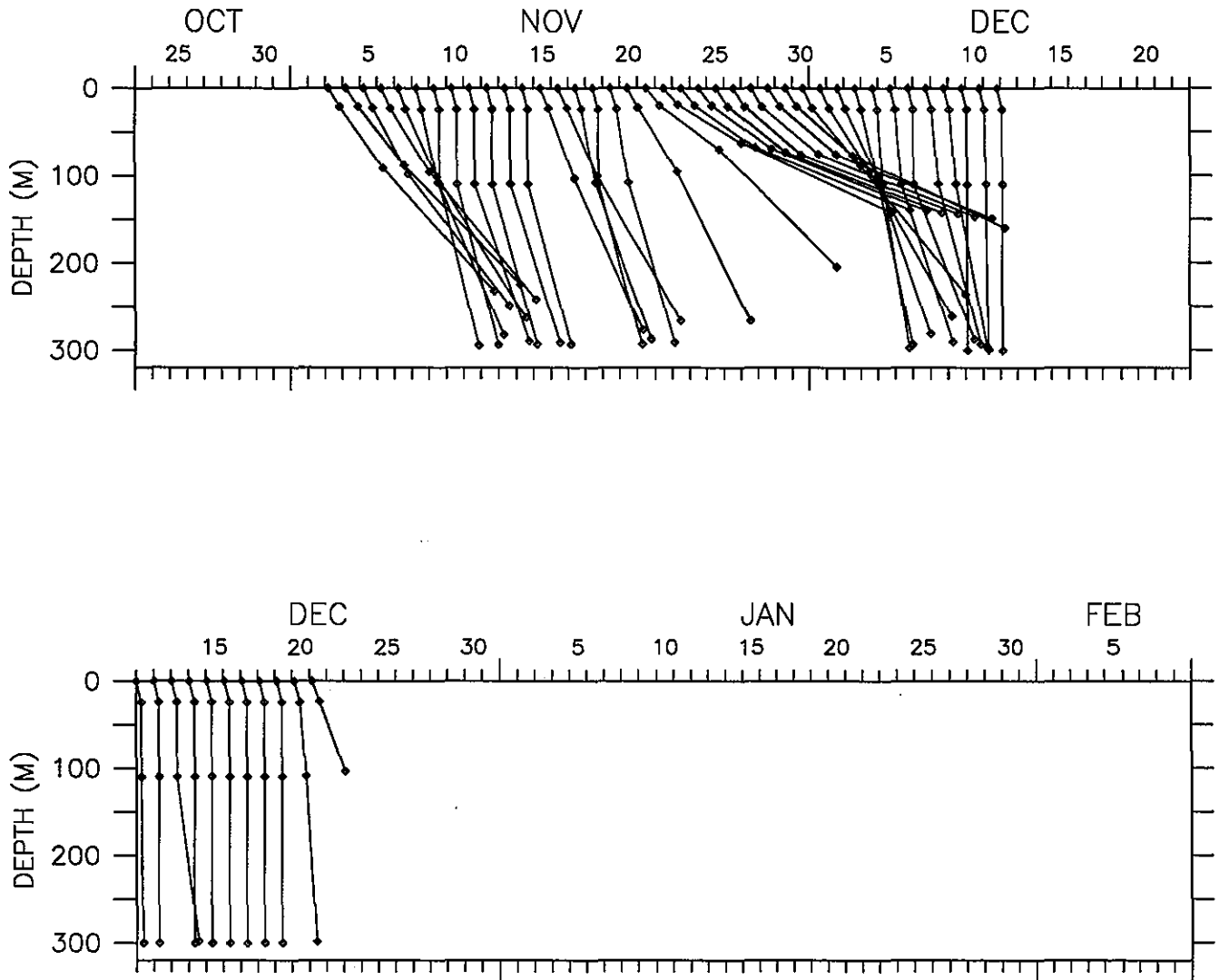


Figure 60.

## CHAIN SHAPE

BUOY 08132 (2.97 S 159.42 E)

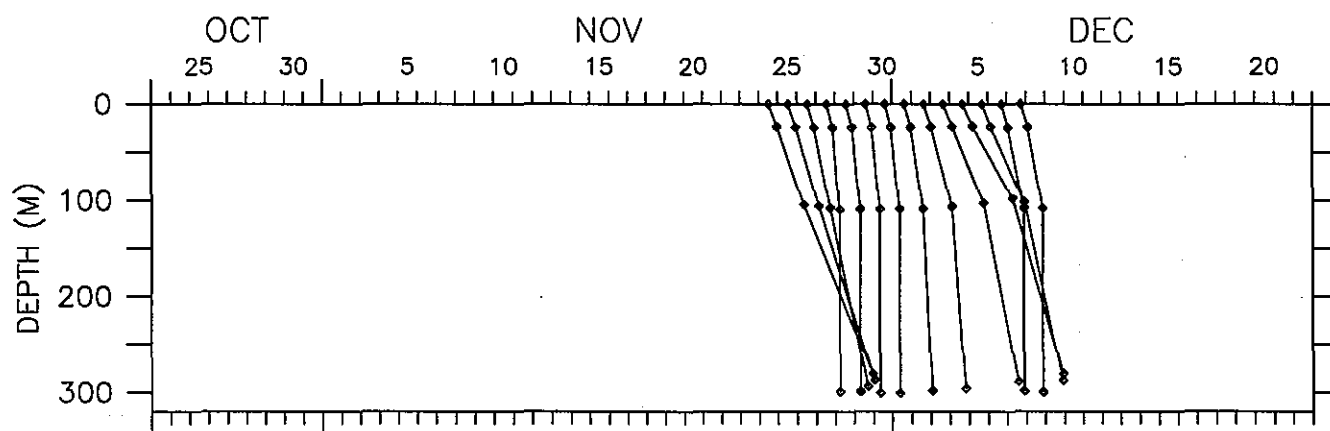


Figure 61.

# CHAIN SHAPE

BUOY 08133 (3.00 S 155.00 E)

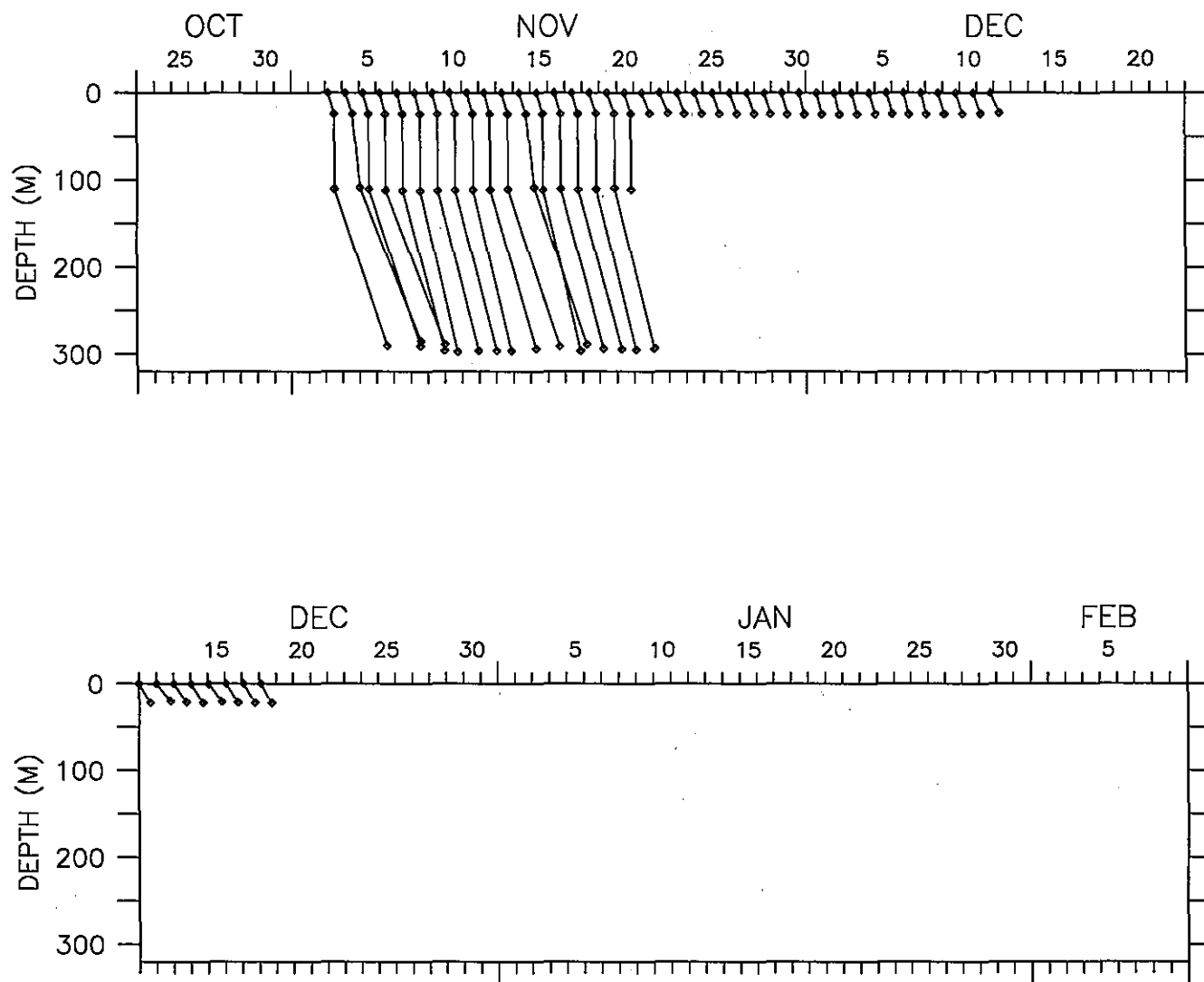


Figure 62.



# CHAIN SHAPE

BUOY 08134 (2.97 N 150.00 E)

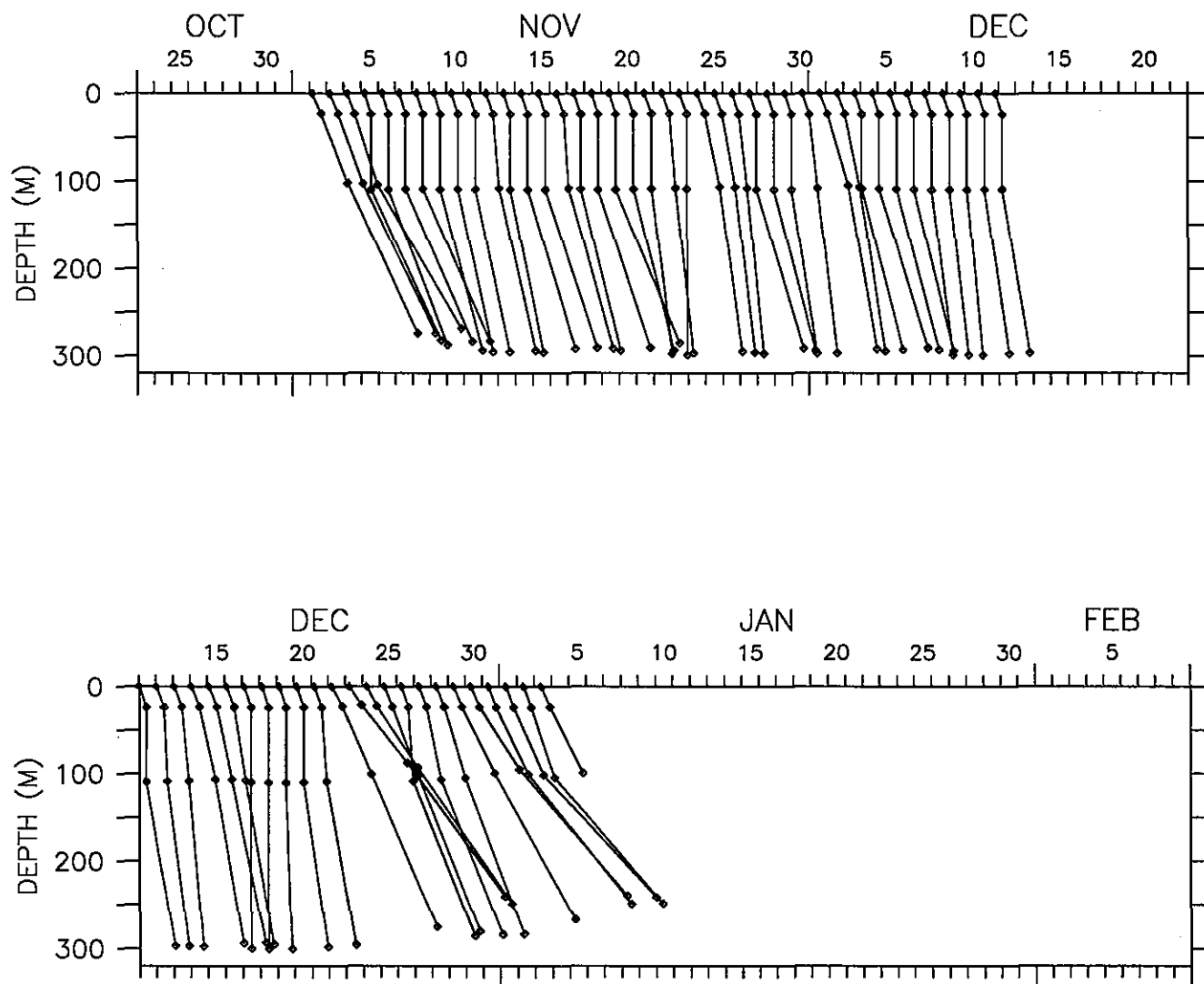


Figure 63.

# CHAIN SHAPE

BUOY 08135 (1.49 N 156.86 E)

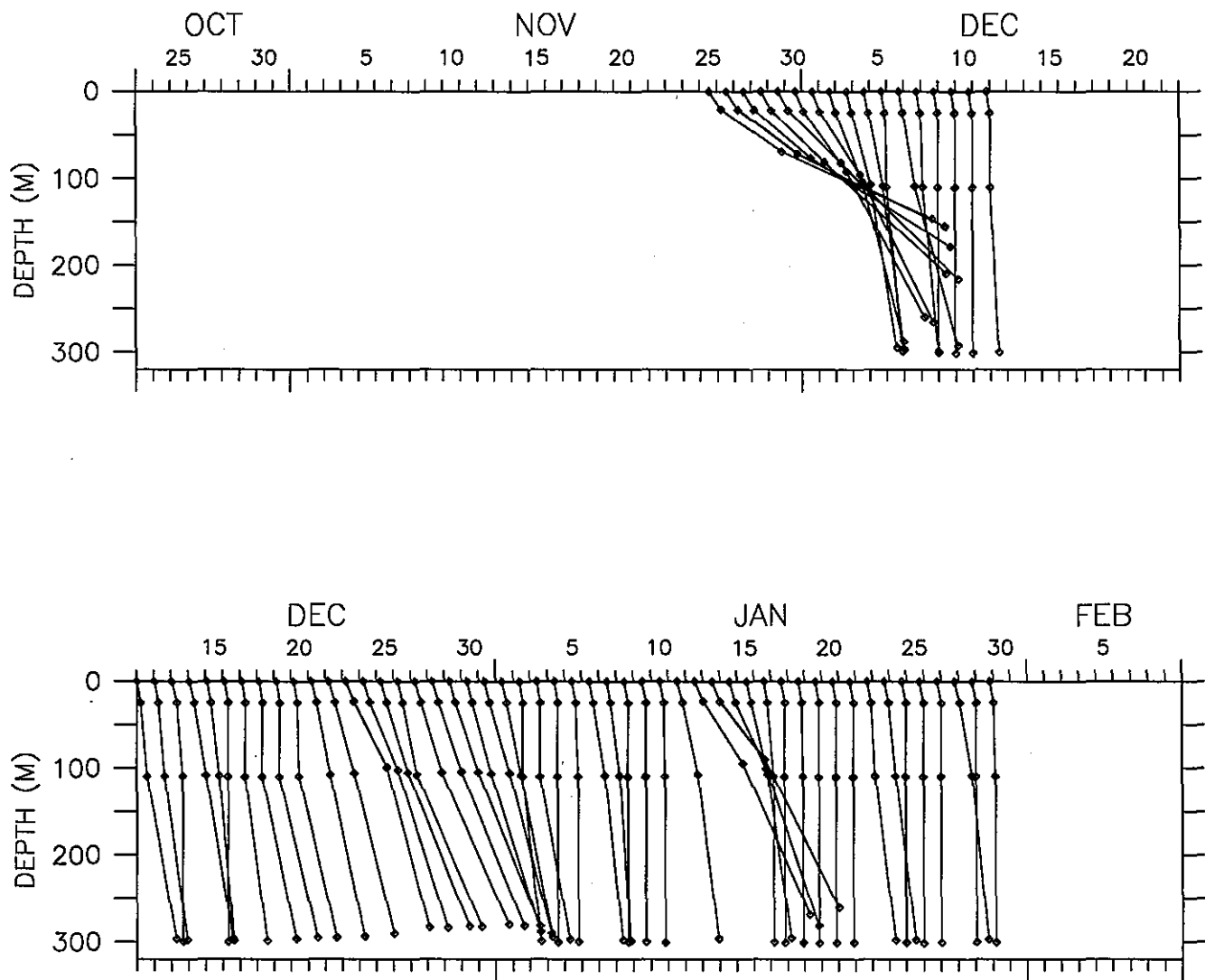


Figure 64.

# CHAIN SHAPE

BUOY 08136 (1.49 N 152.49 E)

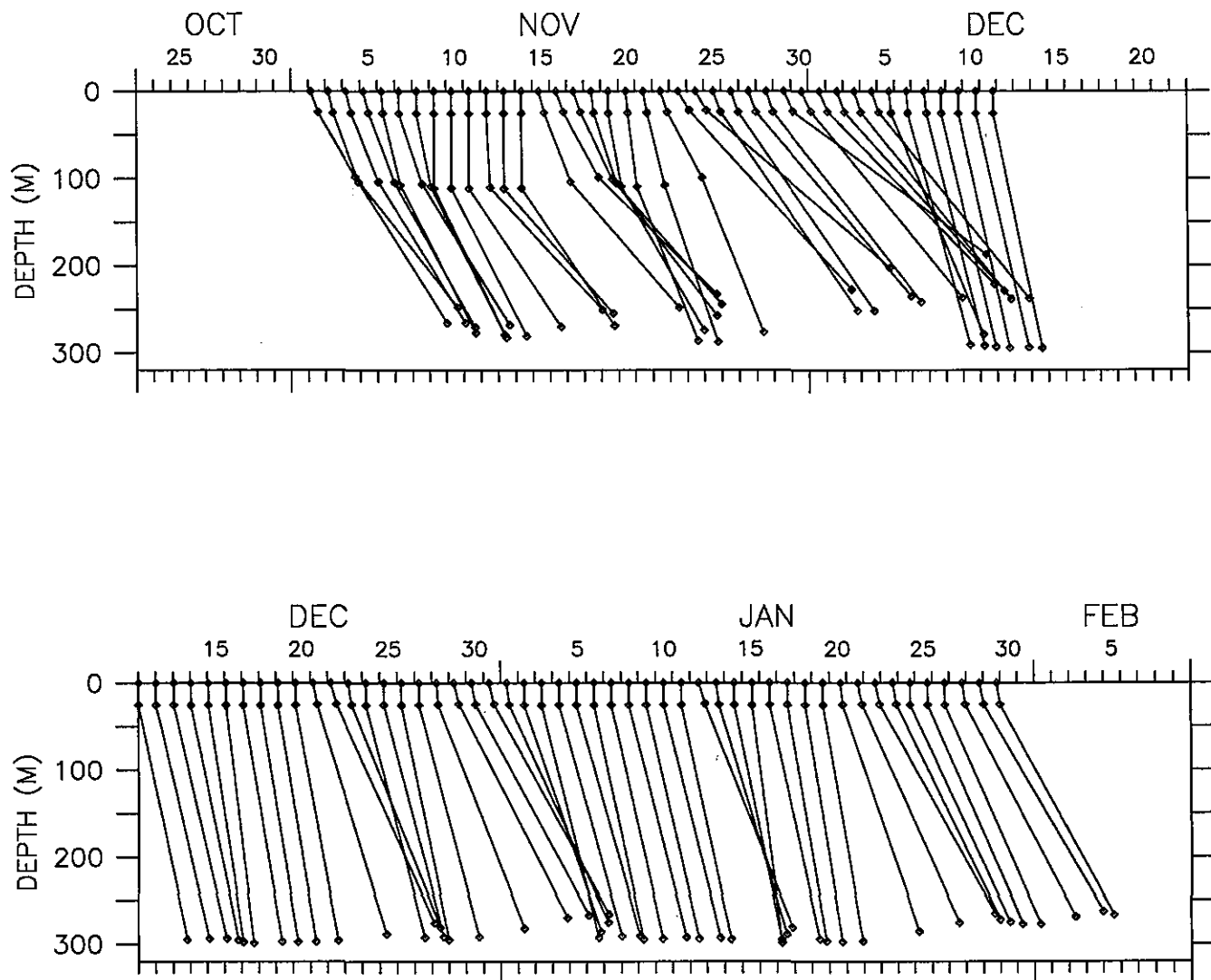


Figure 65.

# CHAIN SHAPE

BUOY 08137 (3.01 S 150.00 E)

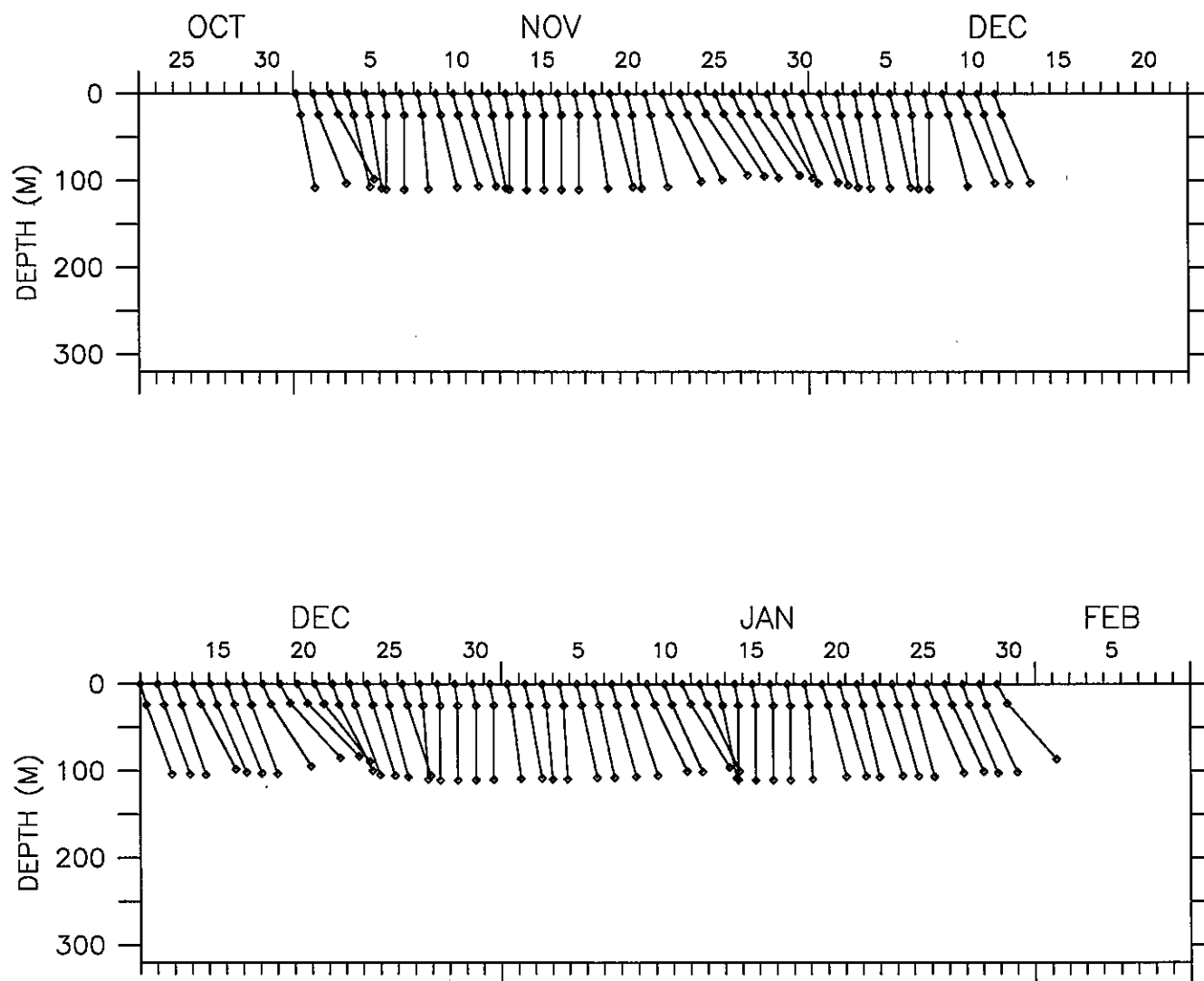


Figure 66.

# CHAIN SHAPE

BUOY 08138 (1.50 S 141.51 E)

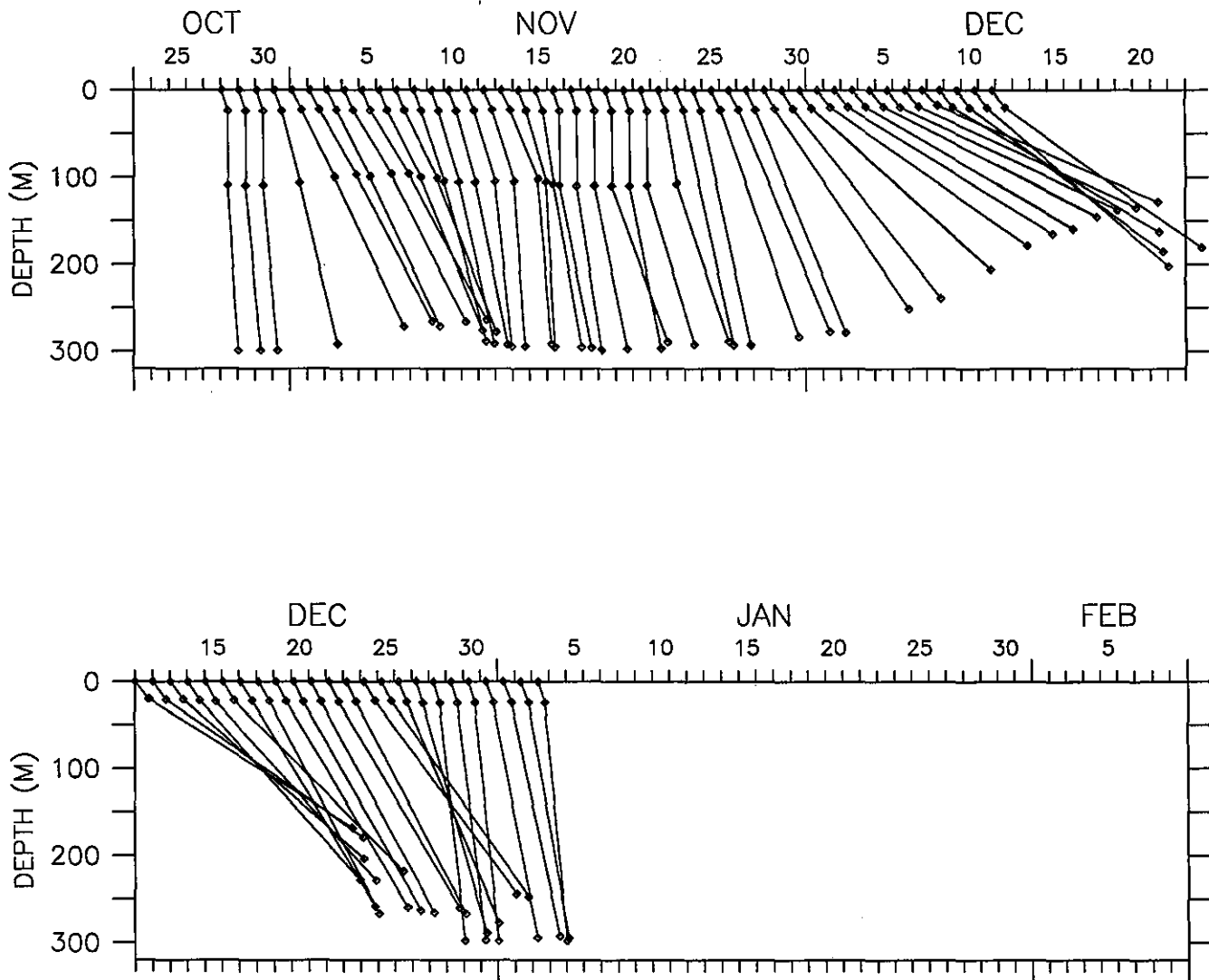


Figure 67.

# CHAIN SHAPE

BUOY 08139 (3.00 S 145.00 E)

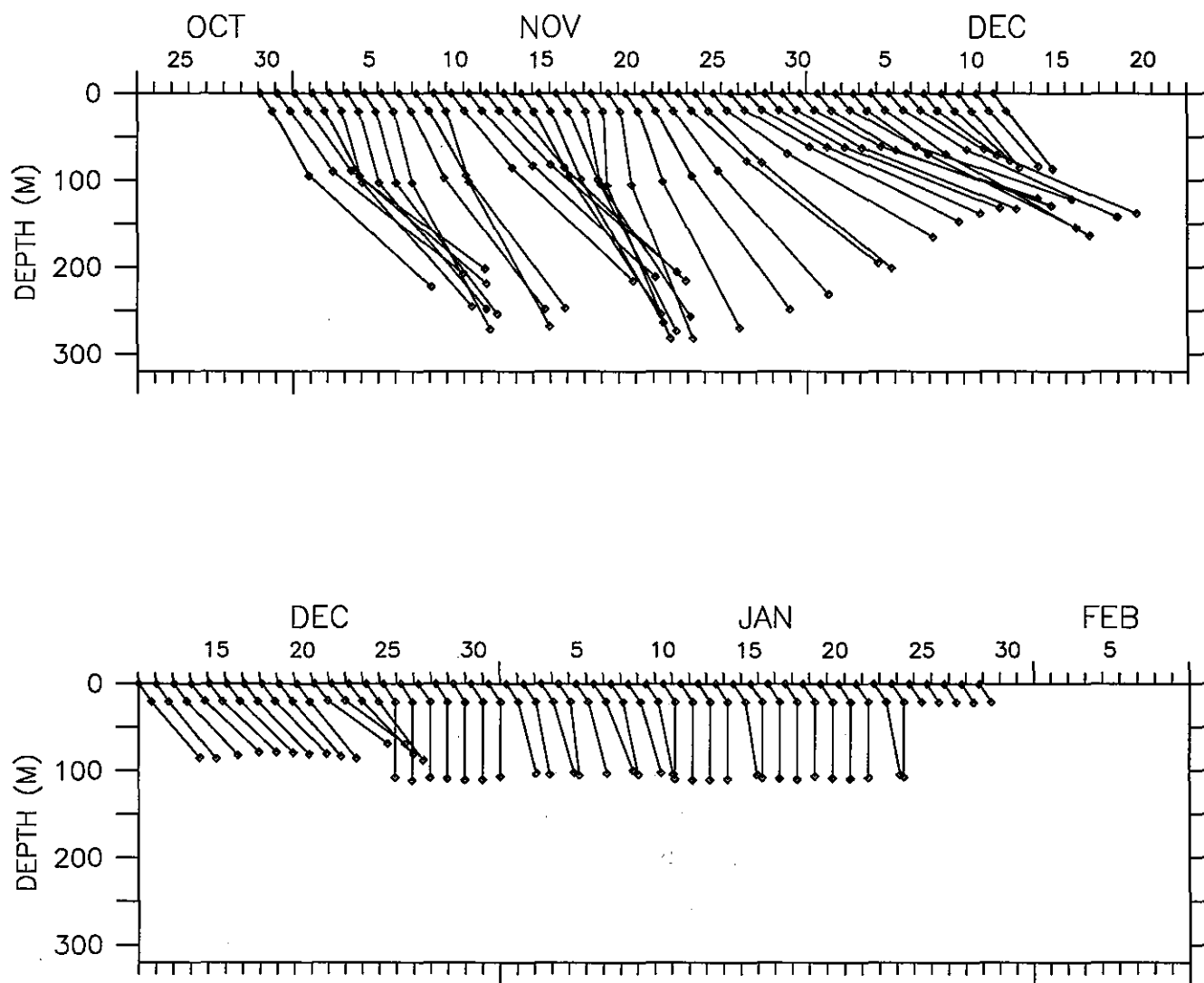


Figure 68.

# CHAIN SHAPE

BUOY 08140 (3.00 N 156.00 E)

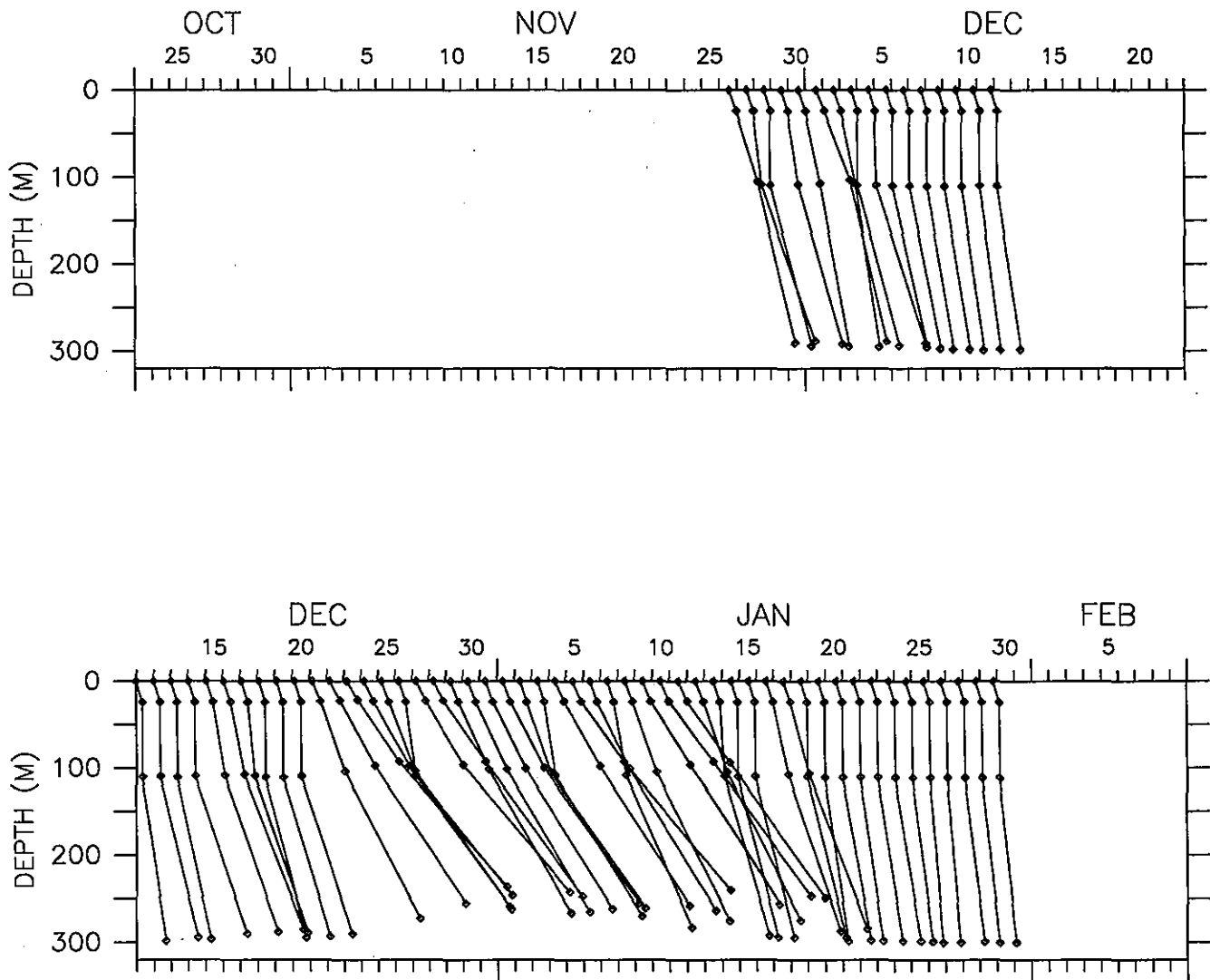


Figure 69.

# CHAIN SHAPE

BUOY 10066 (0.01 N 160.00 E)

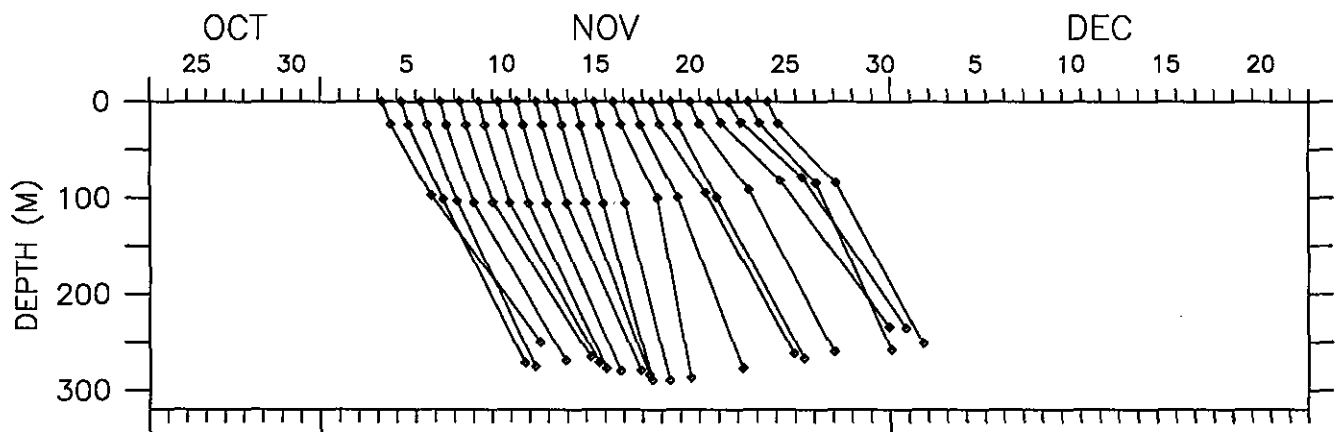


Figure 70.



## CHAIN SHAPE

BUOY 10067 (0.01 N 145.00 E)

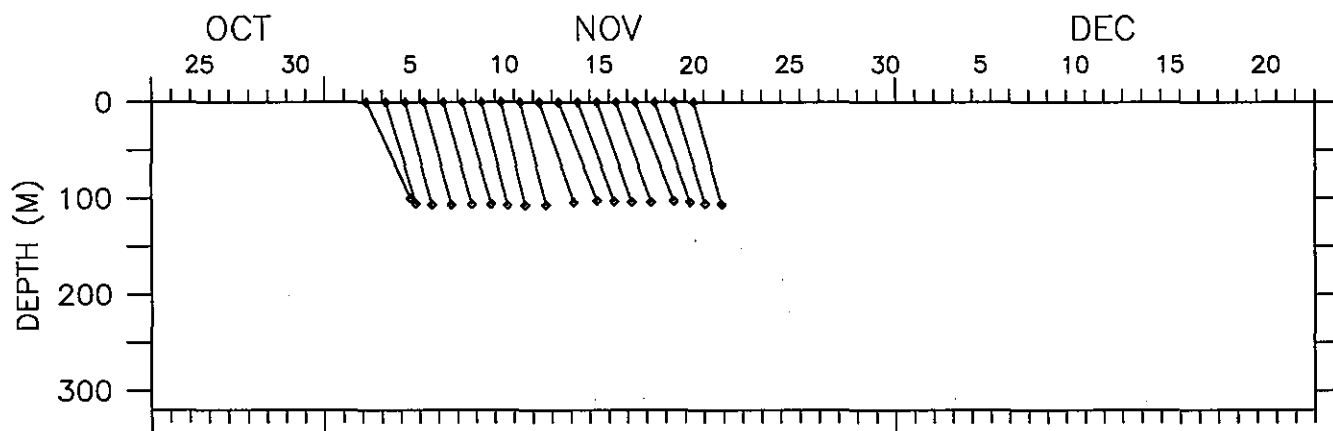


Figure 71.

# CHAIN SHAPE

BUOY 10068 (0.02 N 150.01 E)

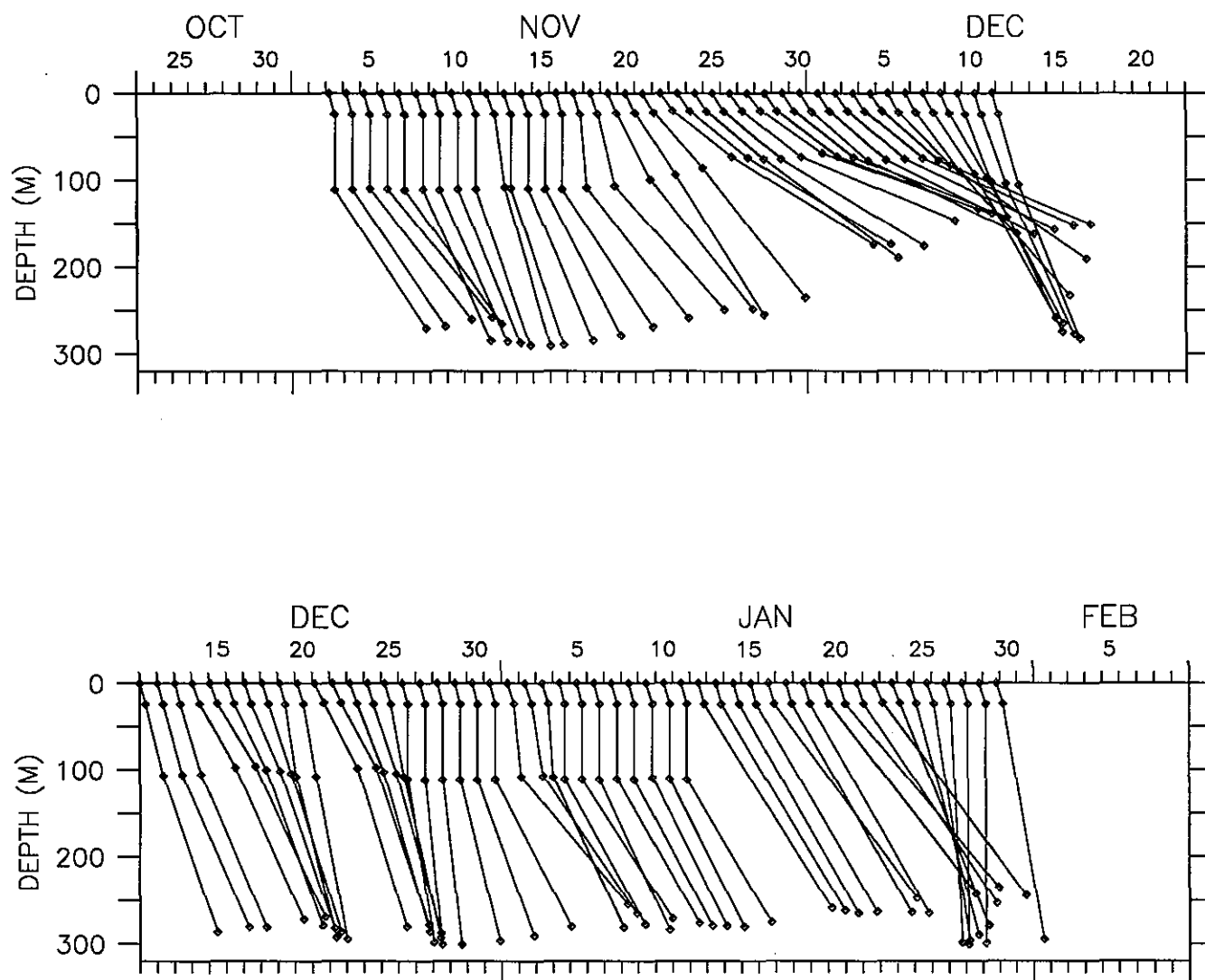


Figure 72.

Figures 73–91. Time series of 3-hourly temperature sensor data for PRL drifters.

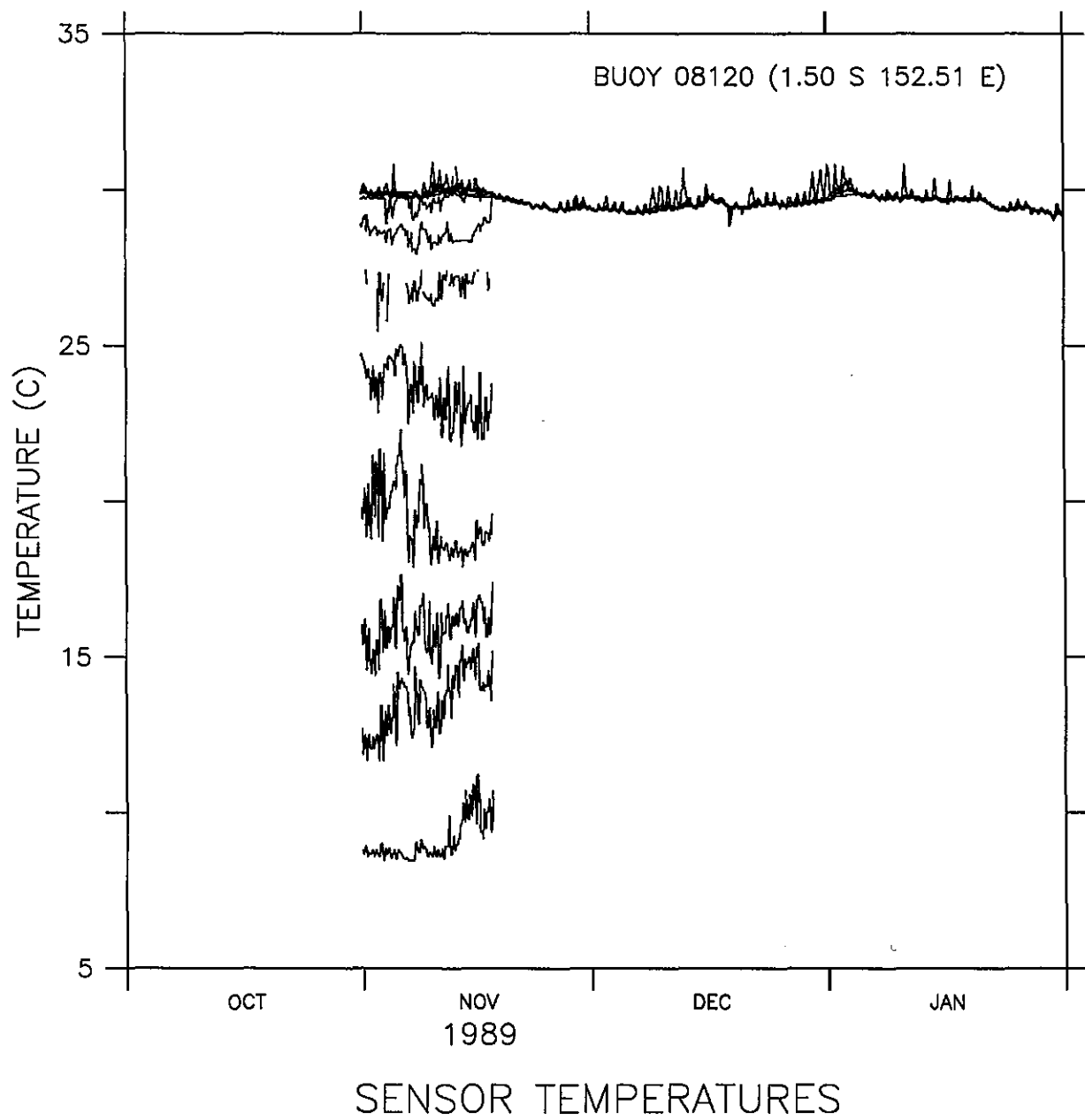


Figure 73.

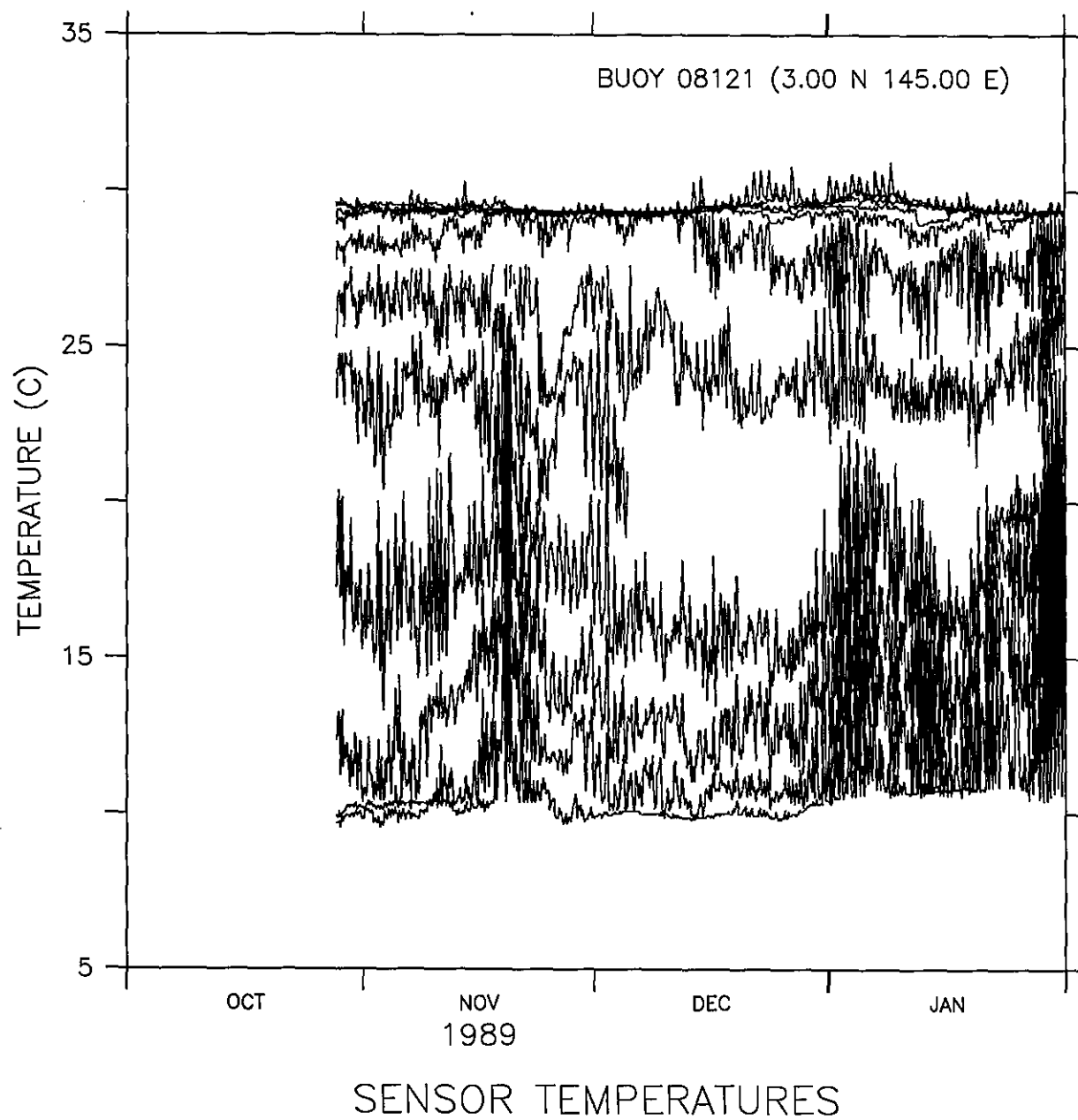


Figure 74.

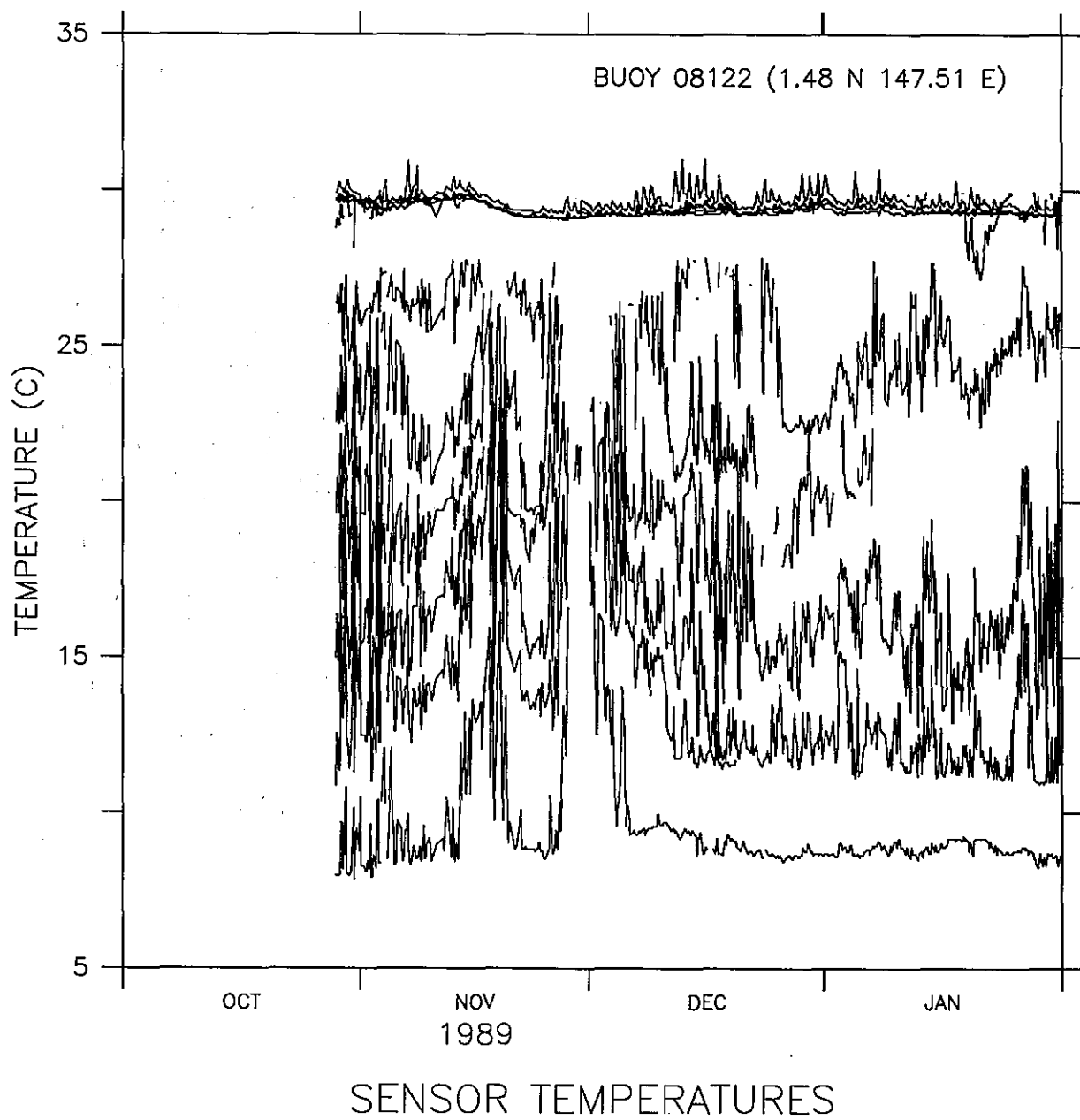


Figure 75.

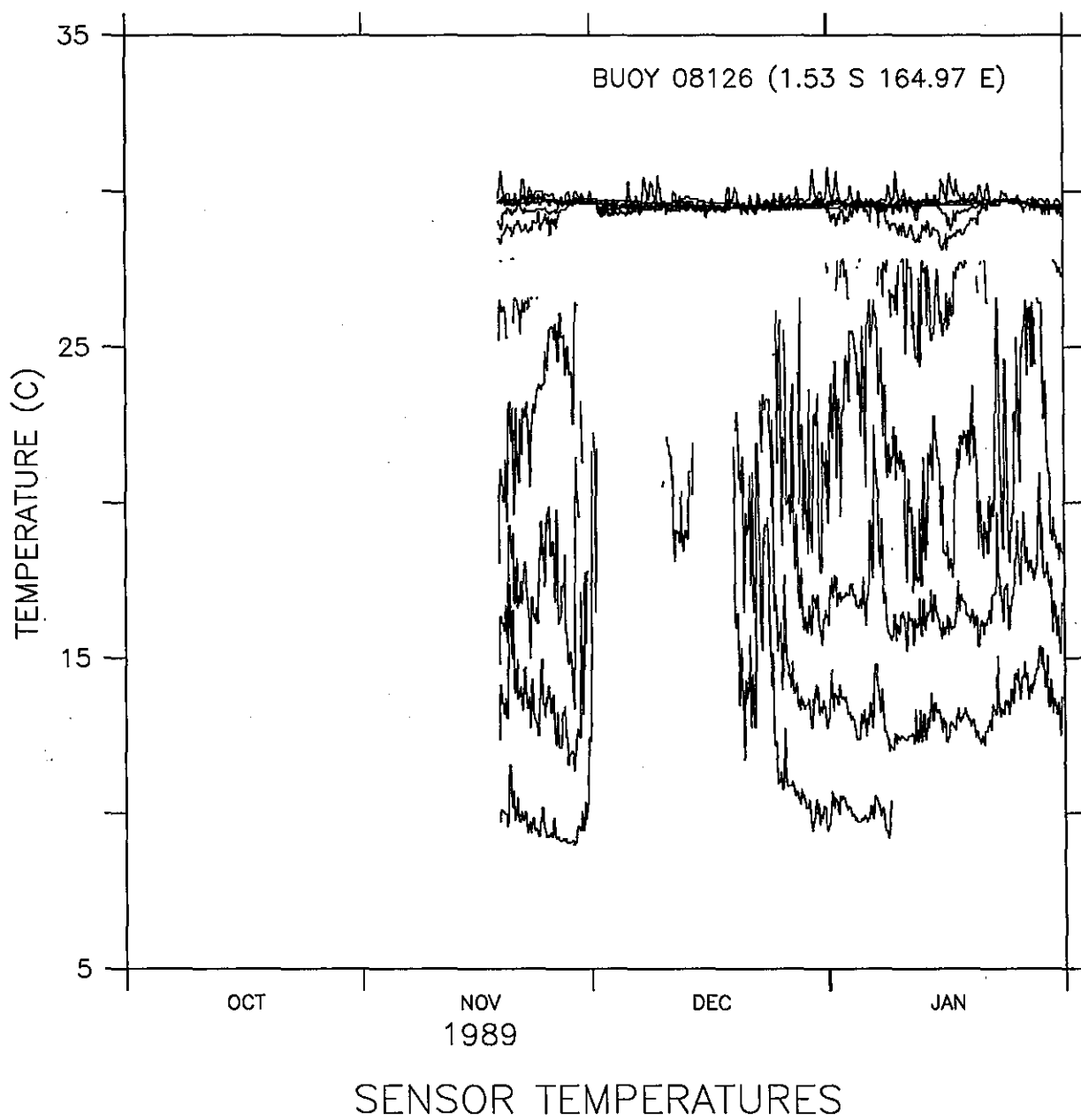


Figure 76.

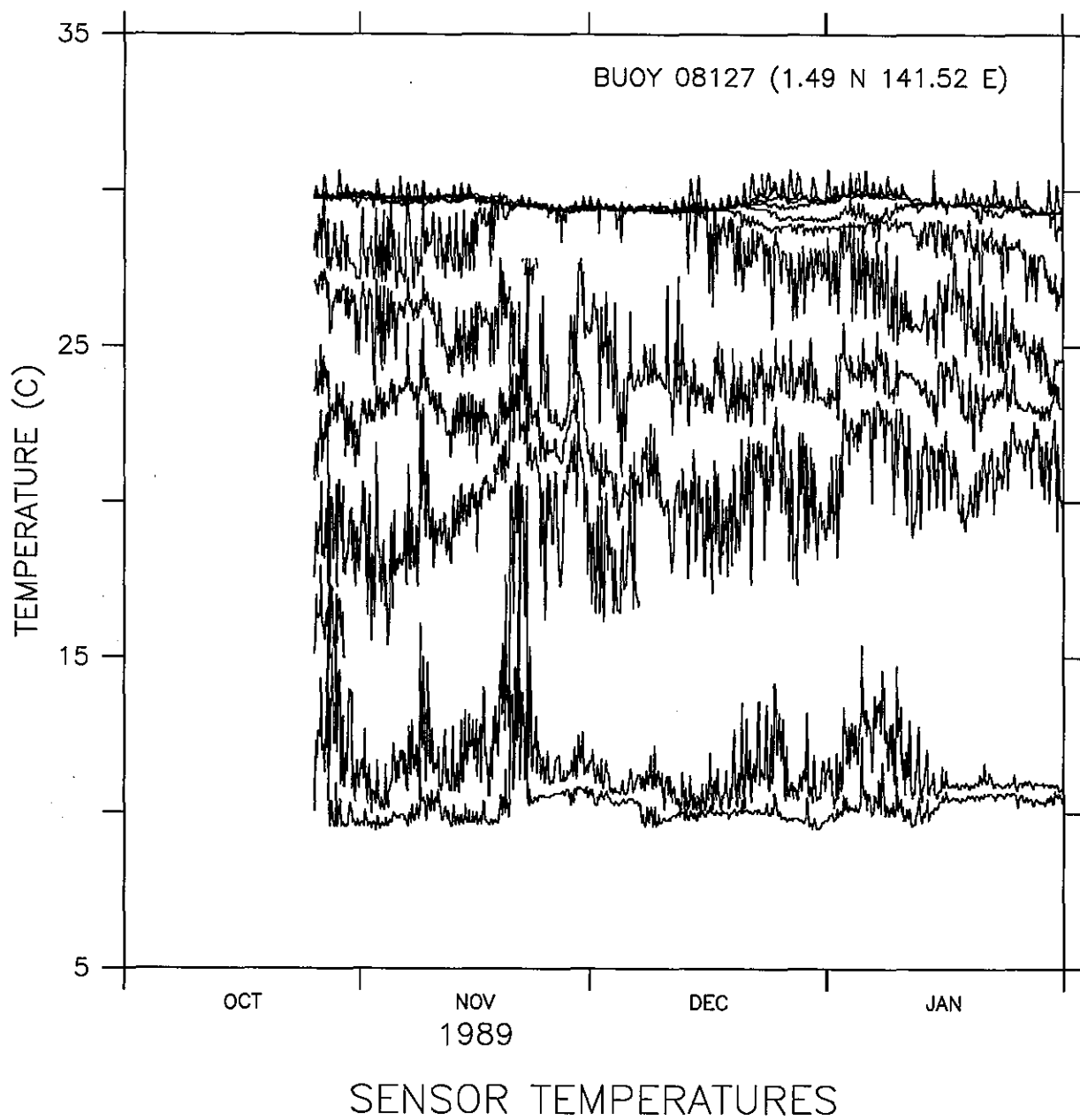


Figure 77.



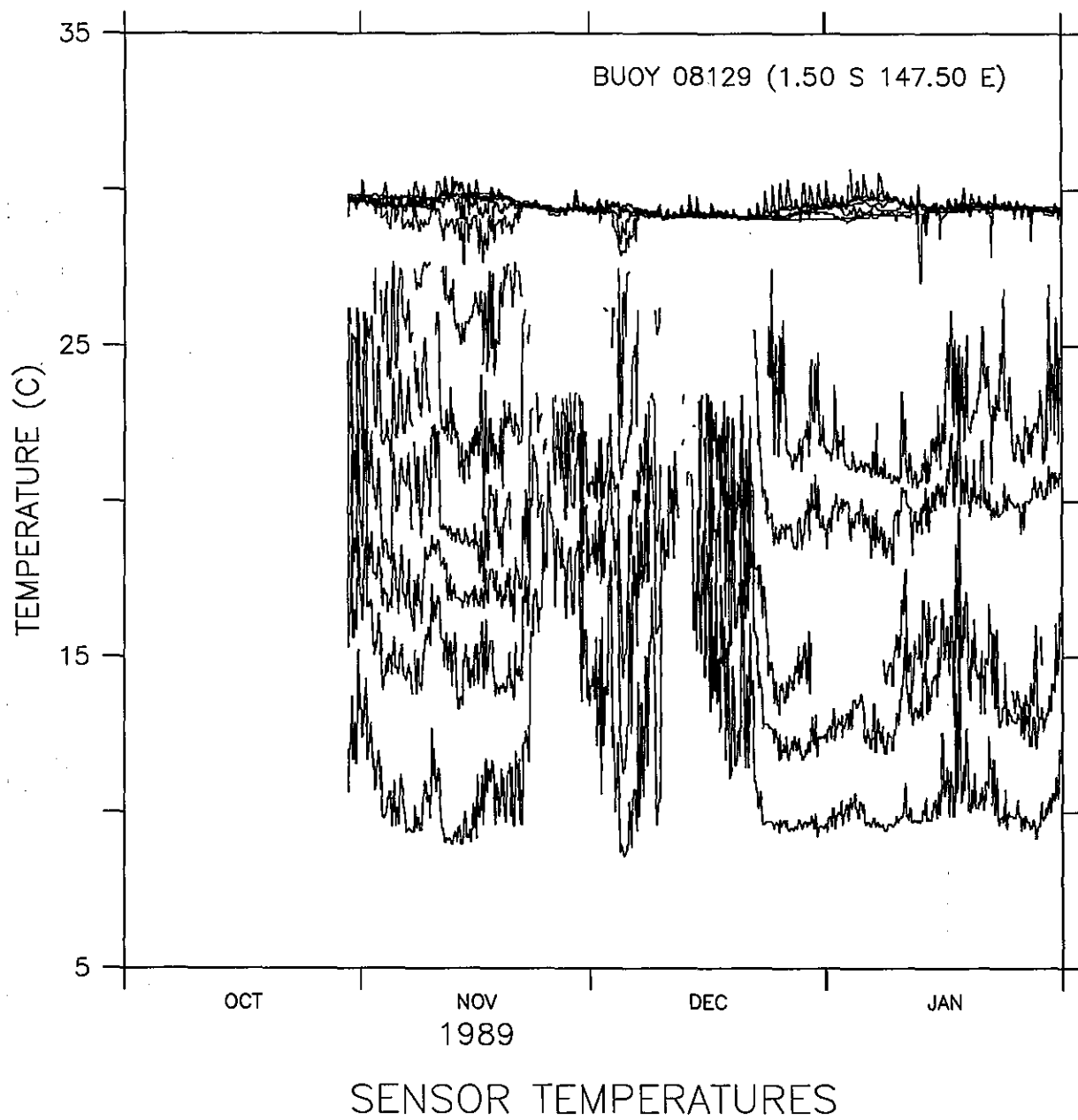


Figure 78.

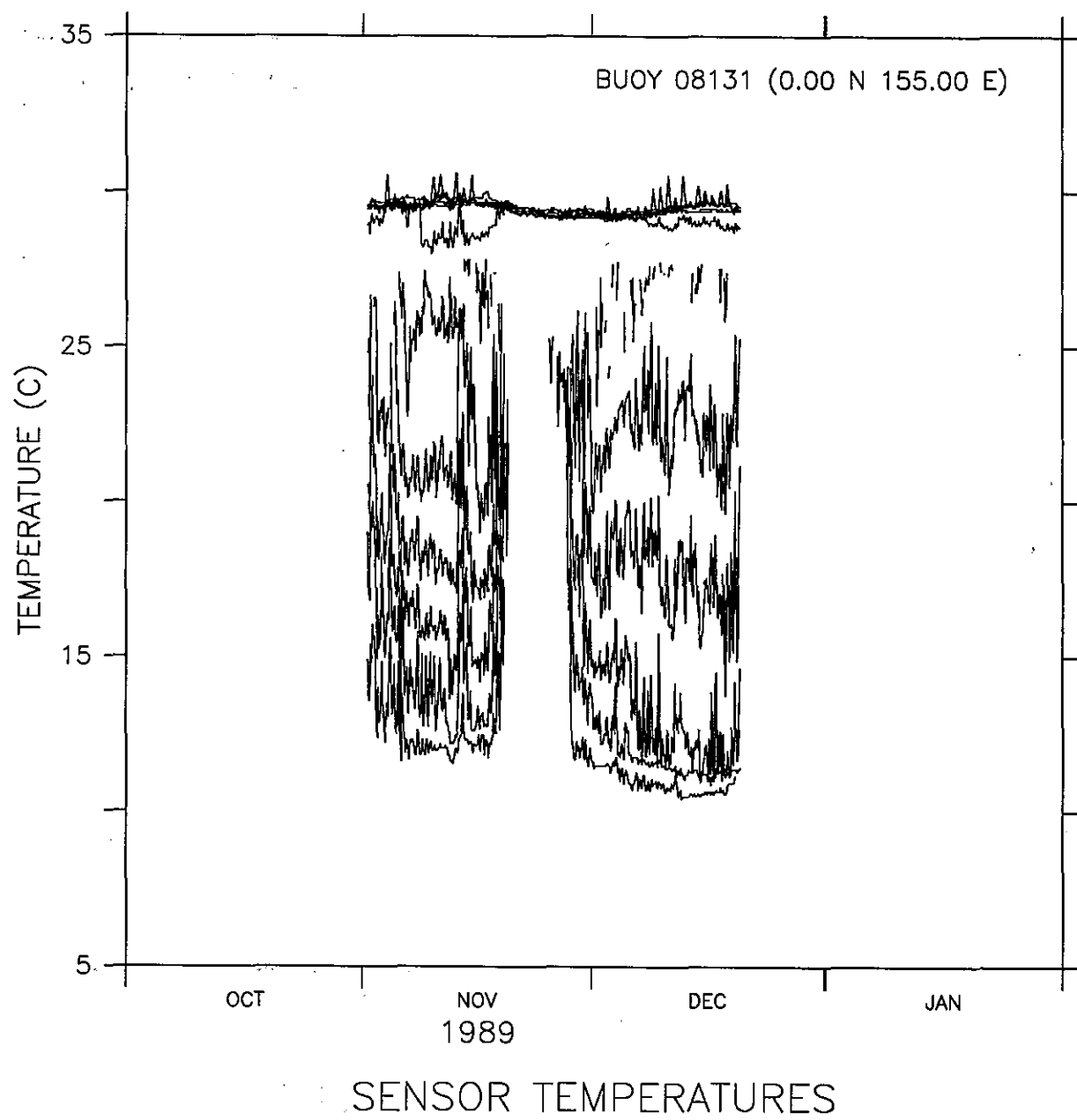


Figure 79.

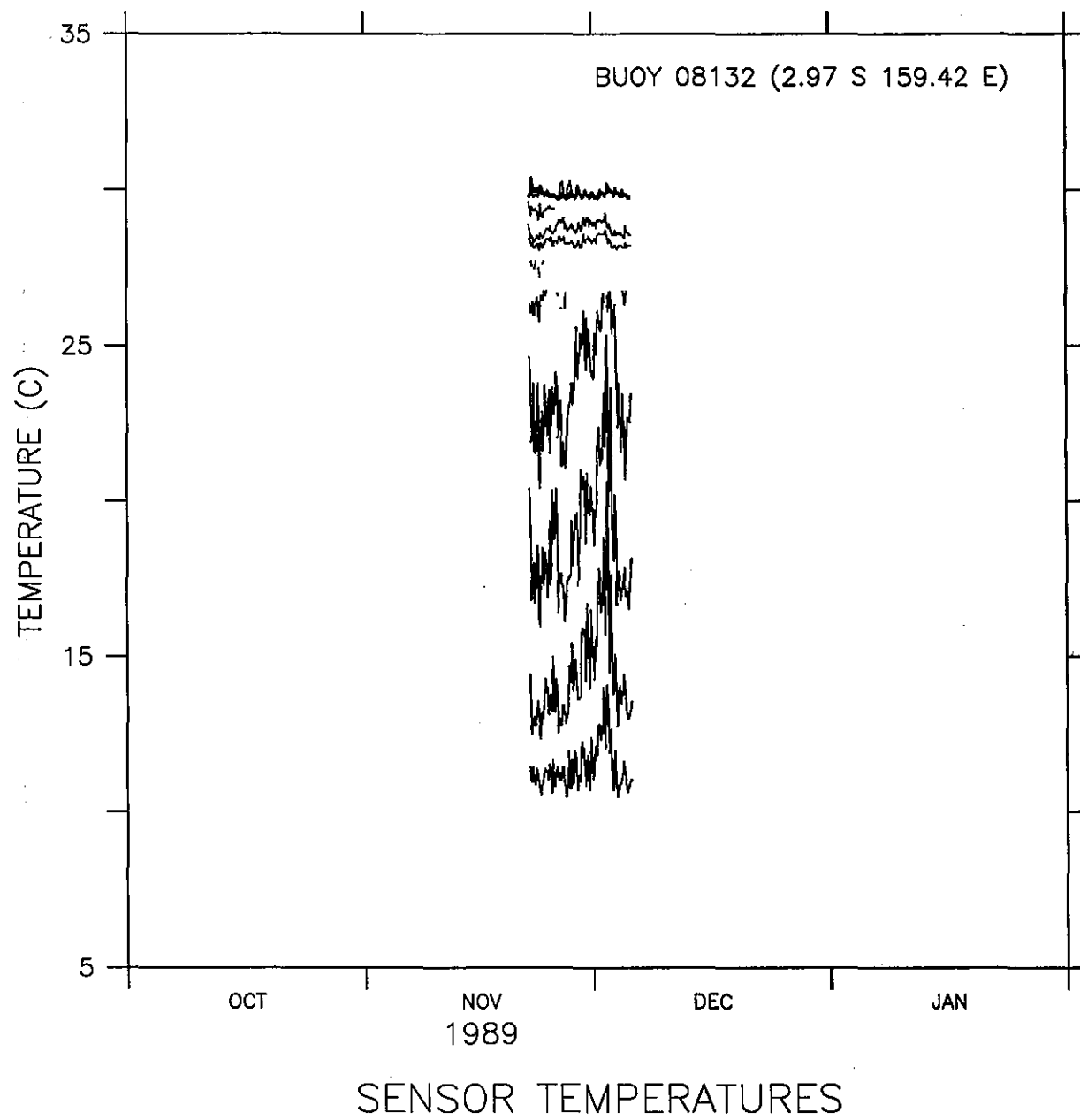


Figure 80.

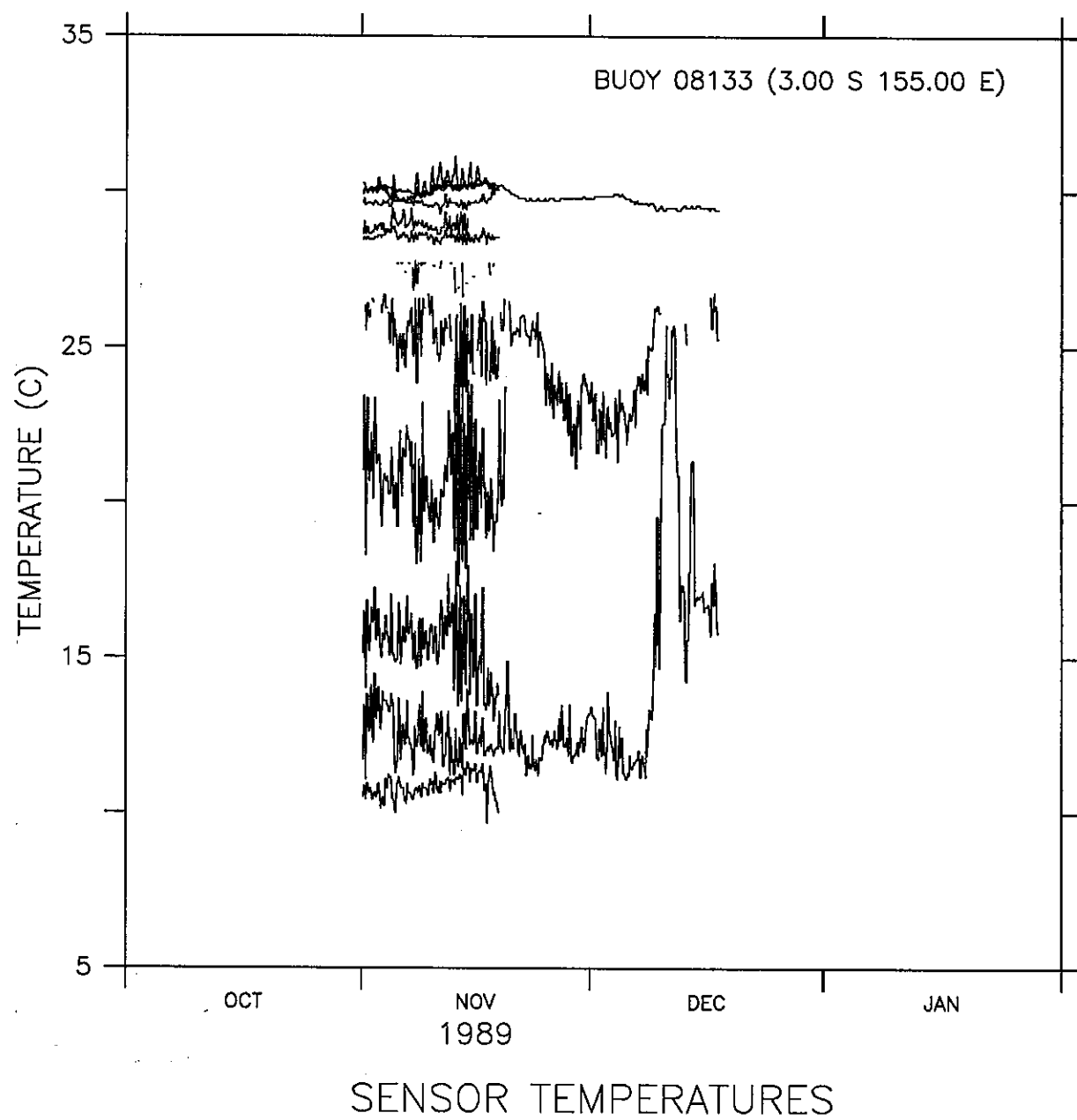


Figure 81.

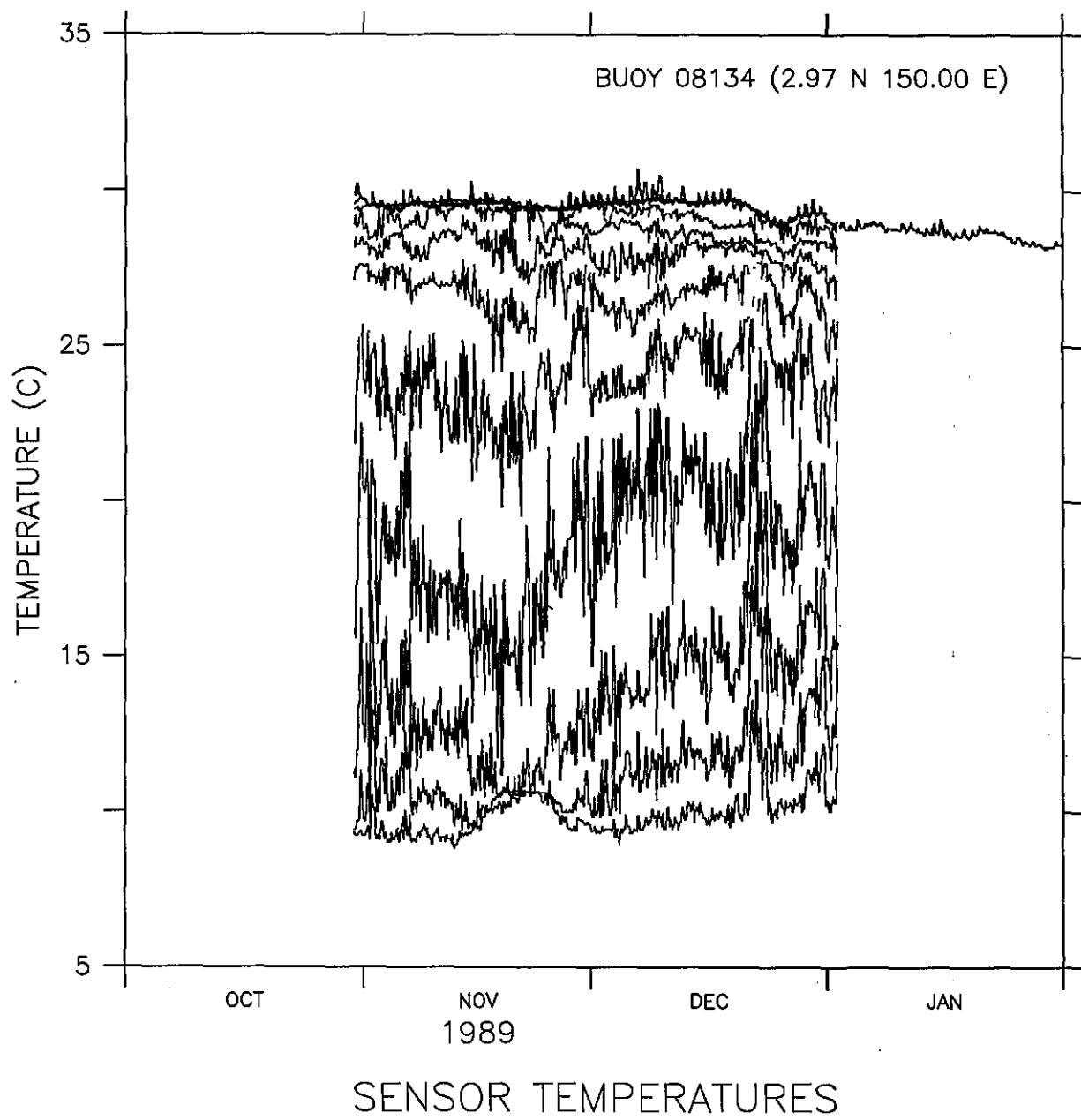


Figure 82.

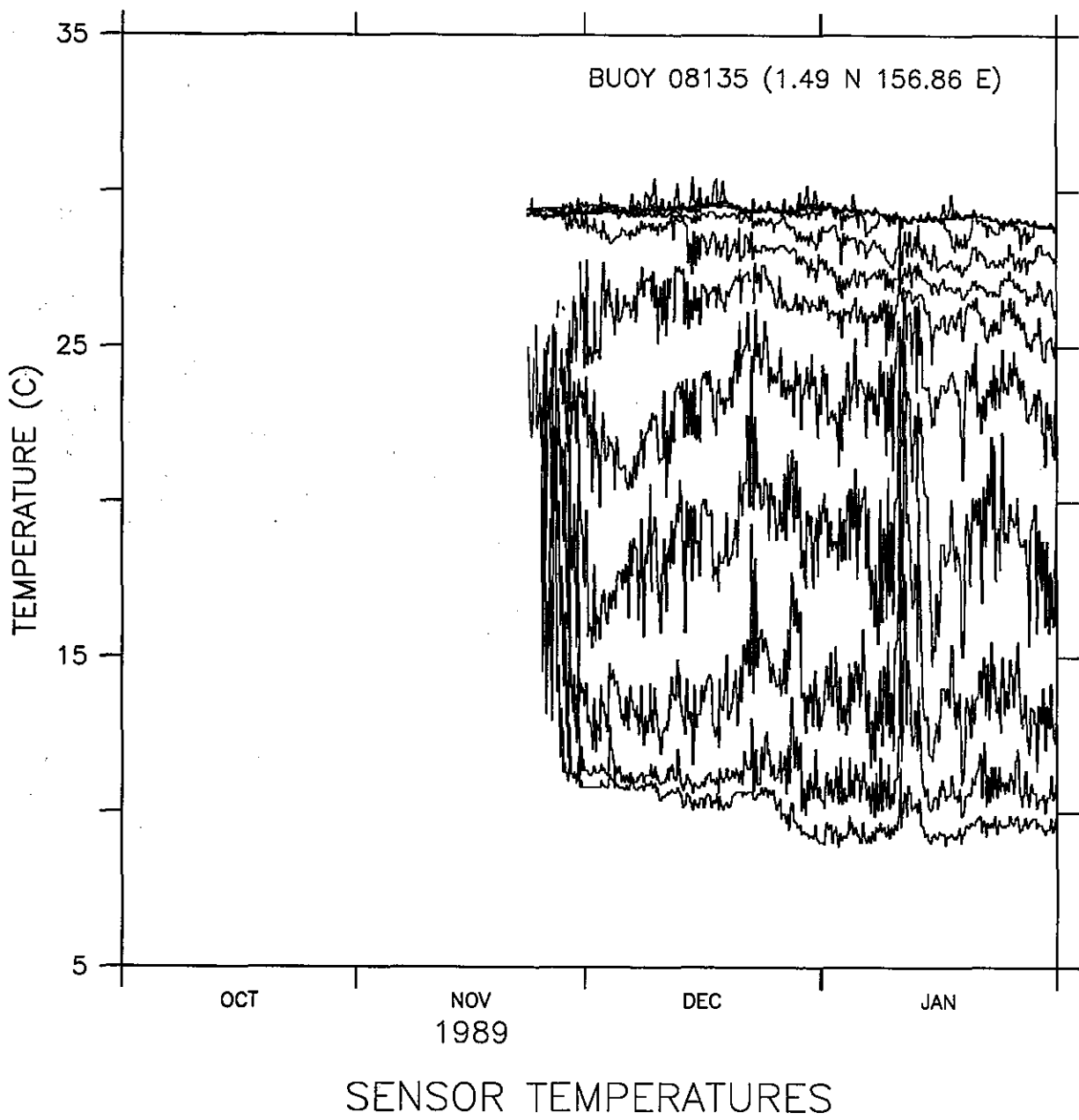


Figure 83.

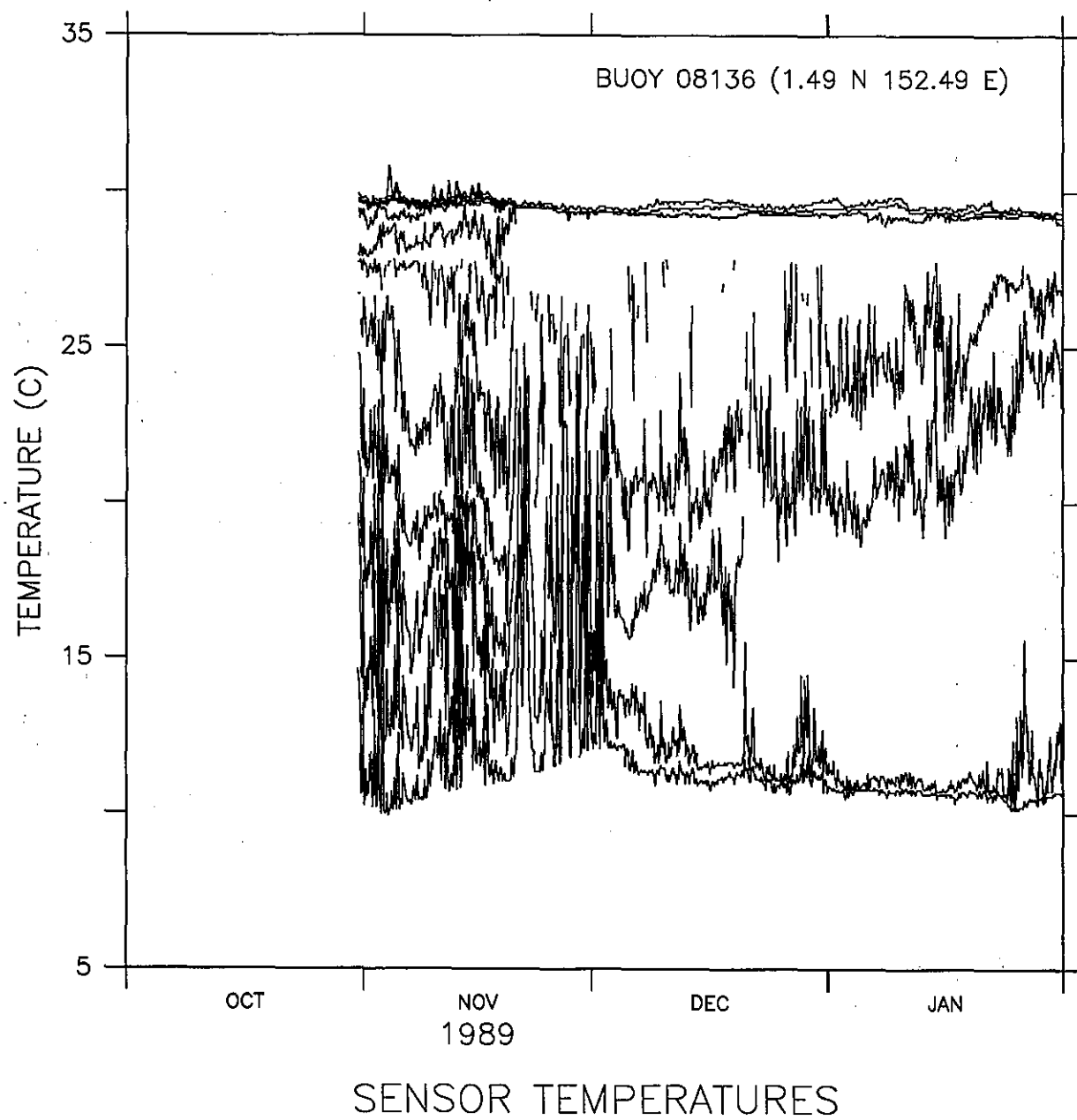


Figure 84.

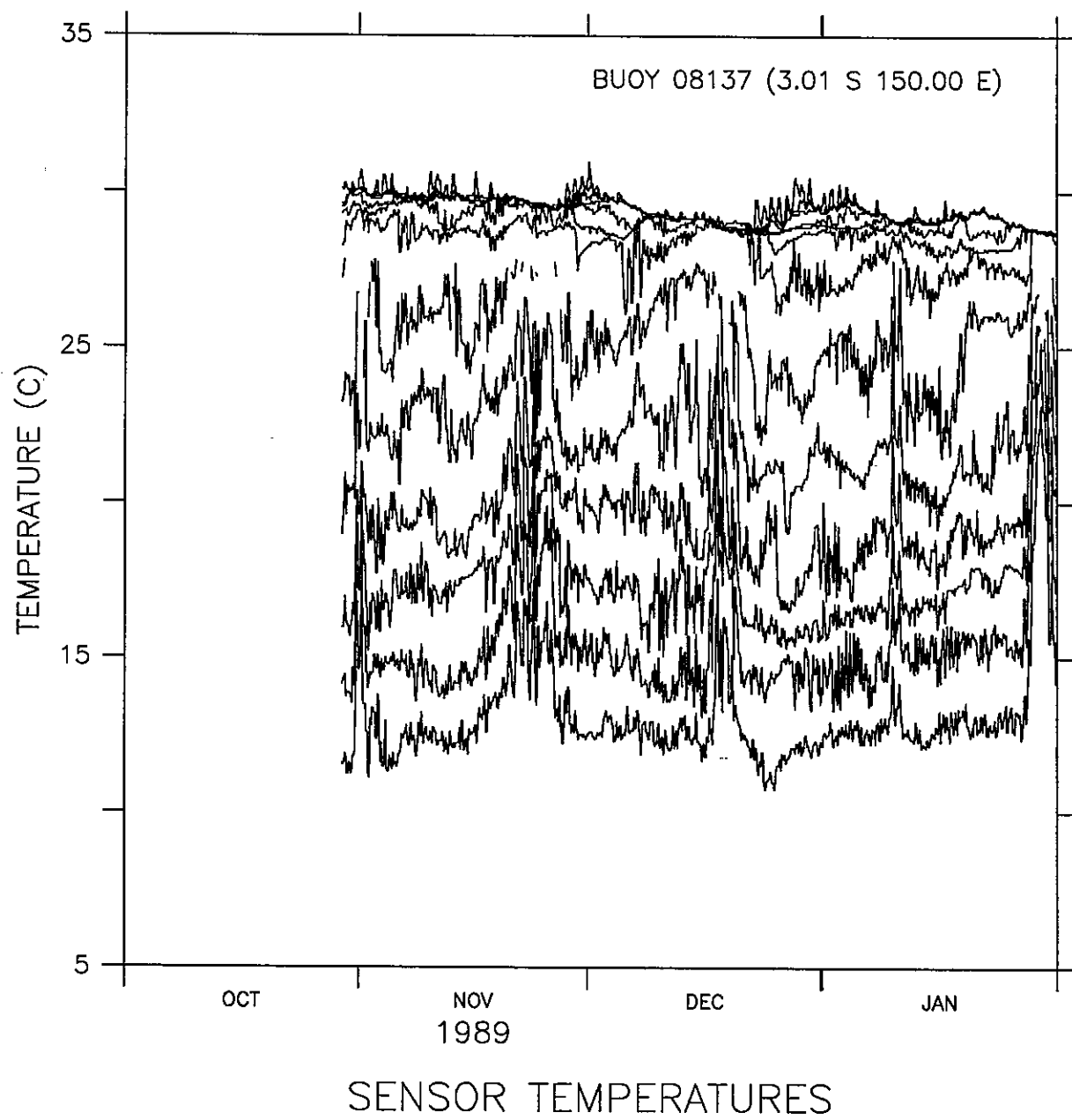


Figure 85.



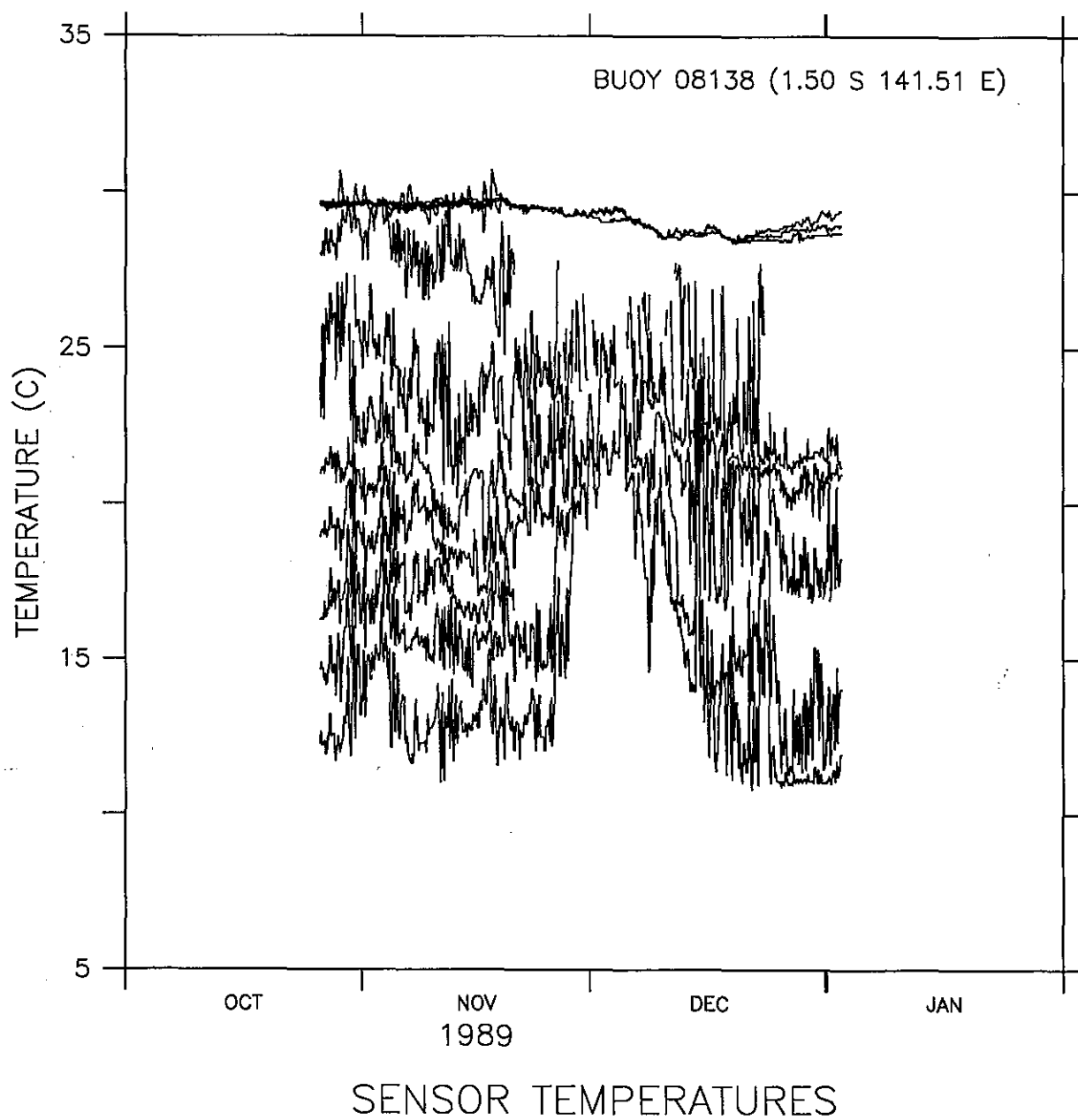


Figure 86.

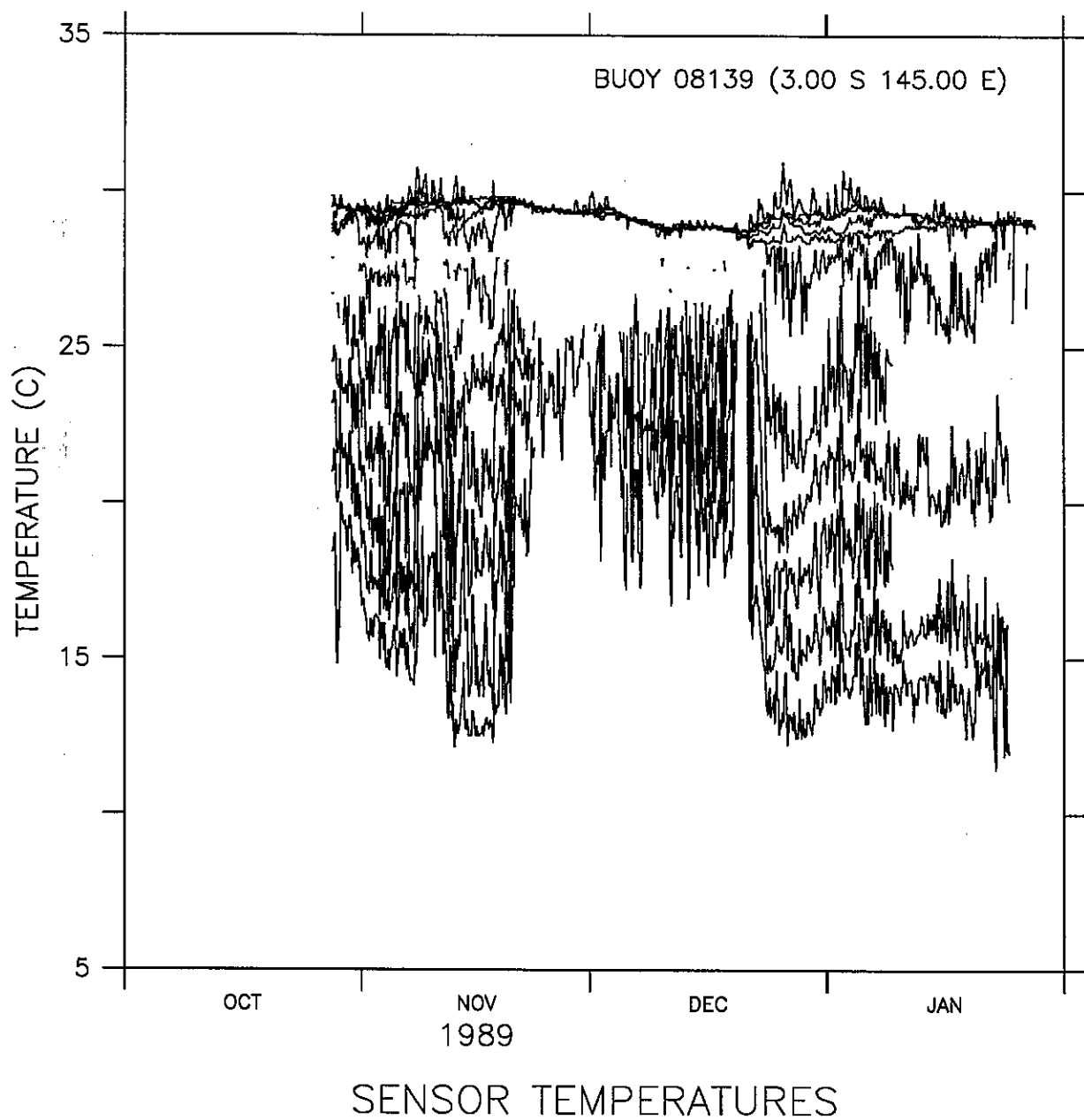


Figure 87.

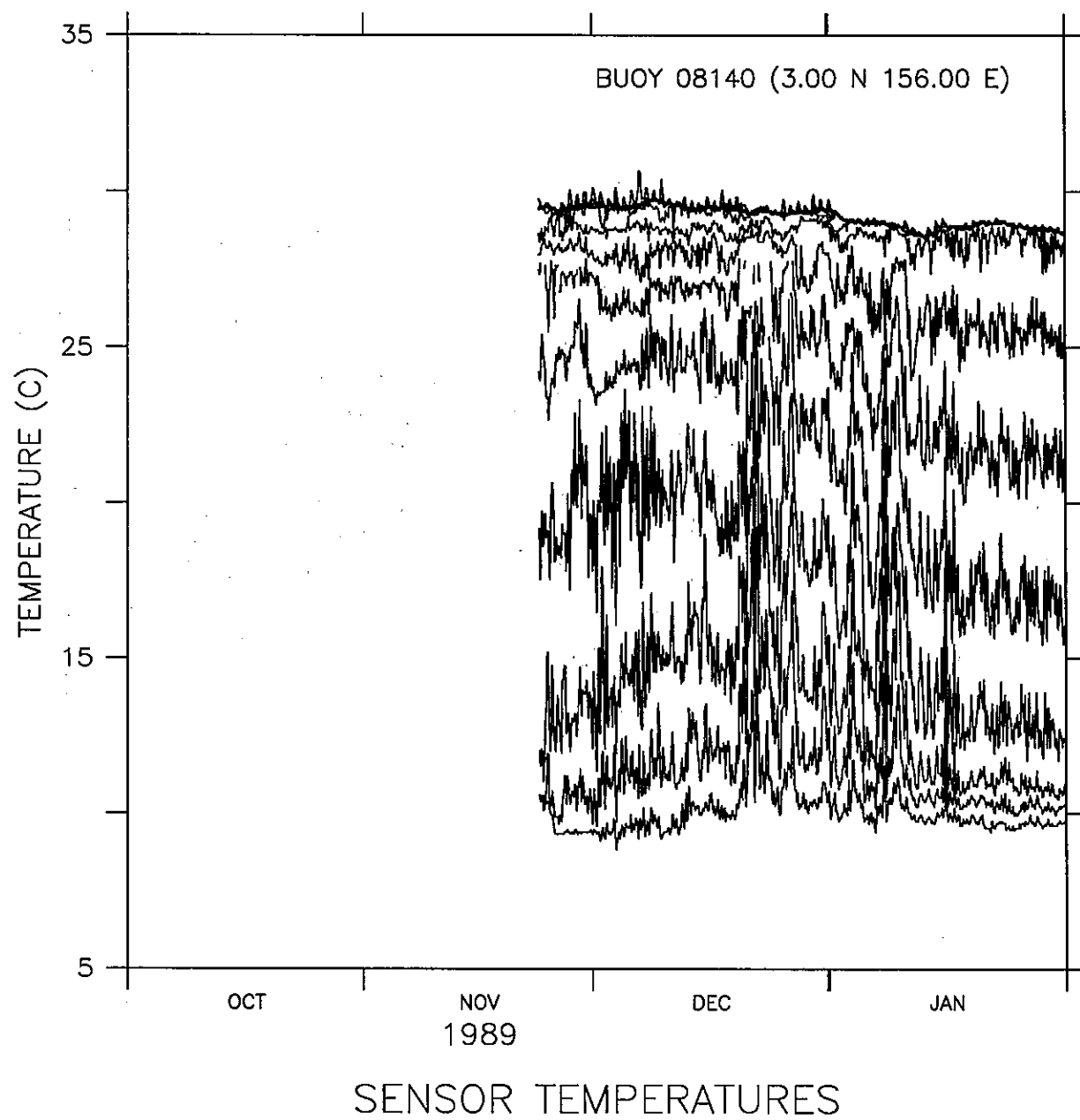


Figure 88.

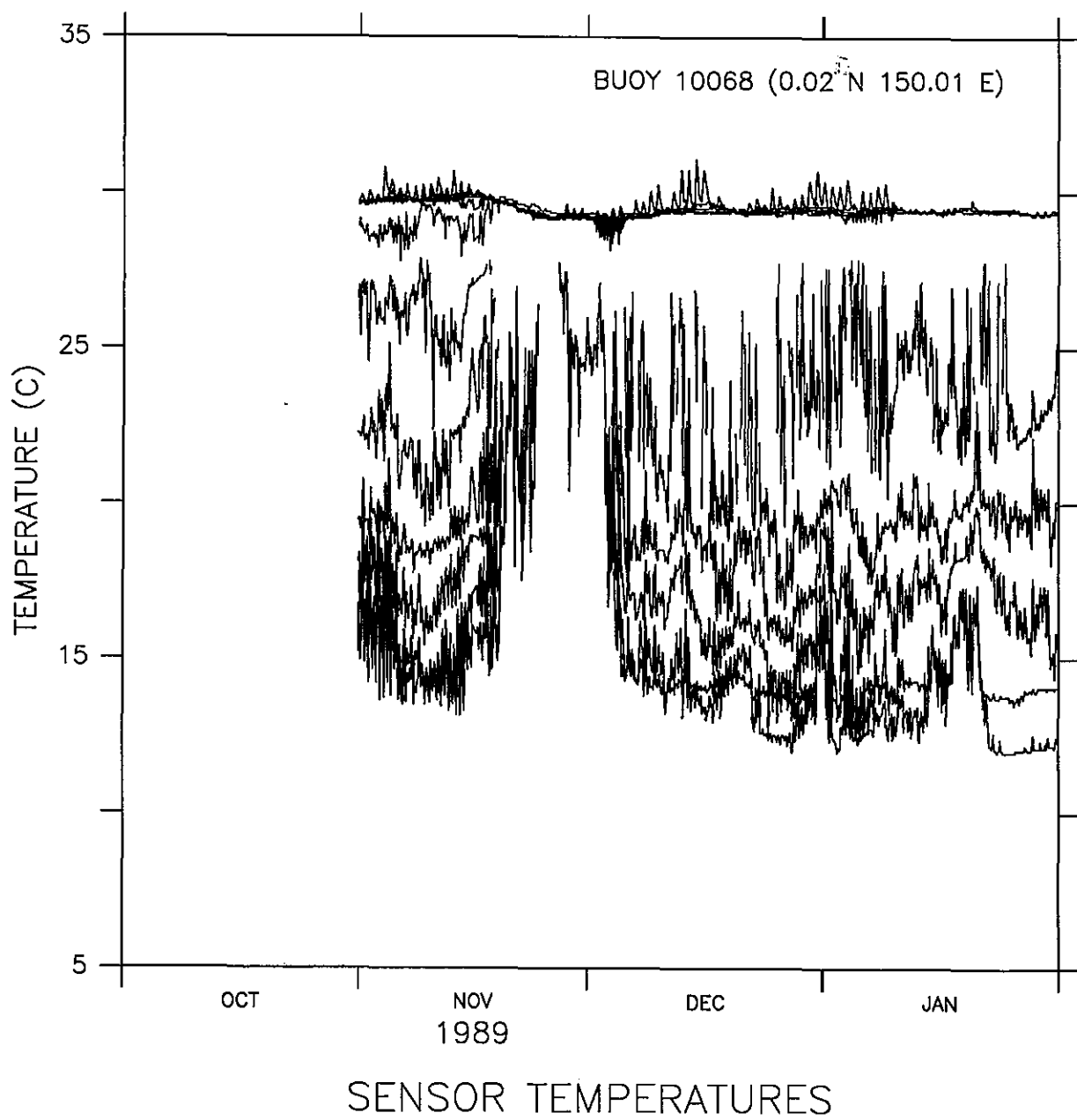
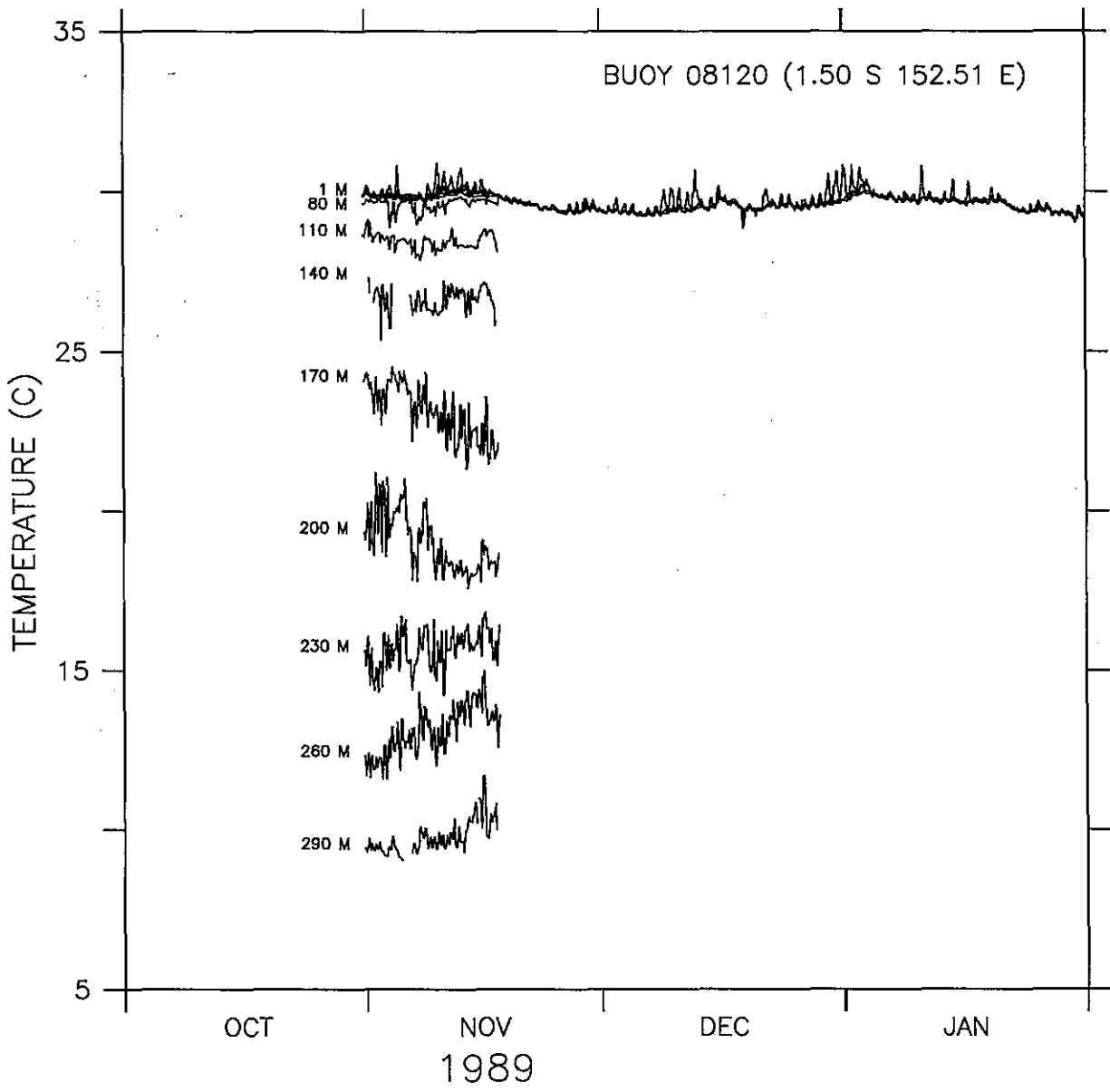


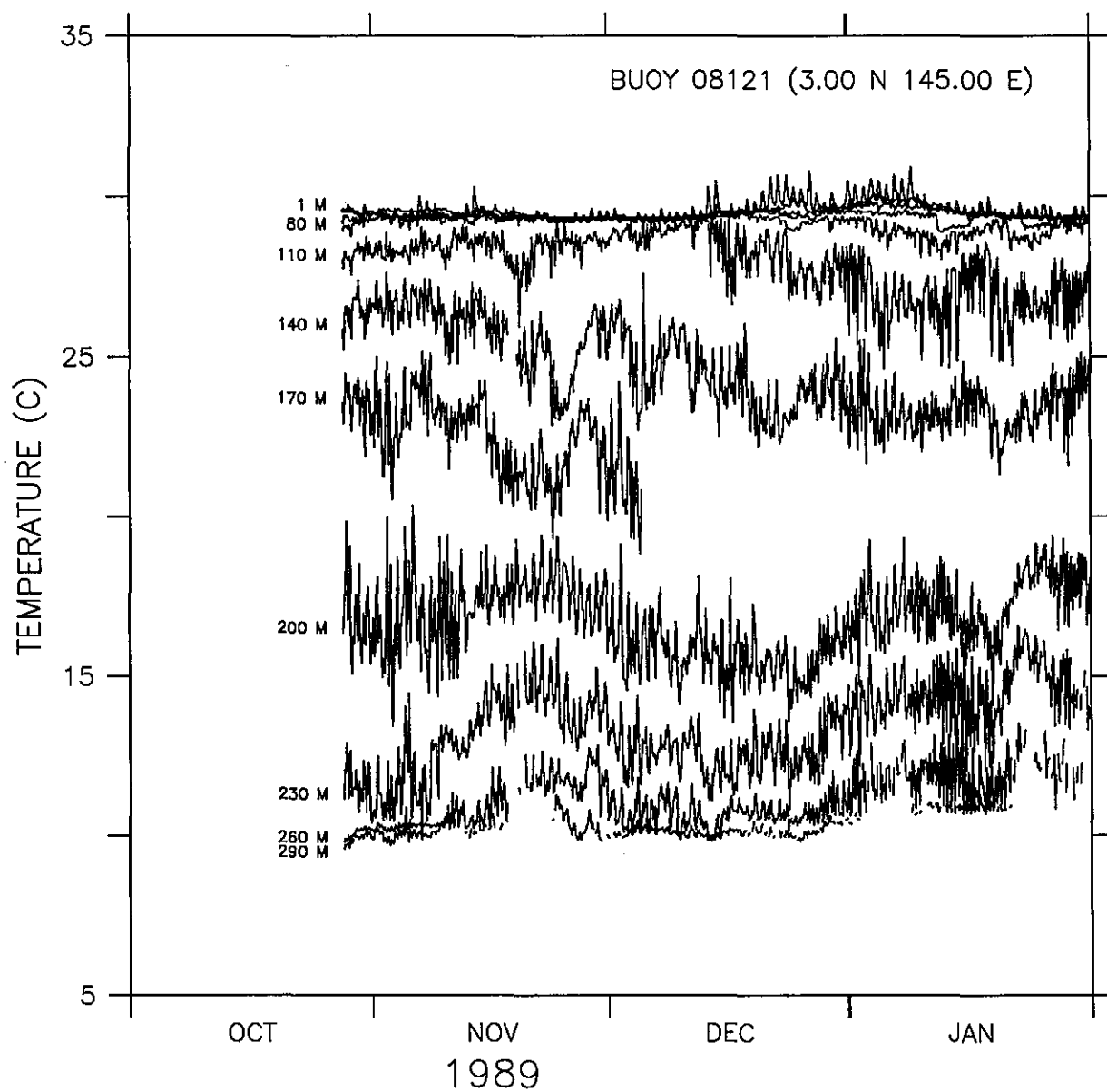
Figure 91.

Figures 92–110. Time series of 3-hourly temperatures at fixed depths for PRL drifters.



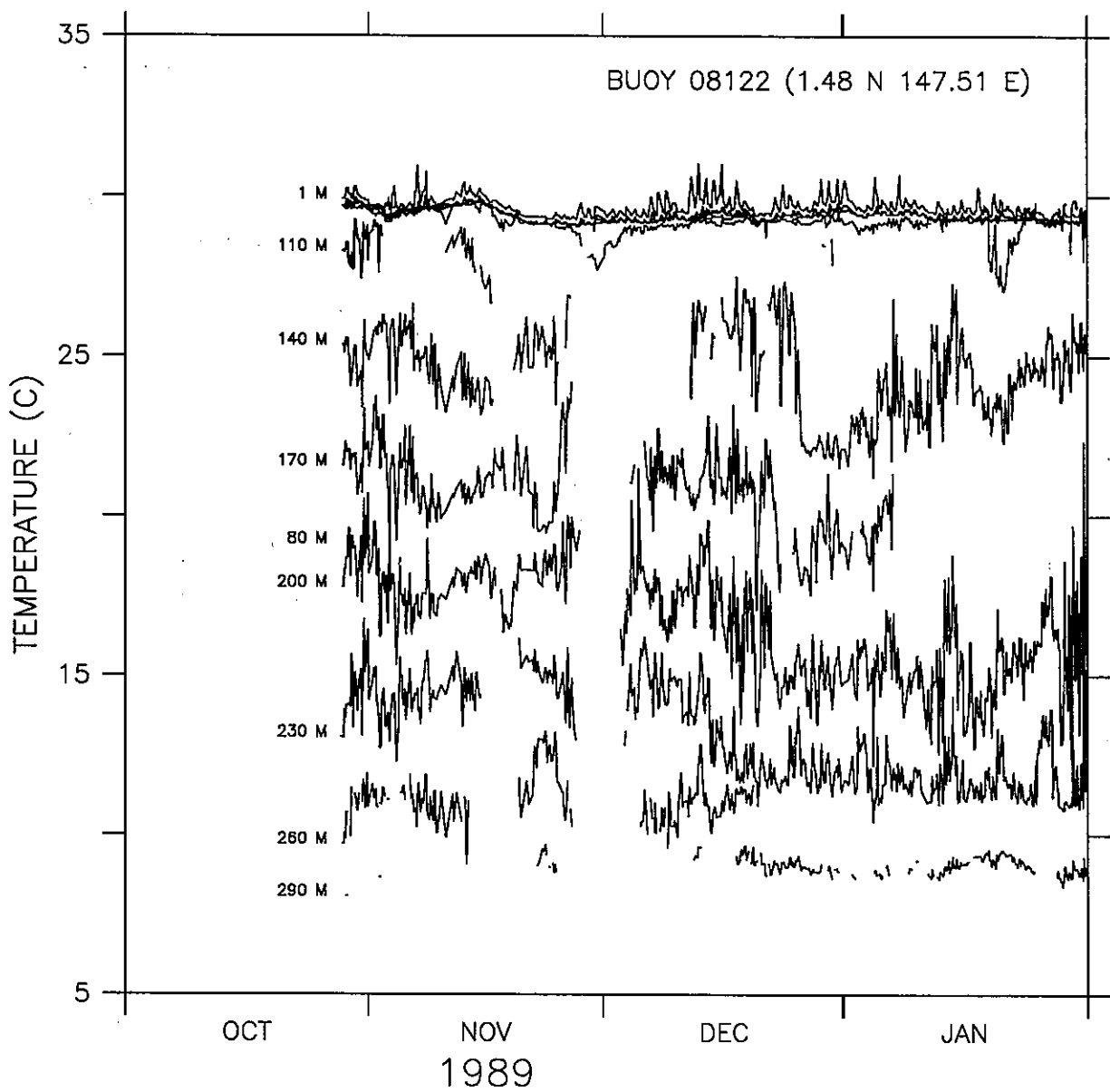
## TEMPERATURES AT FIXED DEPTHS

Figure 92.



## TEMPERATURES AT FIXED DEPTHS

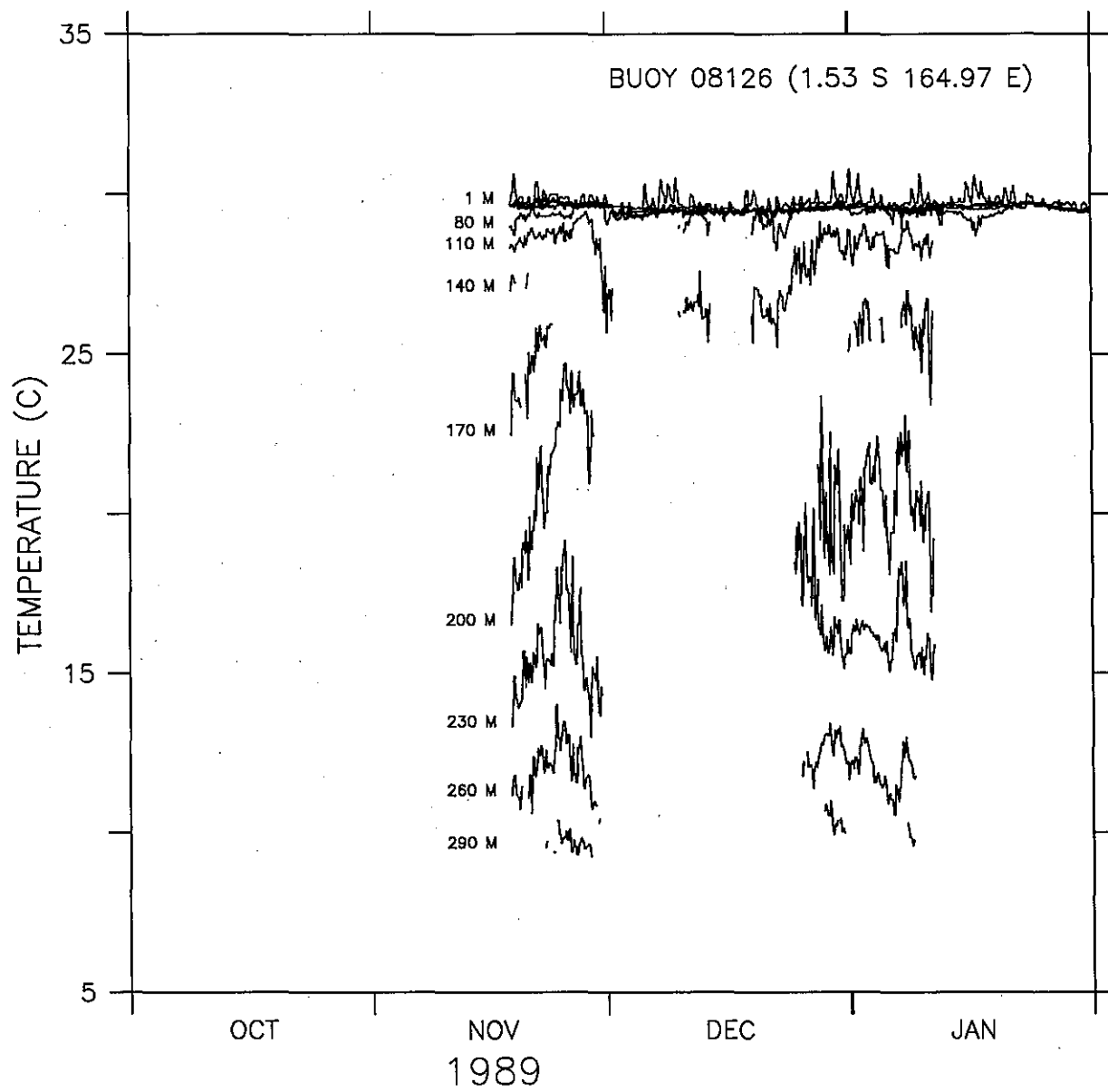
Figure 93.



## TEMPERATURES AT FIXED DEPTHS

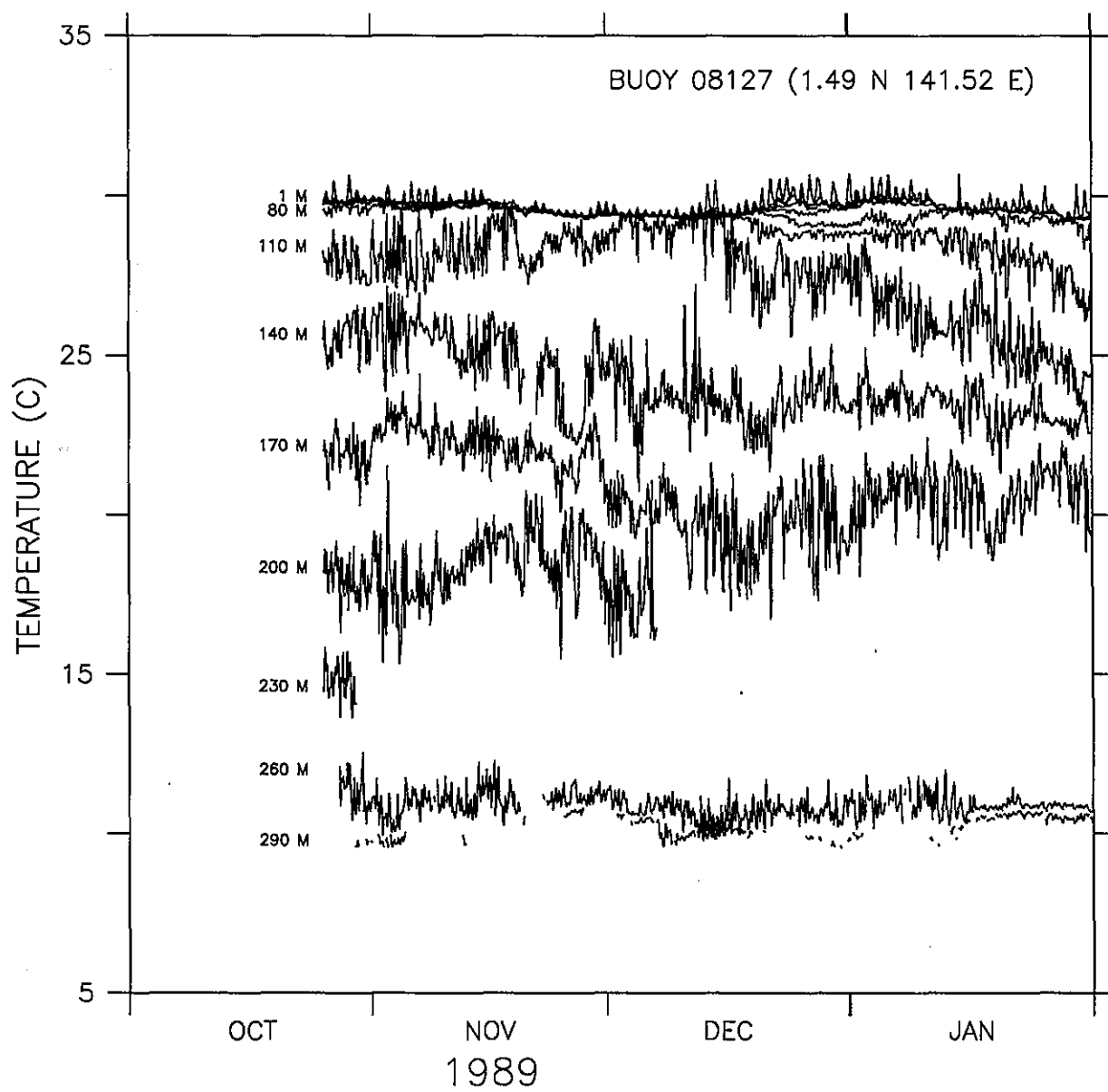
Figure 94.





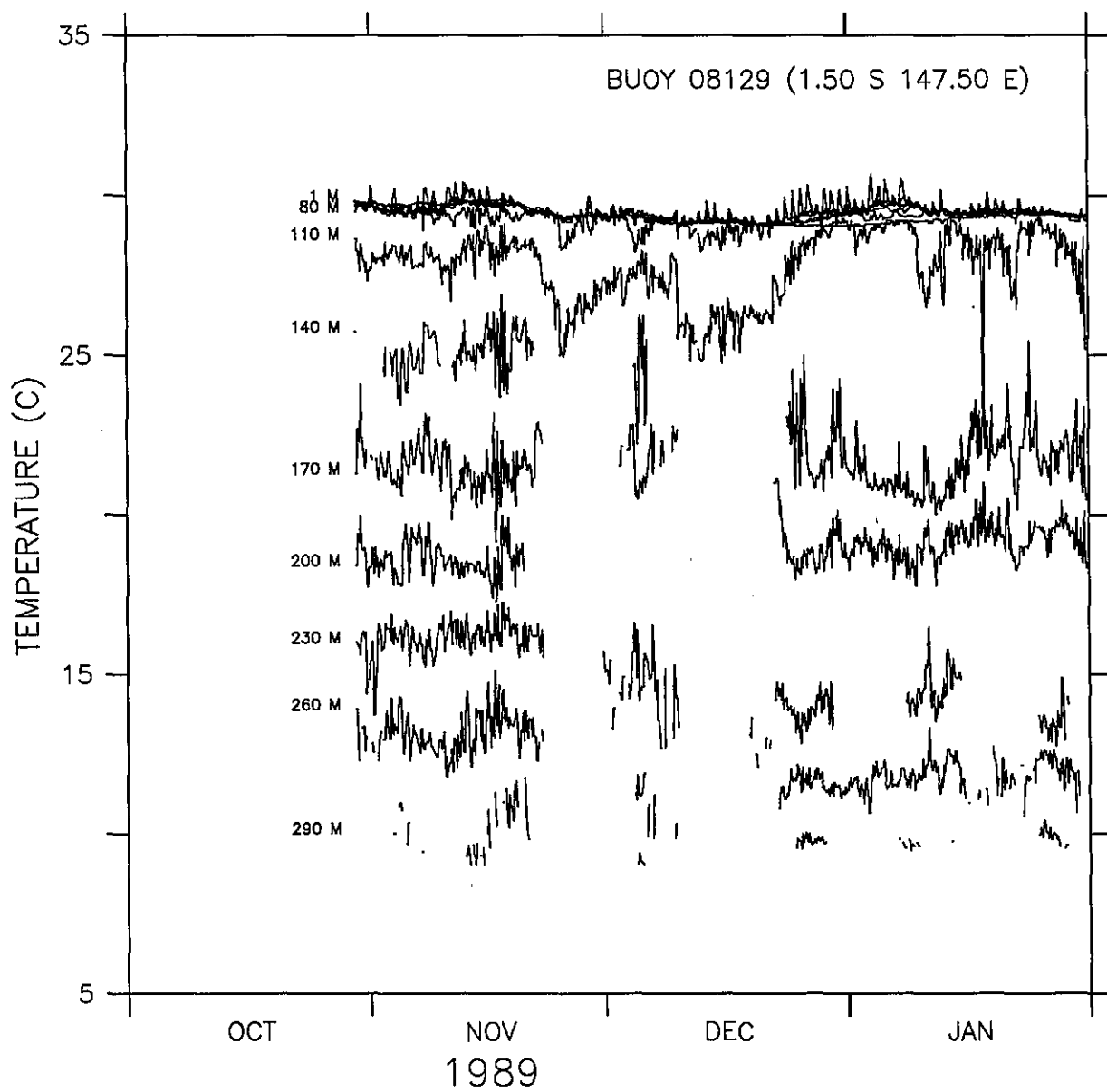
## TEMPERATURES AT FIXED DEPTHS

Figure 95.



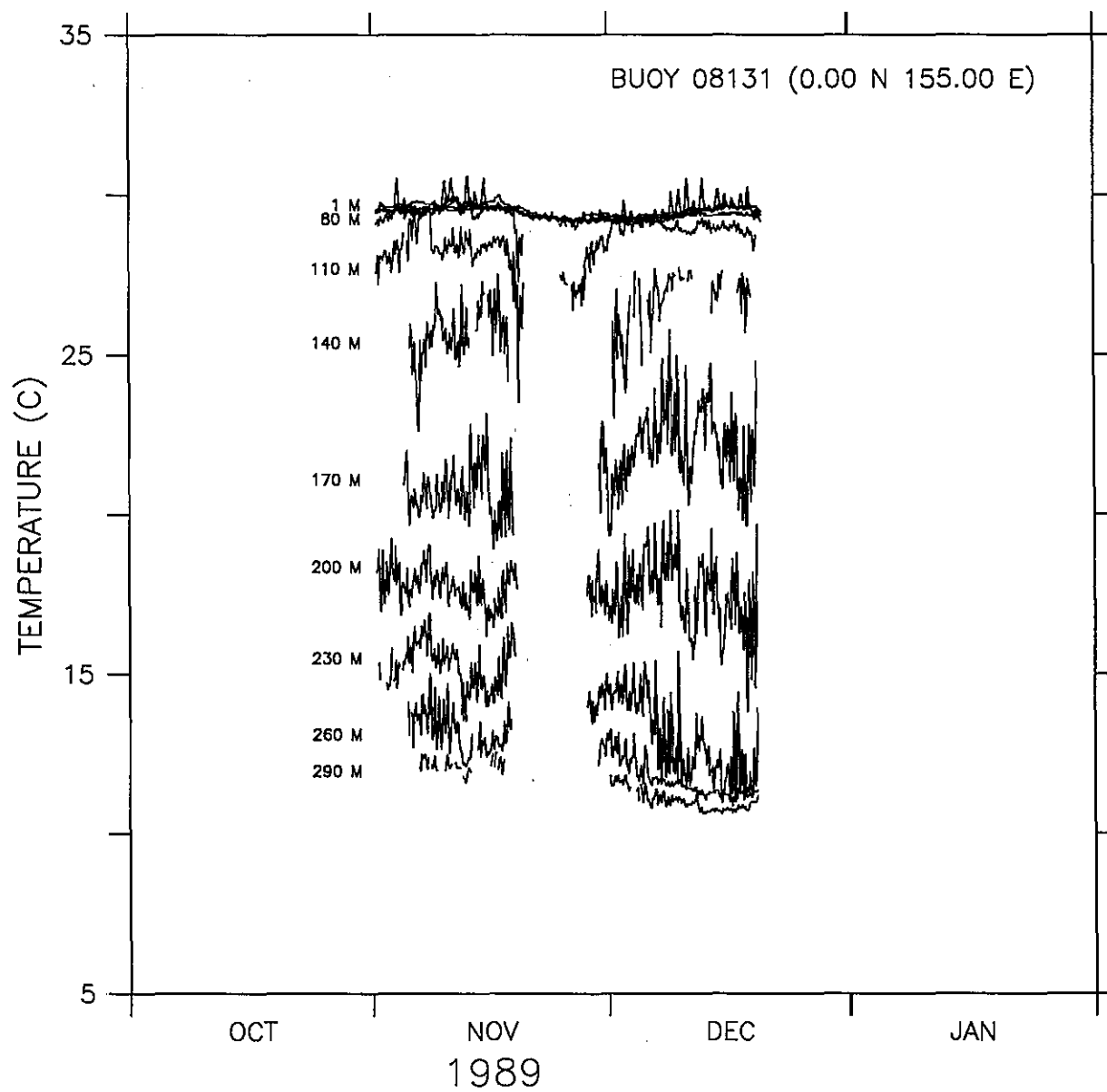
## TEMPERATURES AT FIXED DEPTHS

Figure 96.



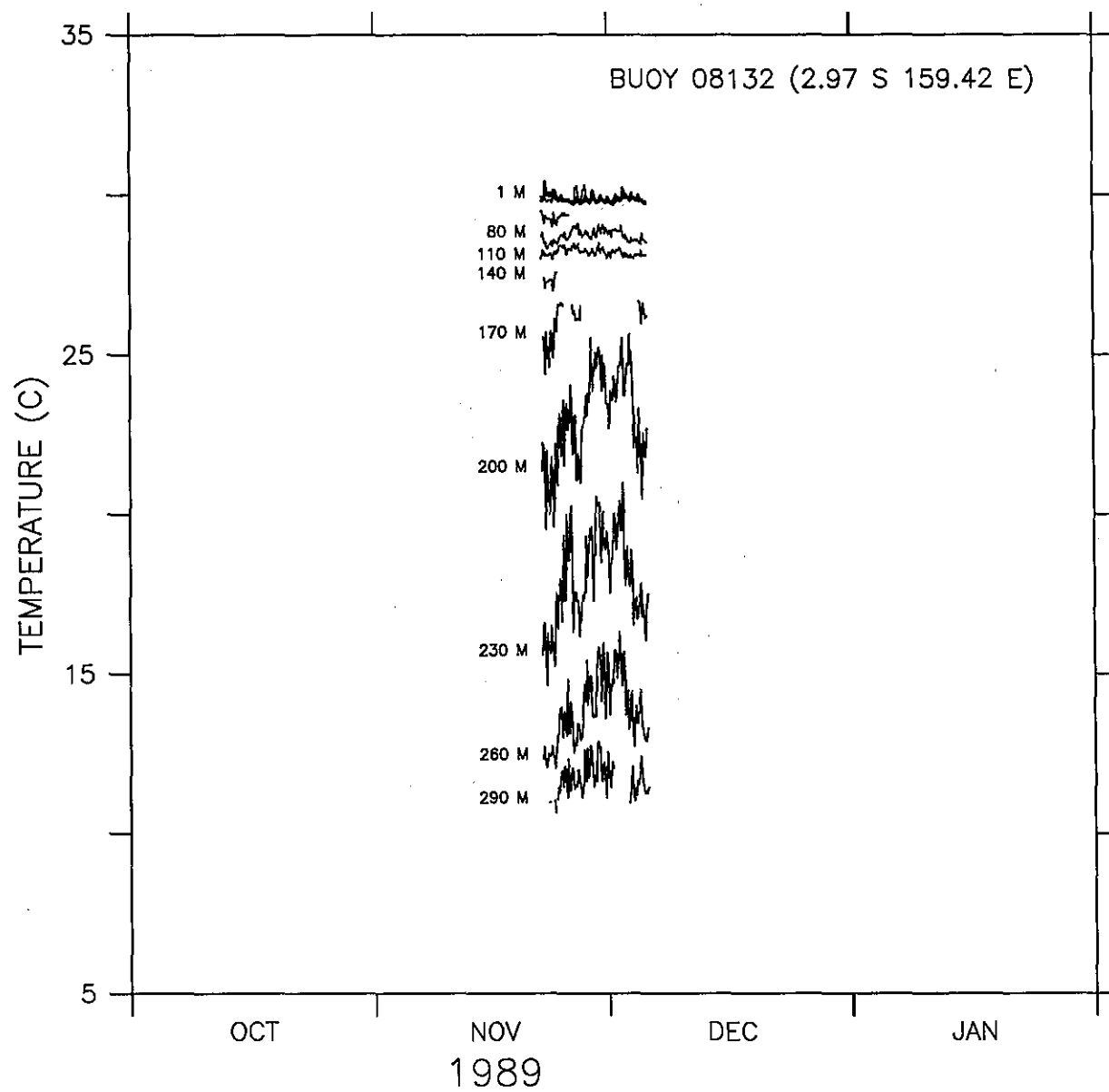
## TEMPERATURES AT FIXED DEPTHS

Figure 97.



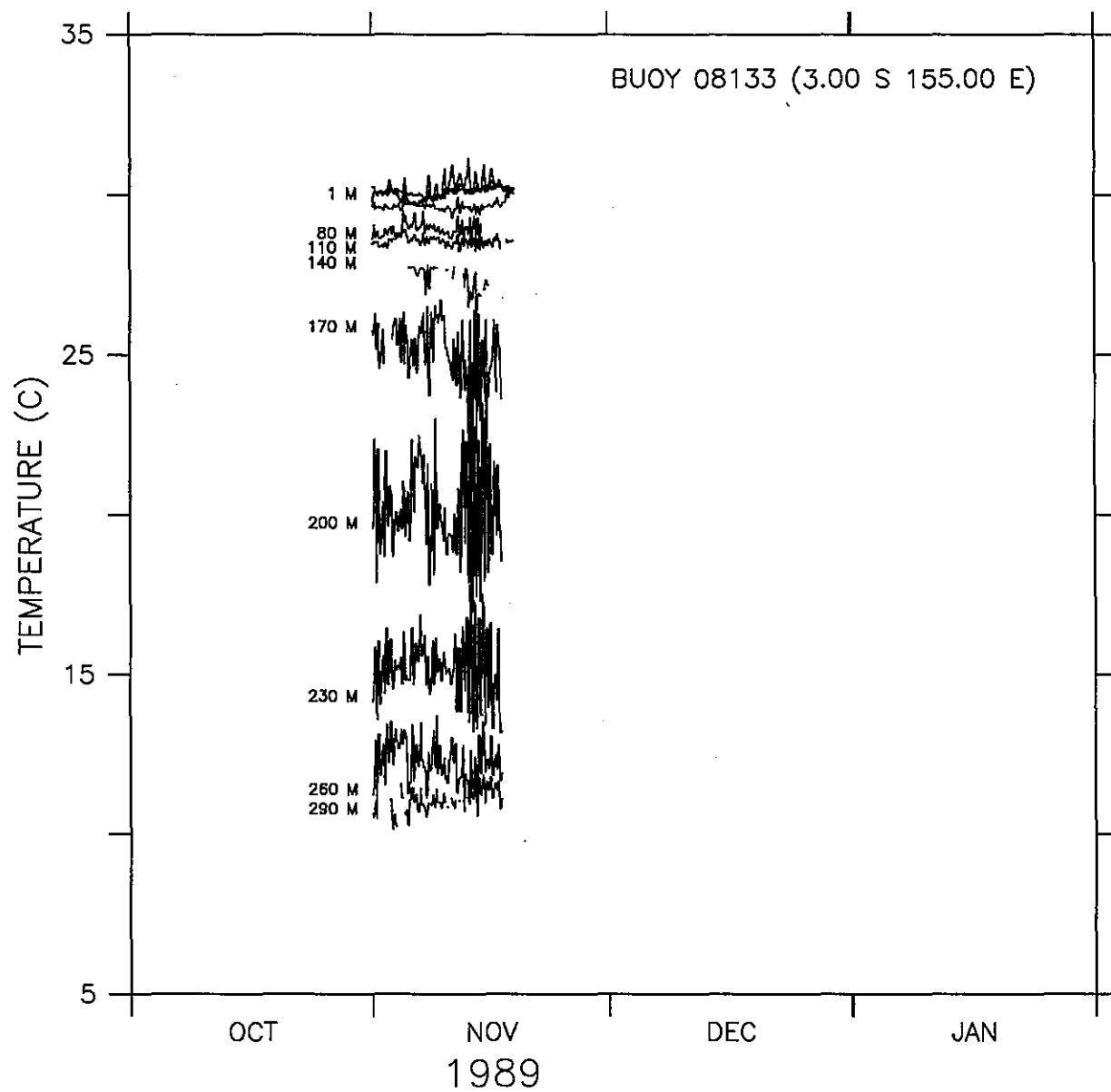
## TEMPERATURES AT FIXED DEPTHS

Figure 98.



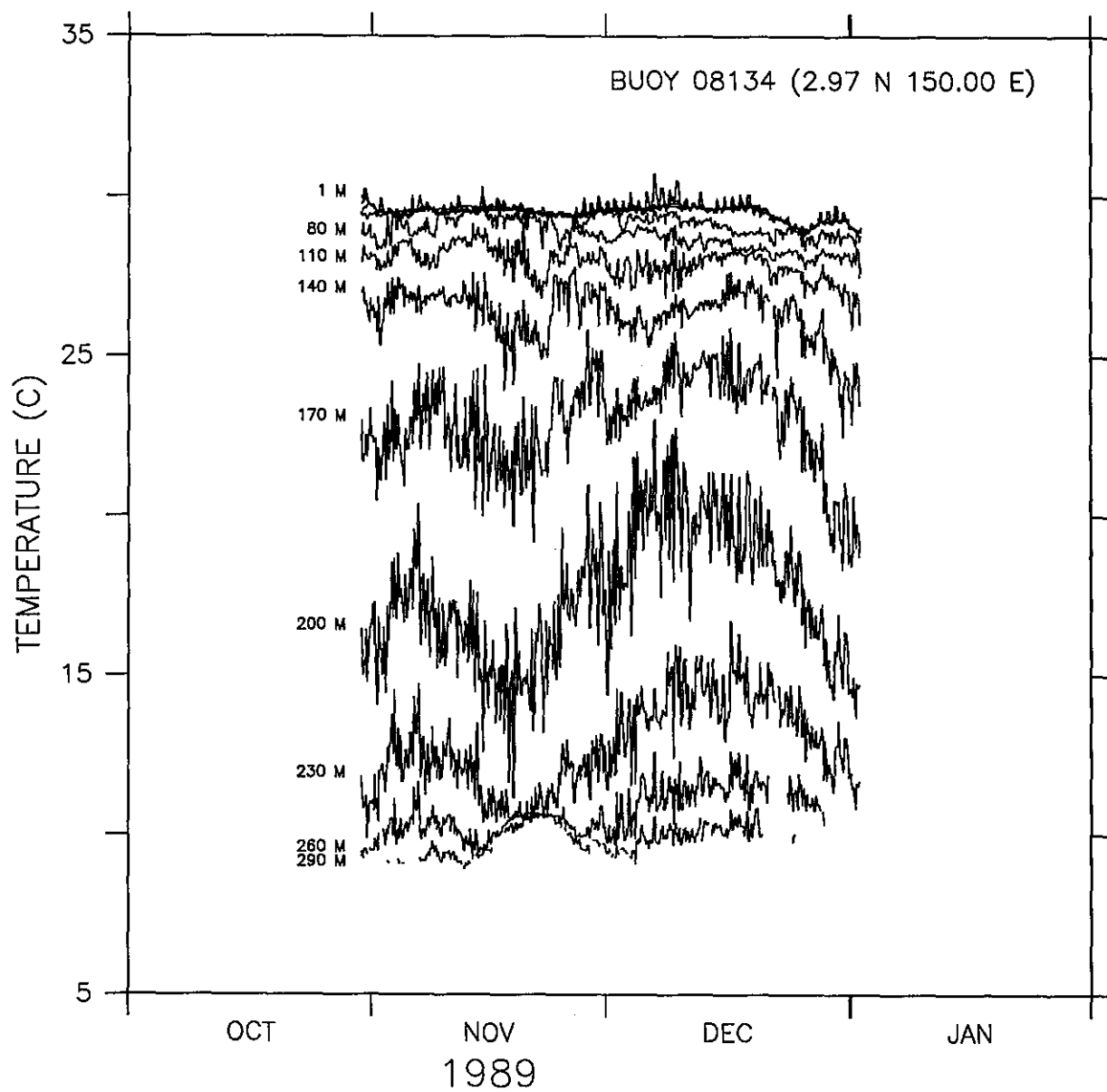
## TEMPERATURES AT FIXED DEPTHS

Figure 99.



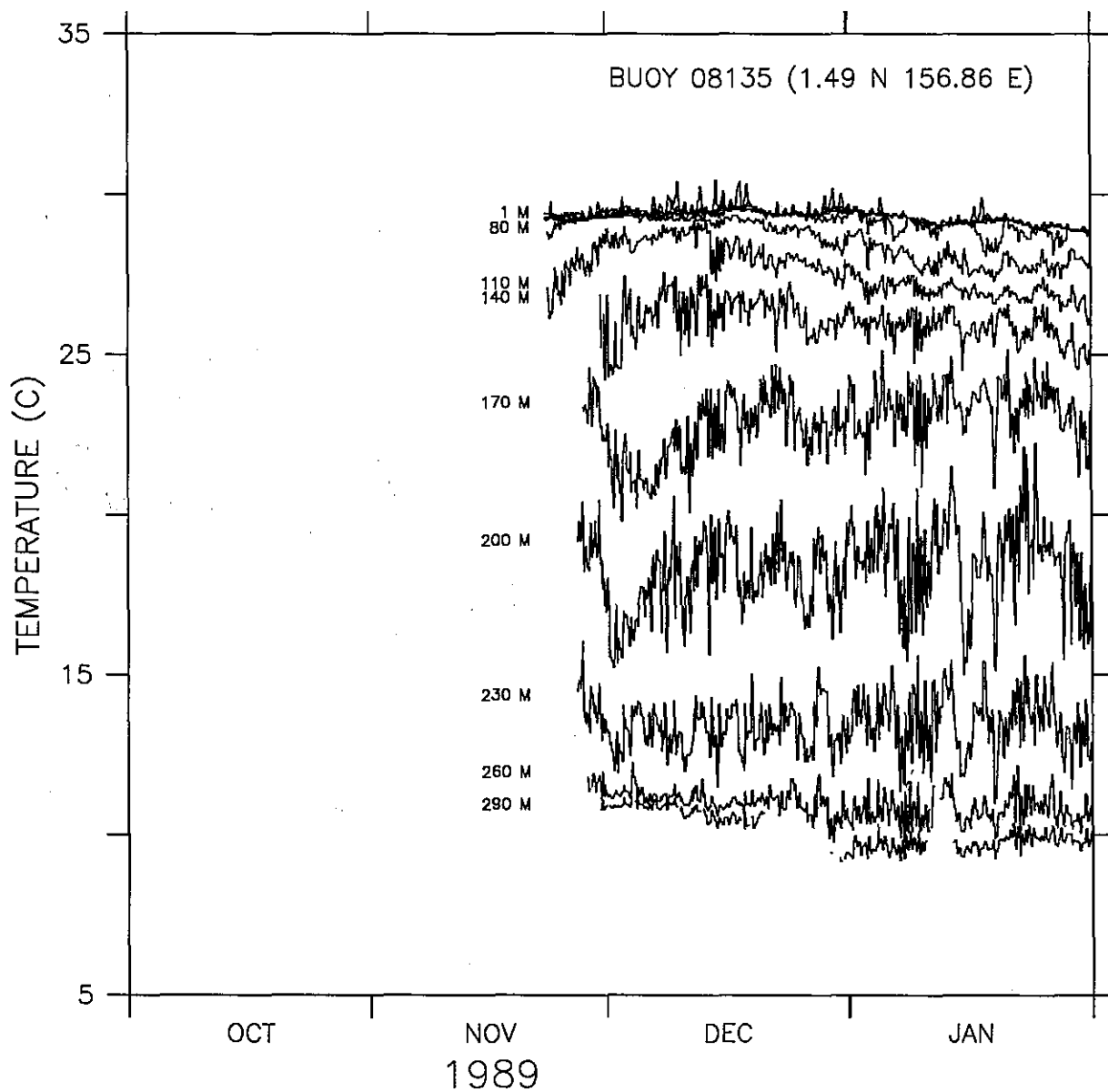
## TEMPERATURES AT FIXED DEPTHS

Figure 100.



## TEMPERATURES AT FIXED DEPTHS

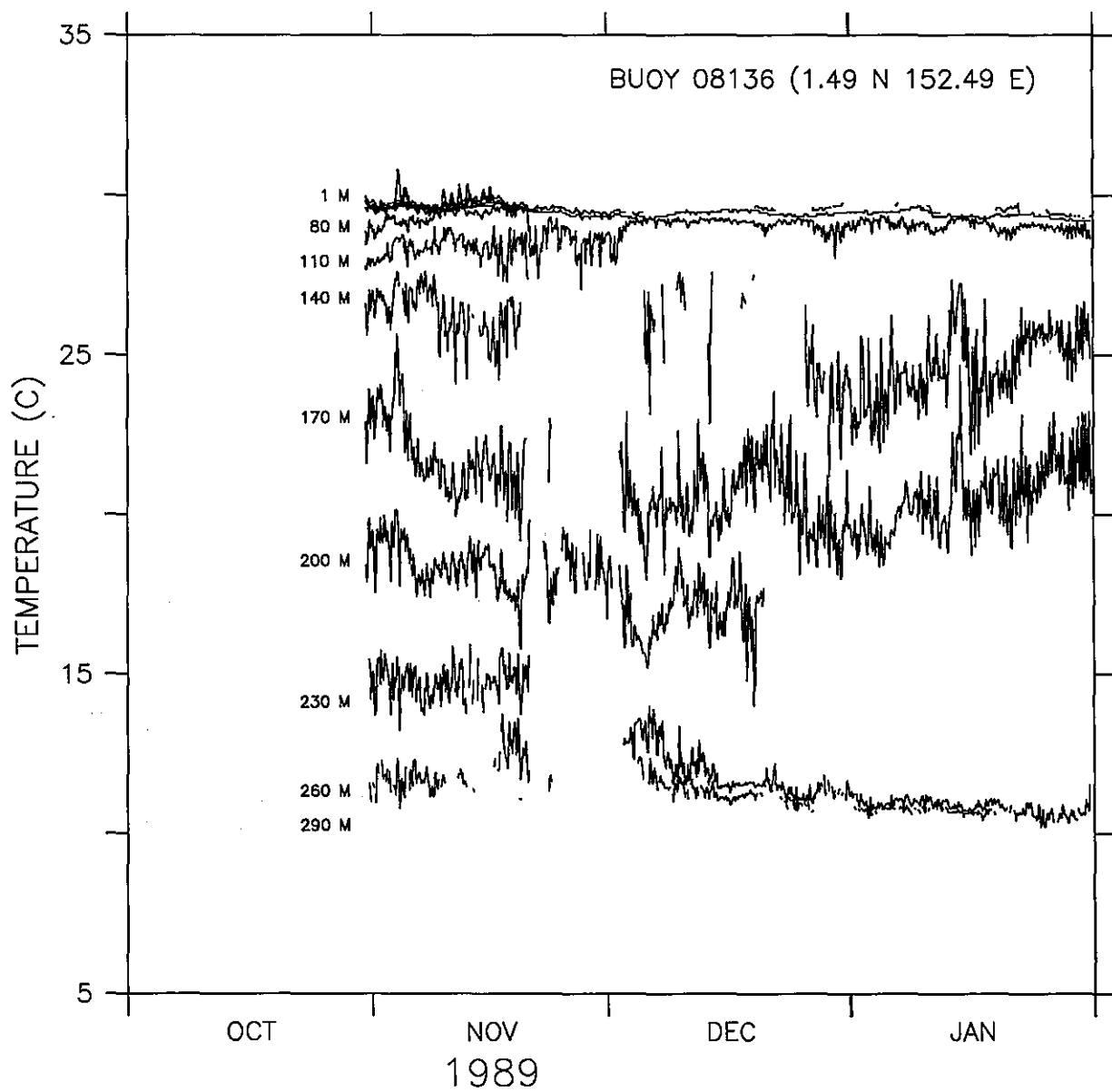
Figure 101.



## TEMPERATURES AT FIXED DEPTHS

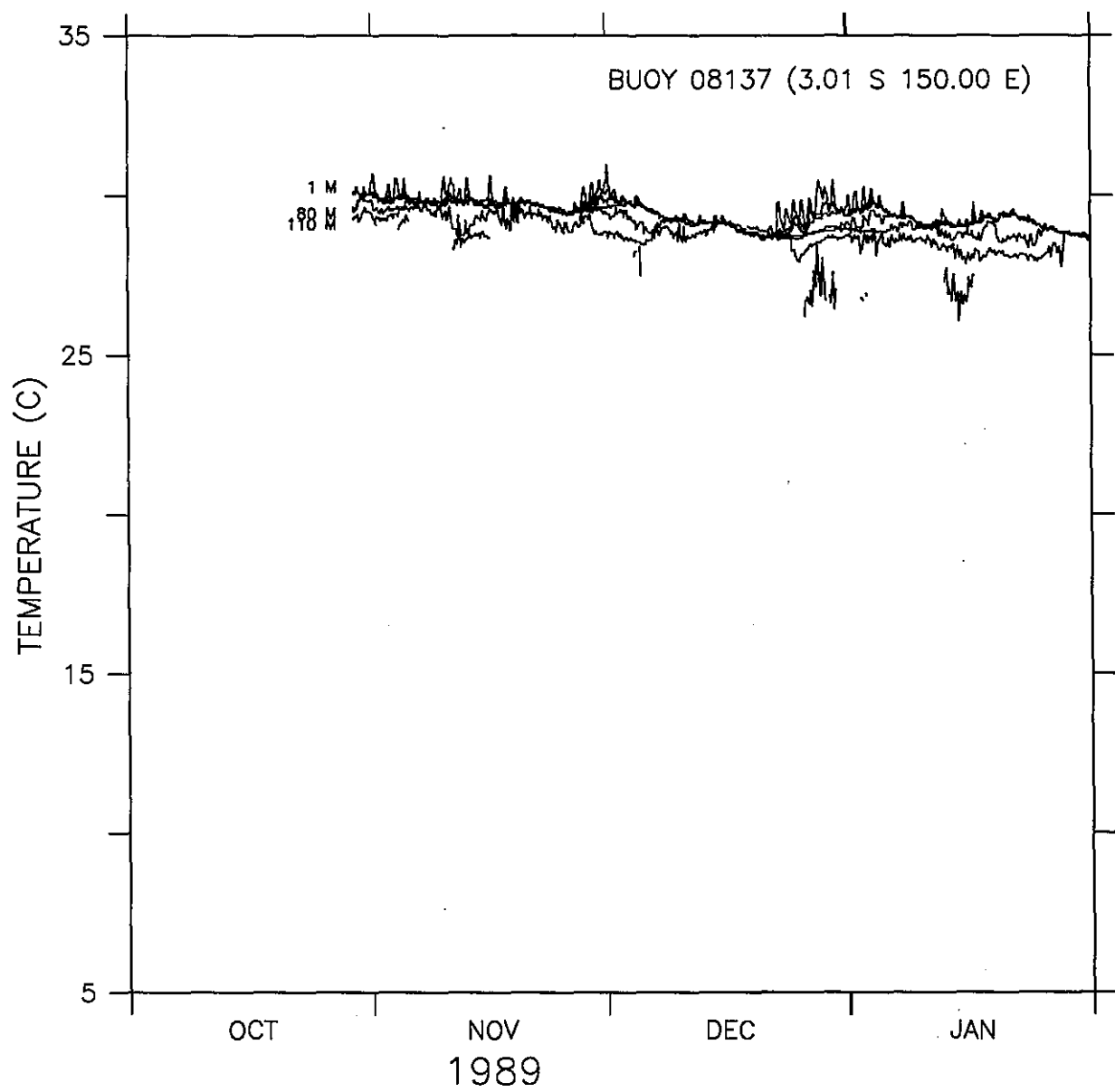
Figure 102.





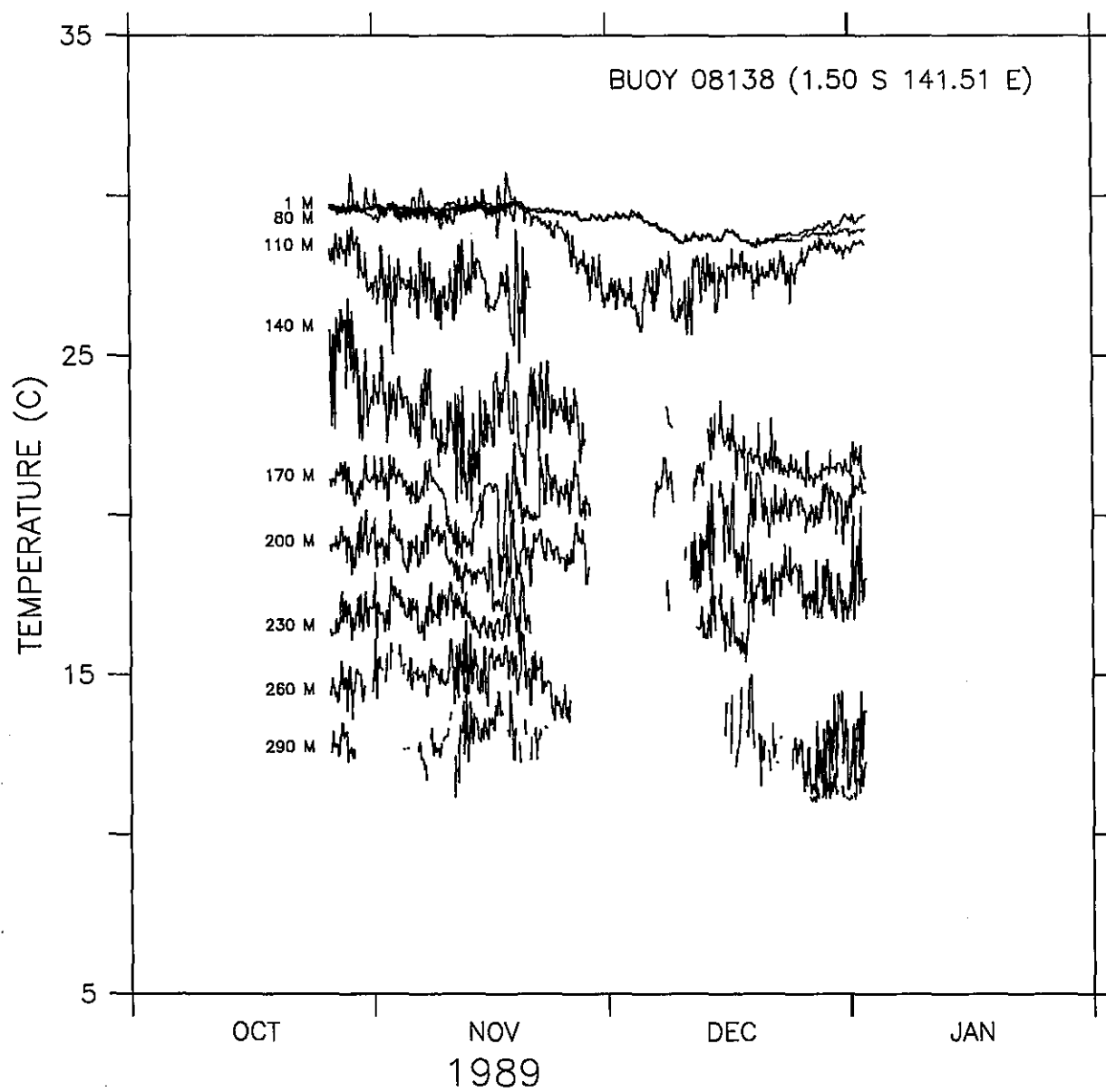
## TEMPERATURES AT FIXED DEPTHS

Figure 103.



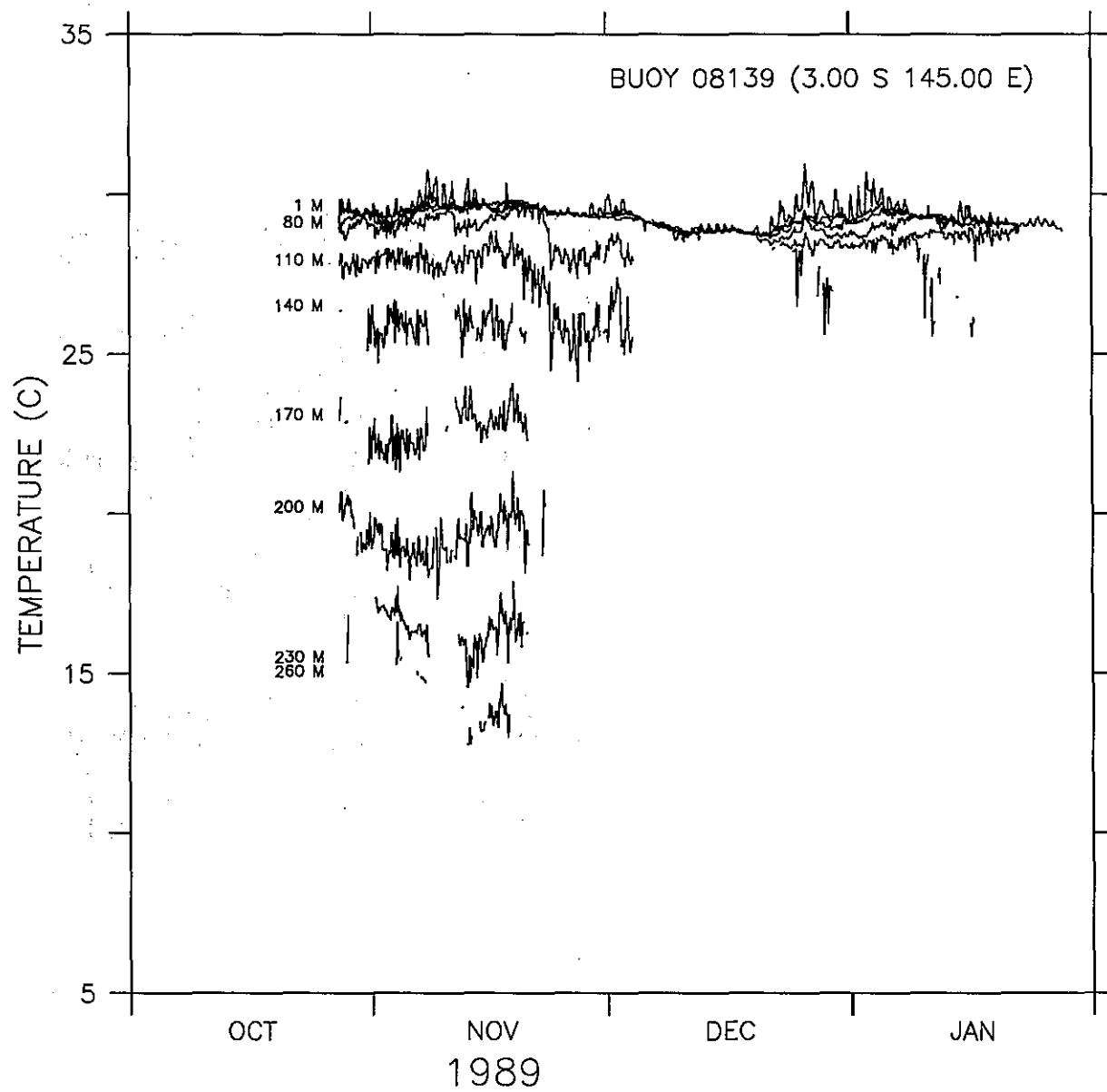
## TEMPERATURES AT FIXED DEPTHS

Figure 104.



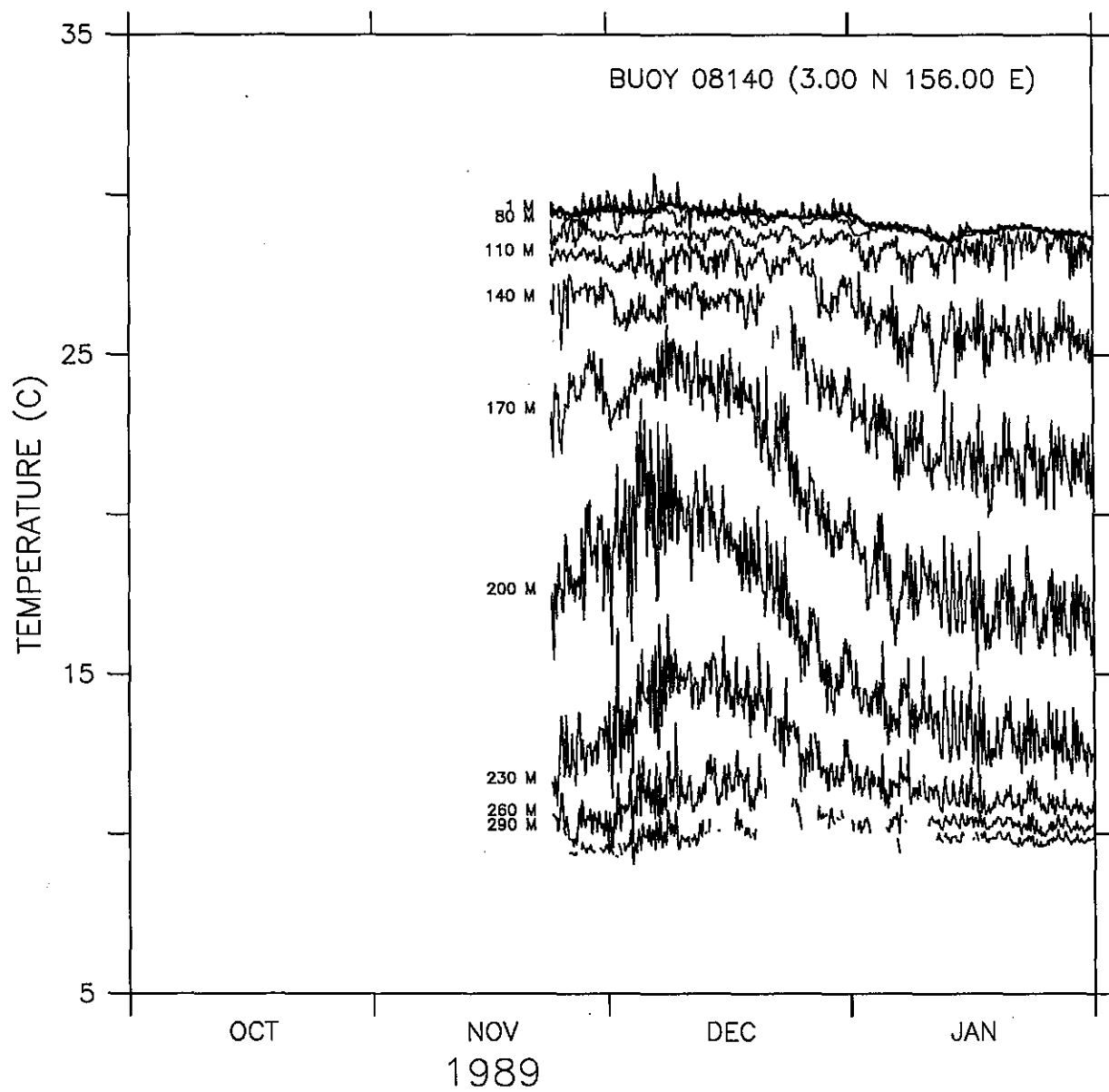
## TEMPERATURES AT FIXED DEPTHS

Figure 105.



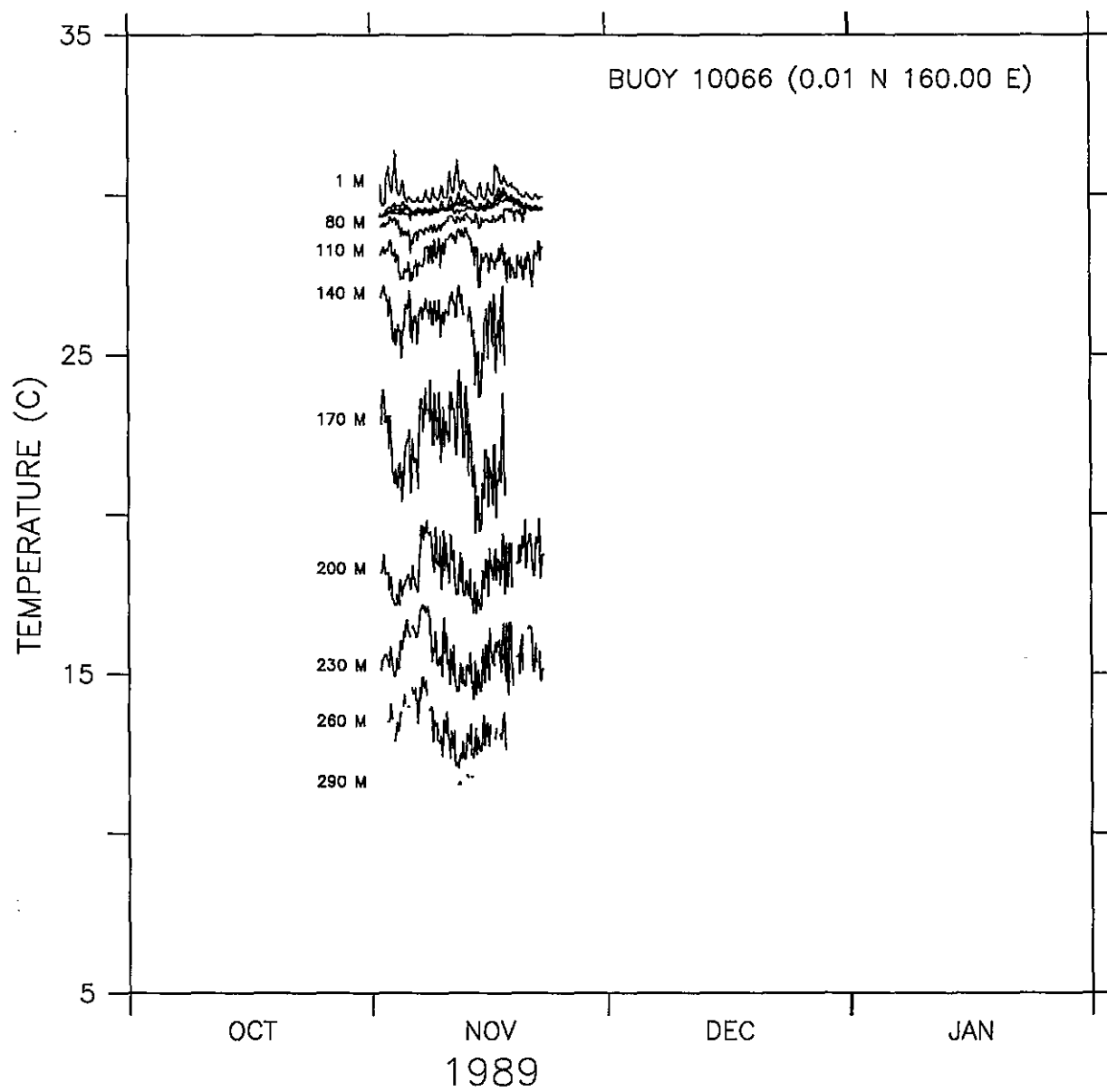
## TEMPERATURES AT FIXED DEPTHS

Figure 106.



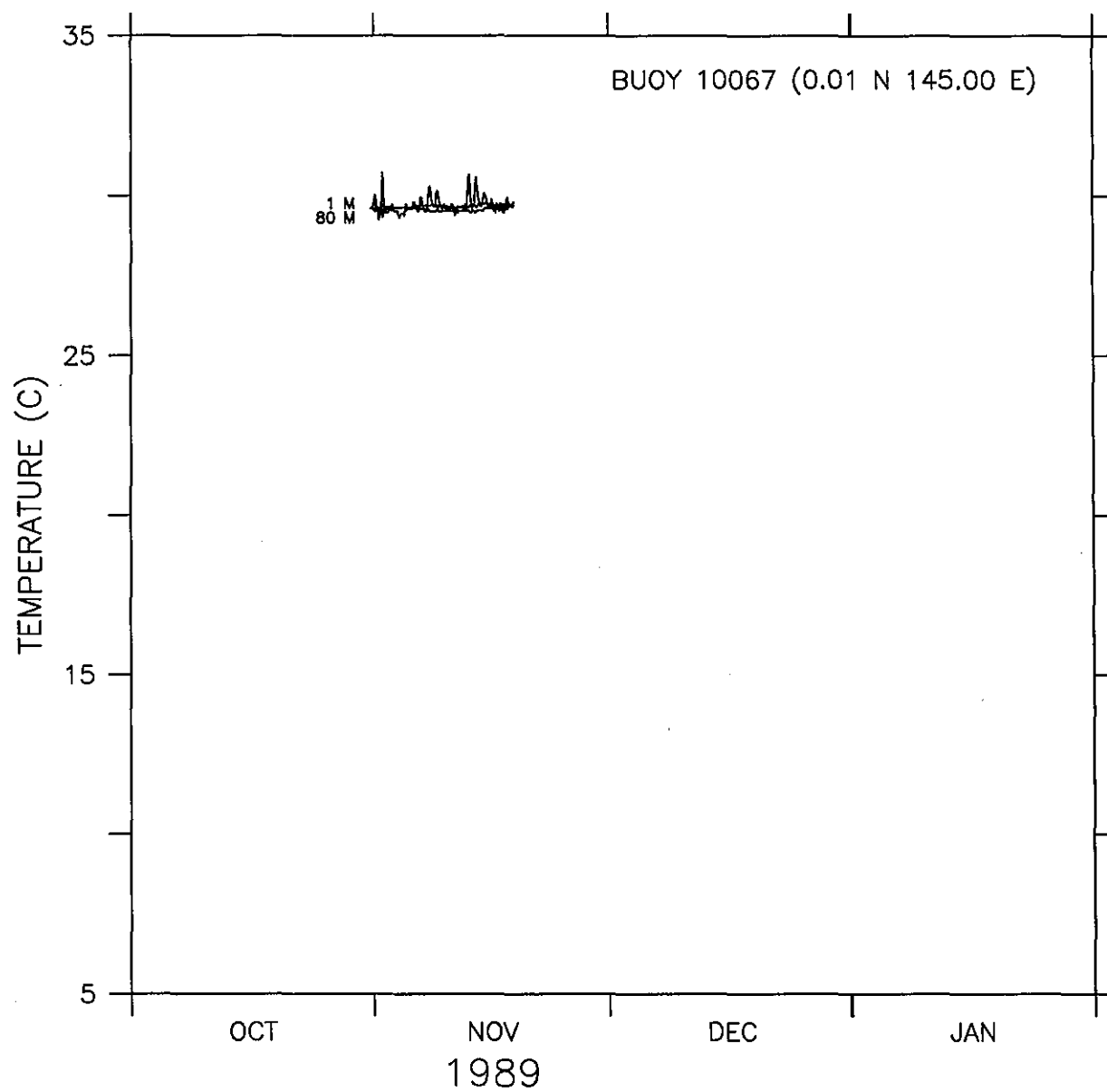
## TEMPERATURES AT FIXED DEPTHS

Figure 107.



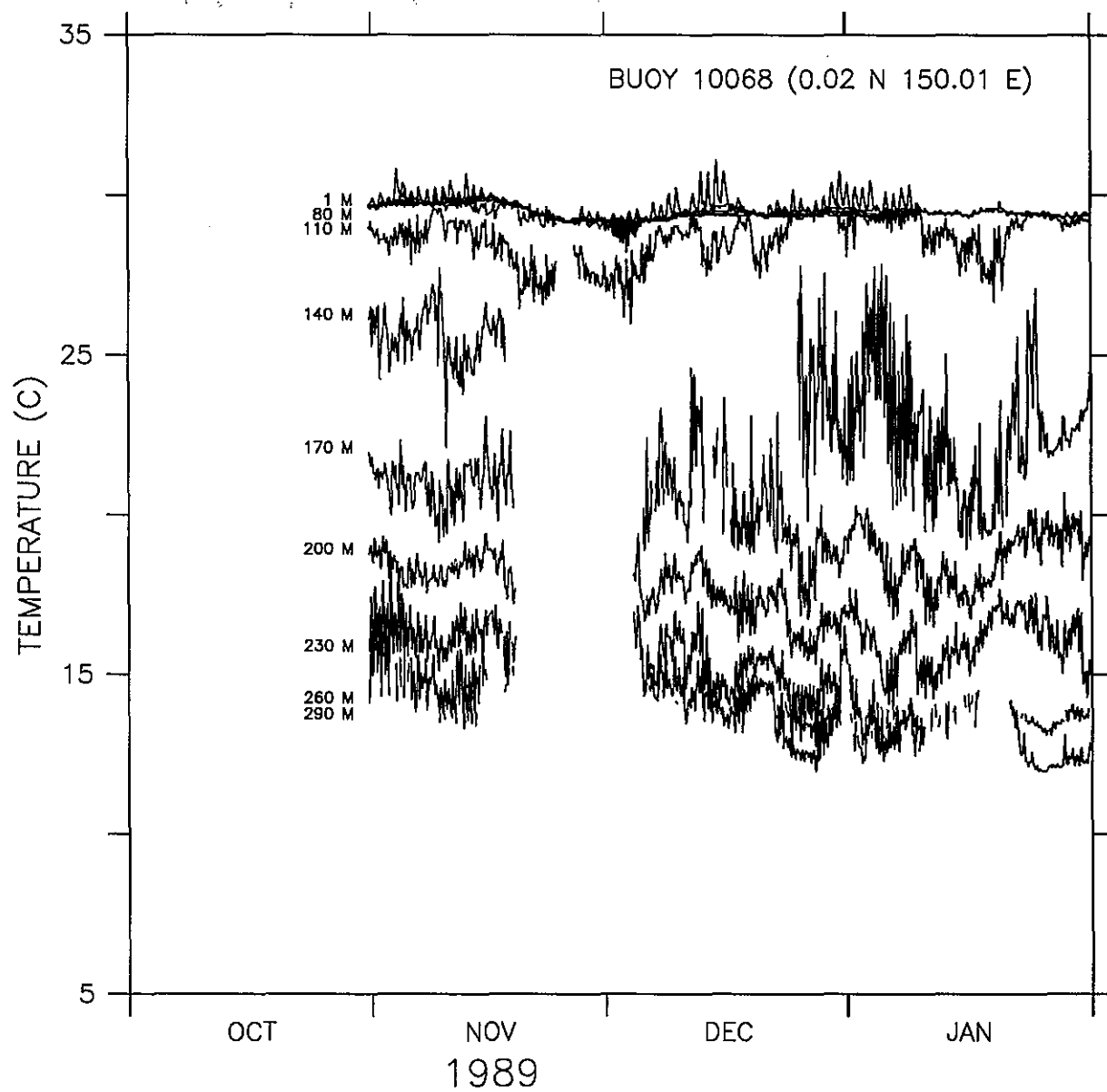
## TEMPERATURES AT FIXED DEPTHS

Figure 108.



## TEMPERATURES AT FIXED DEPTHS

Figure 109.

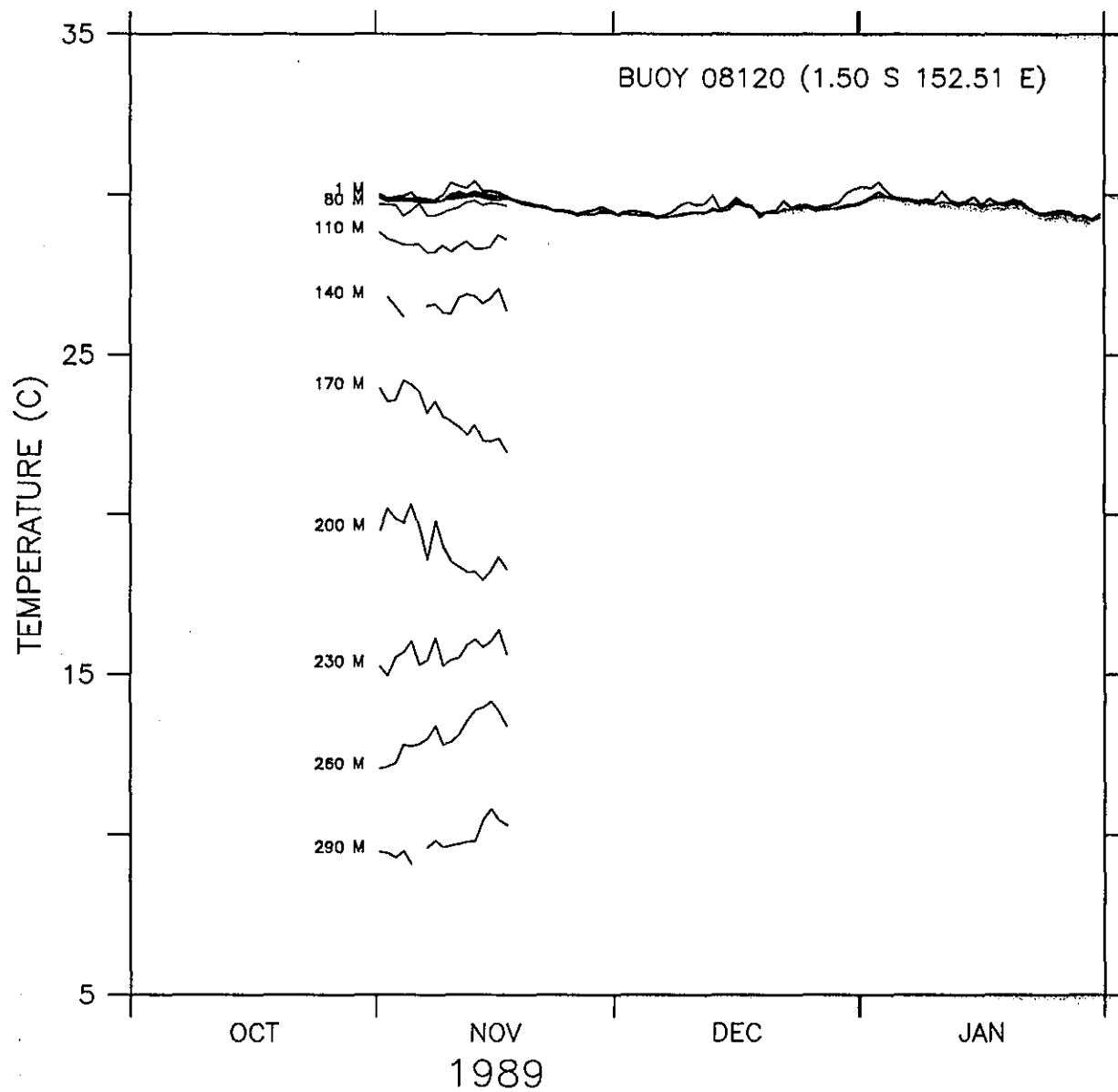


## TEMPERATURES AT FIXED DEPTHS

Figure 110.

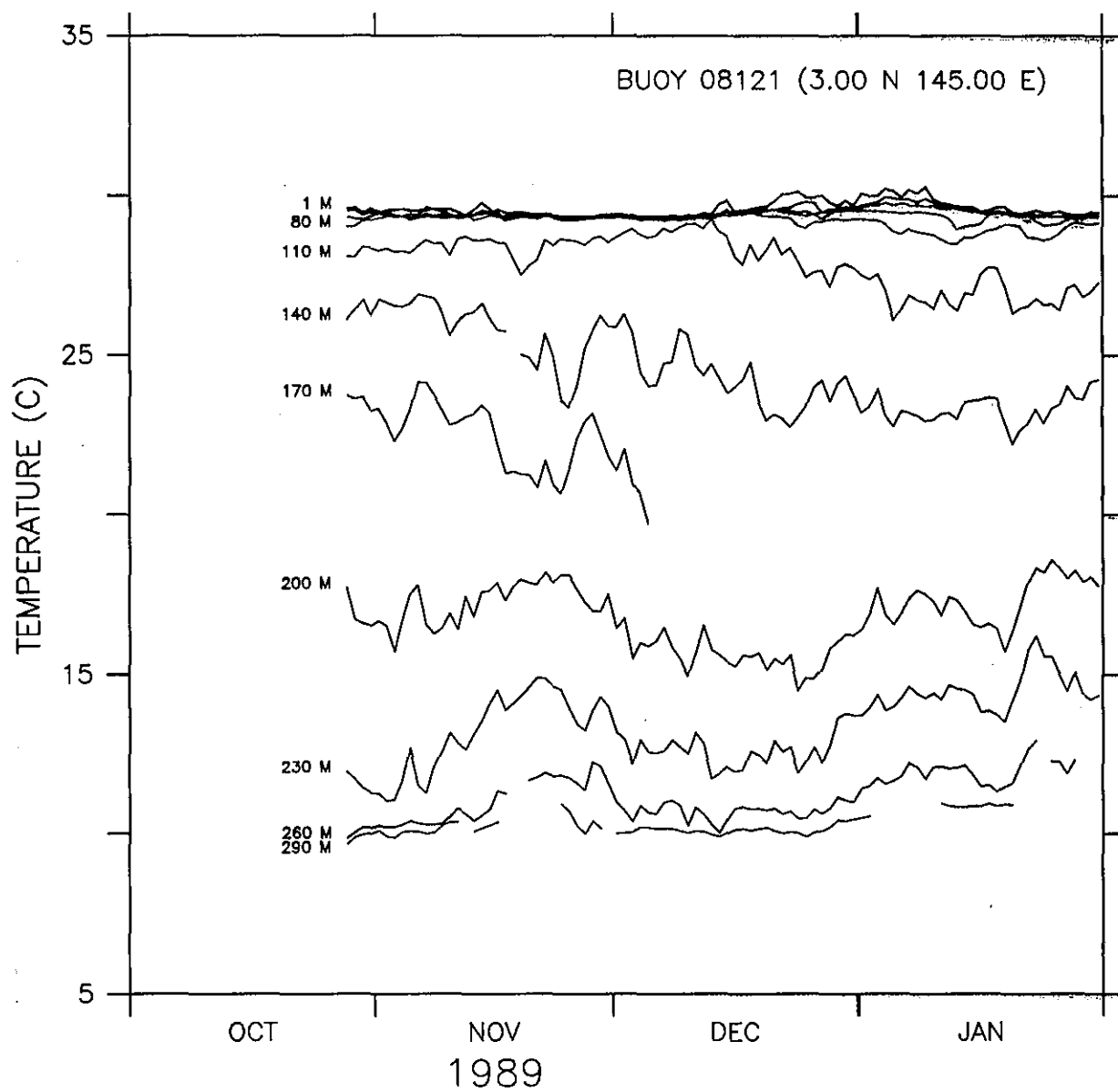


Figures 111–129. Daily averaged temperature time series at fixed depths for PRL drifters.



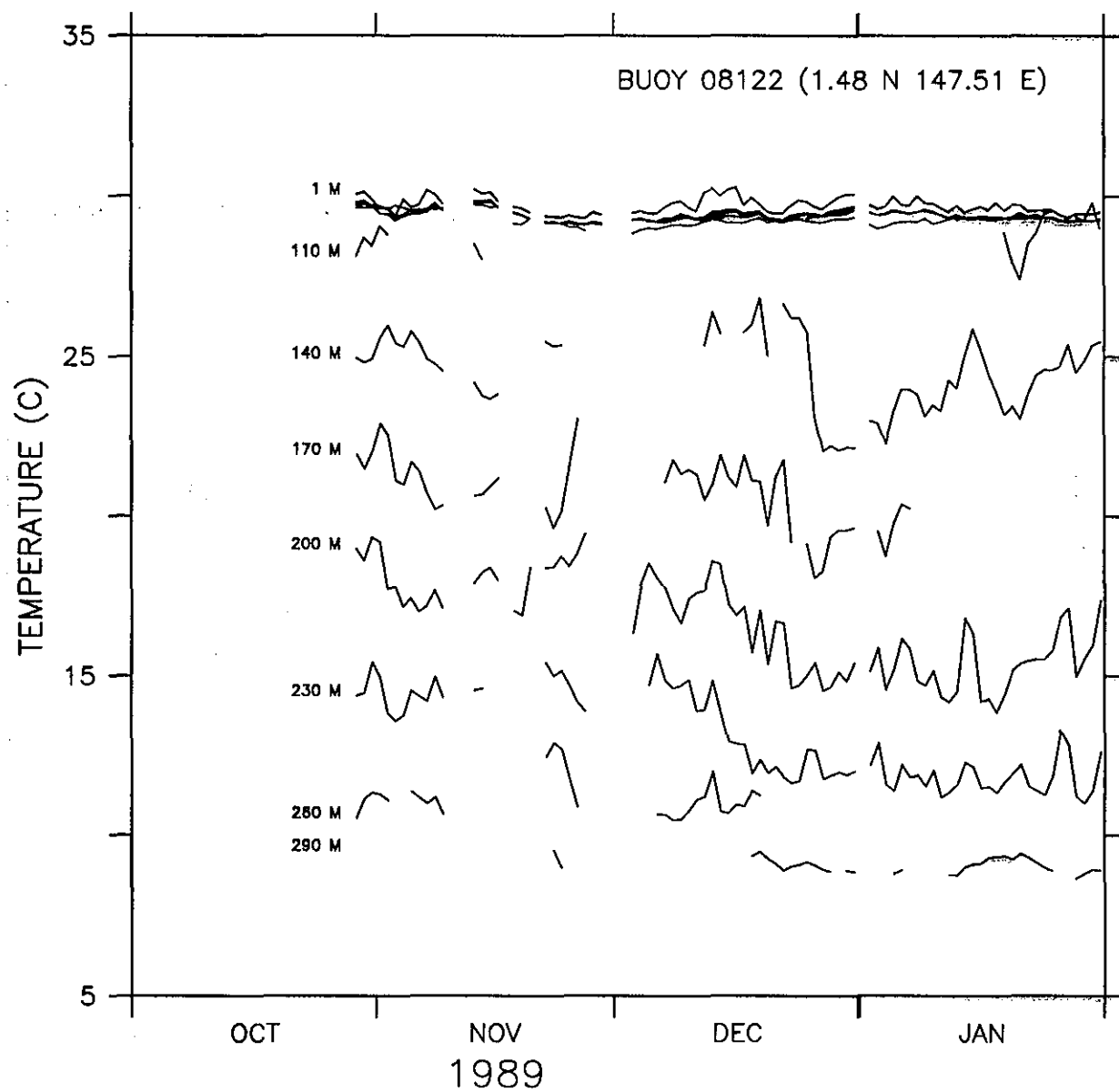
DAILY AVERAGED  
TEMPERATURES AT FIXED DEPTHS

Figure 111.



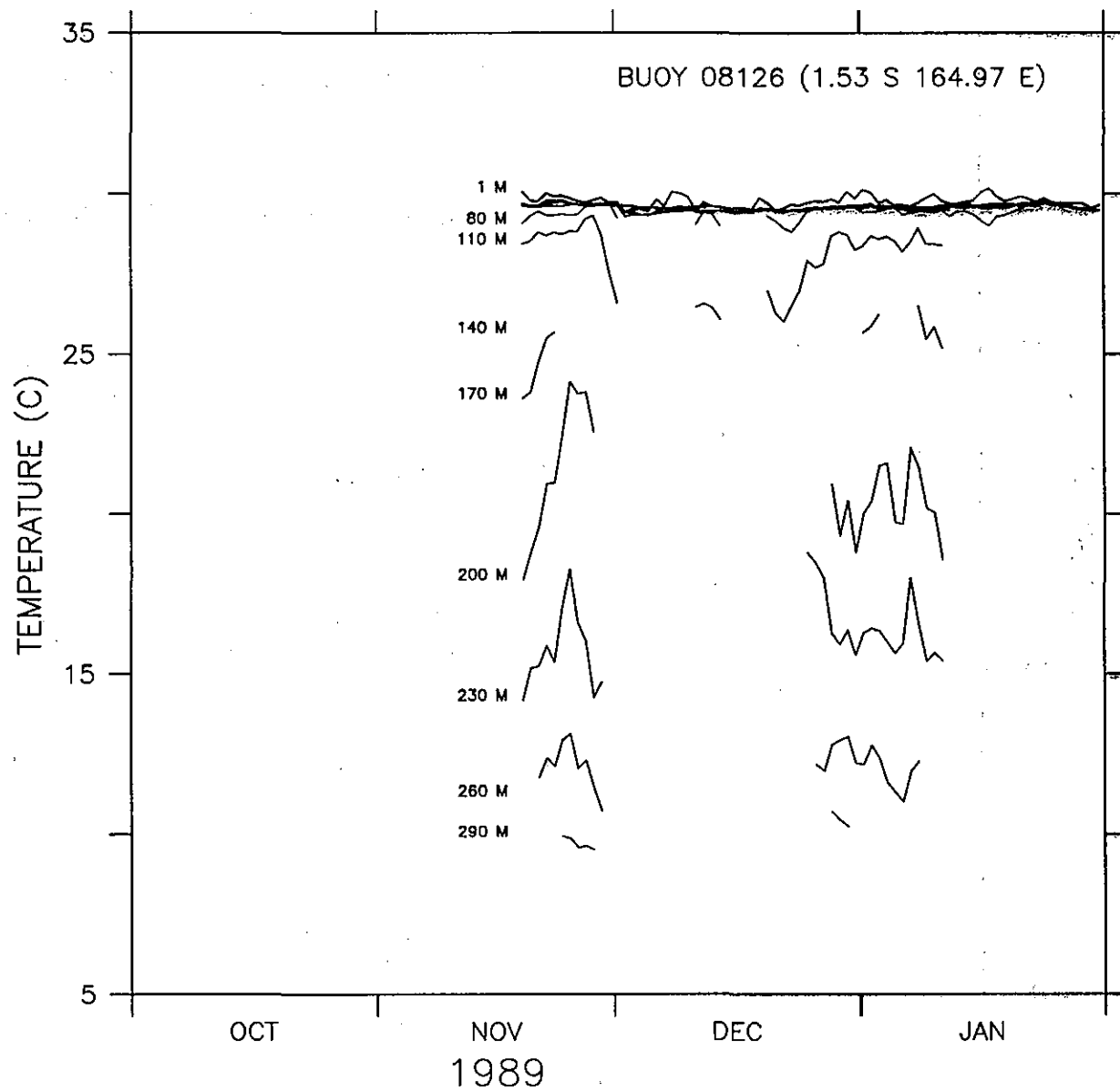
DAILY AVERAGED  
TEMPERATURES AT FIXED DEPTHS

Figure 112.



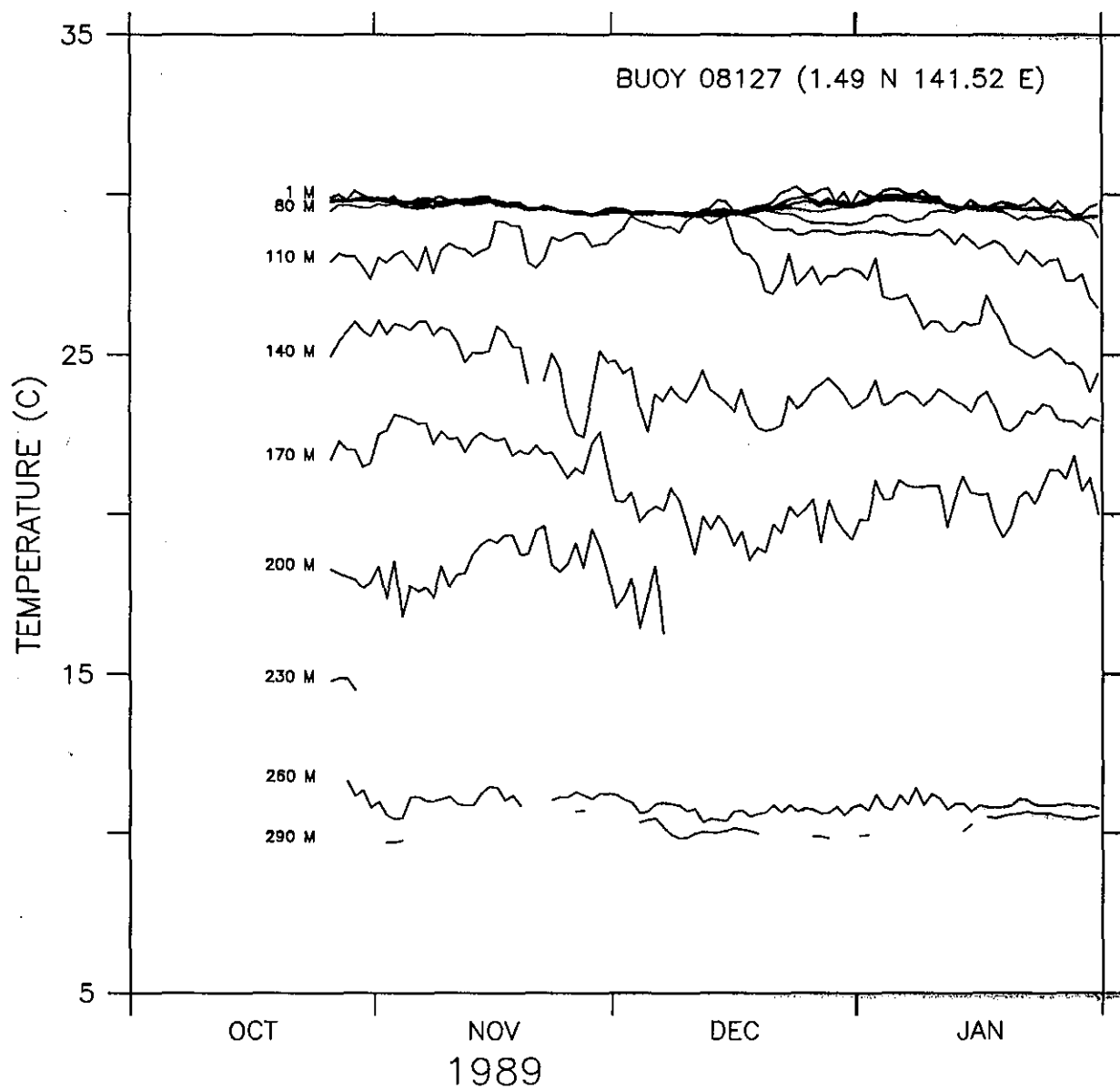
DAILY AVERAGED  
TEMPERATURES AT FIXED DEPTHS

Figure 113.



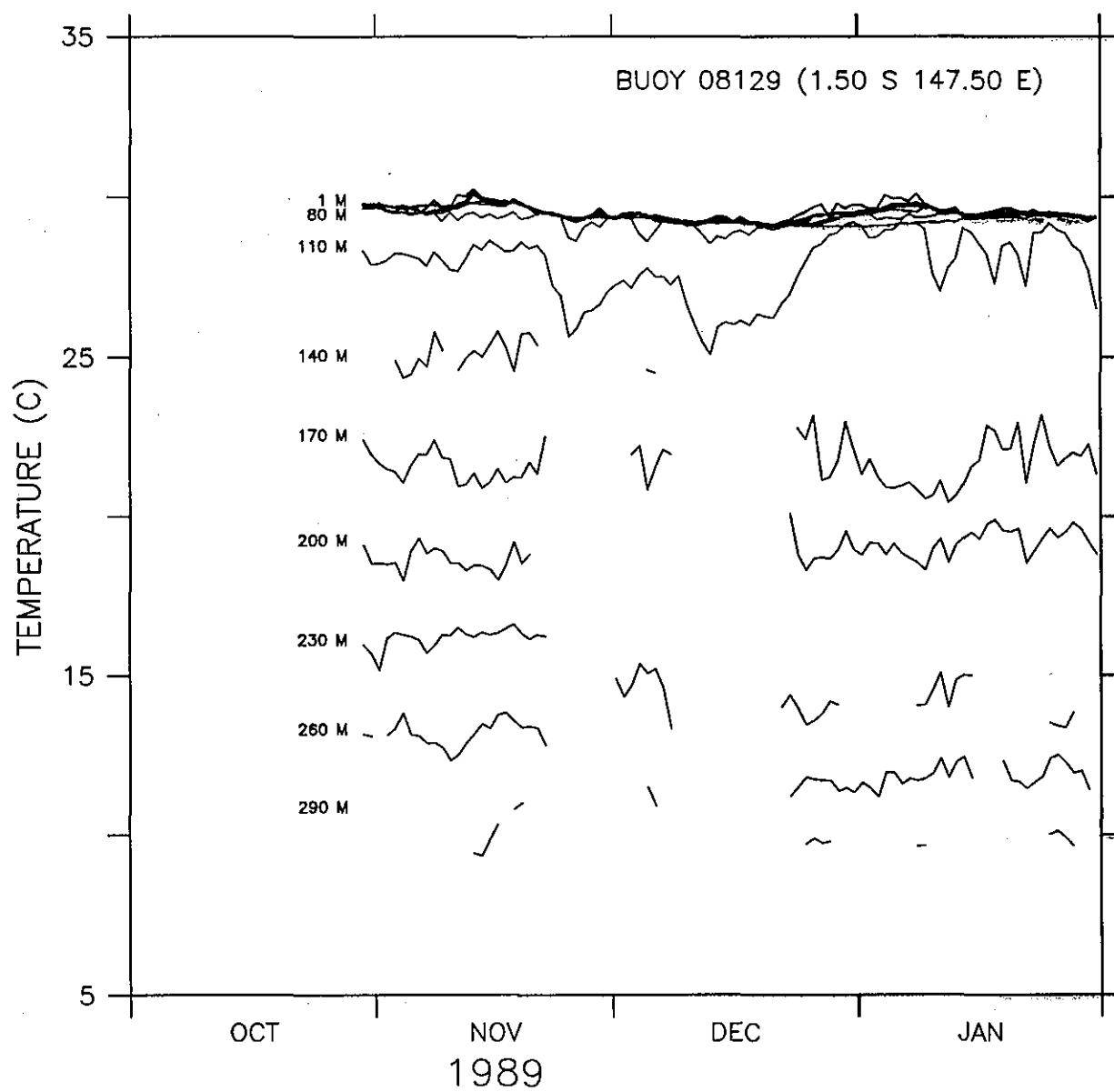
DAILY AVERAGED  
TEMPERATURES AT FIXED DEPTHS

Figure 114.



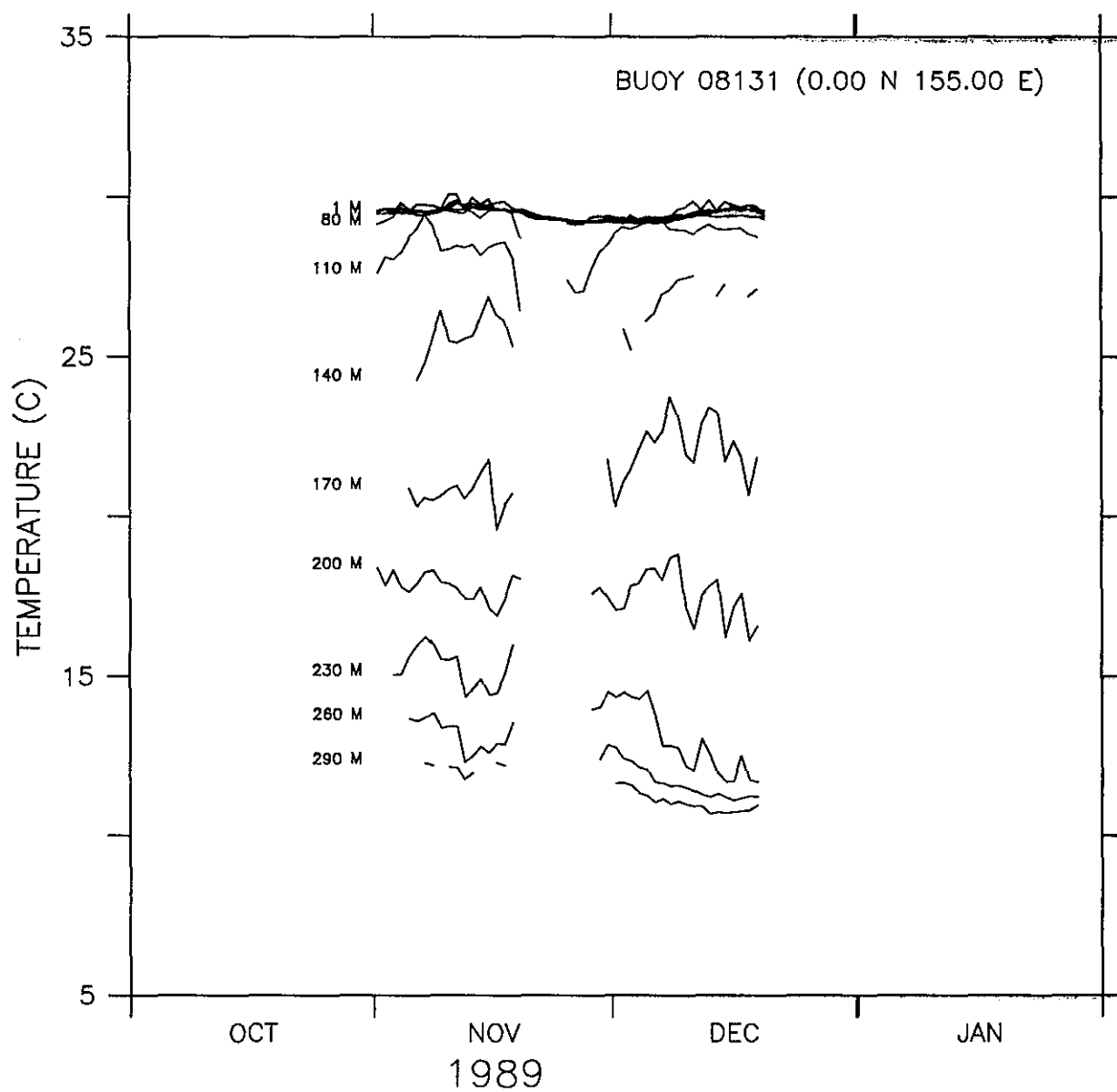
DAILY AVERAGED  
TEMPERATURES AT FIXED DEPTHS

Figure 115.



DAILY AVERAGED  
TEMPERATURES AT FIXED DEPTHS

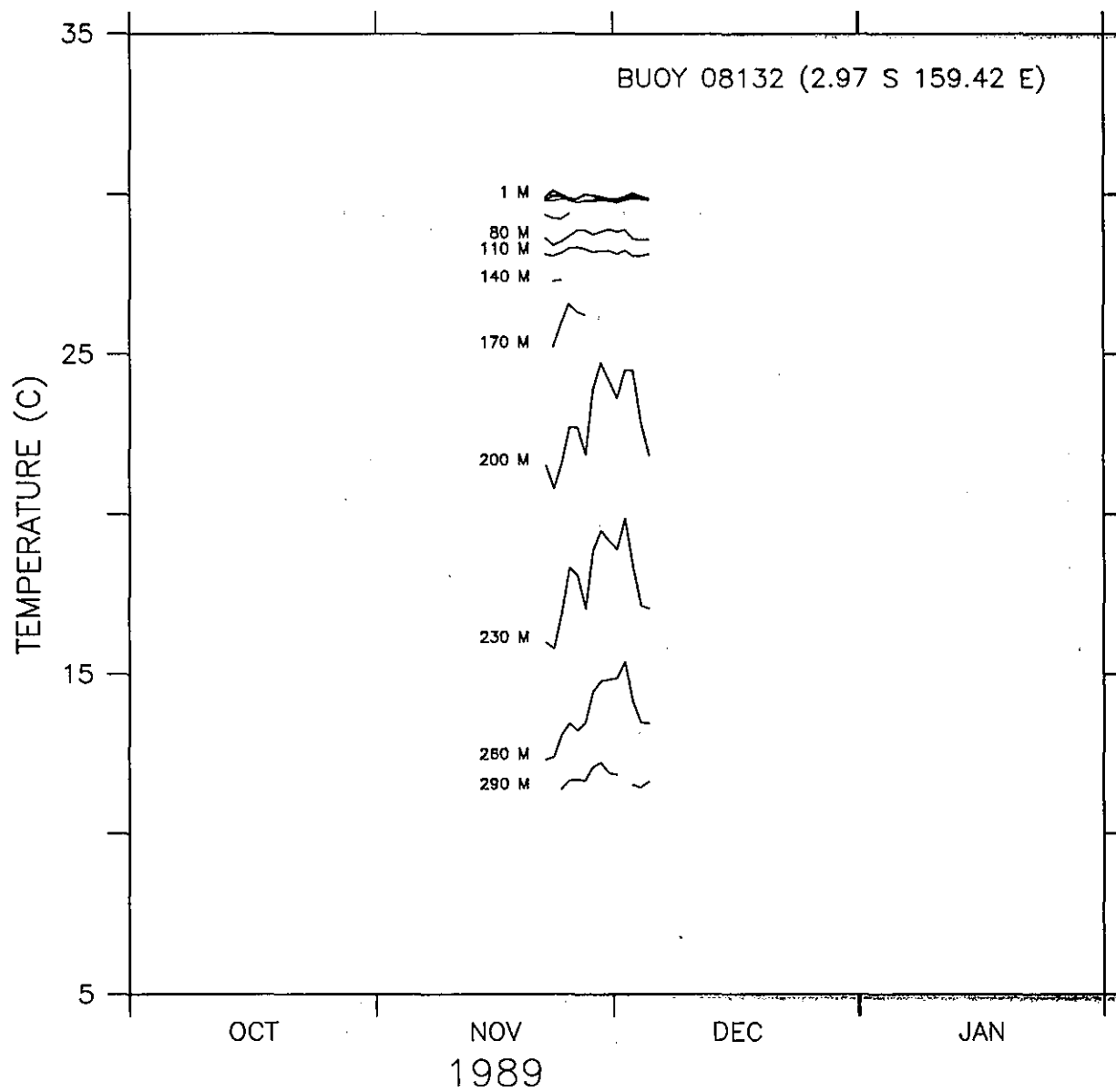
Figure 116.



DAILY AVERAGED  
TEMPERATURES AT FIXED DEPTHS

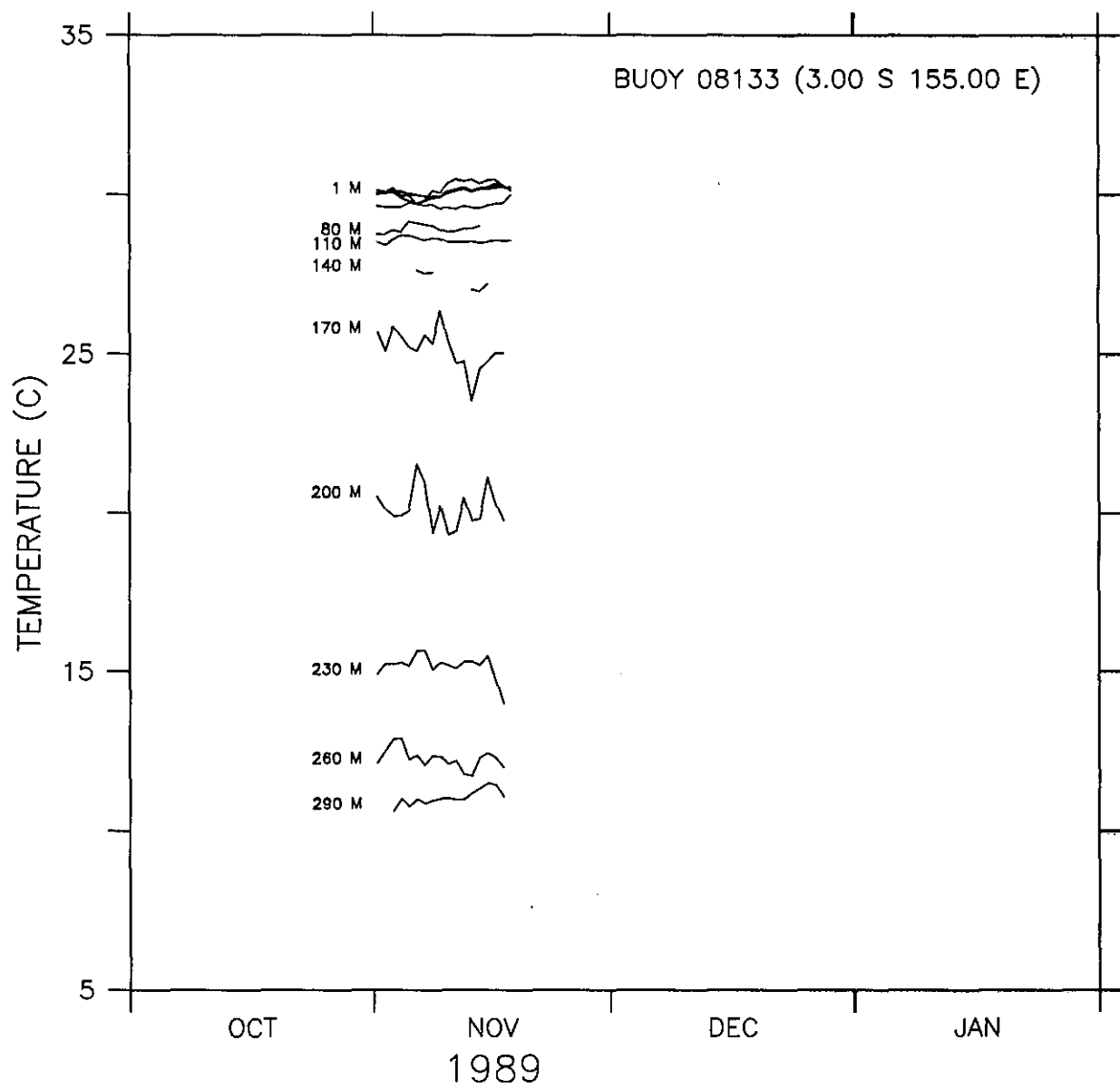
Figure 117.





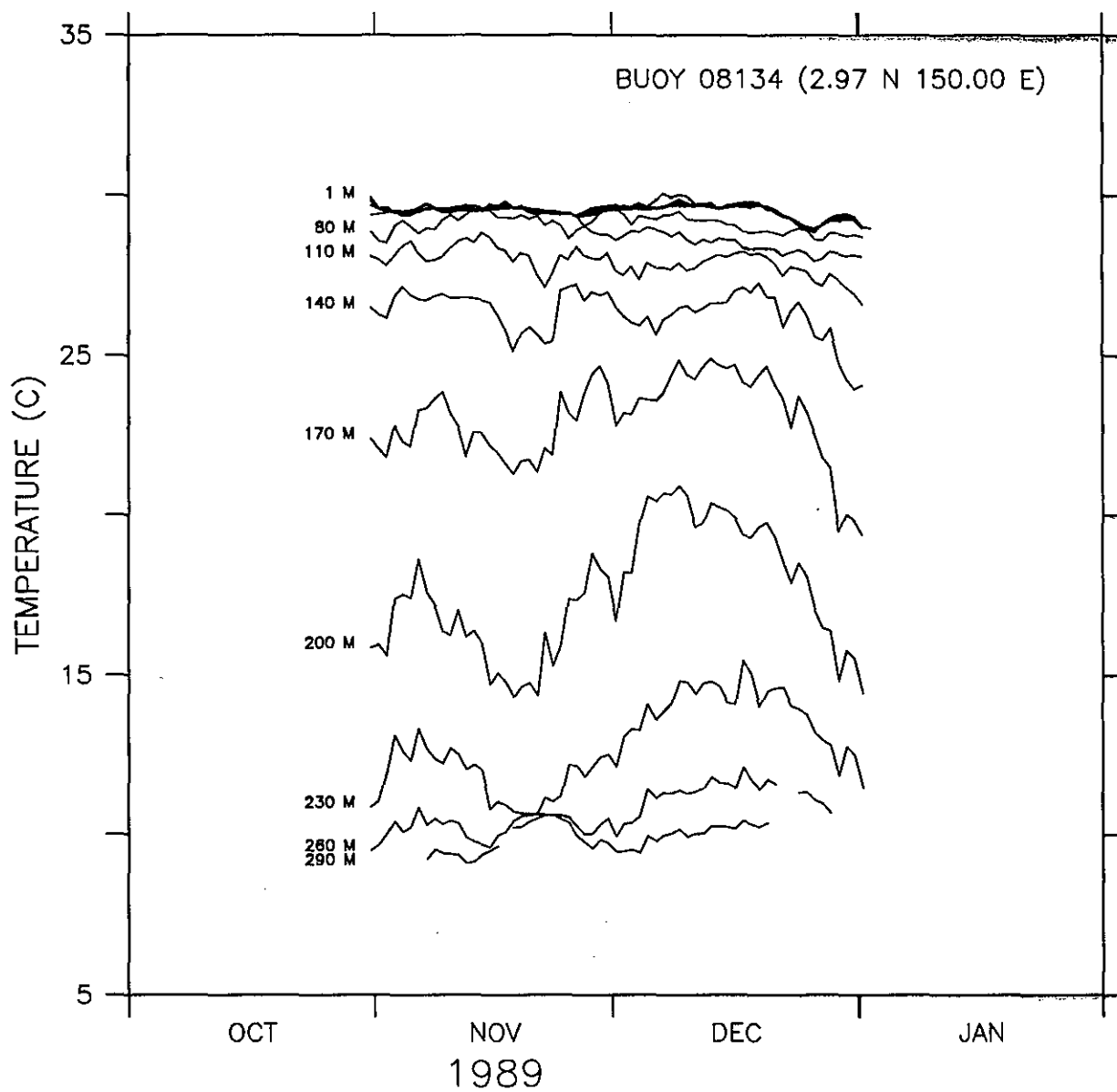
DAILY AVERAGED  
TEMPERATURES AT FIXED DEPTHS

Figure 118.



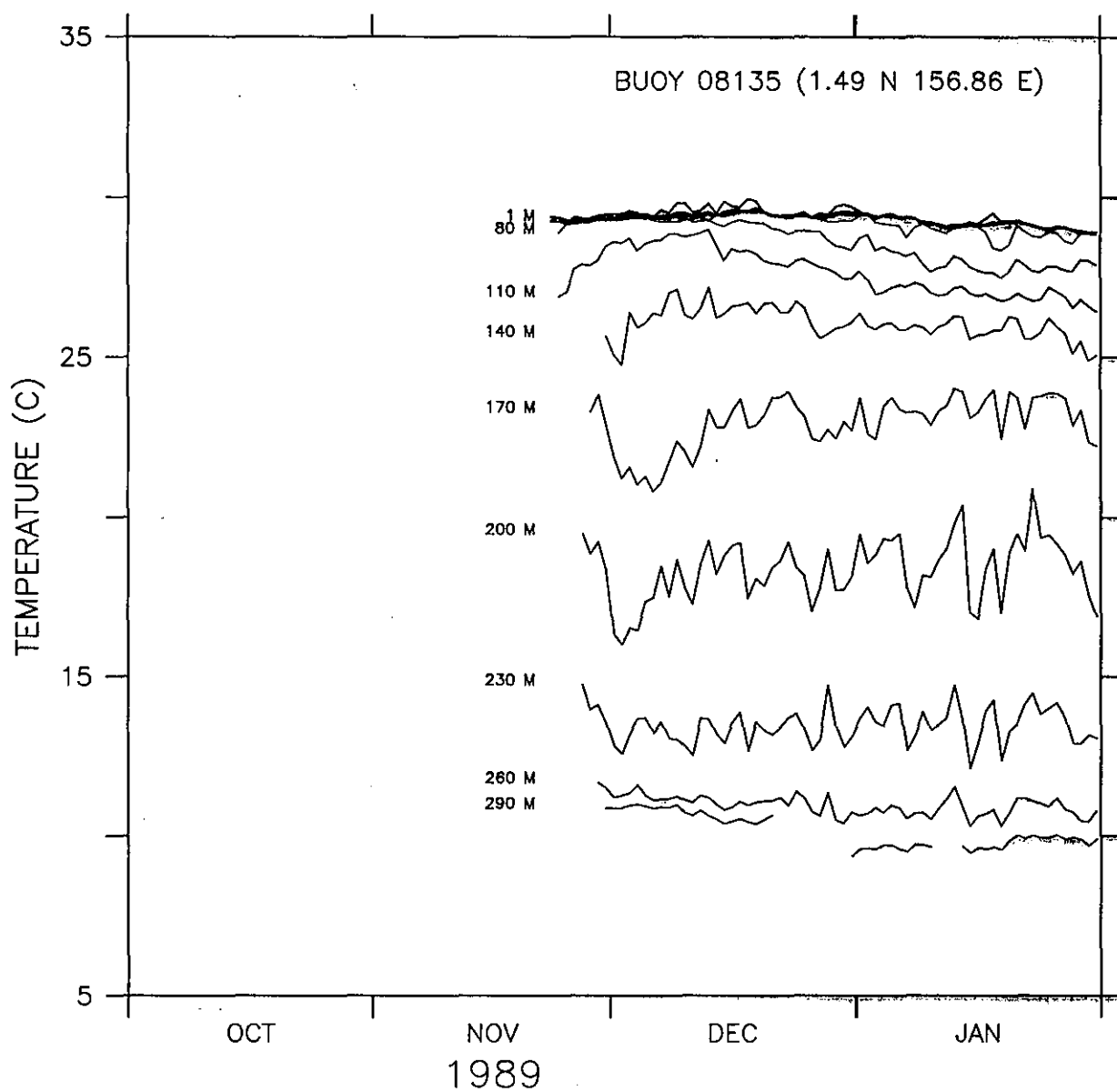
DAILY AVERAGED  
TEMPERATURES AT FIXED DEPTHS

Figure 119.



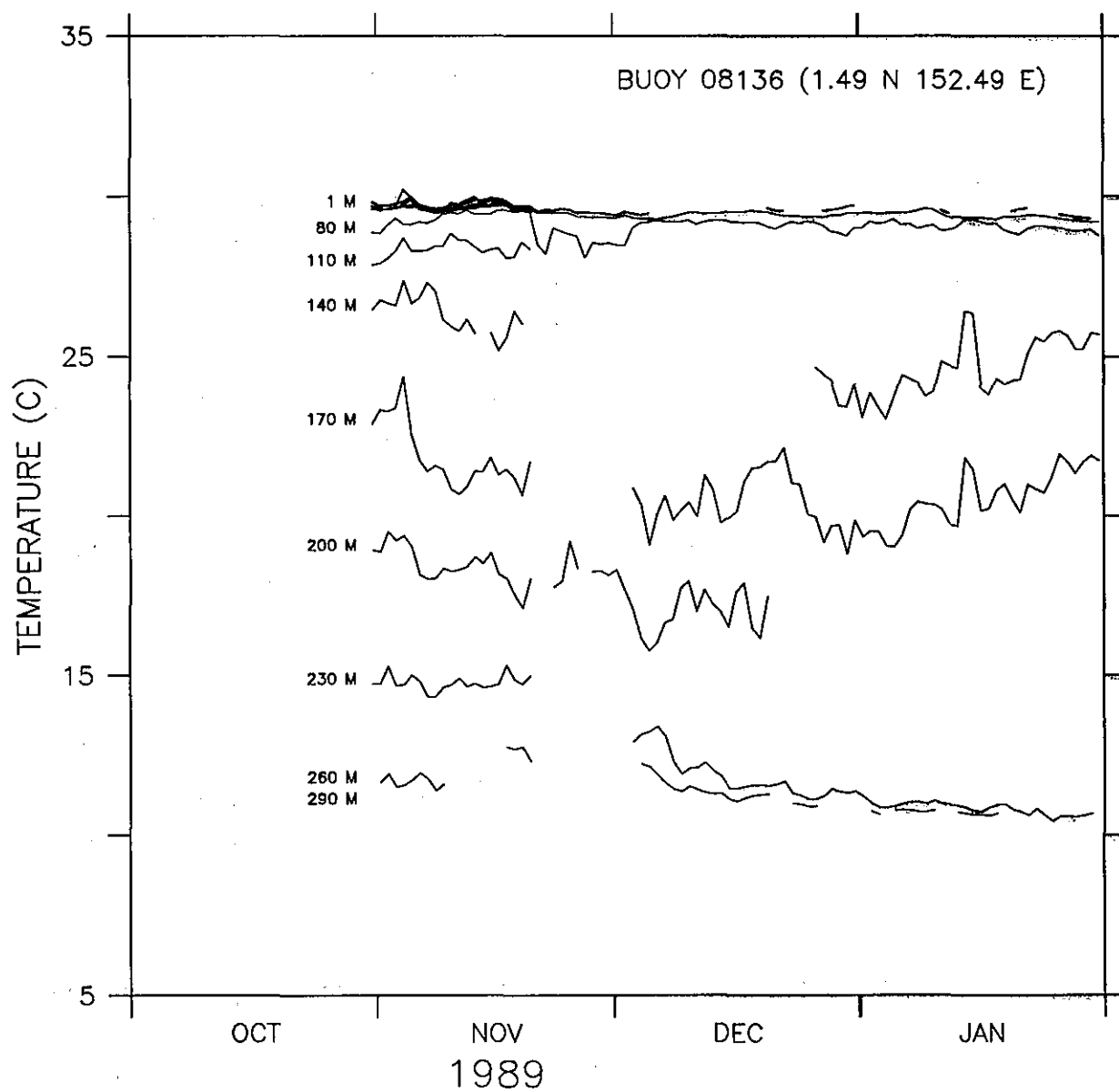
DAILY AVERAGED  
TEMPERATURES AT FIXED DEPTHS

Figure 120.



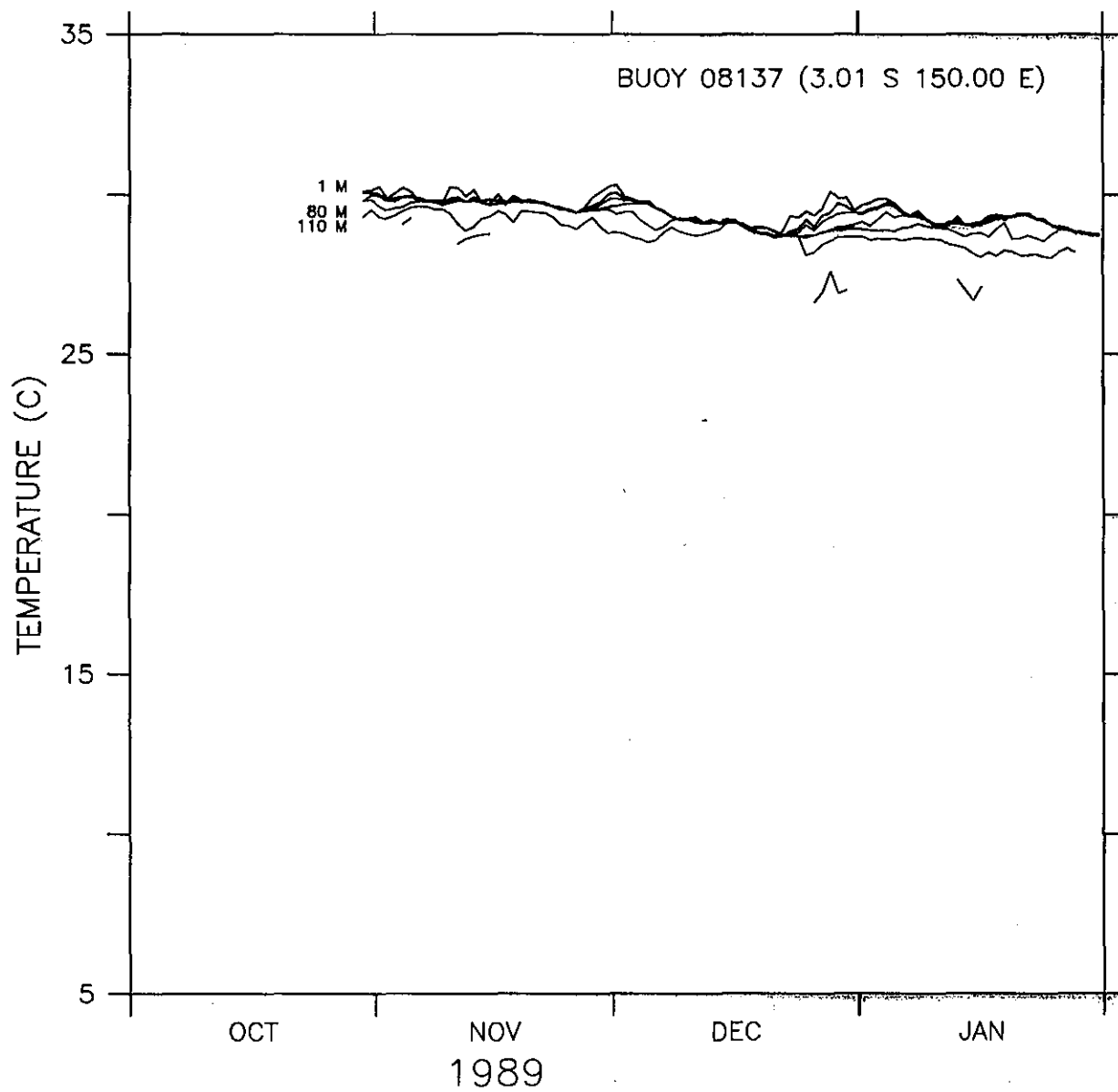
DAILY AVERAGED  
TEMPERATURES AT FIXED DEPTHS

Figure 121.



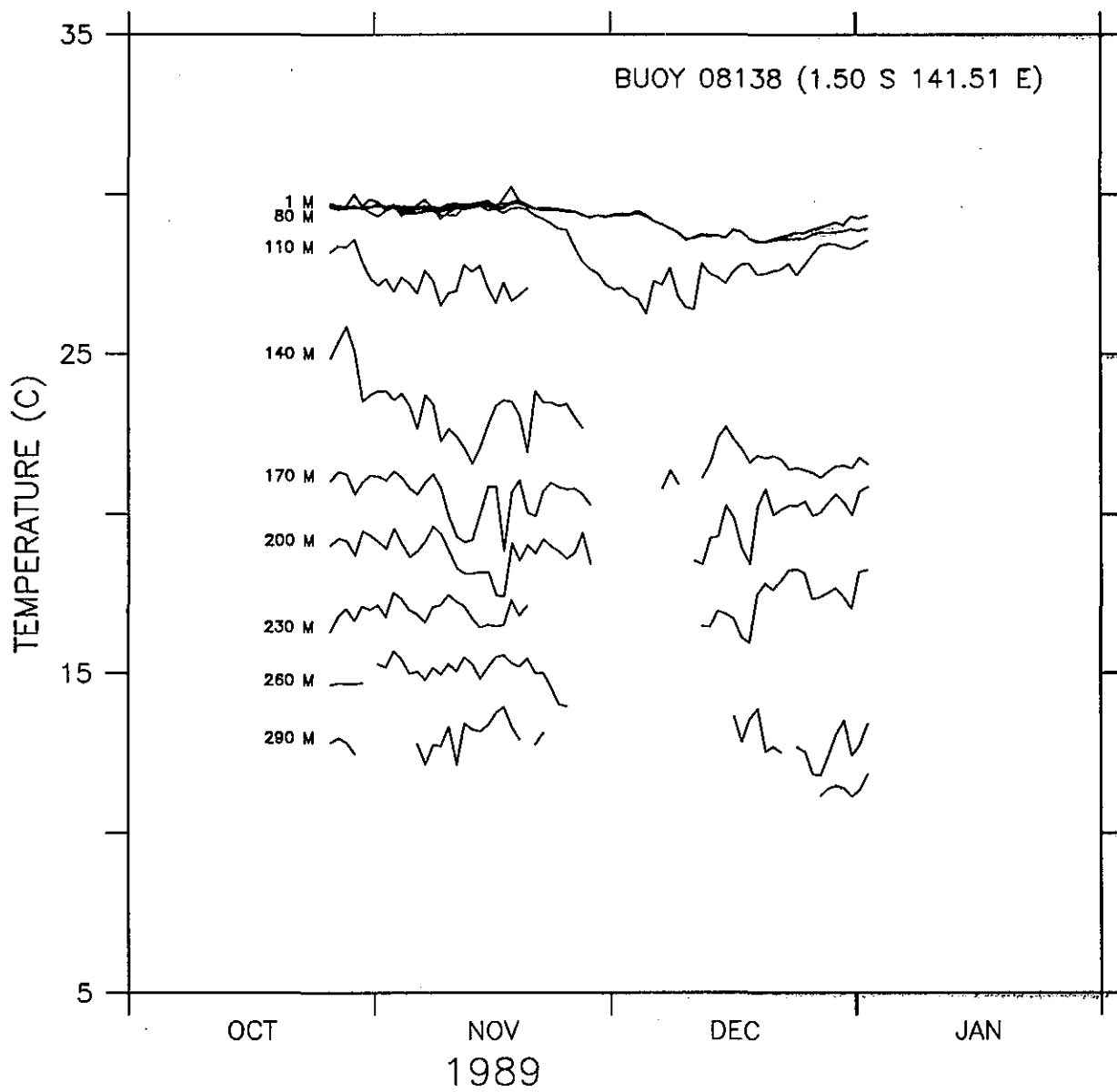
DAILY AVERAGED  
TEMPERATURES AT FIXED DEPTHS

Figure 122.



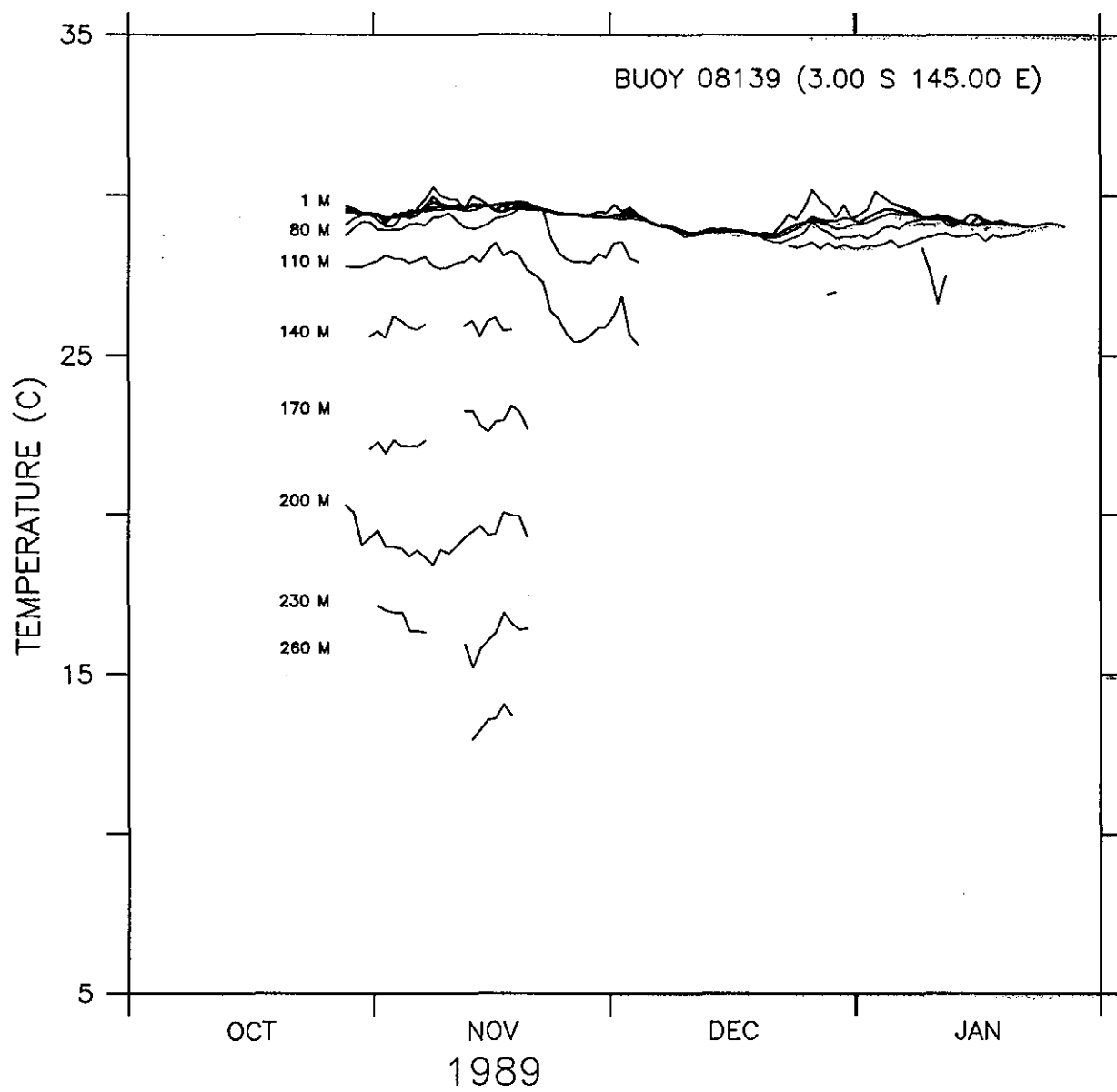
DAILY AVERAGED  
TEMPERATURES AT FIXED DEPTHS

Figure 123.



DAILY AVERAGED  
TEMPERATURES AT FIXED DEPTHS

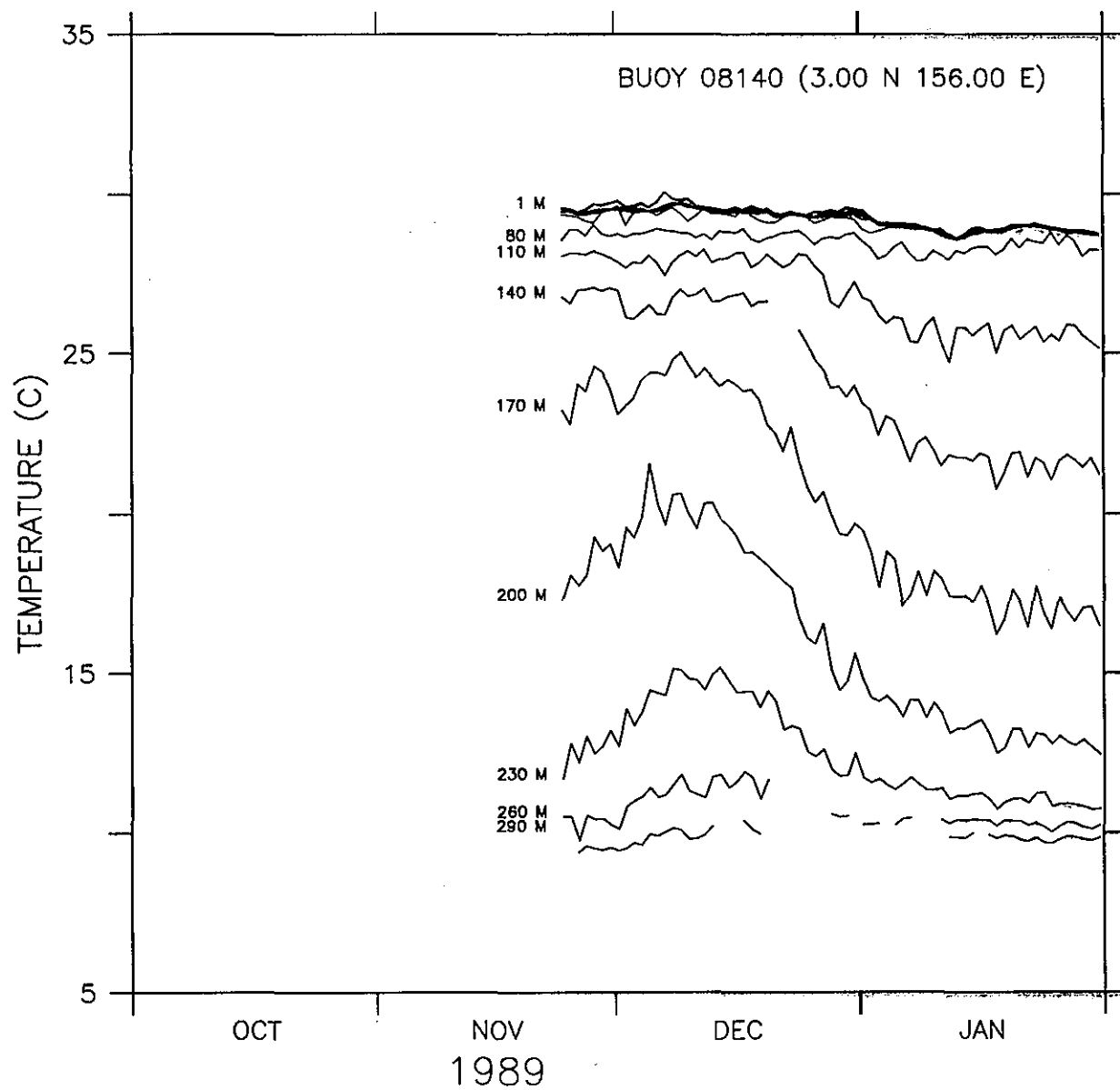
Figure 124.



DAILY AVERAGED  
TEMPERATURES AT FIXED DEPTHS

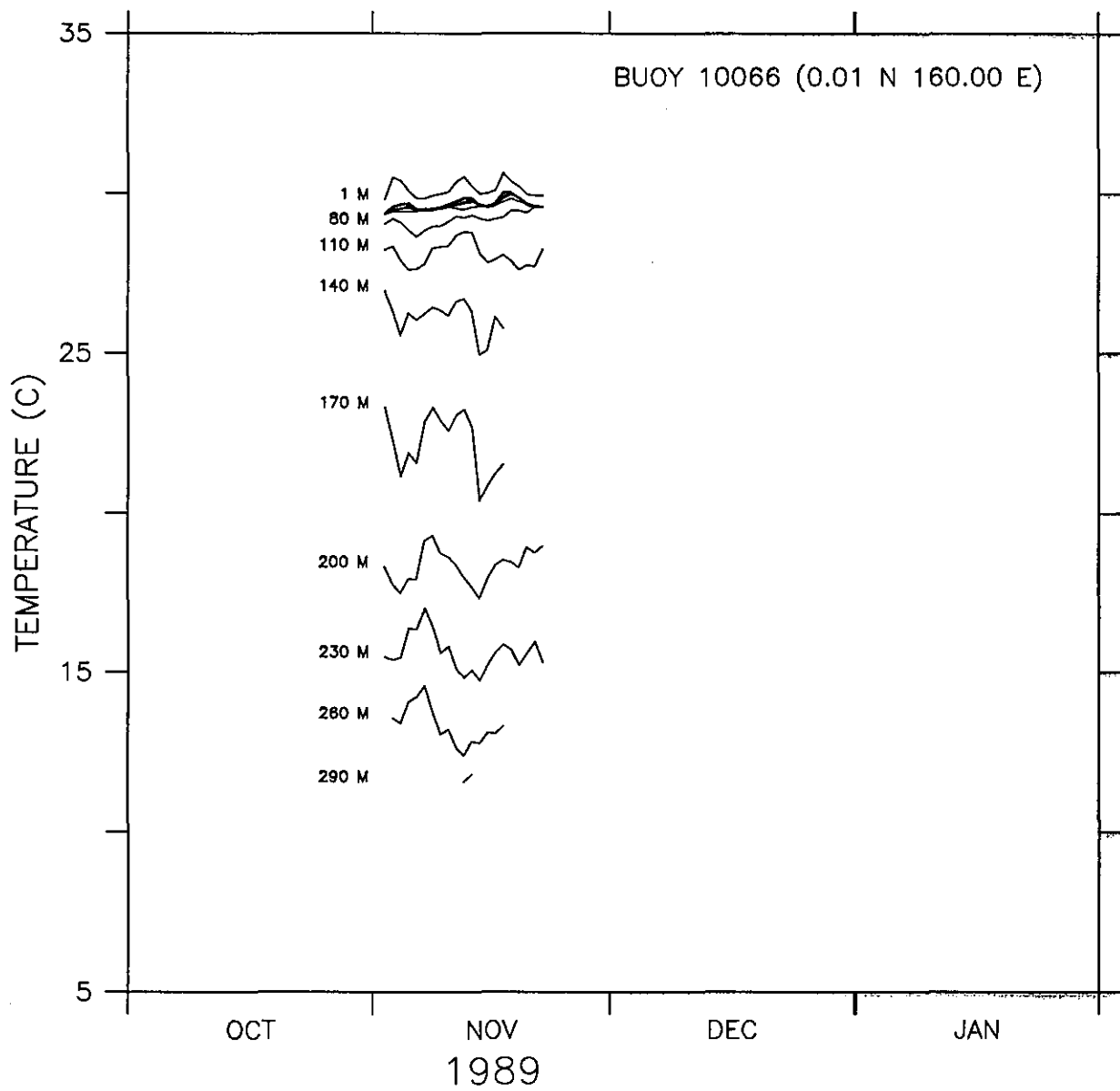
Figure 125.





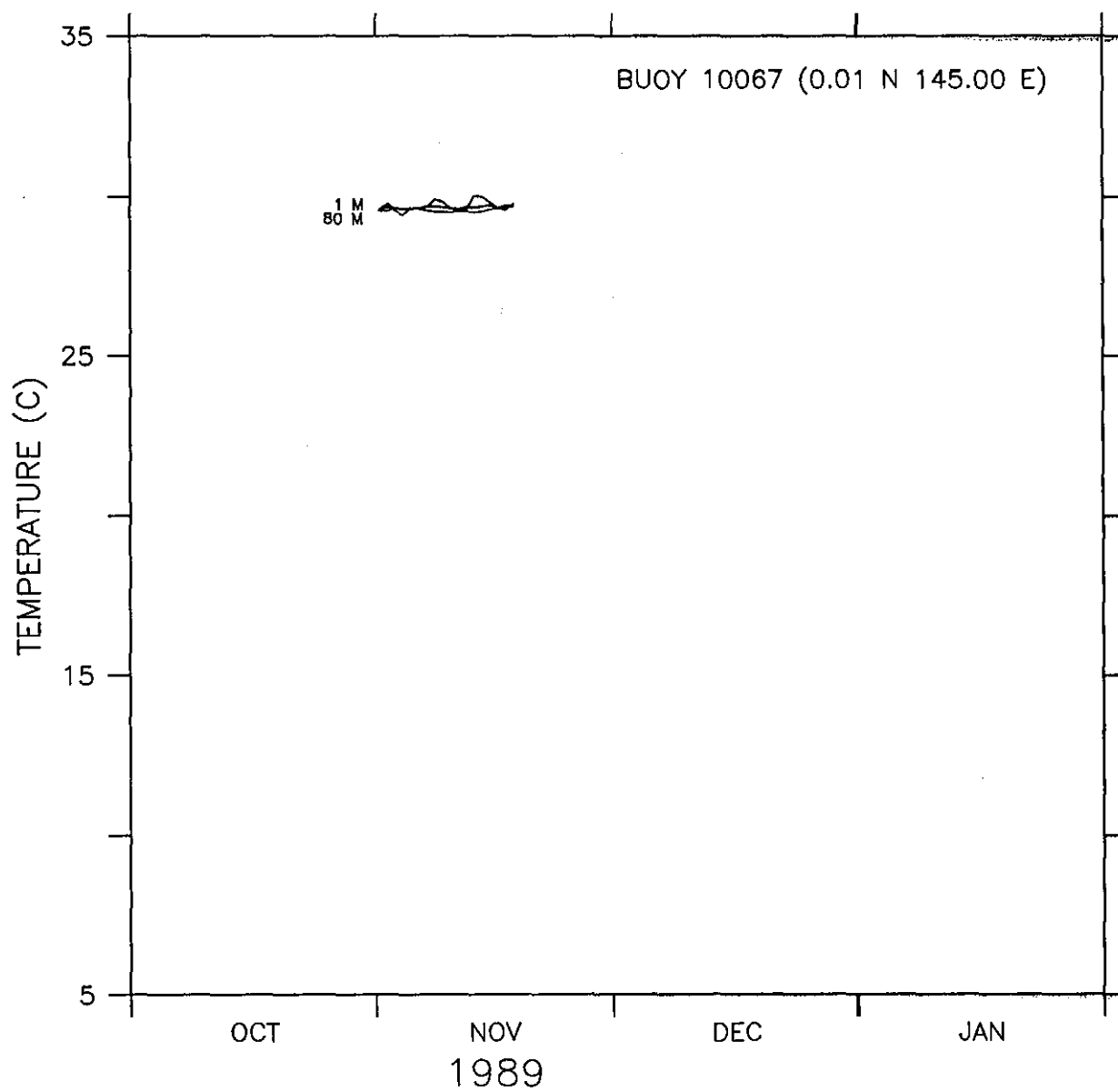
DAILY AVERAGED  
TEMPERATURES AT FIXED DEPTHS

Figure 126.



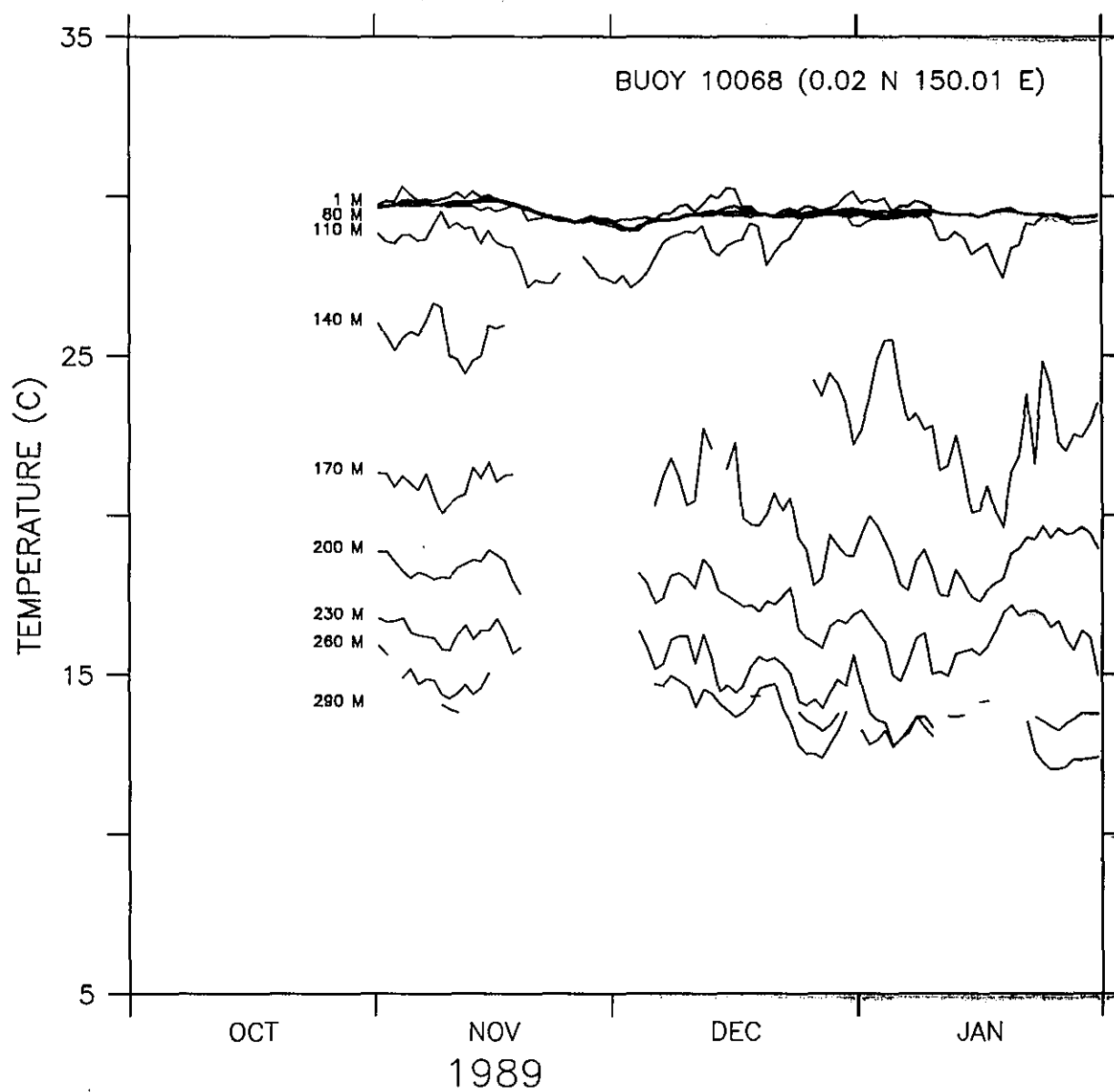
DAILY AVERAGED  
TEMPERATURES AT FIXED DEPTHS

Figure 127.



DAILY AVERAGED  
TEMPERATURES AT FIXED DEPTHS

Figure 128.



DAILY AVERAGED  
TEMPERATURES AT FIXED DEPTHS

Figure 129.

Figures 130–147. Contour plots of daily averaged temperatures for PRL drifters. No plot is shown for buoy #10067 due to lack of sufficient data.

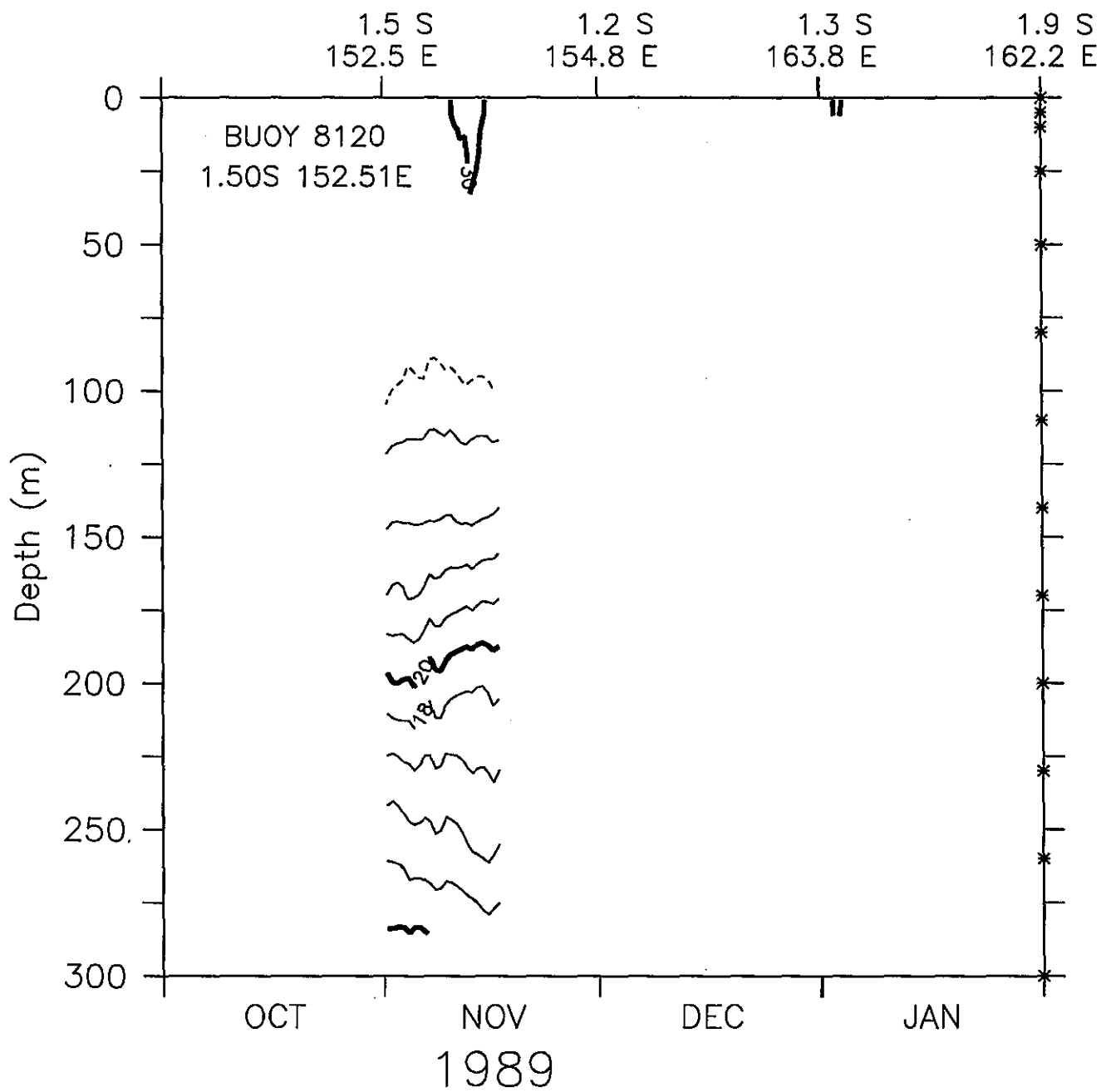


Figure 130.

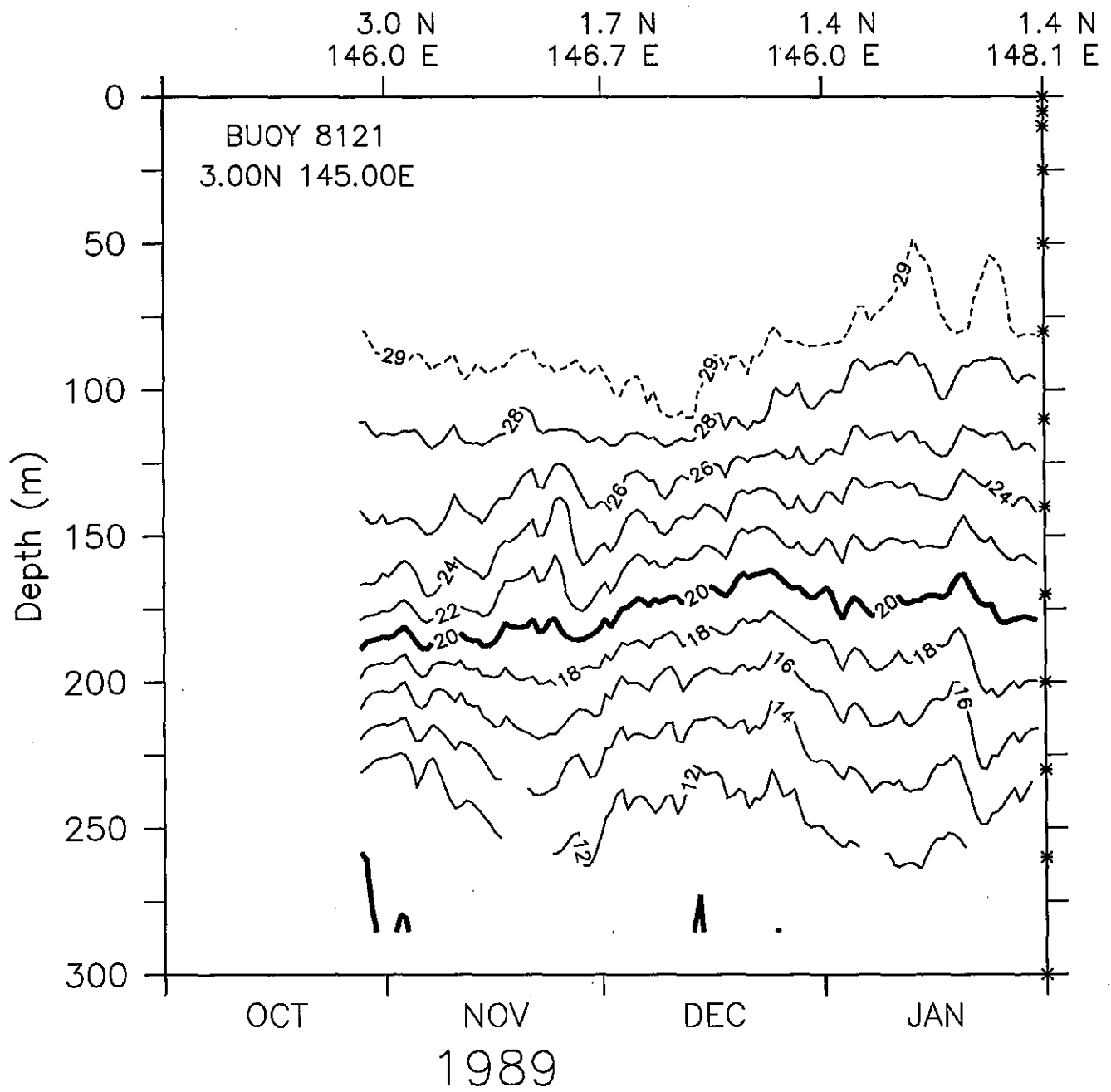


Figure 131.

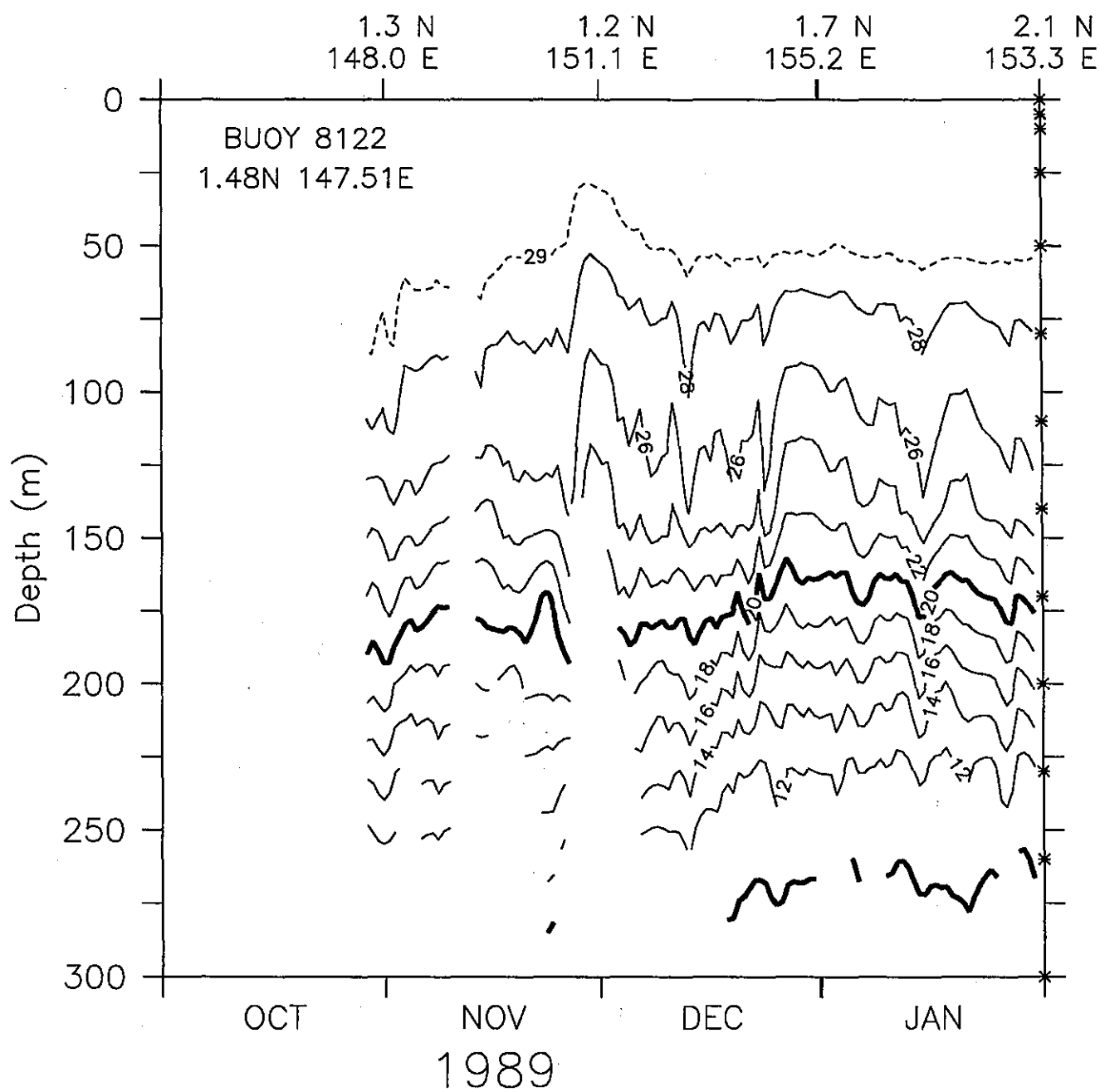


Figure 132.



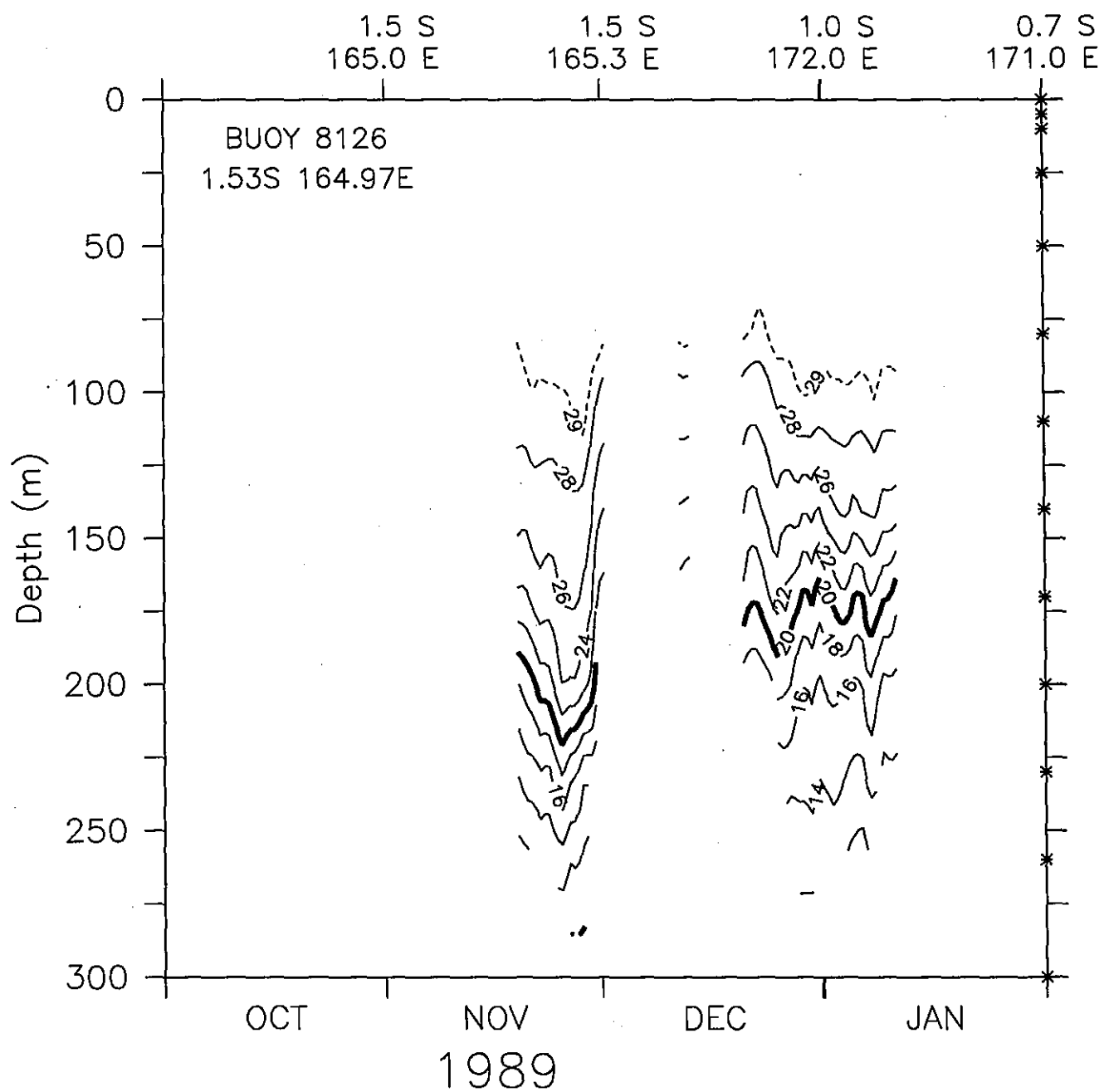


Figure 133.

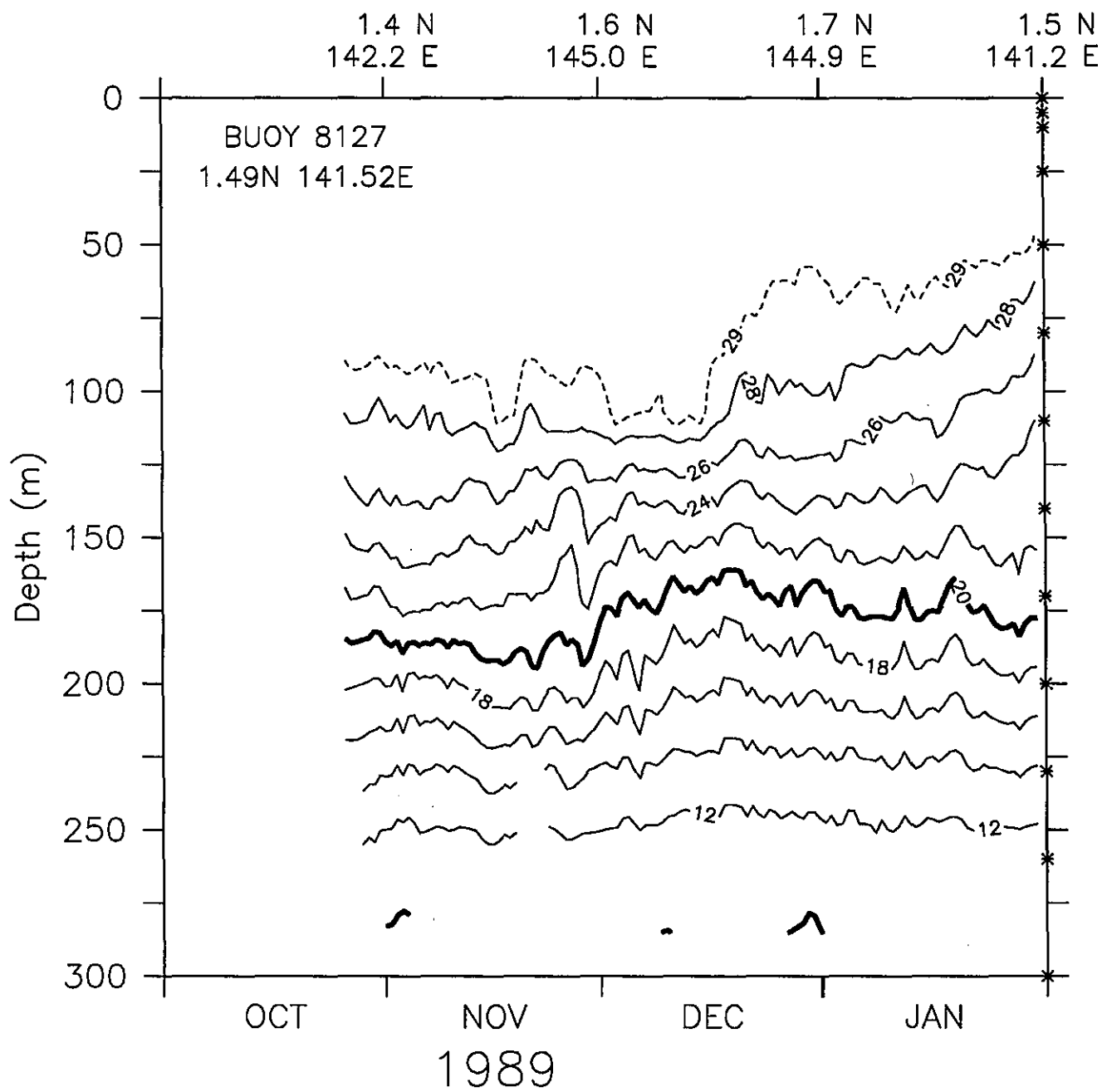


Figure 134.

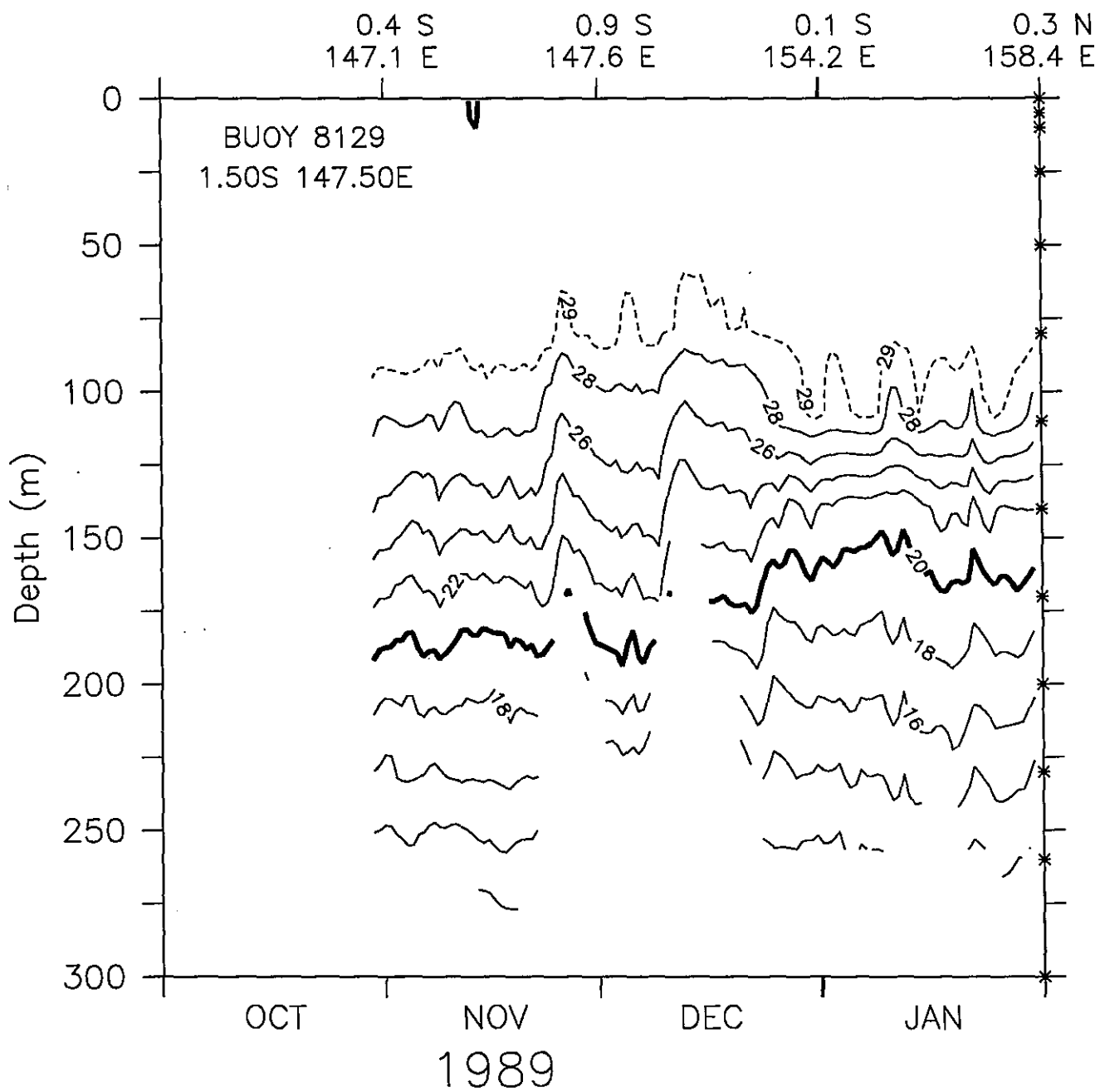


Figure 135.



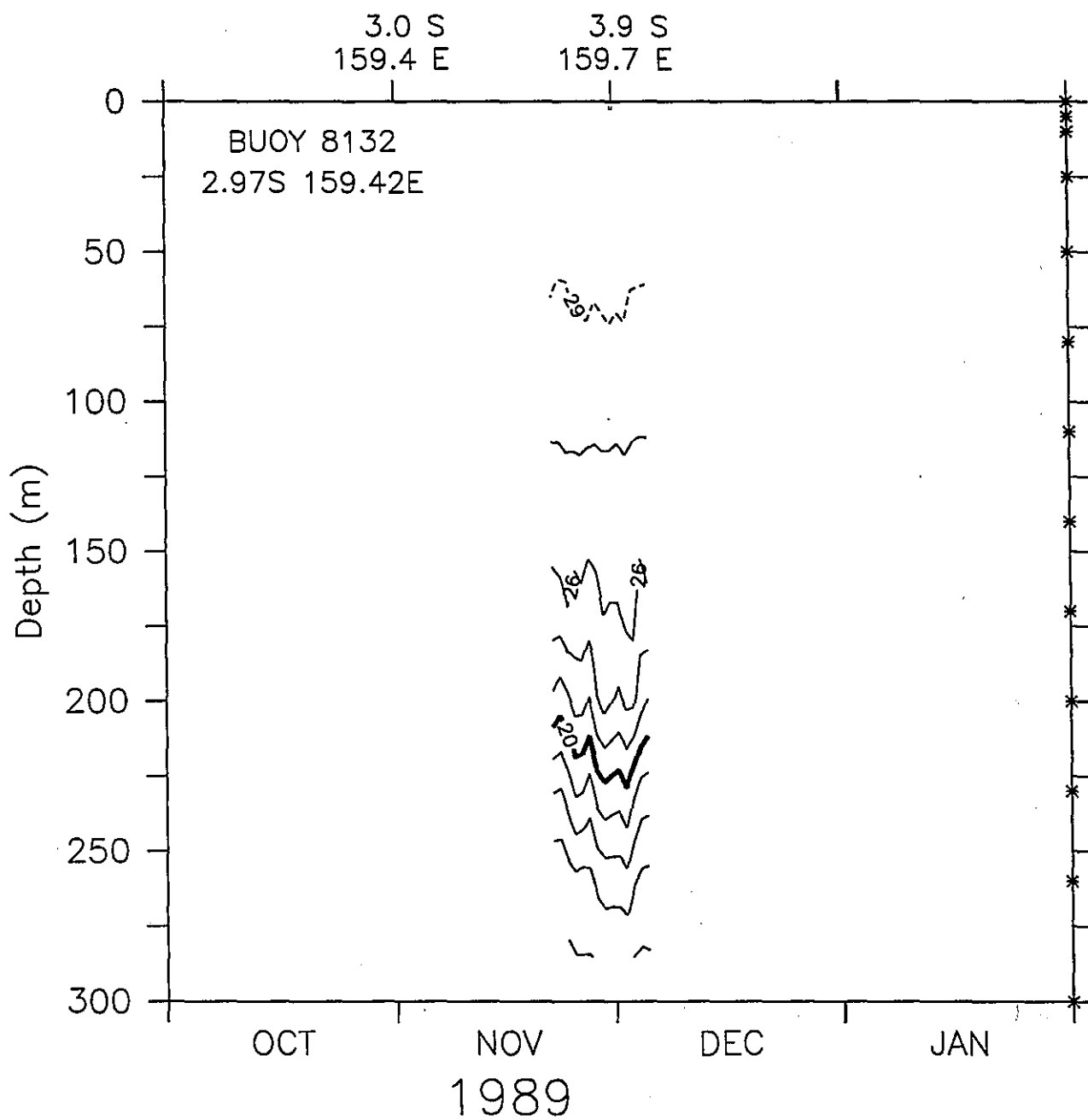


Figure 137.

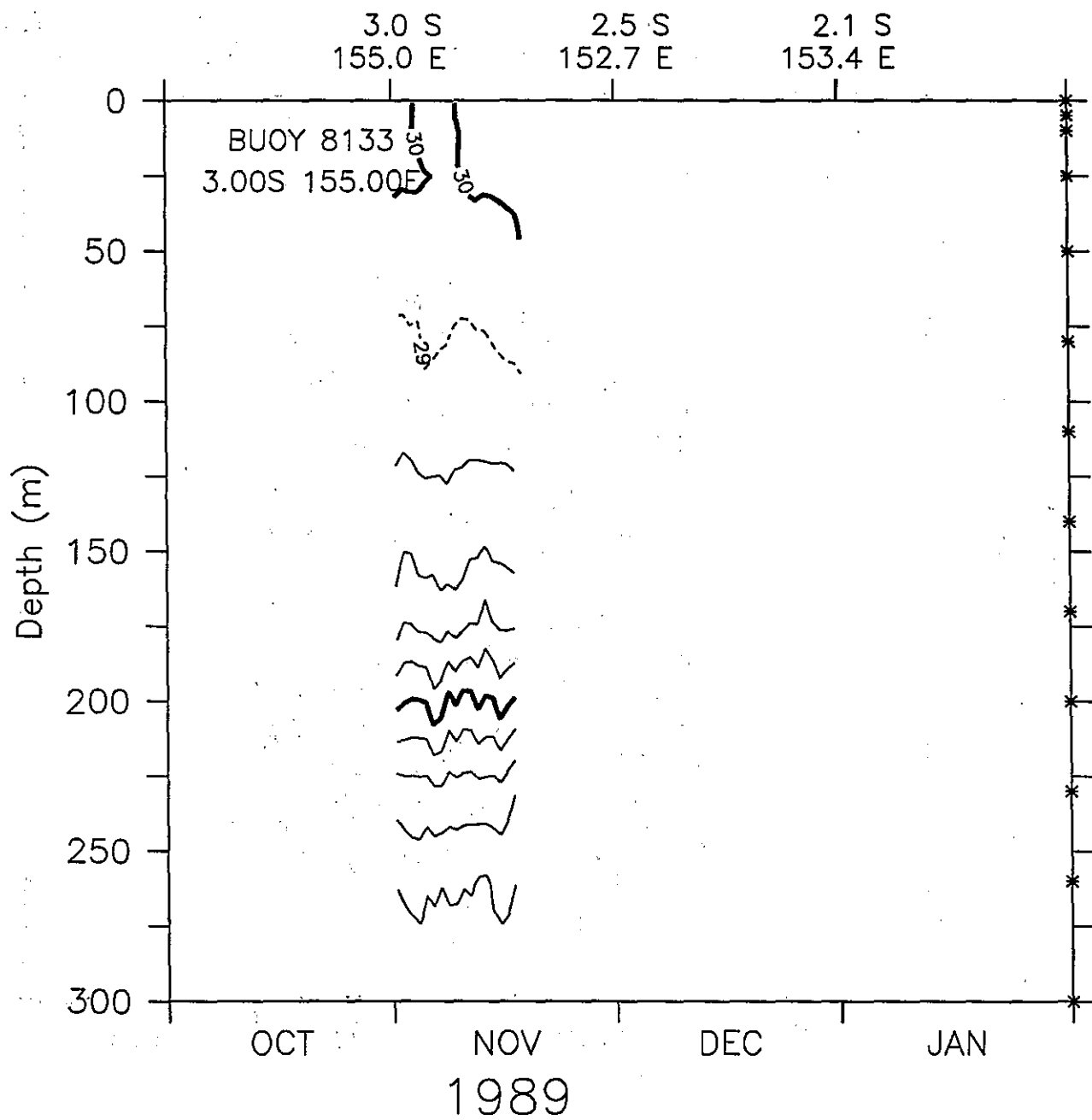


Figure 138.

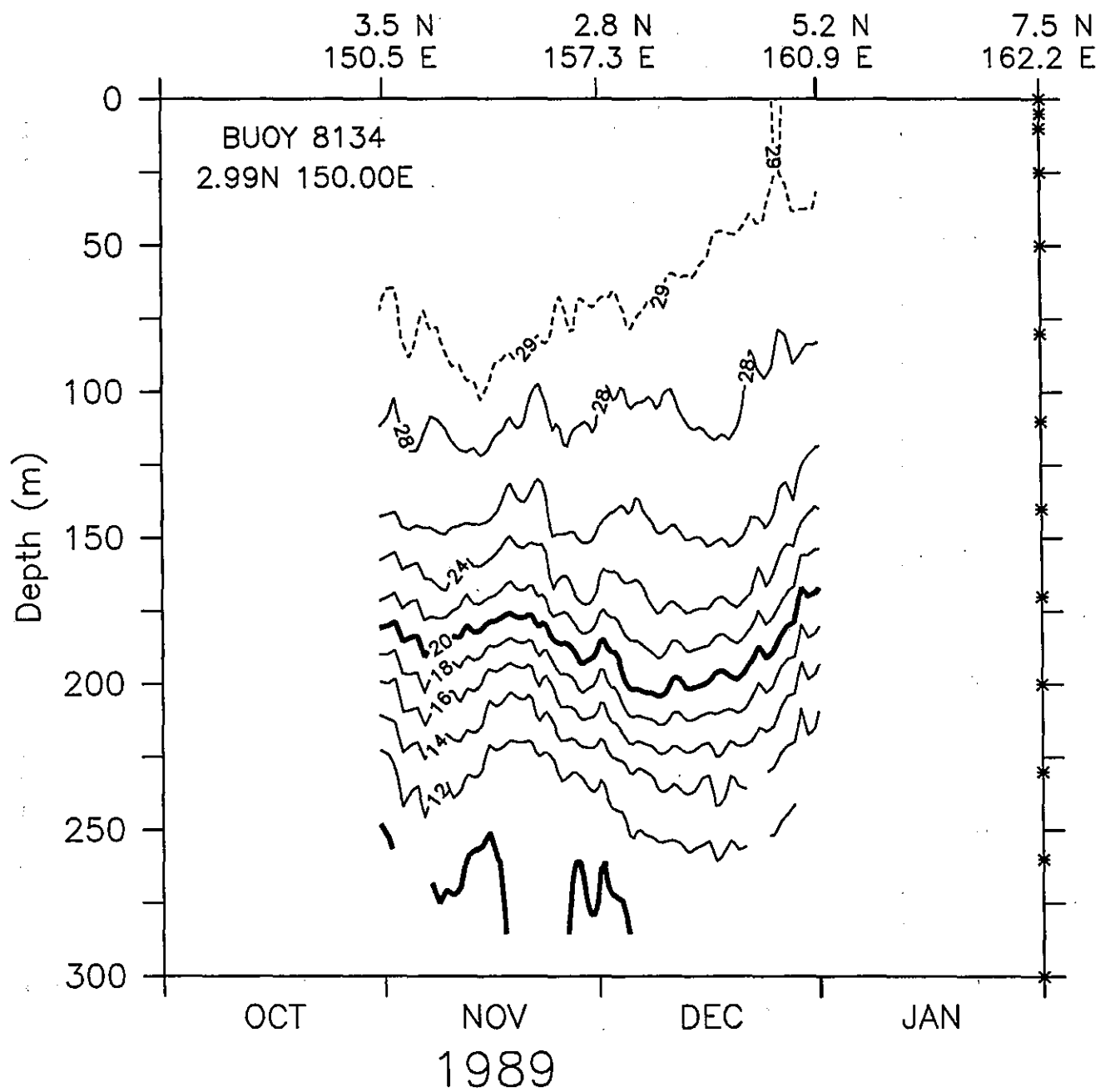


Figure 139.

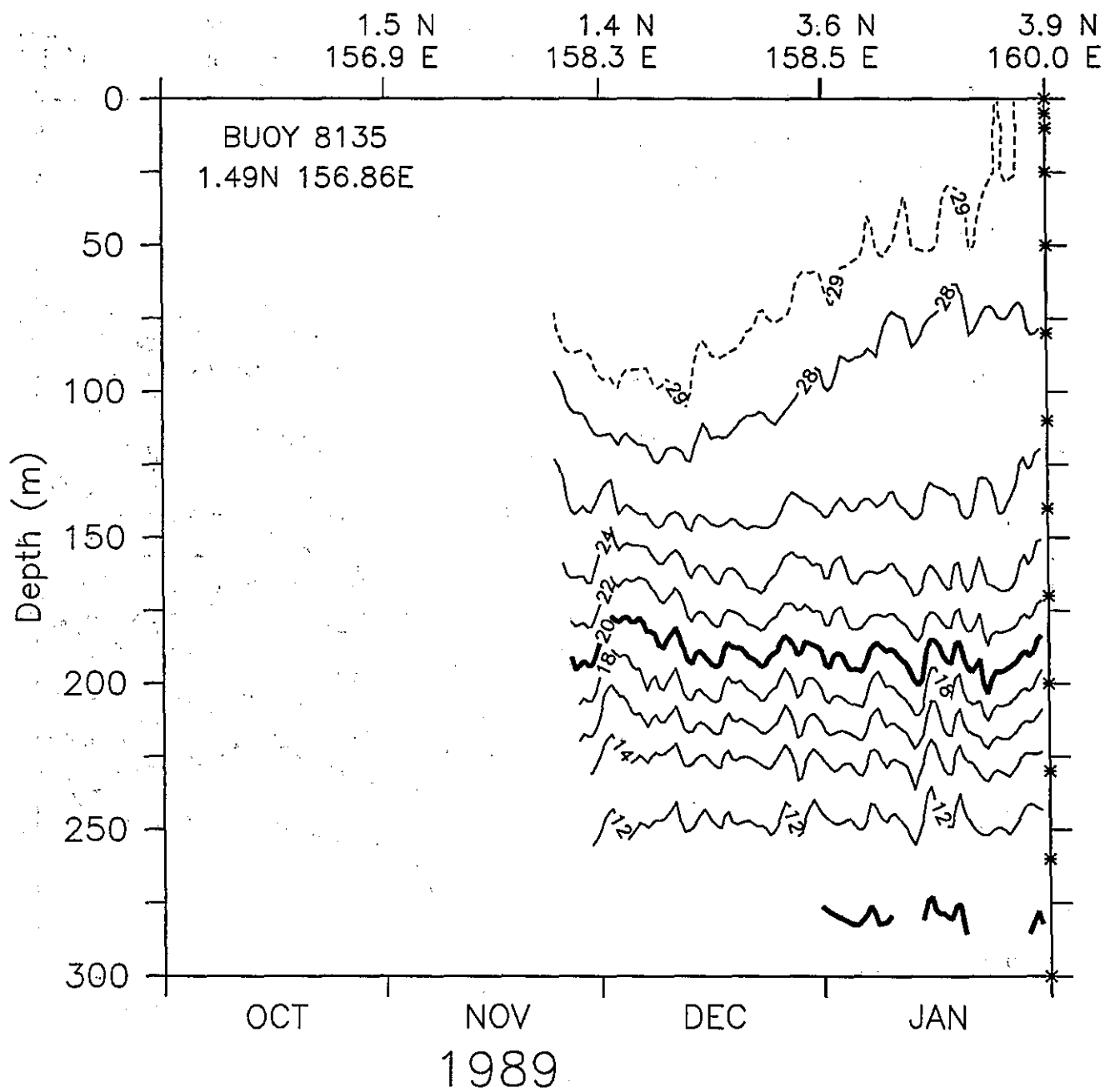


Figure 140.



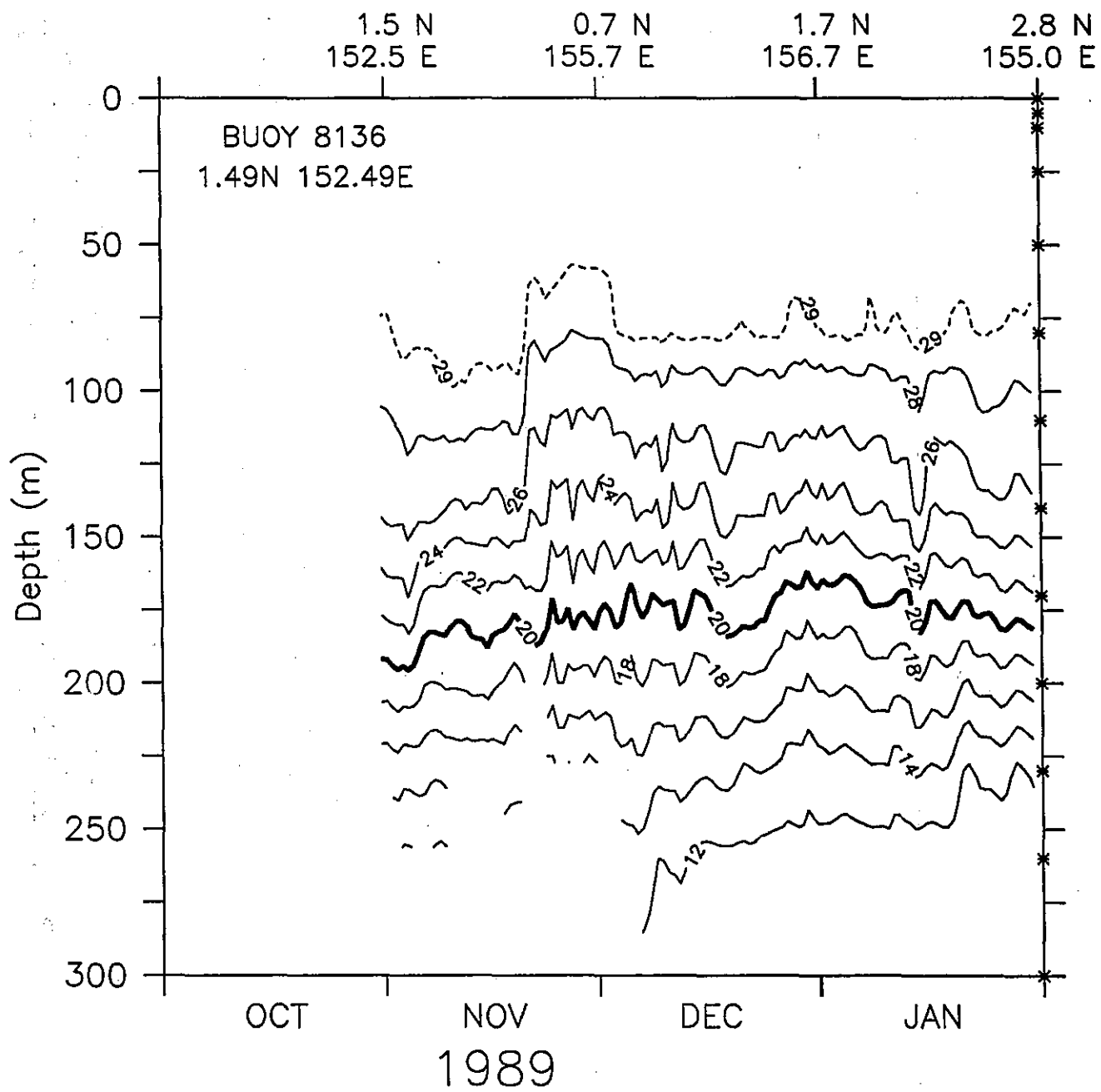


Figure 141.

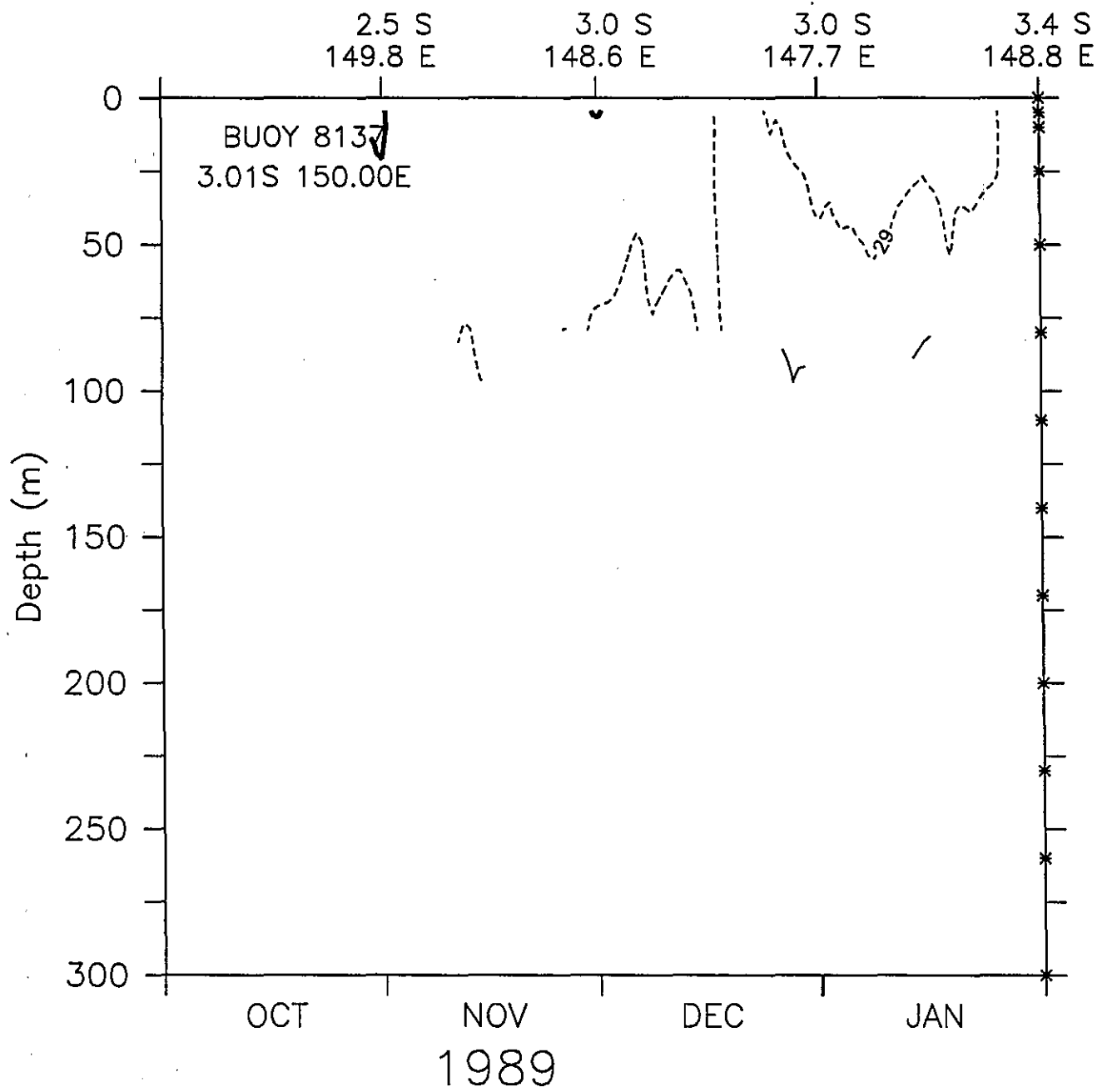


Figure 142.

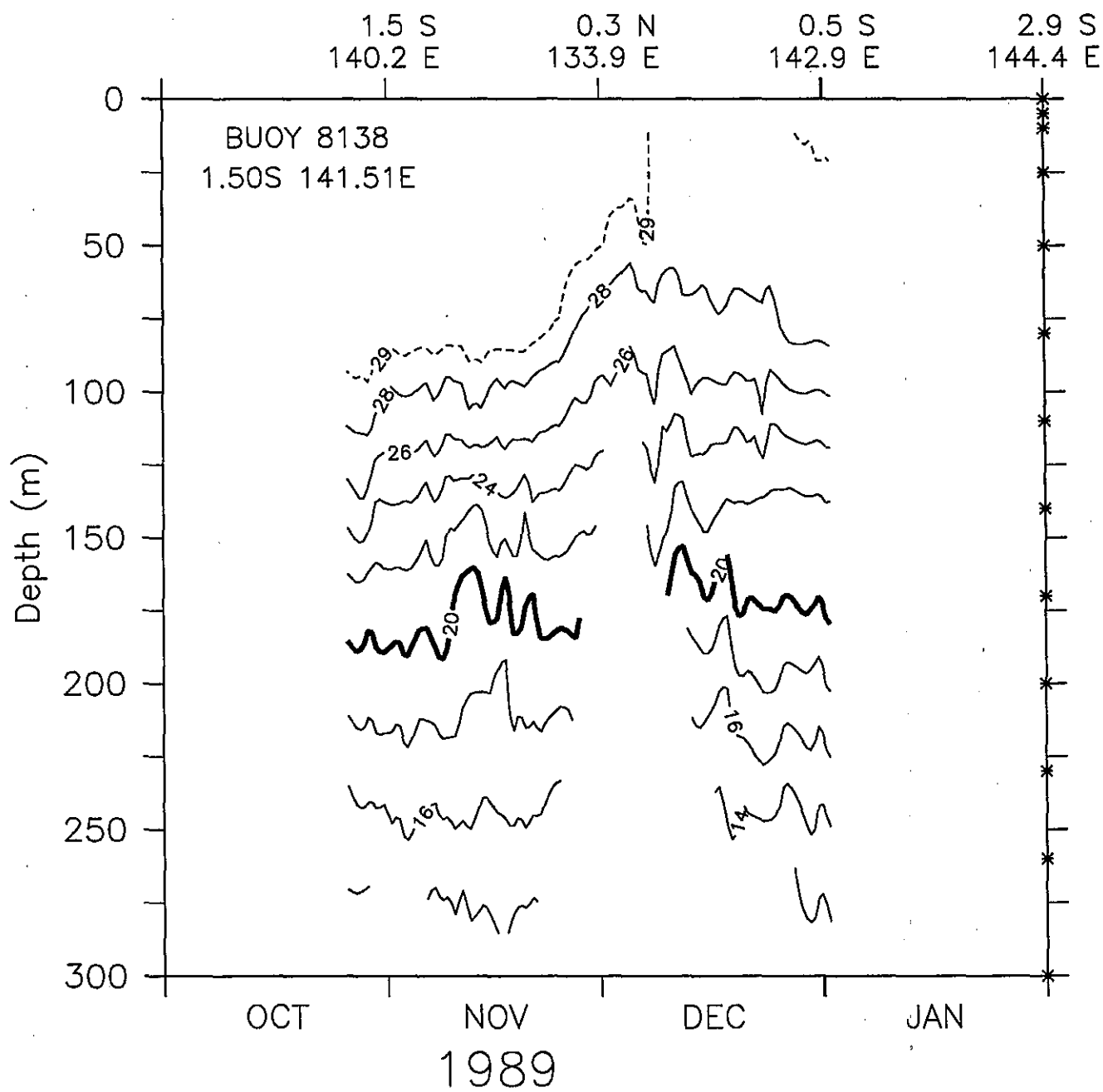


Figure 143.



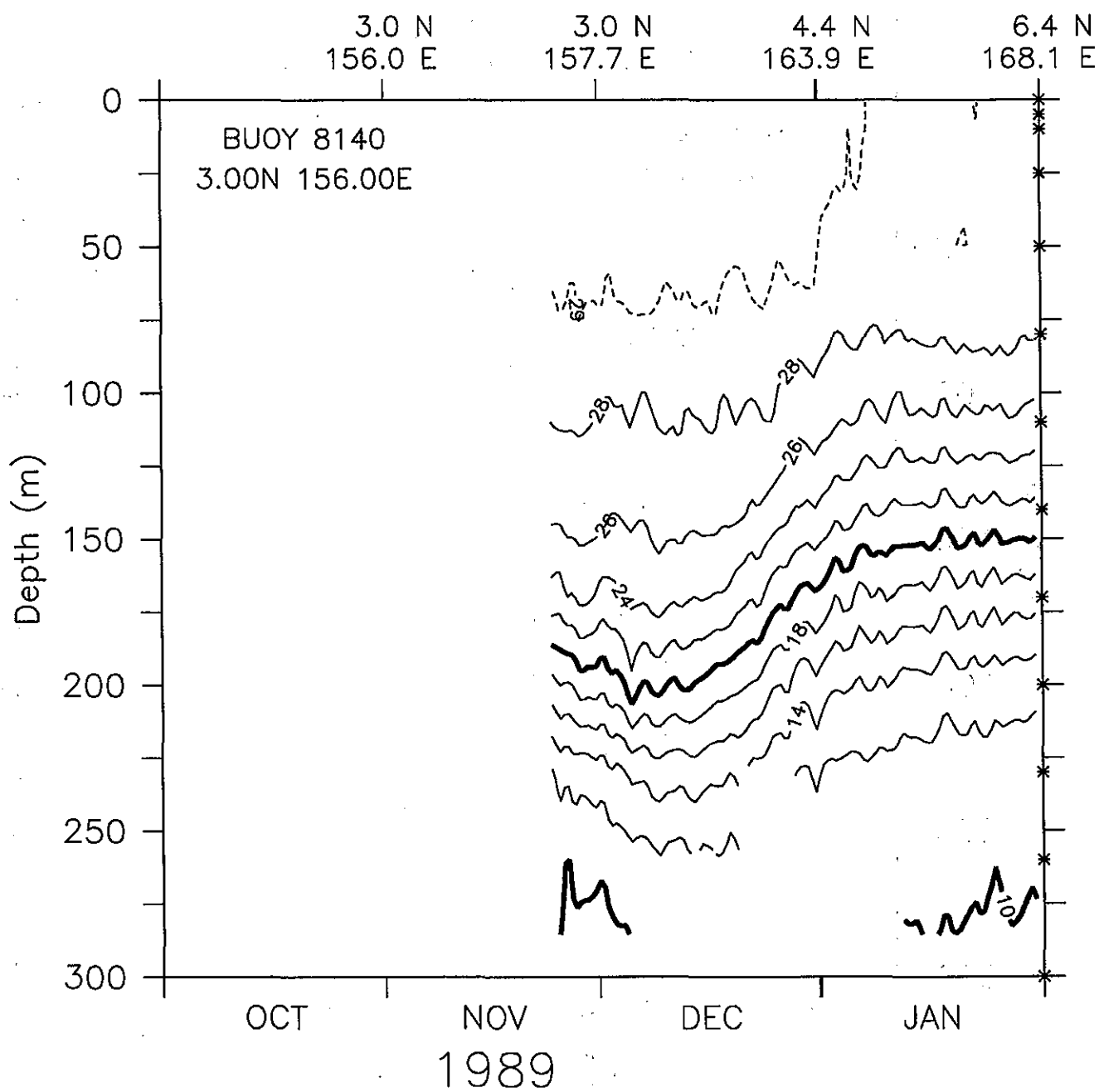


Figure 145.

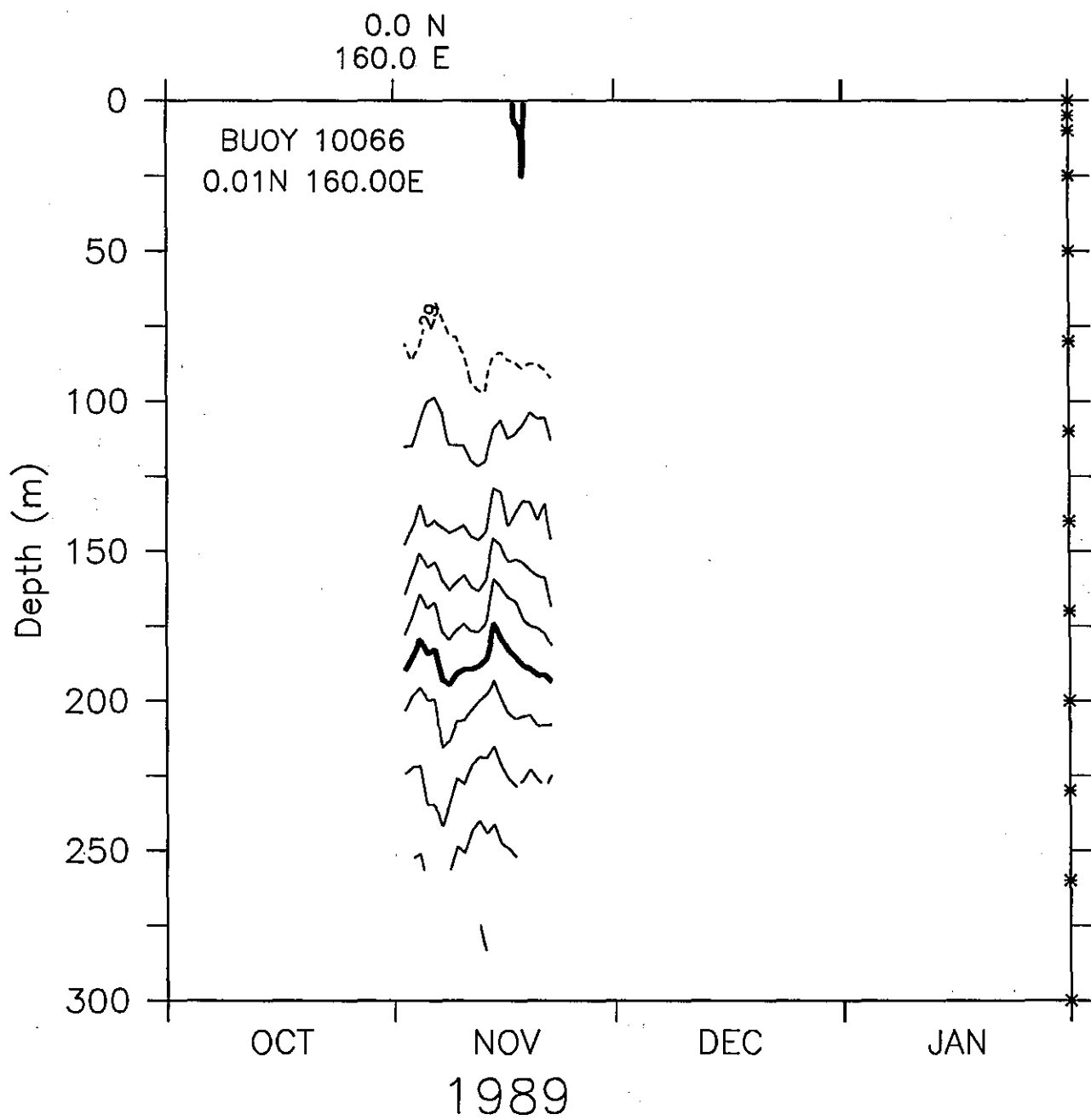


Figure 146.

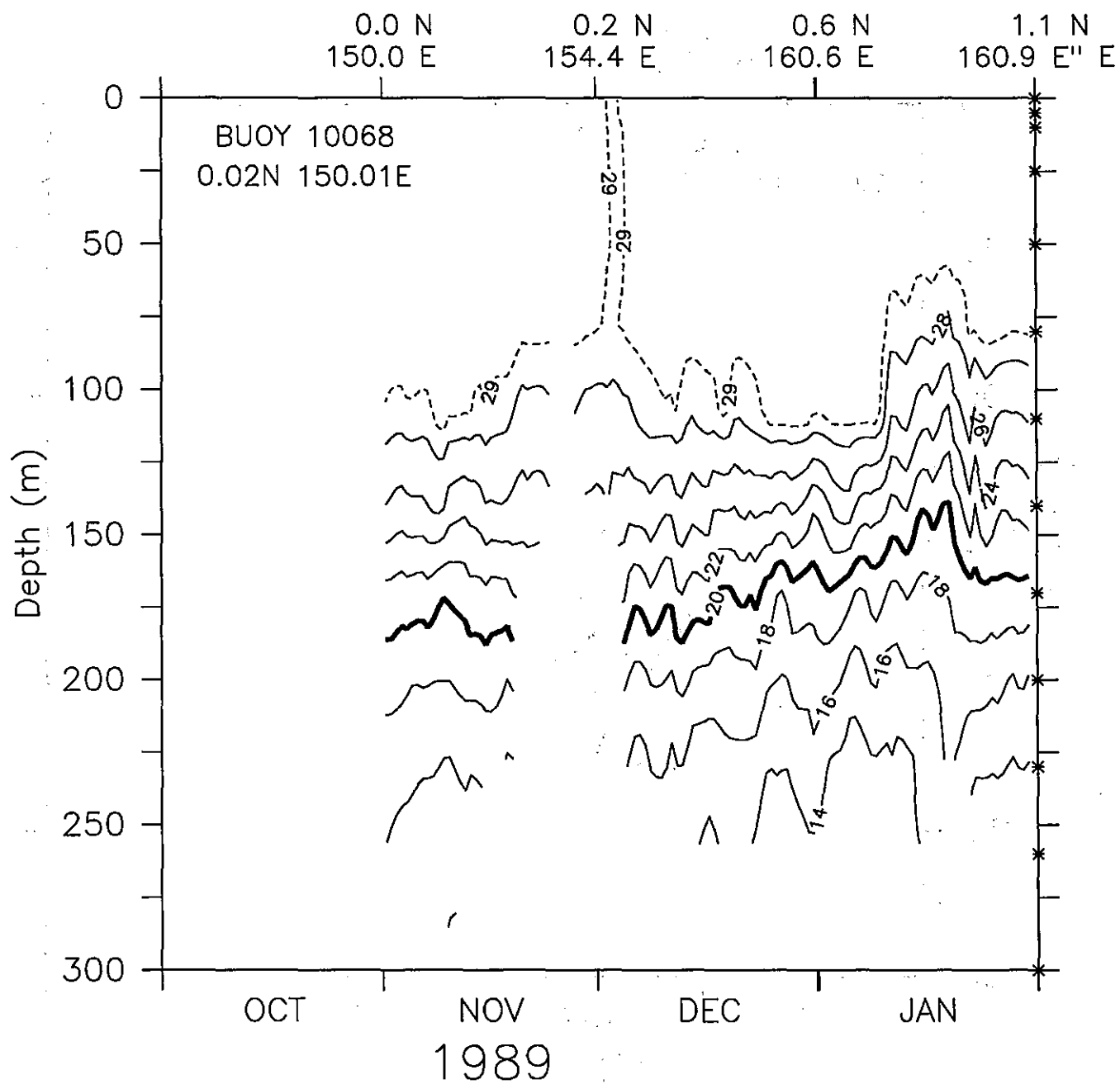


Figure 147.

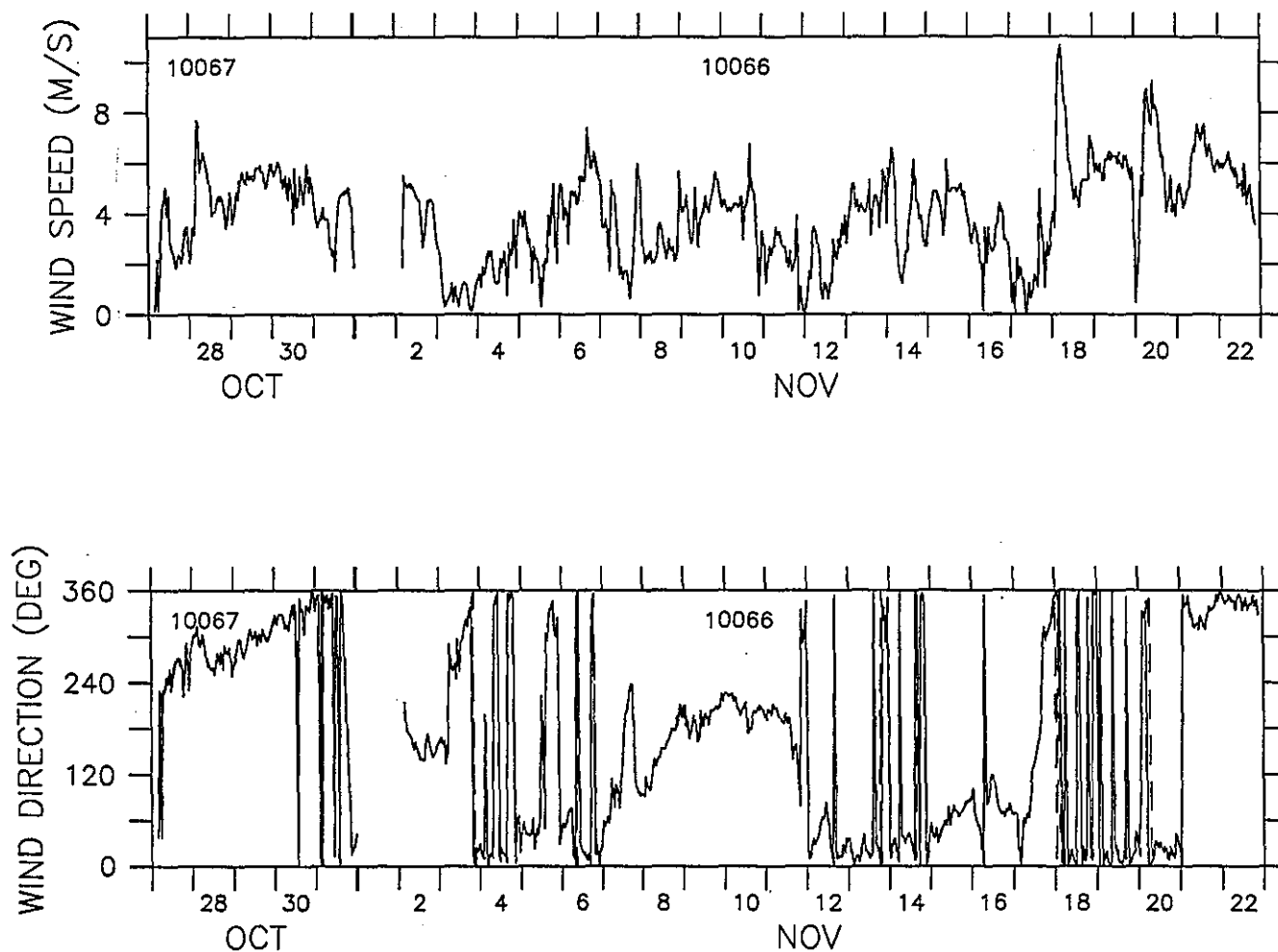


Figure 148. Hourly time series of wind speed and direction (measured counterclockwise relative to east) for PRL buoys #10066 and #10067. Time series from the 2 buoys are non-overlapping and separated by the record gap on November 1. Direction computed from subsampled compass data (solid line) and subsampled compass and vane data (dashed line) are overplotted, as are speeds based on data with and without subsampling. There is almost no distinction between the two methods of subsampling wind speed and direction.



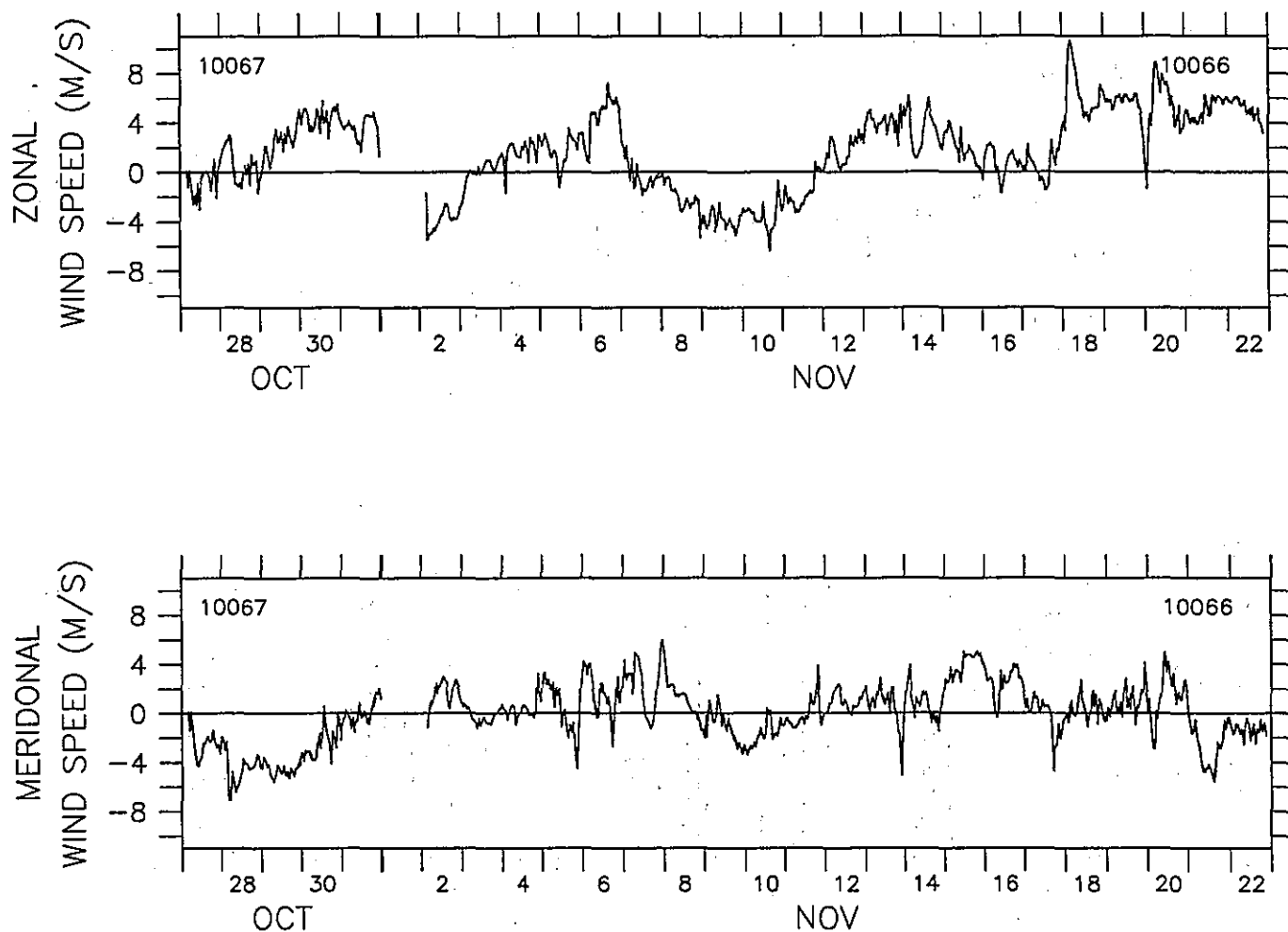


Figure 149. Hourly time series of wind velocity components for PRL buoys #10066 and #10067. Time series from the 2 buoys are non-overlapping and separated by the record gap on November 1. Components computed from subsampled compass only (solid line) and subsampled compass and vane (dashed line) are overplotted. There is almost no distinction between the two methods of computing wind components.

